Ph.D. Mining

ABSTRACT

INTERPRETATION OF GRAVITY DATA DUE TO FAULTS AND DIKES

BY

BIJON SHARMA

Formulas are given for the gravity anomalies of several types of two-dimensional faults and dikes,such as a single fault cutting a series of beds, several parallel faults cutting a bed or a dike inclined at an arbitrary angle to the vertical.

Methods of interpretation of the gravity anomalies of two-dimensional structures based upon the first and the second horizontal derivative of gravity are discussed.Expressions are obtained showing the relationships between the parameters of the various two-dimensional structures and the position and amplitude of the second derivative maximum and minimum.

The Fourier transform formulas for the gravity anomalies of the two-dimensional structures are derived. For small values of ω ,the Fourier transforms give valuable information about the parameters of the structures.Under favorable conditions the amplitude spectrum of the Fourier transforms can give information about the depth as well as the inclination of the anomalous mass.

The validity of the new formulas and the suitability of the new interpretation techniques are tested by comparing results obtained from field measurements with the known geology of the structures.

INTERPRETATION OF GRAVITY DATA DUE TO FAULTS AND DIKES

by

Bijon Sharma
(M.S. Minnesota)

A thesis submitted to the Faculty of Graduate Studies and Research of McGill University in partial fulfilment of the requirements for the degree of Doctor of Philosophy

January

1968

ACKNOWLEDGEMENTS

The author wishes to express his sincere thanks to Dr. L.P. Geldart for his encouragement, interest and guidance throughout this investigation.

The assistance of the members of the staff and fellow graduate students of the Department of Mining and Applied Geophysics, McGill University, is gratefully acknowledged.

My appreciation is also expressed to Mr. R.N. Singh of the Department of Theoretical Physics and Mr. S. Kumarapeli of the Department of Geology, McGill University, for many stimulating discussions.

TABLE OF CONTENTS

Table of Contents (cont'd.)

page

CHAPTER III (cont'd.)

CHAPTER IV

THE FOURIER TRANSFORM OF GRAVITY DATA

Table of Contents (cont'd.) page

Table of Contents (cont'd.) page

LIST OF SYMBOLS AND VARIABLES

The following is a list of some of the important symbols and variables used in this thesis:

G	Universal gravitational constant.
x	Horizontal distance.
z	Vertical depth.
$z_1 , z_2 \cdots z_{N+1}$	Depths to interfaces 1, 2 . . . $N+1$. respectively.
q_i	x/z_i
ρ	Density contrast expressed in gm/cc.
σ	Density of a particular bed or formation expressed in gm/cc.
δ	Vertical displacement of a fault.
d	Vertical displacement of a fault.
δ_1 , δ_2	Vertical displacements due to faults 1 and 2, respectively.
t	Thickness of a bed.
t_i	$z_{i+1} - z_i$.
T	Thickness of a bed or the vertical extent of a dike.
α	Dip of the fault plane or of a dike.
β	Complement of the dip angle $= \frac{\pi}{2} - \alpha$
x_o	Half-width of a dike.
w	Width of a dike.
h	Half the horizontal distance between two parallel faults.

D_1 , D_2	Horizontal distances of secondary faults 1 and 2 from the principal fault.
g_s, g_f, g_m, g_d	The vertical component of the gravity anomalies due to a single block, a fault cutting a single bed, a fault cutting a series of beds and a dike, respectively.
F_{id}	$2G\rho(\psi_{id} \cot\psi_{id} - \log \sin\psi_{id})$.
ψ_{id}	$\theta_{id} - \beta$.
$\tan\theta_{id}$	$\tan\beta + \dfrac{x \mp x_o}{z_i}$.
F_{id}'	$2G\rho(\psi_{id}' \cot\psi_{id}' - \log \sin\psi_{id}')$.
ψ_{id}'	$\theta_{id}' - \beta$.
$\tan\theta_{id}'$	$\tan\beta + \dfrac{x + x_o}{z_i}$.
$f'(x)$	First horizontal derivative of $f(x)$.
$f''(x)$	Second horizontal derivative of $f(x)$.
$\dfrac{dg_s}{dx}$, $\dfrac{dg_f}{dx}$, $\dfrac{dg_m}{dx}$	The gradient or the first horizontal derivative of the gravity anomalies g_s, g_f and g_m, respectively.
$\dfrac{\partial g_s}{\partial z}$, $\dfrac{\partial g_f}{\partial z}$	The first vertical derivative of the anomalies g_s and g_f, respectively.
$G_s(x)$	$x \dfrac{dg_s}{dx} - g_s$. Similar expressions hold for $G_f(x)$ and $G_m(x)$.
g''	Second derivative of the gravity anomaly due to a fault.
g''_{min}	The minimum of g''.
g''_{max}	The maximum of g''.

x_o	Horizontal distance from the fault trace to the point where the second derivative vanishes.
x''_{min}	Horizontal distance from the fault trace to the point where the second derivative is a minimum.
x''_{max}	Horizontal distance from the fault trace to the point where the second derivative is a maximum.
ω	Parameter of Fourier transformation called the 'frequency'.
$F(\omega)$	Fourier transform of the function f(x).
$F\{f(x)\}$	Fourier transform of the function f(x).
$R(\omega)$	Real part of $F(\omega)$.
$X(\omega)$	Imaginary part of $F(\omega)$.
$F_1(\omega)$, $F_2(\omega)$	Fourier transforms of the first and second horizontal derivatives of f(x), respectively.
$R_1(\omega)$, $X_1(\omega)$	Real and imaginary parts of $F_1(\omega)$.
$R_2(\omega)$, $X_2(\omega)$	Real and imaginary parts of $F_2(\omega)$.
$F_s(\omega)$, $F_f(\omega)$, $F_m(\omega)$	Fourier transforms of g_s, g_f and g_m, respectively.
$F_{1s}(\omega)$, $F_{1f}(\omega)$, $F_{1m}(\omega)$	Fourier transforms of $\frac{dg_s}{dx}$, $\frac{dg_f}{dx}$, $\frac{dg_m}{dx}$, respectively.
$F_{2s}(\omega)$, $F_{2f}(\omega)$, $F_{2m}(\omega)$	Fourier transforms of $\frac{d^2g_s}{dx^2}$, $\frac{d^2g_f}{dx^2}$, $\frac{d^2g_m}{dx^2}$, respectively.
$\delta(\omega)$	Dirac 'δ' function.
$R_{1s}(\omega)$, $X_{1s}(\omega)$	Real and imaginary parts of $F_{1s}(\omega)$, respectively.
$R_{2s}(\omega)$, $X_{2s}(\omega)$	Real and imaginary parts of $F_{2s}(\omega)$, respectively.
$R_{1f}(\omega)$, $X_{1f}(\omega)$	Real and imaginary parts of $F_{1f}(\omega)$, respectively.
$R_{2f}(\omega)$, $X_{2f}(\omega)$	Real and imaginary parts of $F_{2f}(\omega)$, respectively.

$R_{1m}(\omega)$, $X_{1m}(\omega)$	Real and imaginary parts of $F_{1m}(\omega)$, respectively.
$R_{2m}(\omega)$, $X_{2m}(\omega)$	Real and imaginary parts of $F_{2m}(\omega)$, respectively.
$g_{+\infty}$	Limiting value of the function $g(x)$ as $x \longrightarrow \infty$.
$g_{-\infty}$	Limiting value of the function $g(x)$ as $x \longrightarrow -\infty$.
g_L	$\begin{cases} g_{+\infty} & \text{for } x > 0. \\ g_{-\infty} & \text{for } x < 0. \end{cases}$
$G(x)$	$g_L - g(x)$.
L	Half the fundamental wavelength of the Fourier series.
ω_o	Fundamental frequency of the Fourier series.
n	Fourier harmonics.
j	$\sqrt{-1}$.
a_n , b_n	Sine and cosine coefficients in the Fourier Expansion of the function $f(x)$.
a_{n1} , b_{n1}	Sine and cosine coefficients in the Fourier Expansion of the function $f'(x)$.
a_{n2} , b_{n2}	Sine and cosine coefficients in the Fourier Expansion of the function $f''(x)$.

CHAPTER I

INTRODUCTION

In the gravitational method of prospecting, small lateral variation in the gravitational pull is measured on the earth's surface. The physical property of the subsurface material which produces the variation in the gravitational pull is small changes in density. Many geological structures produce appreciable variations in the gravity field due to the density contrast between these materials and the surrounding medium. When the variation in the earth's gravitational pull is of sufficiently large magnitude it is often possible to detect the presence of anomalous mass distribution from a knowledge of the variation of the field of gravity.

Compared to the total attraction of the earth, the variation produced by the subsurface anomalous mass distribution is very small, and very sophisticated instrumentation is necessary to detect such small differences in the gravitational field. The advent of very high sensitivity portable gravimeters around 1935 greatly accelerated geophysical exploration by the gravity method.

Among the geologic structures favorable for exploration by the gravity method are faults, dikes, synclines and anticlines. The density differences between these structures and the surrounding medium often produces appreciable variations in the earth's gravitational field. Depending upon the size and shape of the anomalous mass distribution, the

gravity anomaly curve also shows wide variations; however, a general idea about the shape of the structure can often be obtained from the shape of the gravity curve.

In spite of the great value of gravity in the search for oil and minerals, the interpretation of gravity data is often primarily qualitative. The commonest method of interpreting the gravity data is by assuming some simple shape for the causative body and then trying to match the observed anomaly with the calculated anomaly of the assumed structure. As an example, the gravity anomaly produced by a geologic fault is often analyzed by matching the observed anomaly with the calculated anomaly due to a single step with a vertical edge. Interpretation based upon this simple model can give reliable information only under the most favorable geologic conditions. Usually faults cut through a series of beds of different densities and thicknesses; replacing the entire series of beds by a single bed of uniform density is a common simplifying assumption, but it is not always valid. Moreover, in the step model for a fault, we assume that the down-thrown side of the fault is at such a large depth that it has negligible effect on the gravity observations; this also is an important assumption which is often not valid.

Several authors have discussed the theoretical gravity anomaly produced by faulted structures. Perhaps the best known of these is Shaw (1932) who discusses the gradient and curvature anomaly due to a single block terminated by a fault at an arbitrary angle. Other papers relating to gravity anomaly by faults have also appeared before

as, for example, Hedstrom (1938), Barton (1938), Nettleton (1942), Hubbert (1948), and Romberg (1958). All of these papers have been very qualitative and are all based upon the simple model of a block terminated by a vertical or inclined fault. An interpreter faced with the problem of interpreting the gravity anomaly of a fault to extract the maximum information from his gravity data often has to rely upon the simplified models discussed above.

An attempt is made in the present work to obtain more quantitative information from gravity data over two-dimensional faults and dikes. Expressions giving the gravity anomalies of various kinds of two-dimensional faults and dikes are derived. The gravity anomaly of a fault cutting through a number of beds of different densities and thicknesses and the effect on the gravity anomaly of the down-thrown side of the fault is discussed. Interpretation techniques are discussed for obtaining quantitative information about the parameters of two-dimensional faults and dikes.

The starting point for obtaining the gravitational attraction of two-dimensional structures discussed in this paper is a new formula giving the gravitational attraction of a single block terminated by a fault at an arbitrary angle. This formula, derived by Geldart (1966), differs from other single block formulas, such as those given by Jung (1930) and Heiland (1946), in that the new formula is simpler and more readily adaptable to obtaining formulas for other more complicated two-dimensional structures.

For interpreting the gravity anomalies of two-dimensional faults and dikes, the methods of interpretation based upon the derivatives and the Fourier transform of the gravity data are discussed. The use of the horizontal derivative or the gradient of the gravity anomaly due to a single block truncated by a fault at an arbitrary angle is discussed by Shaw (1932). Rosenbach (1954) has successfully utilized the high resolving power of the second derivative to make a detailed study of the Rhine graben in Europe. Romberg (1958), while emphasizing the high resolving and amplifying power of the second derivatives, has pointed out certain inherent weaknesses of the second derivative method of interpretation. Firstly, according to Romberg, second derivatives are calculated from the differences between small variations in gravity and hence are greatly affected by small errors. Secondly, the second derivatives of gravity do not resemble the structure that caused them and no information about the size of the structure can be obtained from the second derivative profiles. In spite of these shortcomings, several authors have shown that second derivatives, when used in conjunction with gravity, can be a very powerful tool in interpreting gravity data. In the present work, expressions for the gradient and the second derivative of some two-dimensional structures are derived and methods of interpreting the gravity anomalies of these structures based upon the use of these derivatives are discussed.

A second method of interpretation based upon the Fourier transformation of the raw gravity data is also discussed. By the

Fourier transformation, the gravity anomaly is transformed from the original distance domain into the frequency domain. If we transform the data into the frequency domain and then carry out the interpretation, we obtain certain advantages; firstly, in transforming into the frequency domain, a new function is obtained which is easier to handle than the original function; secondly, in finding the Fourier transforms all available gravity data are used in the interpretation.

Dean (1958) pointed out that electrical filter theory has considerable applications to the spectrum analysis of potential field data since many sampling operations, such as calculations of derivatives, also upward and downward continuation of fields, are exactly analogous to the filtering action of electrical network. Odegard and Berg (1965) made frequency analysis of several bodies of simple geometric shapes such as cylinder, sphere, single fault with a vertical edge, and have shown how the depth and size of the causative body may be obtained from the frequency spectrum of the anomaly. In the present work, Fourier transform formulas are derived for a wide variety of geologic structures, such as a single block truncated by a fault at an arbitrary angle, faults cutting a series of beds having different densities and thicknesses, dikes, etc. Techniques are discussed for obtaining information about the parameters of the two-dimensional structures from the frequency spectrum of these anomalies.

To verify the validity of the new formulas and to investigate the usefulness of the interpretational techniques, several gravity surveys were carried out over known faults and a dike. Since the

geology of the surveyed structures is fairly well known, the value of the new formulas and interpretational techniques can be evaluated by comparing the results from our interpretation with the known geology of the structures.

CHAPTER II

GRAVITY ANOMALIES OF FAULTS AND DIKES

Gravity Anomalies For Single Blocks

General: The formula and curves for a single block will be discussed in some detail because these are fundamental in obtaining results for more complicated forms. In addition the results for a single block can be applied in studying faults with very large displacements and therefore have intrinsic value in fault interpretation.

Discussion of the Formulas: The basic formulas are derived in Appendix A where it is shown that the vertical component of gravity, g_s, due to a horizontal semi-infinite block truncated by a plane dipping at an angle α is given by

$$g_s = 2G\rho(\pi-\alpha)t + x \sin^2\alpha(F_2-F_1) \qquad \ldots\ldots (1)$$

$$= 2G\rho(1/2\pi+\beta)t + x \cos^2\beta(F_2-F_1) \qquad \ldots\ldots (1')$$

G is the universal gravitational constant, ρ the density contrast, t the bed thickness, x the distance from the fault trace to the given point, and β the complement of the dip angle, α . The function F_i, where $i = 1,2$, is defined by the relations

$$F_i = 2G\rho(\psi_i \cot\psi_i - \log \sin\psi_i),$$

$$\psi_i = (\theta_i - \beta), \quad \tan\theta_i = \tan\beta + x/z_i,$$

z_i, z_2 = depth to top and bottom of the block respectively.

Figure 1 shows the relationship between the various parameters. The distance x is positive when P is to the right of the fault trace; all angles are measured in the clockwise direction, β and θ_i being measured from the vertical, α and ψ_i from the fault plane.

Formula (1) holds when the block is to the right of the fault plane. When the block is to the left of the fault plane, the formula becomes

$$g_s' = 2G\rho\alpha t - x \sin^2\alpha(F_2-F_1) \qquad \ldots\ldots (1'')$$

$$= 2G\rho(1/2\pi-\beta)t - x \cos^2\beta(F_2-F_1) \qquad \ldots\ldots (1''')$$

Thus, $g_s + g_s' = 2\pi G\rho t$.

It is shown in Appendix A that g_s has the following limiting values:

$g_s = 0$ when $x = -\infty$ or when $\alpha = +\pi$,

$= 2\pi G\rho t$ when $x = +\infty$ or when $\alpha = 0$,

$= 2\pi G\rho(\pi-\alpha)t$ when $x = 0$ or when $z_1 = +\infty$.

If all the dimensions in Figure 1 are multiplied by the factor k, the angles, ψ_1 and ψ_2, are preserved and consequently the factor (F_2-F_1) remains the same. Therefore g_s is increased by the factor k. This fact has been noted in several papers, but its full value has not been appreciated by most interpreters. It is invaluable in deriving curves for various depths or thicknesses from a few standard curves,

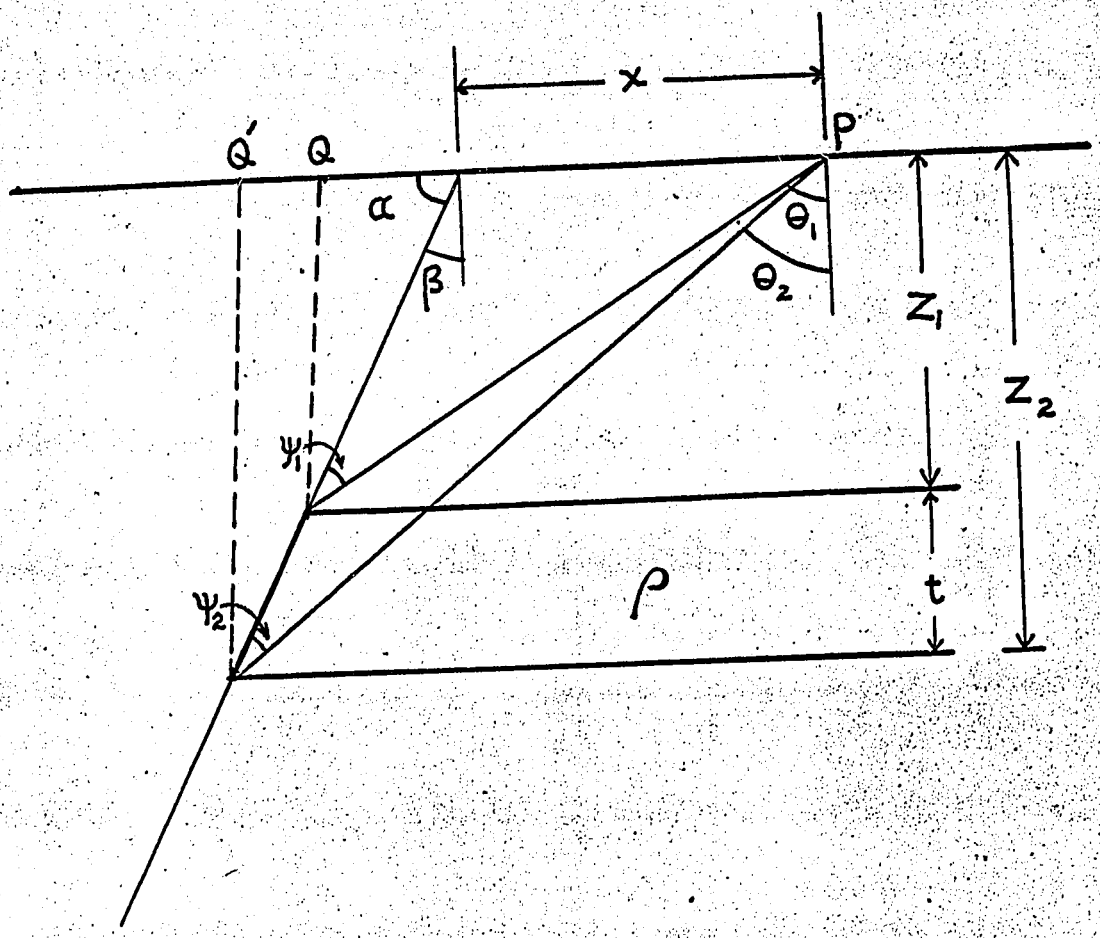

FIG. 1. Parameters and variables used in calculating g_s.

also in reducing observed data to a standard thickness of bed or depth.

The function, F_i, can be regarded as an even function of ψ_i (see Appendix A). Therefore the term (F_2-F_1) is unaltered when ψ_1 and ψ_2 both change signs. If g_+ denotes the value of g_s for given values of x and β while g_- is the value of g_s corresponding to the values of $-x$ and $-\beta$, then

$$g_+ + g_- = 2\pi G\rho t,$$

hence

$$g_- = g_s'$$

Therefore the curves corresponding to negative values of β can be obtained by reflecting the curve for g_s' in the axis of g_s, as shown in Figure 2. The curves for block A and block B add up to give $2\pi G\rho t$ at every point, whereas the value for block B at $x = +x_o$ is the same as the value for block C at $x = -x_o$. The sum of the intercepts for block A and either block B or block C equals $2\pi G\rho t$. Because of this relation, curves are not required for negative values of β, that is, α greater than 90^o.

Curves for single blocks: g_s can be expressed in terms of three parameters: the dip, thickness and depth of the block. Figures 3-6 illustrate the effects of varying each of these parameters. In calculating the values for these curves, ρ was given the value unity and all dimensions expressed in units of 1,000 ft. This results in a value of 4.064 mg/1,000 ft for $2G\rho$. Except for Figure 5, the curves are for blocks of unit thickness; this rather large thickness, together

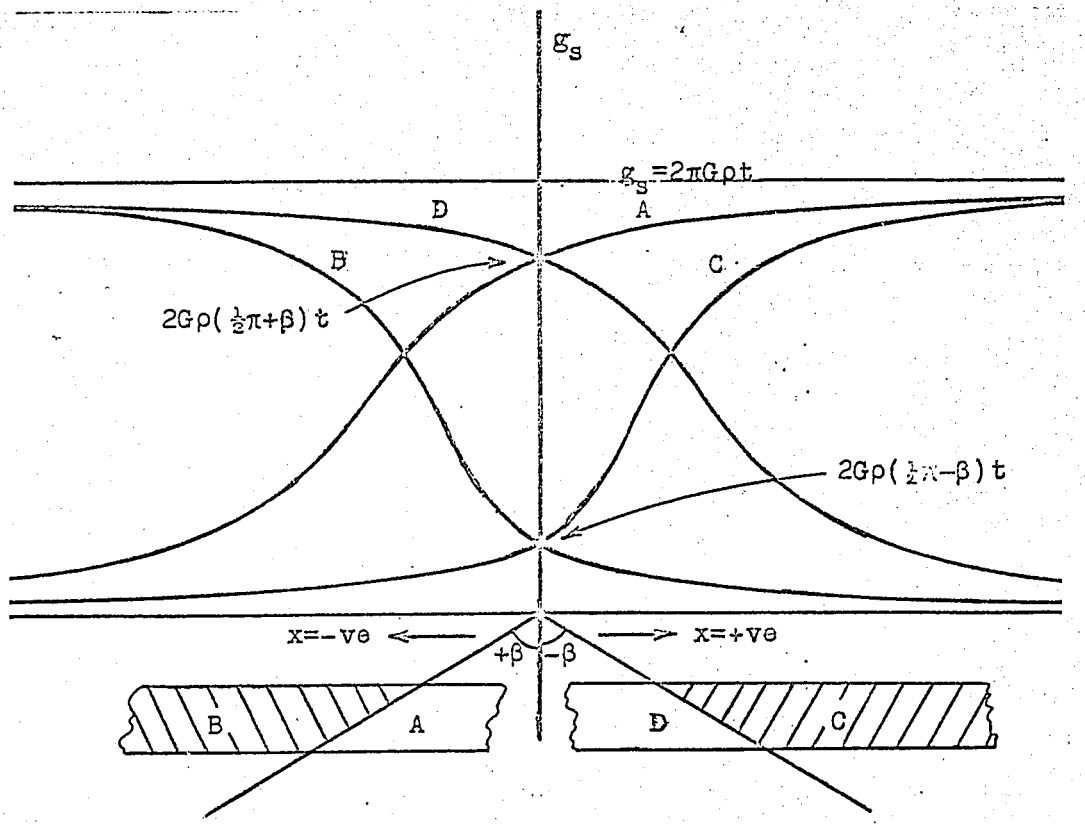

FIG. 2. Relation between g_s and algebraic signs of x and β.

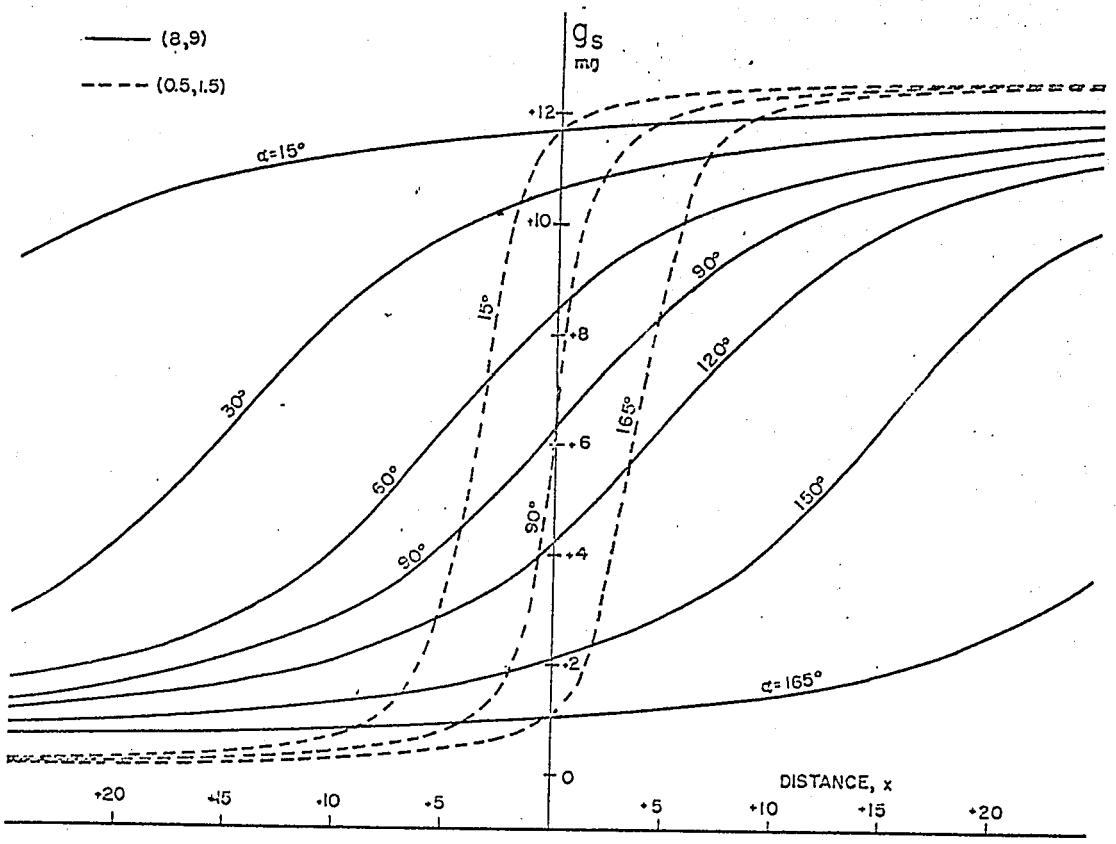

FIG. 3. Variation of g_s with dip.

with the large value of ρ, results in amomalies which are approximately an order of magnitude larger than those commonly encountered in field work, a fact which should be kept in mind in studying the curves.

To simplify the discussion and labelling of the curves, the expression (z_1, z_2) will be used to designate specific blocks; thus, (0.5, 1.8) refers to a block extending from a depth of 500 ft to a depth of 1,800 ft. This notation will be used later in an expanded form to designate faults as well.

Figure 3 shows the effect of varying the dip. Curves are given for two blocks at different depths, the intermediate curves being omitted for the shallow block.

The striking feature about the curves in Figure 3 is that all curves for a given depth are essentially identical in form. A tracing of any one of the curves, if translated parallel to the x-axis without rotation, can be made to coincide with any other curve for the same depth. Although the curves coincide within the accuracy of plotting, the agreement is probably not mathematically exact. Exact agreement requires the existence of an equation of the form

$$g_s(x, \alpha_1) = g_s(x + h, \alpha_2)$$

where $g_s(x, \alpha)$ denotes that g_s is regarded as a function of x and α and the quantity h is independent of x.

If two faults having dip angles α_1 and α_2 intersect at the surface of the ground, the gravity curves resulting from the faults

truncating a given bed will be separated as in Figure 3. Let h be the horizontal distance between corresponding points on the two curves. If one of the faults is displaced an amount h away from the other in the proper direction, the two curves will coincide, that is the value of g_s at any point is the same for both faults. If a vertical section is now drawn as in Figure 4, it will be found that the two faults intersect at a point O which is slightly above the center line of the bed. Probably this relation is equivalent to the statement that a point O can be found such that the values of g_s for the infinitely long wedges, OAC and OBD, are approximately equal for every point on the surface.

The invariance of curve shape as the dip varies permits one to interpolate readily for the intermediate values of dip. Also, if the location of the surface trace of the fault is known, the dip could be found by comparing the observed curve with the curves in Figure 3 (assuming ρ and t are known).

Figure 5 illustrates the effect of varying the block thickness. Results are given for two blocks, one having its upper surface coinciding with the ground surface, the other having its upper surface at a depth of 4 units. For each block, curves are given for t = 0.25, 0.50, and 1.0 units. The dip is 90° for all curves except the dotted curve corresponding to $\alpha = 15^\circ$ which illustrates the translation of the curve resulting from the change in dip.

The curves are asymptotic to the horizontal lines given by $g_s = 0$ and $g_s = 2\pi G\rho t = 3.19$, 6.38, and 12.77 mg respectively for the

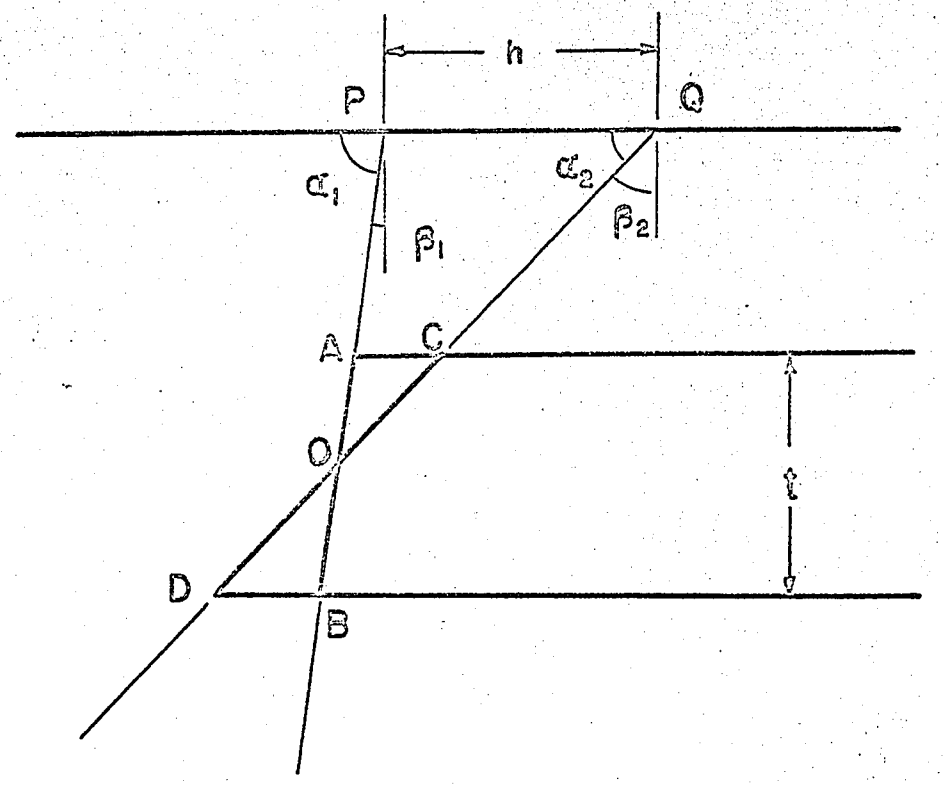

FIG. 4. Geometrical relationship between equivalent faults.

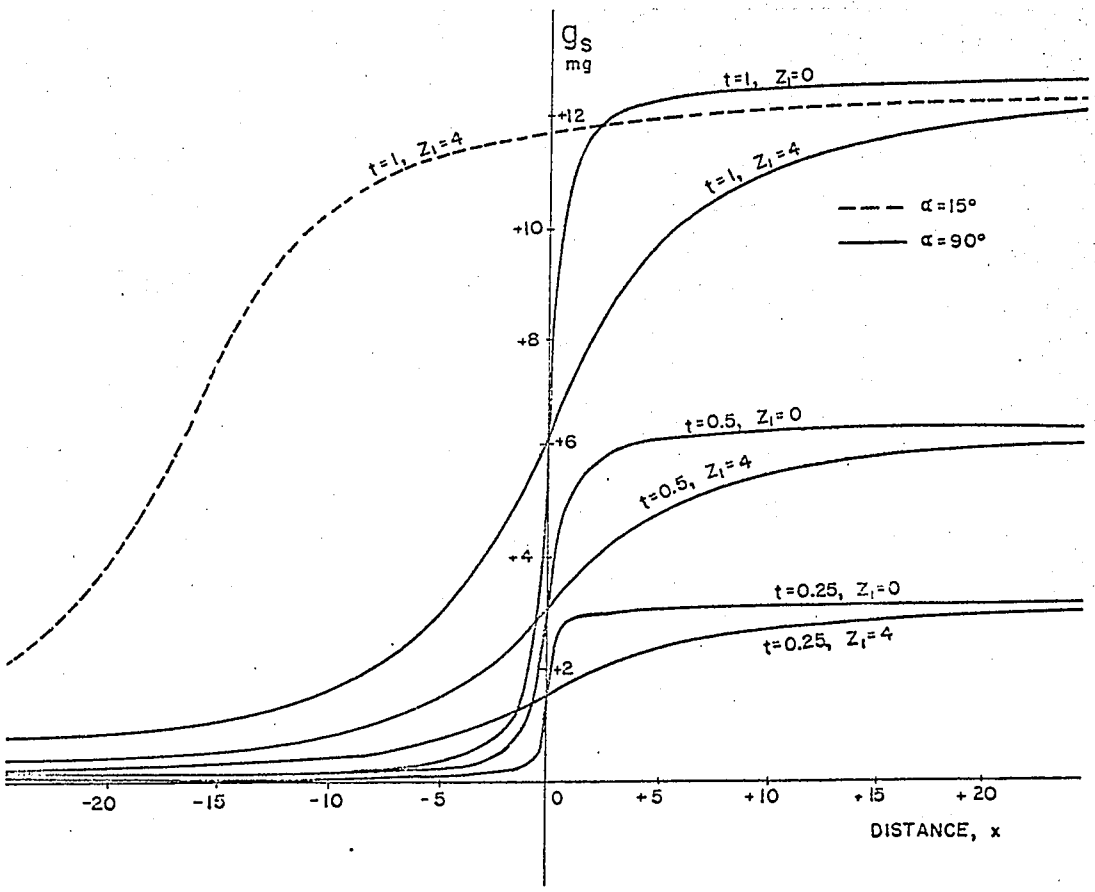

FIG. 5. Effect on g_s of varying the block thickness.

three sets of curves. The slopes of the curves at the origin depend upon both the depth and the thickness, except when $z_1 = 0$, when the slope is infinite regardless of the thickness (see Appendix A).

The curves in Figure 6 show the manner in which g_s changes as the depth, z_1, varies when the dip is 90°. As the depth approaches infinity, the curve approaches the horizontal straight line corresponding to

$$g_s = 1/2(2\pi G\rho t) = 6.38 \text{ mg when } t = 1.$$

The curves for other values of dip can be visualized by mentally displacing the appropriate curve, to the left for α less than 90°, to the right for α greater than 90°, the amount of the displacement depending upon α and the depth. For a given α and t, the intercept on the g_s axis is $2G\rho(\pi-\alpha)t$. O' and O'' are two such intercepts corresponding to $\alpha = 60^\circ$ and $\alpha = 120^\circ$ respectively.

The range of the anomaly, that is, the difference between the values of g_s for $x = \pm \infty$, is often used to obtain the quantity (ρt). If ρ is known, t can be found in this way, after which the depth z_1 could be obtained by comparison with curves such as those in Figure 6. However, if t cannot be found, the ratio (t/z_1) can be determined from the slope of the gravity curve. It is shown in Appendix A that the slope of the curve for g_s at $x = 0$ is

$$\frac{dg_s}{dx} = 2G\rho \sin^2\alpha \log(1 + t/z_1).$$

For a given block, the slope at $x = 0$ is a maximum when the dip is 90°.

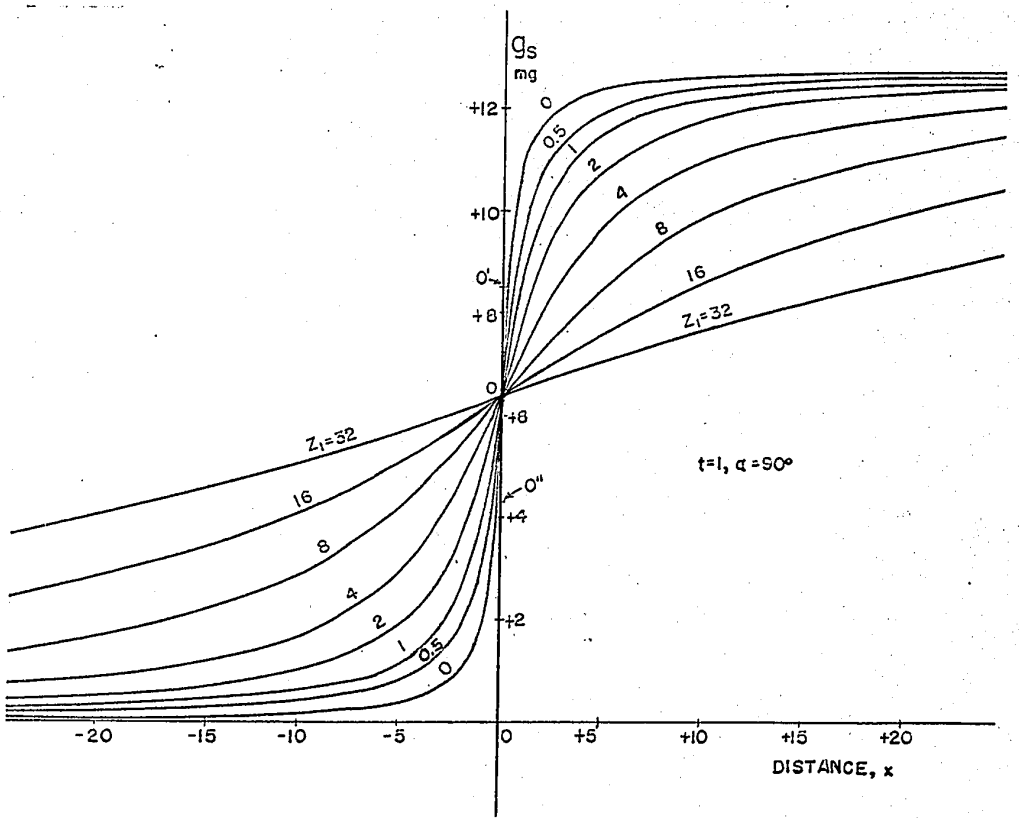

FIG. 6. Effect of depth on g_s.

If it were possible to rotate the fault plane, the gravity curve would be displaced laterally without any appreciable change in shape as α is varied. This would cause the origin to move along the curve, each point on the curve becoming the origin in its turn. The slope at the origin would reach its maximum when α became 90°; however, because the curve would not change shape, this maximum slope would be identical with the maximum slope along the entire curve. Consequently, regardless of the actual dip, the maximum observed slope of the gravity curve is equal to $2G\rho \log(1 + t/z_1)$ from which the ratio (t/z_1) can be found if ρ is known.

The curves in Figures 3-6 can be applied in the limiting case of a fault having infinite displacement provided the constant term equal to $2G\rho\alpha t$ due to the lower block (see Appendix A) is taken into account where necessary.

Gravity Anomaly Of A Fault Cutting A Single Bed

Discussion of Formula: In Appendix B it is shown that the vertical component of gravity due to the normal fault shown in Figure 7 is

$$g_f = 2\pi G\rho t + x \sin^2 \alpha\{(F_2-F_1) - (F_4-F_3)\} \quad \ldots\ldots (2)$$

For the reverse fault represented by the cross-hatched beds in Figure 7, the formula becomes

$$g_f' = 2\pi G\rho t - x \sin^2 \alpha\{(F_2-F_1) - (F_4-F_3)\} \quad \ldots\ldots (2')$$

When the anomaly corresponding to g_f or g_f' is obtained from field data, the constant term $2\pi G\rho t$ will be removed automatically, at least in large part, when the regional effect is removed. Therefore it will be dropped from these formulas also, except when the effect of varying t is being considered. When this is done, the anomalies produced by a normal fault and the corresponding reverse fault differ only in algebraic sign.

If the signs of both β and x are changed in the expression for g_f, the only effect is to change the sign of g_f, hence curves are not required for negative values of β.

Figure 8 illustrates the general relationship between the geometry of the fault and the resulting anomaly (for positive ρ). The negative anomaly is always over the downthrown side. For a normal fault the amplitude of the negative anomaly is larger than that of the positive, the opposite being true for a reverse fault. The fault

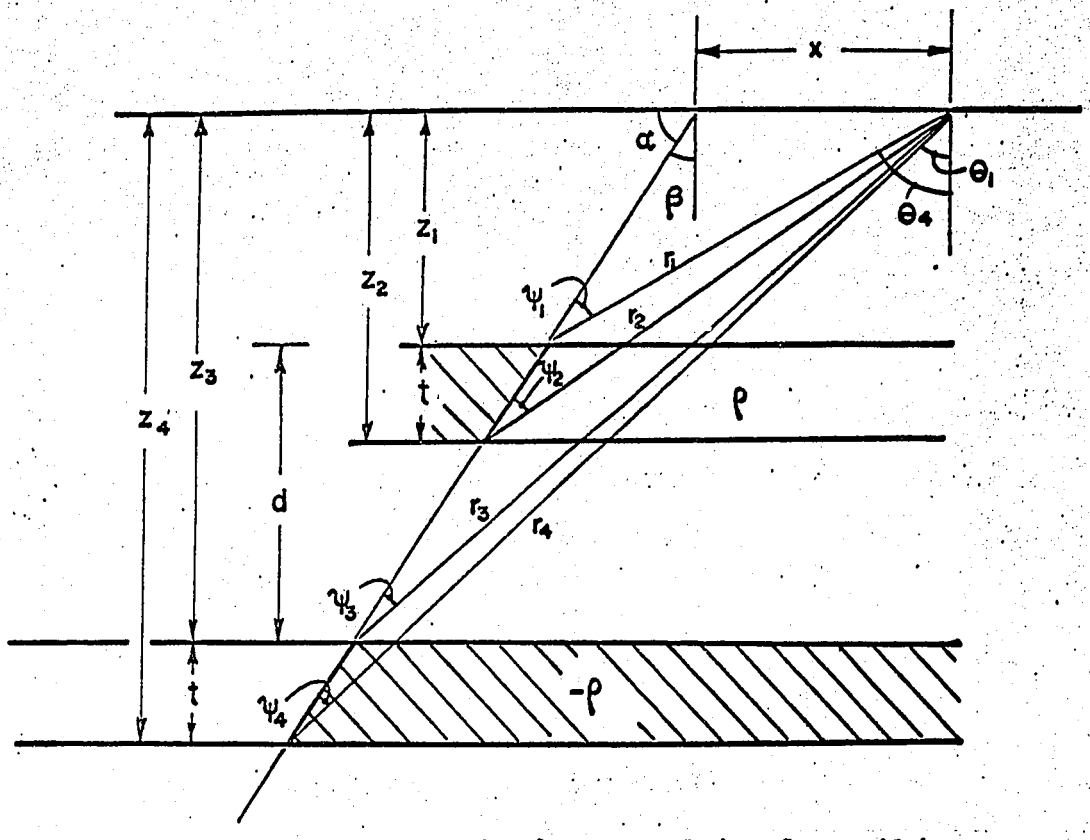

FIG.7 Parameters and variables used in describing g_f.

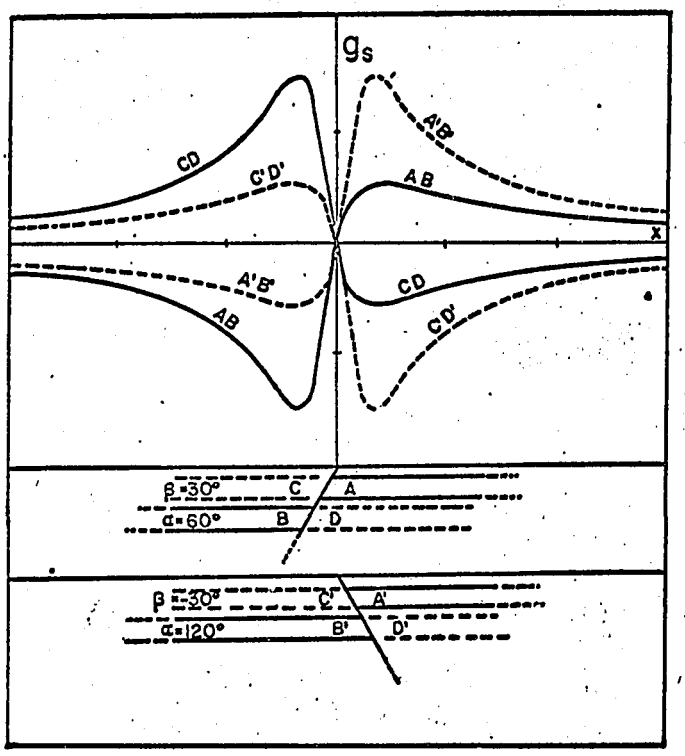

FIG 8. General relationship between g_f and the type of faulting

curves presented in Figures 9-16 correspond to AB, that is, a normal fault with β positive (α between 0° and 90°), but curves for the other cases can be obtained from them readily with the aid of Figure 8.

The notation used to designate single blocks will be adapted to the description of faults. Thus, a fault is denoted by the expression (z_1, z_2, z_3, z_4); for example, the fault (1, 4, 3, 6) is a normal fault displacing a 3,000 ft bed from a depth of 1,000 ft to a depth of 3,000 ft (depths to the top of the bed).

Curves for fault anomalies: The expression for g_f can be written in terms of four parameters: the dip, fault displacement, bed thickness, and depth to the top of the upper block. The effects of varying these parameters are shown in Figures 9-16. In these curves ρ and t are equal to unity as before, except for t in Figures 13 and 14.

Many of the properties of the curves in Figures 9-16 are well known in a qualitative sense, for example, the increase in amplitude and width of the anomaly as the bed thickness and displacement are increased, the decrease in amplitude and increase in width of the anomaly as the entire fault is moved downward. Less predictable, however, are the variations in amplitude and position of the anomaly as the dip is varied, the remarkable similarity in slope of the curves for a given z_1 in the region between the fault trace and the minimum, the wide range of slopes of the curves at the origin.

Probably the most striking feature of the curves is the large effect resulting from changes in dip. The curves are symmetrical about

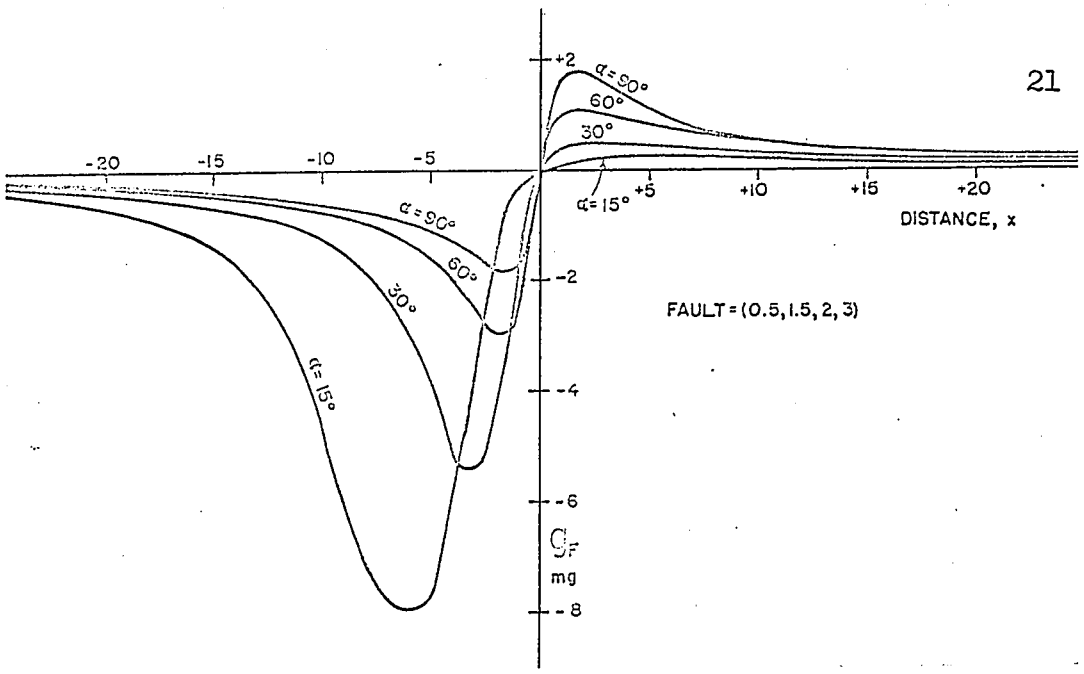

FIG. 9. Variation of g_f with dip for a thin bed.

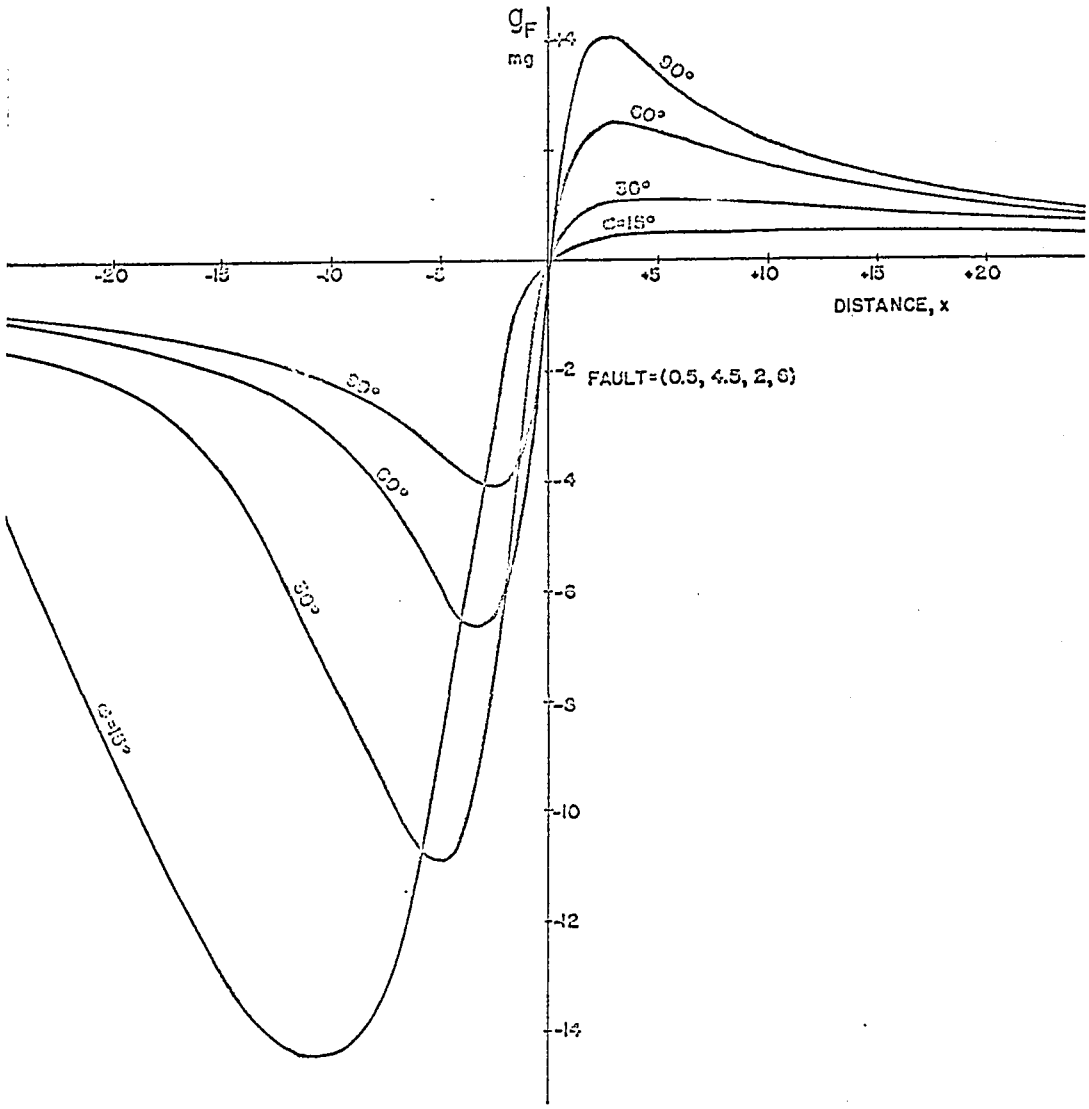

FIG. 10. Variation of g_f with dip for a thick bed.

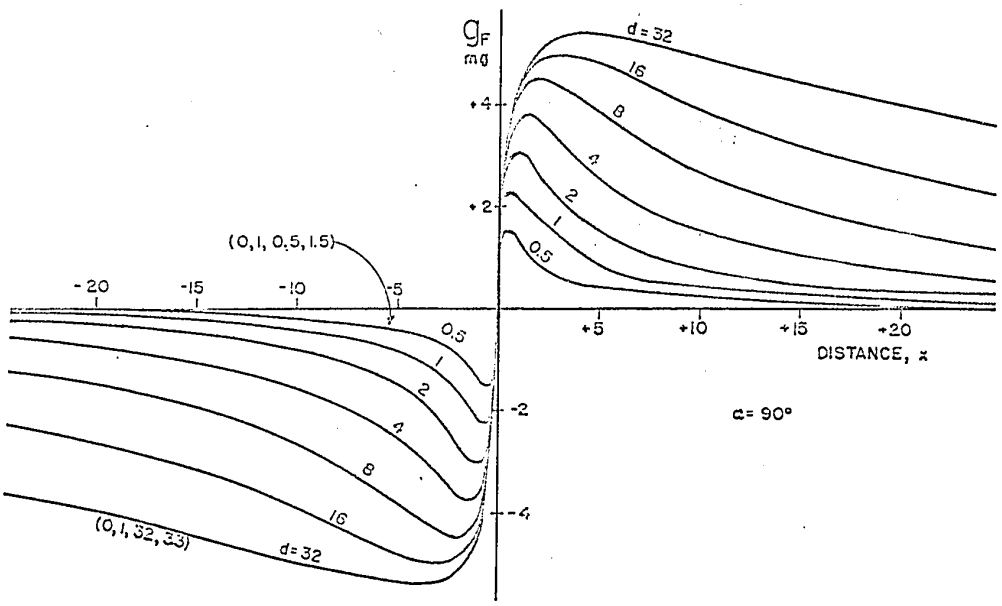

FIG. 11. Relation between g_f and the displacement for a vertical fault.

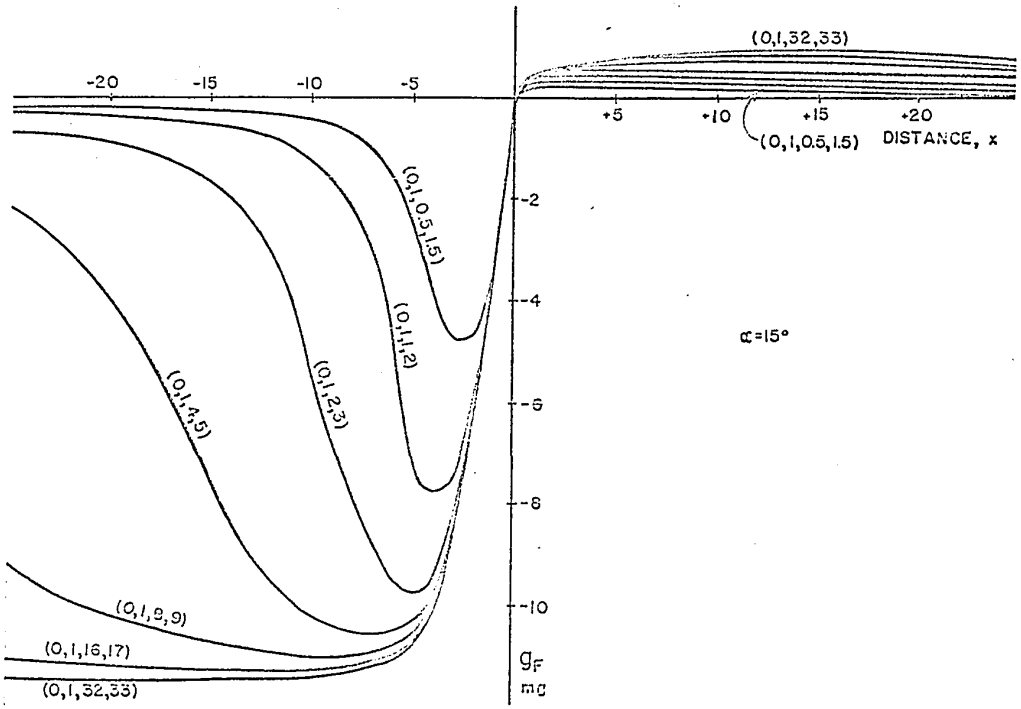

FIG. 12. Relation between g_f and the displacement for a fault with 15 degree dip.

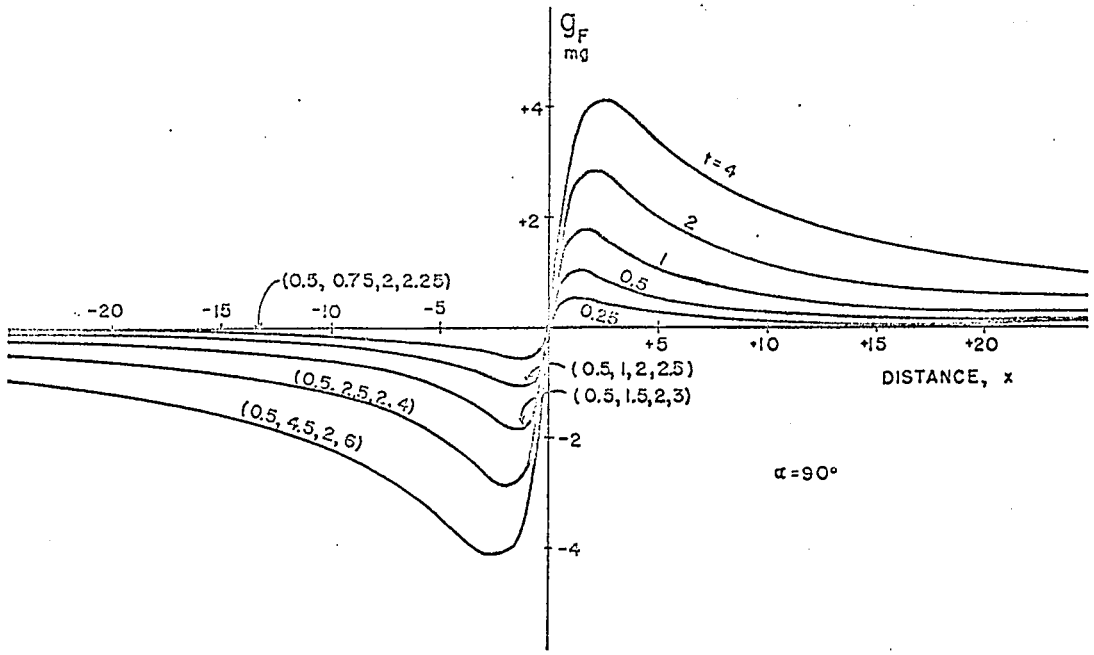

FIG. 13. Dependence of g_f upon bed thickness for a vertical fault.

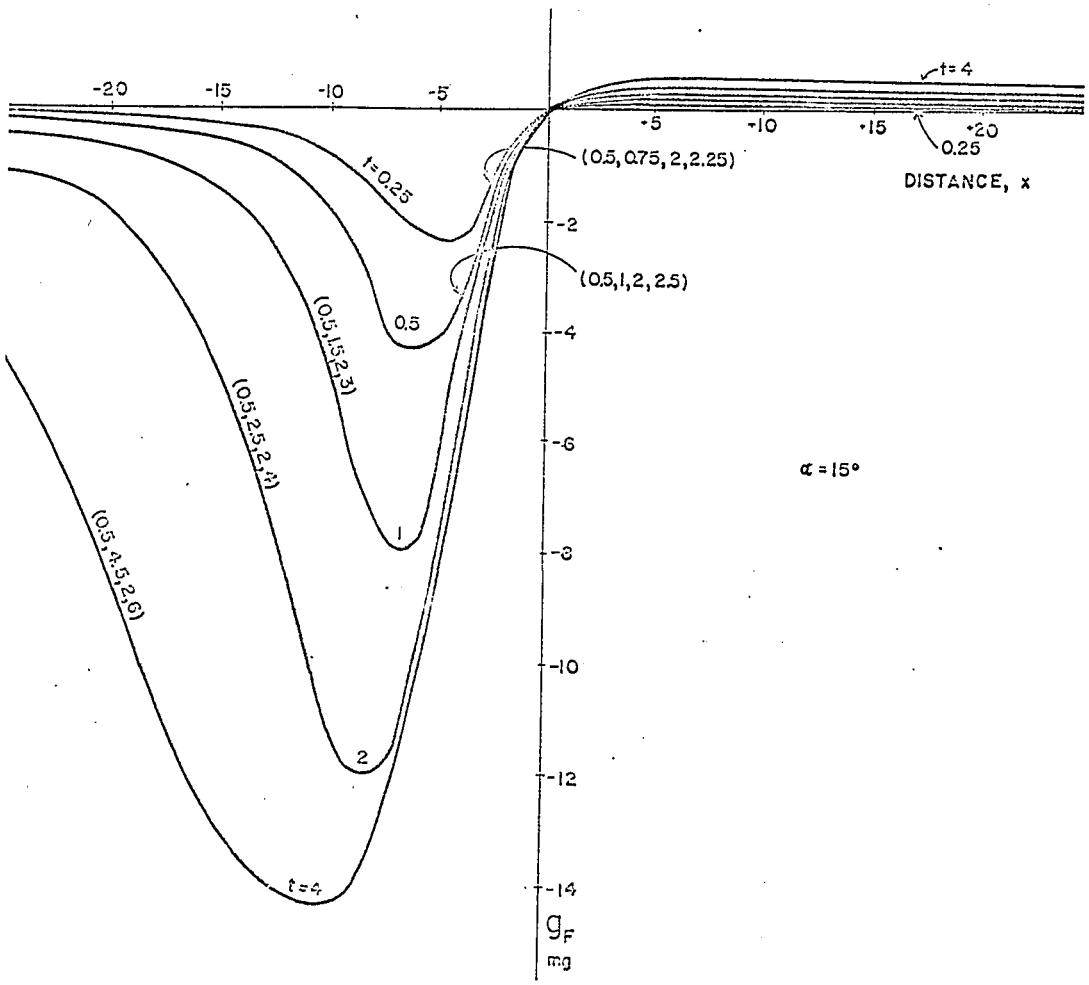

FIG. 14. Dependence of g_f upon bed thickness for a fault with 15-degree dip.

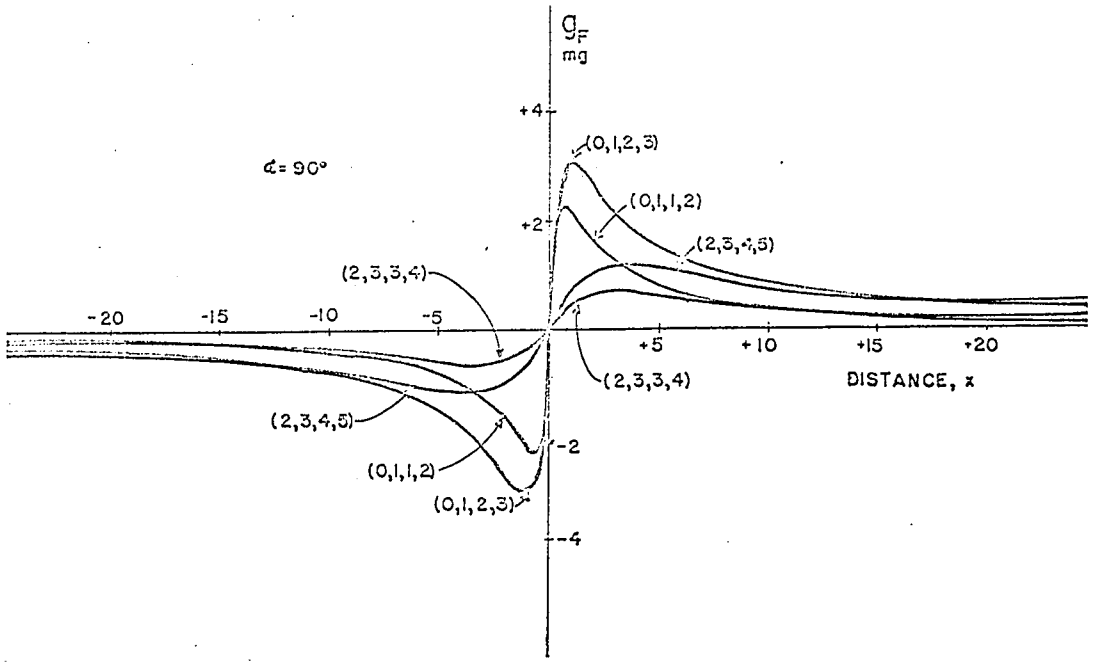

FIG. 15. Relation between g_f and z_1 for a vertical fault.

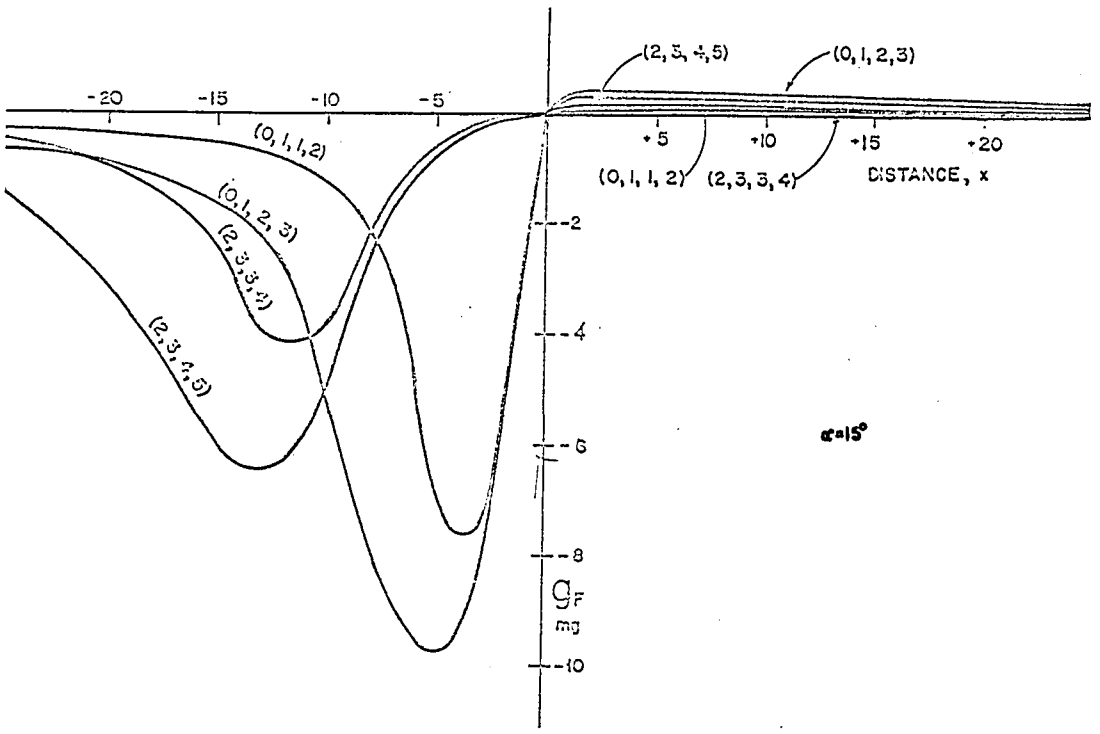

FIG. 16. Relation between g_f and z_1 for a fault with 15-degree dip.

the origin for vertical dip; as α decreases from 90°, the negative anomaly increases while the positive anomaly decreases and both move away from the origin.

The fault curves can be used to illustrate the fundamental ambiguity of gravity interpretation. If overlays of the curves are made, it will be found that increasing z_1 by a small amount gives approximately the same result as changing the dip by the appropriate amount. Likewise, a small displacement of a thick bed can cause the same change as a large displacement of a thin bed provided the dips are chosen judiciously. Consequently, the geometry of a fault cannot be worked out from the gravity data alone.

In the majority of interpretive problems, the fault anomaly cannot be isolated accurately, often as a result of the superposition of several effects. In addition, sub-surface data are usually non-existent or at most very sketchy. Under circumstances such as these, it is folly as well as wasted effort to attempt to make a precise interpretation in terms of dip of the fault plane, bed thickness, and displacement. Nevertheless, the foregoing curves will be useful in defining the limiting values of the fault parameters and in analyzing the causes of changes in the anomaly between adjacent profiles.

Determination of the fault parameters: On certain auspicious occasions a well-isolated fault will occur in an area where regional effects can be accurately removed. Provided sufficient sub-surface information is available, the geometrical parameters of the fault can then be found

using the gravity and geological data in conjunction with the fault curves.

The problem can no doubt be solved in several ways. The method outlined here has the virtues of simplicity and as much accuracy as the nature of the problem warrants. It requires that the density contrast and thickness be known for the bed producing the anomaly; the solution is then obtained from measured values of the amplitudes of the negative and maximum anomalies, g_o and g_1, and the distance between them. When the dip is small, the gravity maximum, g_1, is small and the results become inaccurate. The method is usable for $\alpha = 30^\circ$, but breaks down by the time α has decreased to 15°. However, other techniques probably would run into similar difficulties under the same circumstances.

The ratio (g_o/g_1) is a measure of the asymmetry of the fault curve and will be denoted by the letter A (the minus sign being disregarded). For a vertical fault, A is of course equal to unity. Values of A have been computed for dips of 30° and 60° (a few values were computed for 15° dip also - see below) for a series of faults with upper blocks (0,1), (0.5,1.5), ...,(4,5), and for lower blocks (0.5,1.5), (1,2),.....(24,25). The results may be summarized as follows:

(1) A decreases slowly as the displacement increases and as z_1 decreases,

(2) A has a value between 2.6 and 3.0 for 60° dip, between 9 and 14 for 30° dip, except under the following conditions: (a) $z_1 = 0$ -- in this case A is about 2.6 or 9 for small displacement and decreases to 2.3 or 6 for a displacement of 24 units, (b) $z_1 \neq 0$, $z_3 \geq 10z_1$ -- when

$z_3 = 10z_1$, A has the value 2.6 or 9 and decreases thereafter as the displacement increases until it reaches the value 2.3 or 6 when $z_3 = 50z_1$.

A less extended series of calculations for 15° dip gave values of A in the range 25-40, but the positive anomaly is so small for this dip that it is unlikely that meaningful results can be obtained when the dip is this small.

Multiplying all the dimensions of a fault by a scale factor has no effect on A. Moreover, A is independent of the density contrast, ρ. Consequently A must depend only upon the dip and the ratios z_3/z_1 and t/z_1. The result of varying these ratios over a wide range is relatively small, as shown above. Therefore, to the first approximation, A can be considered to be a function of dip only. Thus the dip can be found from the value of A on the basis of the above summary or by interpolation in Figure 17. If it is found later that z_1 is approximately zero or that z_3 is greater than $10z_1$, a second approximation could be made; however, this probably will rarely be justified.

The principal limitation in finding the dip is the difficulty in finding a sufficiently accurate value of the maximum, g_1. The accuracy with which the regional is removed will be critical, particularly when the dip is less than 45°. Assuming that A is accurate within 10% for 60° dips and within 20% for 30° dips, it should be possible to determine the dip within approximately $\pm$ 10°.

The next step after finding the dip is to locate the fault

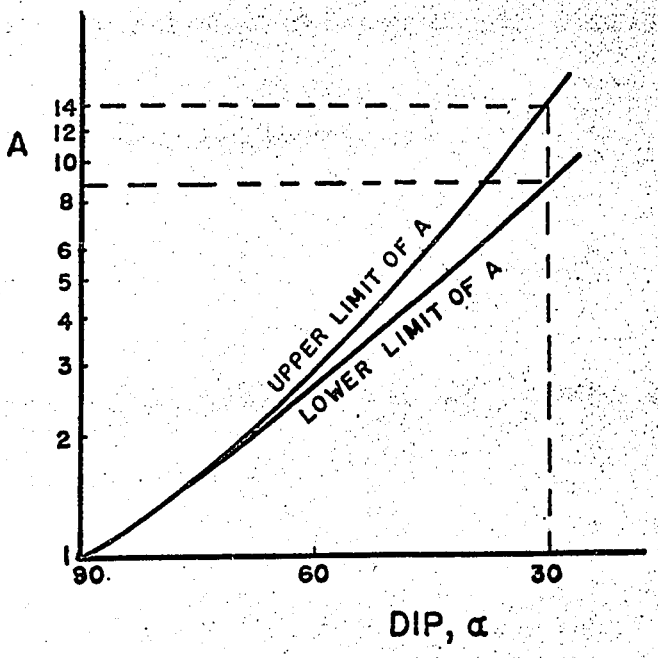

FIG. 17. Limiting values of the asymmetry, A.

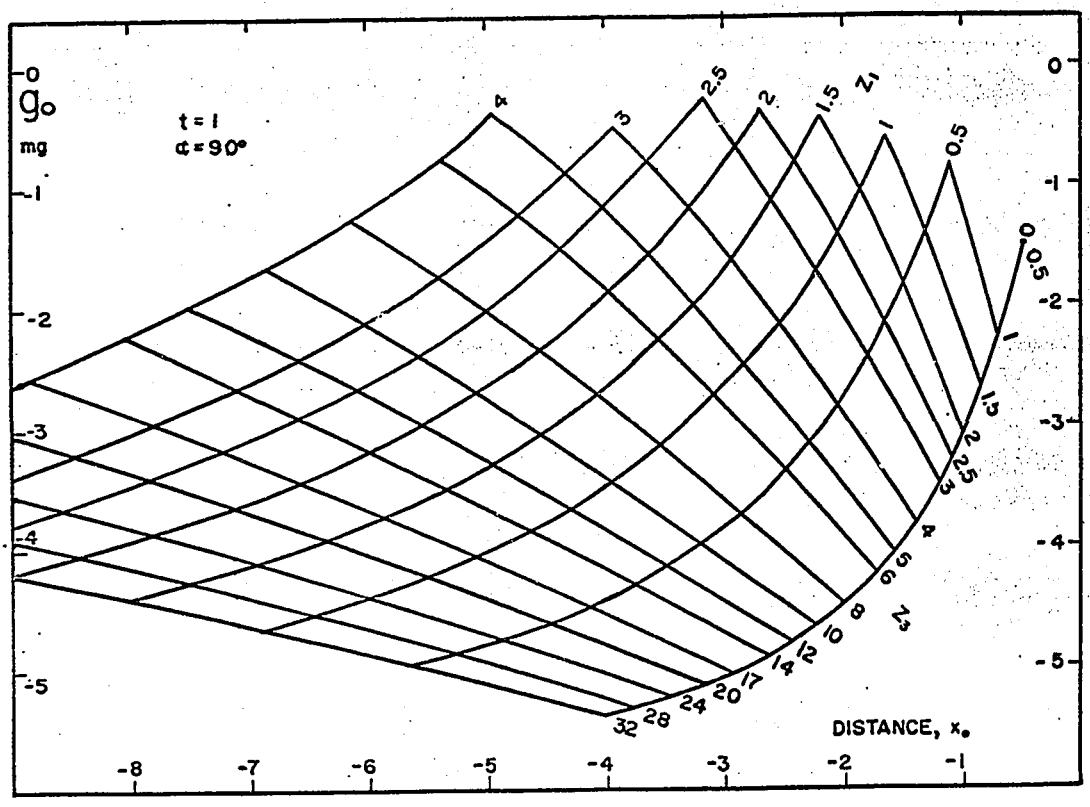

FIG. 18. Variation of size and position of gravity minimum with z_1 and z_3 for vertical dip.

trace. The abscissae of g_o and g_1 will be represented by x_o and x_1 (minus signs being ignored). The ratio $B = x_o/x_1$ was calculated for the same series of faults that were used in calculating A. It was found that B behaves in much the same way that A does. The results may be summarized as follows:

(1) when $z_1 \geq 0.5$, $\alpha \geq 30^\circ$, then $1.0 \leq B \leq 1.1$,

(2) when $z_1 = 0$, and $\alpha = 60^\circ$, then $1.0 \leq B \leq 1.2$,

(3) when $z_1 = 0$, and $\alpha = 30^\circ$, then $1.0 \leq B \leq 1.3$.

Thus, to the first approximation, the fault trace can be taken as the point midway between the locations of the gravity maximum and the gravity minimum. The maximum error resulting from this assumption is about 15%.

Once the dip and the fault trace location are known, it is possible to find z_1 and z_3 provided ρ and t are known. The procedure is to multiply g_o, g_1, x_o, and x_1 by the appropriate conversion factor to convert them to values corresponding to a bed of unit density contrast and unit thickness (the conversion factor being $1/\rho_o t_o$ where ρ_o and t_o are the actual values for the given bed), and then make use of the appropriate charts of Figures 18-23 to obtain z_1 and z_3.

Referring back to Figures 11 and 12, as the lower block is moved downward, the upper block being fixed, the minimum moves downward and to the left. The loci of the minimum gravity value are plotted in Figures 18-21 for dips of 90°, 60°, 30°, and 15° (the latter curves

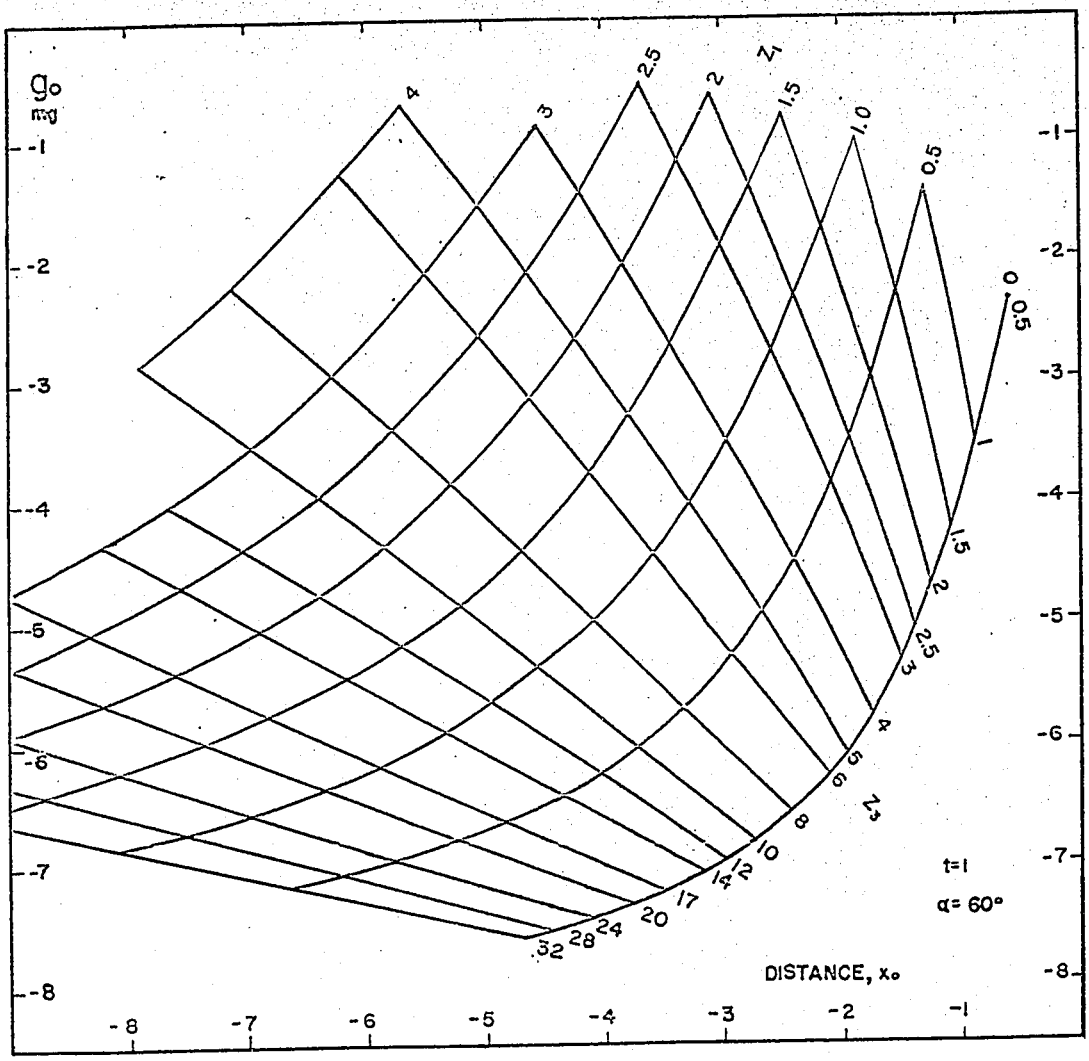

FIG. 19. Variation of size and position of gravity minimum with z_1 and z_3 for $\alpha = 60^\circ$.

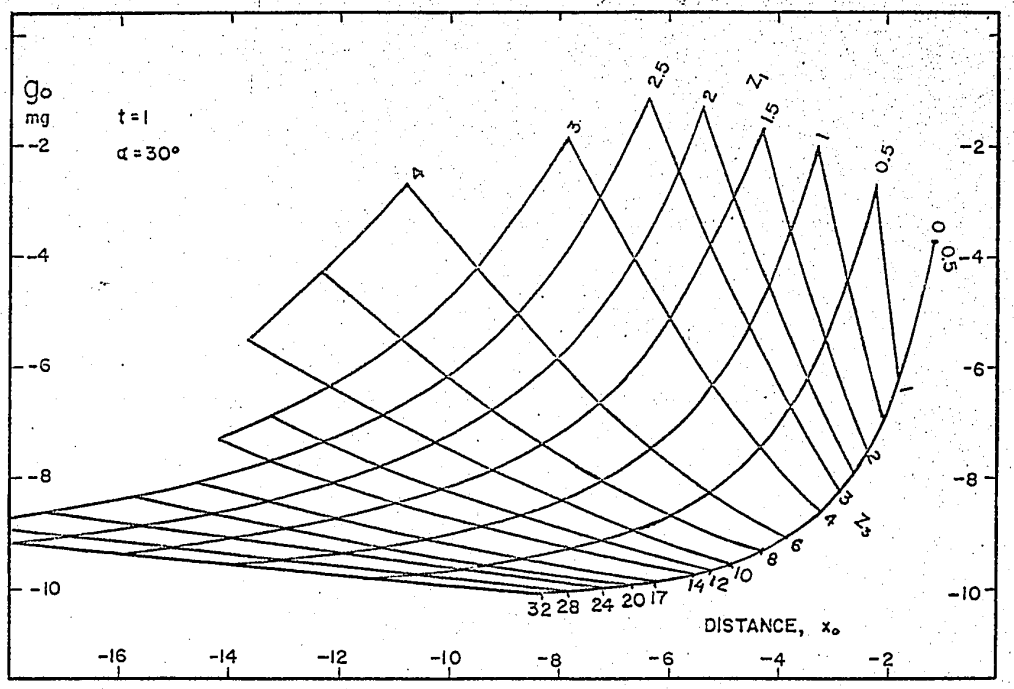

FIG. 20. Variation of size and position of gravity minimum with z_1 and z_3 for $\alpha = 30^o$.

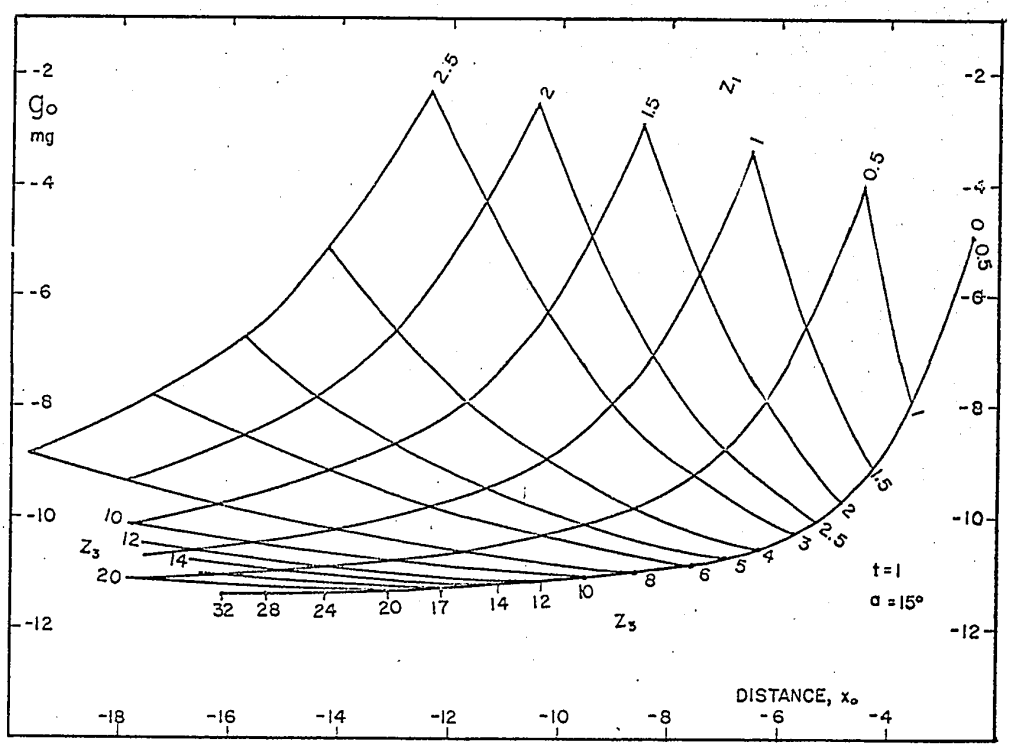

FIG. 21. Variation of size and position of gravity minimum with z_1 and z_3 for $\alpha = 15^o$.

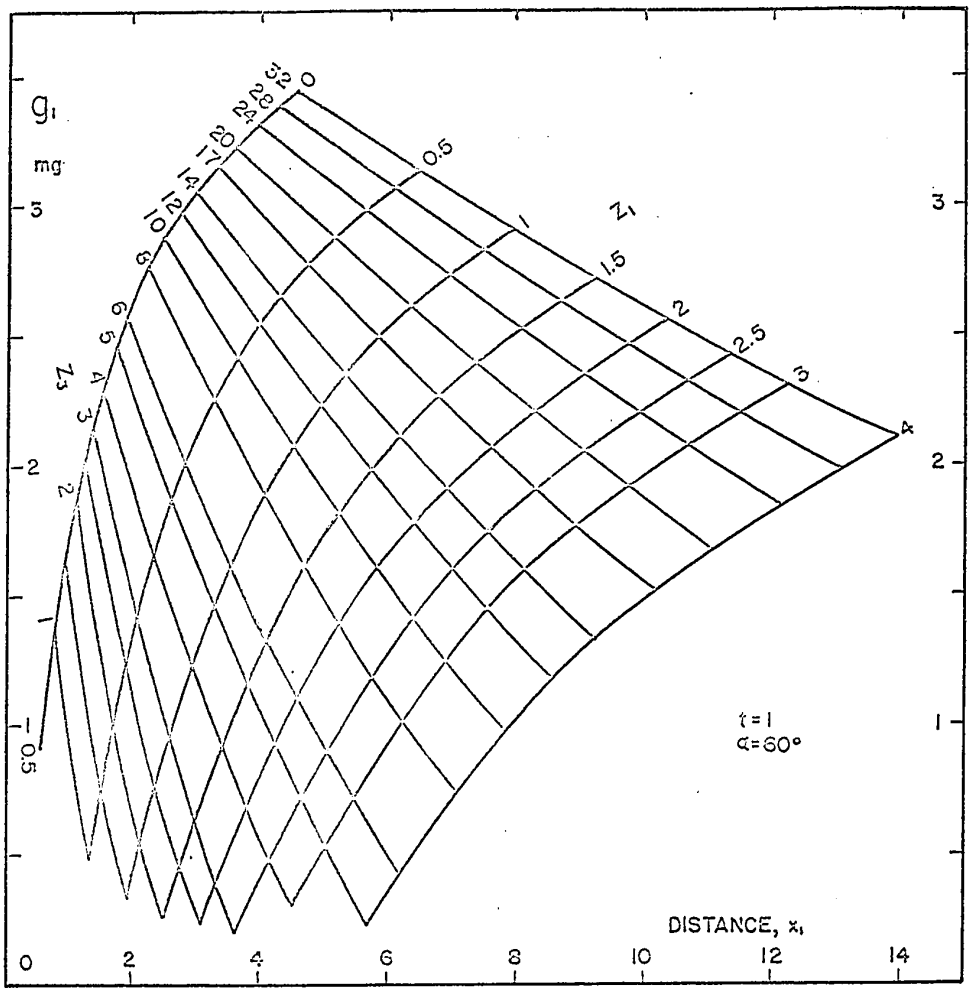

FIG. 22. Variation of size and position of gravity maximum with z_1 and z_3 for $\alpha=60^{\circ}$.

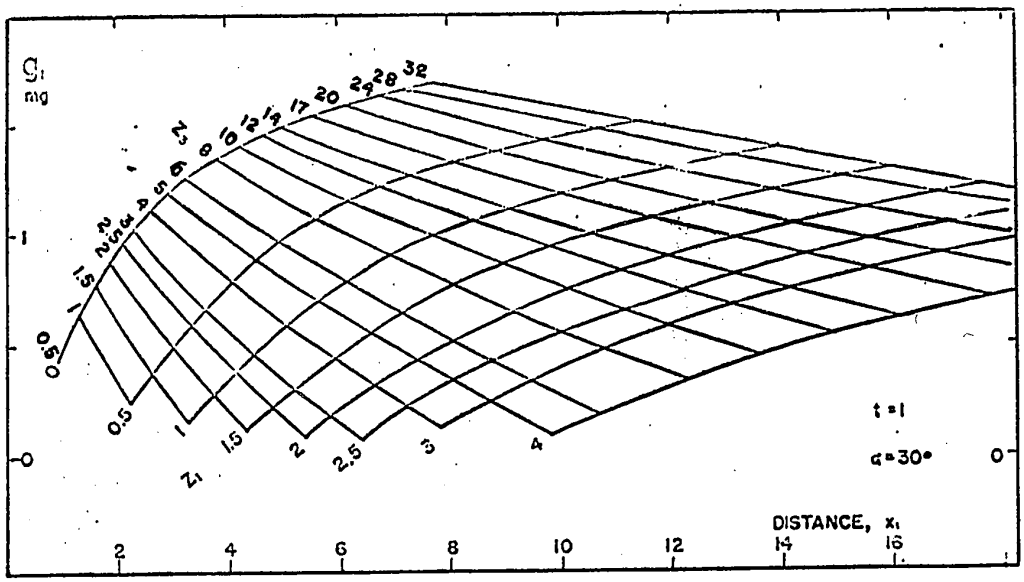

FIG. 23. Variation of size and position of gravity maximum with z_1 and z_3 for $\alpha = 30^\circ$.

being principally of academic interest) for blocks of unit thickness and a series of values of z_1 and z_3. The curves sloping downward to the left are obtained by keeping z_1 fixed and allowing z_3 to vary. The curves sloping downward to the right correspond to z_3 fixed and z_1 variable. For given values of z_1 and z_3, the minimum, g_o, and its abscissa, x_o, are fixed by the coordinates of the point of intersection of the two curves specified by the values of z_1 and z_3. Conversely, if g_o and x_o are given, z_1 and z_3 are fixed by the parameters of the two curves intersecting at the point (x_o, g_o).

The curves in Figures 22 and 23 are the loci of the maximum value, g_1, for dips of 30° and 60° (the curves for $\alpha = 75^\circ$ are omitted because they have little practical value). These curves are not required normally; they are redundant because the data for the maximum have already been used to find A and B and, through them, the dip and x_o. However, the curves may be useful in those instances where the ratio (z_3/z_1) is large or z_1 very small such that the quantities A and B lie outside the usual range of values.

Calculation of curves: In spite of the large number of curves given in this paper for single beds and faults, occasions will arise where other curves, or perhaps more accurate curves, are required. If a large number of curves is required for a definite range of parameters, the obvious solution is to program Formula (2) for a digital computer. However, even if this is done, it may be necessary at times to obtain a small number of curves for special values of the parameters. There-

fore a rapid method of calculating g_s or g_f using a desk calculator is a valuable adjunct to the interpretation techniques given earlier. The following methods have been used for this purpose.

(a) Formula (1) was programmed for a computer for various values of the dip, z_1, and t; fault anomalies were then found by subtracting the effects of the appropriate blocks.

(b) A computer was used to calculate values of the function $F(\psi)$, where

$$F(\psi) = 2G\rho(\psi \cot \psi - \log \sin \psi),$$

for $0 \leq \psi \leq 180$; to obtain g_f, ψ_i is calculated from the relations

$$\psi_i = \theta_i - \beta, \tan \theta_i = \tan \beta + x/z_i, \; i = 1,2,3,4,$$

the corresponding values of F_i obtained and substituted in Formula (2).

(c) Isolated values of g_s or g_f can be found by using the results calculated in (a) or (b) above and then multiplying all dimensions and gravity values by a scale factor to give the required value of g_s or g_f.

Fault Cutting A Series Of Beds

In the discussion of the gravity anomalies of two-dimensional fault above, it is assumed that the fault truncates a single bed of uniform density. However, a fault cutting a single bed of uniform density is most unusual. More often, faults cut through a series of beds of different densities and thicknesses. If the densities and thicknesses of the different beds vary widely then the interpretation based on replacement of the series of beds by a single bed of uniform density may be quite inaccurate.

To obtain the expression for the gravitational attraction of a fault truncating a series of beds, we refer to Figure 24 in which FF' is a normal fault cutting through N different beds of densities σ_1, σ_2, σ_3 .....σ_N. If H denotes the gravitational effect due to the part of the beds lying to the right of the fault plane FF' and below the surface at depth z_1, then from equation (1), after omitting the constant term, we have

$$H = x \cos^2\beta\left[\sigma_1(L_2-L_1) + \sigma_2(L_3-L_2) + \ldots\ldots + \sigma_N(L_{N+1}-L_N) + \sigma_r(L'_{N+1}-L_{N+1})\right]$$

where σ_r is the density of the material immediately below the Nth bed in the upthrown side, the functions L_i and L'_i for $i = 1,2,3, \ldots (N+1)$ are defined by the relations

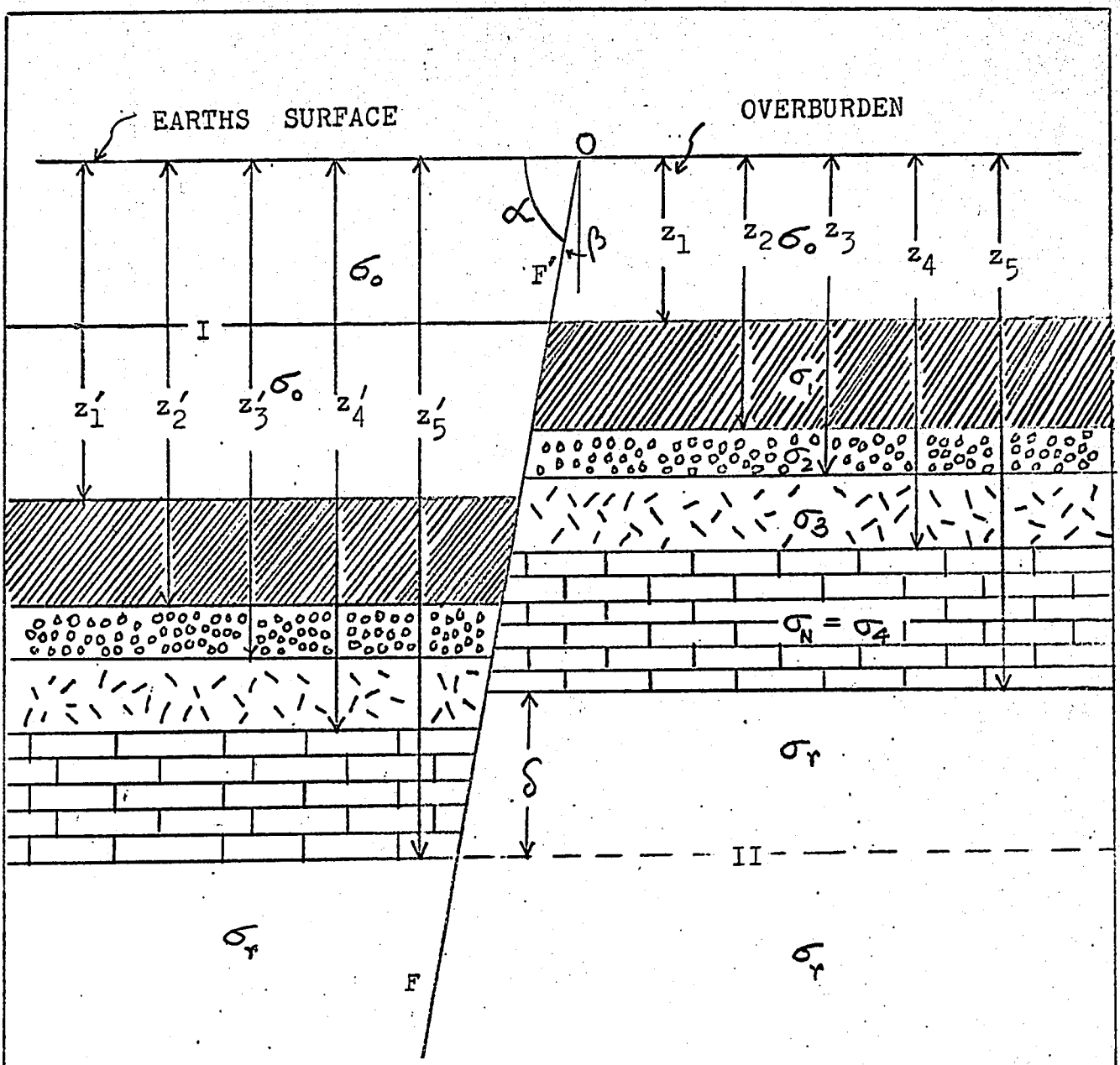

FIG. 24. Parameters and variables used in calculating g_m.

$$L_i = 2G(\psi_i \cot \psi_i - \log \sin \psi_i)$$

$$L_i' = 2G(\psi_i' \cot \psi_i' - \log \sin \psi_i')$$

$$\psi_i = \theta_i - \beta; \quad \tan \theta_i = \tan \beta + \frac{x}{z_i}$$

$$\psi_i' = \theta_i' - \beta; \quad \tan \theta_i' = \tan \beta + \frac{x}{z_i'}$$

$z_i = z_i + \delta$ where δ is the vertical displacement of the fault.

Similarly, if we denote by H' the gravity effect of the part of the beds lying to the left of the fault plane and below the depth z_1, then from equation (1), after omitting the constant term, we get

$$H' = - x \cos^2\beta \left[\sigma_o(L_1'-L_1) + \sigma_1(L_2'-L_1') + \ldots\ldots \right.$$

$$\left. \sigma_N(L_{N+1}'-L_N')\right]$$

where σ_o is the density of the rocks immediately above the first bed on the downthrown side of the fault plane.

The observed gravity anomaly due to the fault, g_m, is given by

$$g_m = H + H' = x \cos^2\beta \left[(\sigma_o-\sigma_1)(L_1-L_1') + (\sigma_1-\sigma_2)(L_2-L_2') + \ldots \right.$$

$$\left. + (\sigma_N-\sigma_r)(L_{N+1}-L_{N+1}')\right] \ldots\ldots (3)$$

The limiting values of the above functions when x is very large may be obtained following the same procedure as in the case of the single

block. As x becomes very large, ψ_i approaches the value α or $\alpha-\pi$ according as x is positive or negative. When x is positive and much larger than z_i,

$$\psi_i = \alpha - \frac{z_i}{x},$$

$$\psi_i \cot \psi_i = \alpha \cot \alpha + (\alpha \csc^2 \alpha - \cot \alpha)\frac{z_i}{x},$$

$$\text{Log}(\sin \psi_i'/\sin \psi_i) = -\left(\frac{z_i'-z_i}{x}\right)\cot \alpha$$

Hence
$$L_i - L_i' = 2G\left[\psi_i \cot \psi_i - \psi_i' \cot \psi_i' - \log\left(\frac{\sin \psi_i}{\sin \psi_i'}\right)\right]$$

$$= 2G\left[(\alpha \csc^2 \alpha - \cot \alpha)\left(\frac{z_i-z_i'}{x}\right) - \left(\frac{z_i'-z_i}{x}\right)\cot \alpha\right]$$

$$= \frac{2G\alpha}{\sin^2\alpha}\left(-\frac{\delta}{x}\right)$$

and
$$g_m = x \cos^2\beta \frac{2G\alpha}{\sin^2\alpha}\left(-\frac{\delta}{x}\right)\left[(\sigma_o-\sigma_1) + (\sigma_1-\sigma_2) + \ldots\ldots (\sigma_N-\sigma_r)\right]$$

$$= 2G\delta\alpha \quad (\sigma_r-\sigma_o)$$

It can be shown, in a similar way, that for large negative values of x, the limiting value of g_m is

$$g_m = 2G\delta \quad (\alpha-\pi)(\sigma_r-\sigma_o)$$

Hence the total change in gravity due to the fault is

$$2\pi G\delta(\sigma_r-\sigma_o) \qquad \ldots\ldots (3a)$$

The last result shows that the total change in gravity due to a fault truncating a series of beds is determined by the density difference $(\sigma_r-\sigma_o)$, the displacement of the fault δ and is independent of the dip of the fault plane α or the density of the intermediate beds. Knowing the density difference $(\sigma_r-\sigma_o)$, the displacement of the fault can be obtained. This result is similar to the expression for the gravity change due to a single block, that is, $2\pi G\rho t$, this also being independent of the dip of the fault plane.

In equation (2) for a fault truncating a single bed, it is assumed that $\sigma_r = \sigma_o$ so that g_m is zero for large positive and negative values of x.

If the fault truncating the N beds has sufficiently large displacement that on one side of the fault plane we have N beds of different thicknesses and densities and on the other side of the fault plane a material of uniform density σ_o, then the equation giving the gravity anomaly of such a fault may be written as

$$g_m' = x\cos^2\beta\left[(\sigma_1-\sigma_o)(L_2-L_1) + (\sigma_2-\sigma_o)(L_3-L_2) + \right.$$

$$\left. (\sigma_N-\sigma_o)(L_{N+1}-L_N)\right]$$

Following the same line of argument as in the case of the single block, it can be shown that the limiting values of the above function for very

large positive and negative values of x may be written as

$$g'_{m+} = 2G\alpha \left[(\sigma_1-\sigma_o)t + (\sigma_2-\sigma_o)t_2 + \ldots (\sigma_N-\sigma_o)t_N\right]$$

$$g'_{m-} = 2G(\alpha-\pi) \left[(\sigma_1-\sigma_o)t_1 + (\sigma_2-\sigma_o)t_2 + \ldots (\sigma_N-\sigma_o)t_N\right]$$

respectively.

where $t_i = z_{i+1} - z_i$; $i = 1, 2, 3, \ldots\ldots N$

Hence the total change in gravity is equal to

$$2\pi G \left[(\sigma_1-\sigma_o)t_1 + (\sigma_2-\sigma_o)t_2 + \ldots (\sigma_N-\sigma_o)t_N\right]$$

Figure 25 shows the curves for the gravity effect of a series of four beds truncated by a normal fault dipping 60^o. In curve I all four beds have the same density 2.5 gm/cc and the same thickness 0.5 units while σ_o and σ_r are both 2.0 gm/cc. This curve has a prominent maximum and minimum, the minimum having a slightly larger amplitude than the maximum. The effect of changing σ_r from 2.0 to 2.1 gm/cc but keeping all the other variables, including σ_o, the same is shown in curve II of the same Figure. This curve also has a prominent maximum and minimum but the amplitudes of the maximum and the minimum in this curve are larger compared to curve I. In curve III, σ_r is changed to 2.5 gm/cc while all the other variables are kept the same as in curves I and II. The difference between curves I and II on the one hand and curve III on the other is striking, although the density distributions are the same except for σ_r. The effect of giving lower density to one

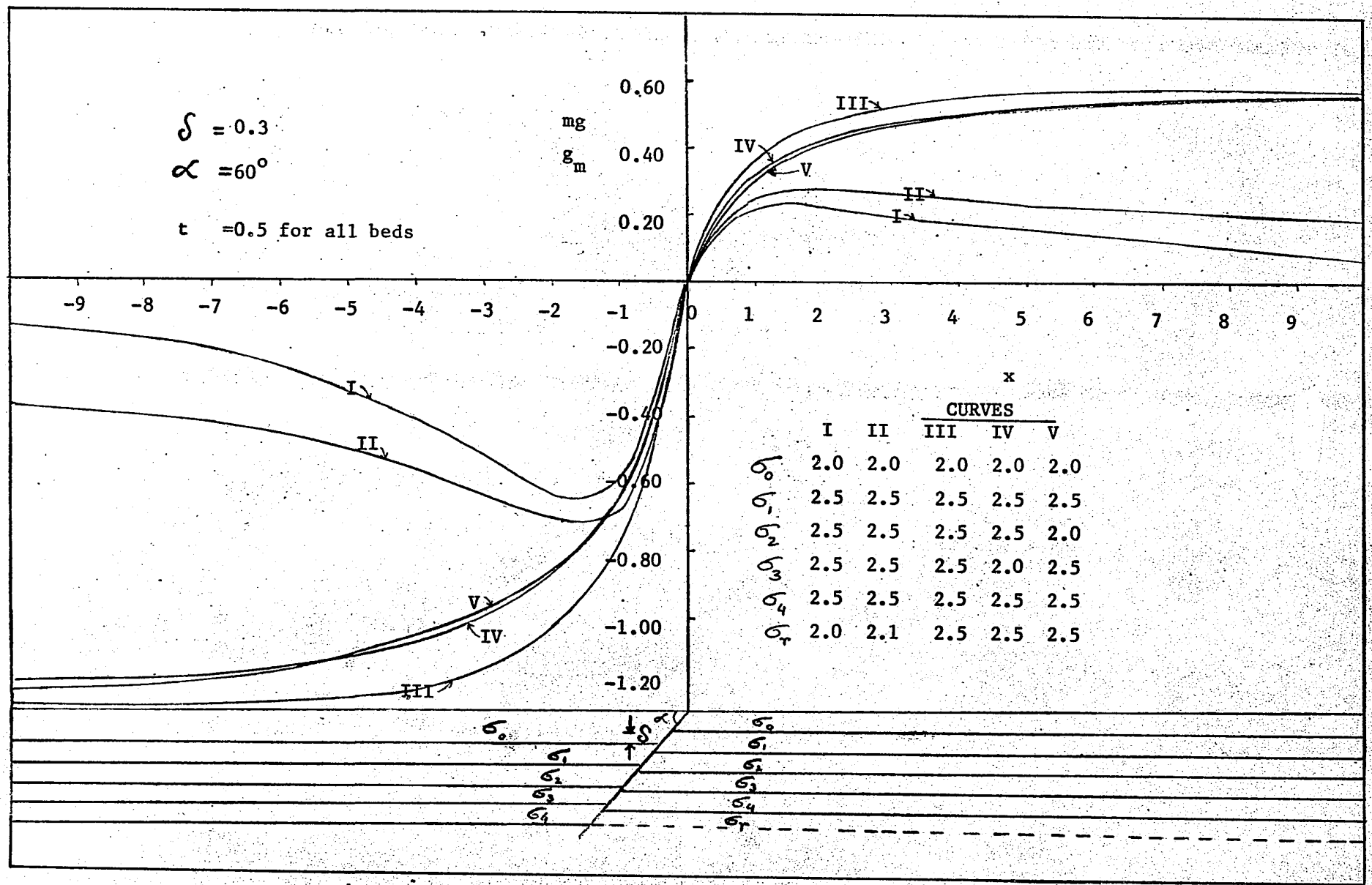

FIG 25 Effect on g_m of varying the densities of different beds

of the intermediate beds is shown in curves IV and V of Figure 25. In curve IV all the beds have the same thickness (0.5 units), σ_o and σ_3 are equal to 2.0 gm/cc while the densities of all the other beds are 2.5 gm/cc. This curve also does not show any maximum or minimum and the general shape of the curve is the same as curve II. In curve V, σ_o and σ_2 are equal to 2.0 gm/cc and the densities of all the other beds are 2.5 gm/cc. The general shape of curve V is very similar to curve IV excepting that near the fault trace curve IV has a slightly larger amplitude than curve V.

Parallel Faults

The faults encountered in gravity prospecting are not always the simple case of displacement of rocks along a single plane. A major fault is often accompanied by a number of secondary faults approximately parallel to the principal fault trend.

The gravity anomaly of the principal fault and the associated secondary faults may be readily obtained when the principal and the secondary faults lie parallel to each other. In Figure 26 is shown the principal fault F_1 and the secondary fault F_2 truncating a bed of density σ_1 at an angle β with the vertical. Let 2h be the distance between the two faults and let δ_1 and δ_2 be the displacements of the bed due to the two faults F_1 and F_2 as shown in Figure 26. To find the gravity expression of the above fault we add together the expressions for the gravity effects of individual blocks. In this way, we get

$$g_p = (x - h)\cos^2\beta \left\{(\sigma_1-\sigma_o)(L_B-L_A)\right\} +$$

$$(x - h)\cos^2\beta\left\{(\sigma_2-\sigma_o)(L_C-L_B)\right\} + (x + h)\cos^2\beta\left\{(\sigma_1-\sigma_o)(L_F-L_E)\right\}$$

$$+ (x - h)\cos^2\beta\left\{(\sigma_2-\sigma_1)(L_D-L_C)\right\}$$

$$+ (x + h)\cos^2\beta\left\{(\sigma_2-\sigma_o)(L_G-L_F)\right\} + (x + h)\cos^2\beta\left\{(\sigma_2-\sigma_1)(L_H-L_G)\right\}$$

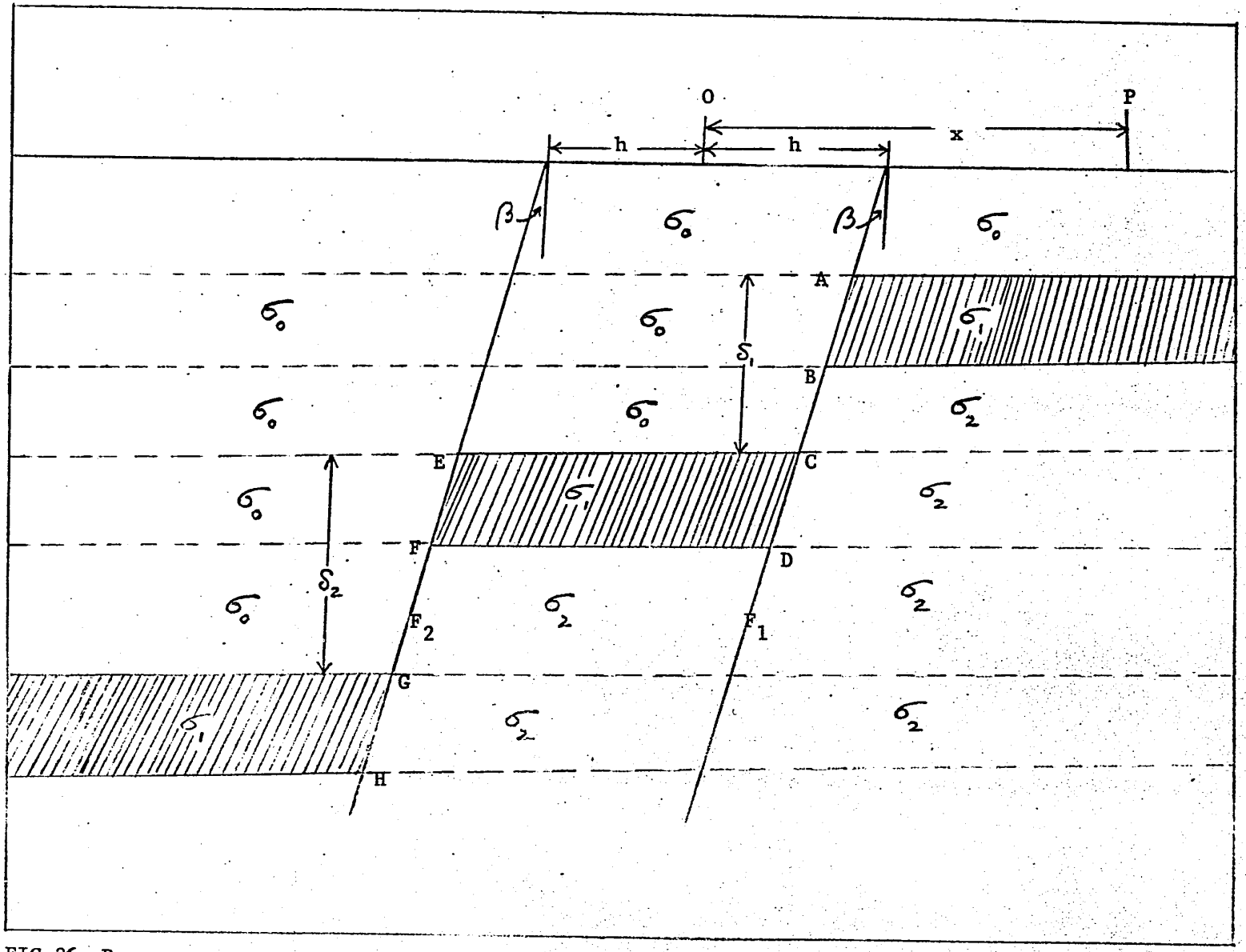

FIG 26 Parameters and variables used in calculating g_p

$$= (x - h)\cos^2\beta \left\{(\sigma_1-\sigma_o)(L_B-L_A) + (\sigma_2-\sigma_o)(L_C-L_B)\right.$$

$$\left. + (\sigma_2-\sigma_1)(L_D-L_C)\right\} + (x + h)\cos^2\beta \left\{(\sigma_1-\sigma_o)(L_F-L_E)\right.$$

$$\left. + (\sigma_2-\sigma_o)(L_G-L_F) + (\sigma_2-\sigma_1)(L_H-L_G)\right\}$$

$$= (x - h)\cos^2\beta \left\{(\sigma_2-\sigma_1)(L_D-L_B) + (\sigma_1-\sigma_o)(L_C-L_A)\right\}$$

$$+ (x + h)\cos^2\beta \left\{(\sigma_2-\sigma_1)(L_H-L_F) + (\sigma_1-\sigma_o)(L_G-L_E)\right\}$$

The total change in gravity due to the parallel fault may be obtained following the same procedure as in the case of multiple beds. By calculating the limiting values of each term in the expression for g_p it can be shown that for very large values of x in the positive and negative directions, the total change in gravity due to the parallel fault is given by

$$2\pi G(\sigma_2-\sigma_o)(\delta_1+\delta_2)$$

Thus, the total change in gravity due to the two parallel faults depends upon the density contrast $(\sigma_2-\sigma_o)$ and is independent of the density of the bed itself. Also, the total change in gravity is proportional to the total displacement $(\delta_1+\delta_2)$ of the two faults and does not depend upon the individual values of δ_1 and δ_2.

The four curves in Figure 27 show the gravity anomalies of two parallel faults for different values of the parameters h, δ_1 and δ_2.

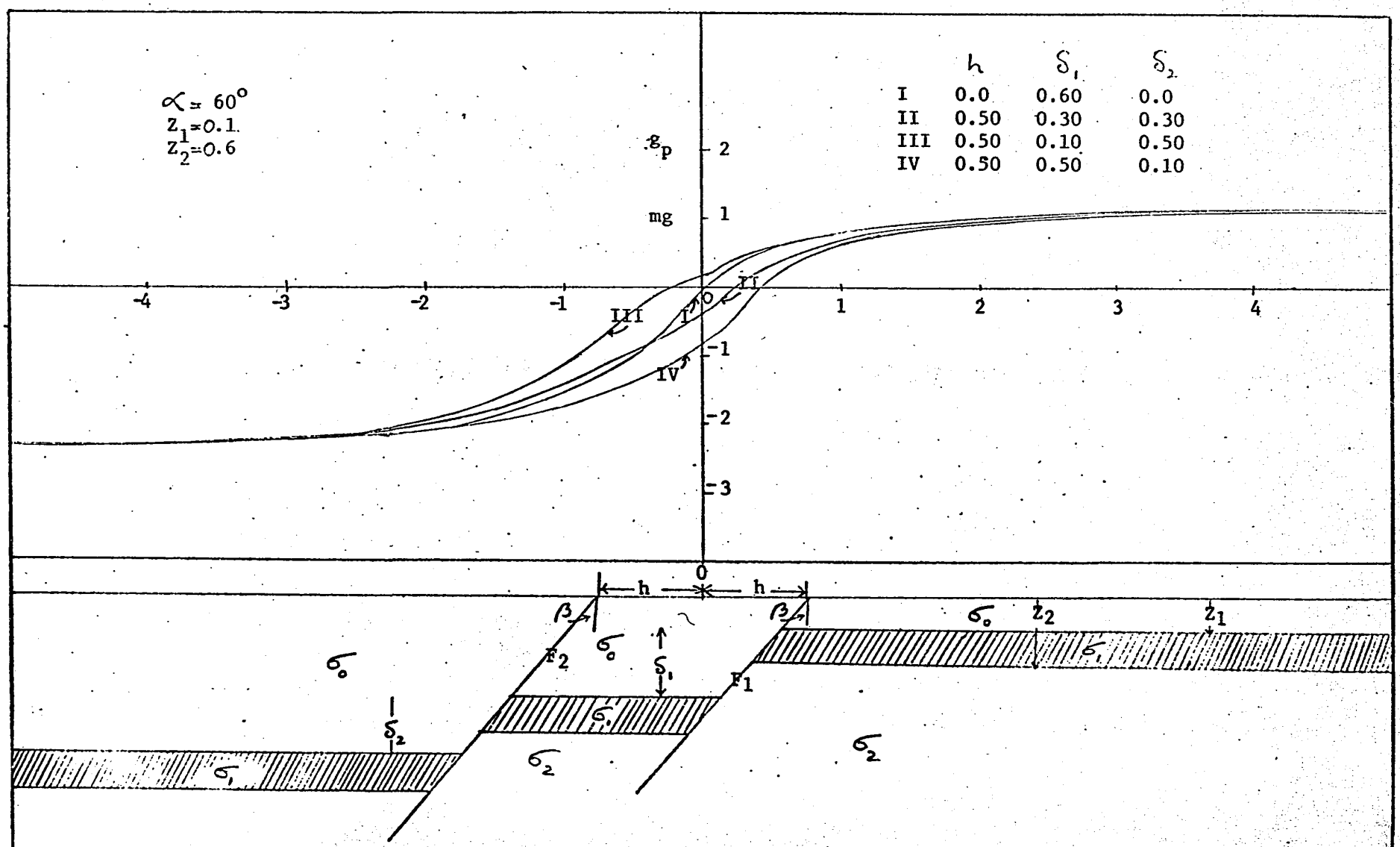

Figure 27 Relation between g_p and displacements for a fault with 60° dip.

In curve I of Figure 27 the displacement δ_2 is zero and the displacement δ_1 due to the fault F_1 is equal to 0.6. This curve, in effect therefore, represents the gravity anomaly of a single fault F_1. In curves II, III and IV the total displacement due to the two faults is kept fixed at 0.6 while the individual values of δ_1 and δ_2 are varied. The difference between curve I and the remaining three curves is confined mainly to the region between the two fault traces, the differences between the four curves being very small whenever x is greater than about $3(\delta_1+\delta_2)$. For large δ_1 the gravity anomaly in between the two parallel faults decreases (curve IV) compared to the case of the fault having small δ_1 (curve III).

The influence of parallel faults on the gravity anomaly under slightly different geologic conditions may also be obtained by combining the effect of the gravity anomalies of single blocks. Figure 28 could represent a major fault and two parallel secondary faults, the net effect of faulting being to bring basement rocks of density σ_B near to the surface. The beds of densities σ_1 and σ_2 could be due to deposition of sedimentary rocks during the period of faulting. The effect of the secondary faults in this case is to produce two step-like structures at distances D_1 and D_2 from the principal fault. Let z_1, z_2, z_3 and z_4 represent the depths from the surface to the different geologic horizons as shown in Figure 28.

To find the combined effect of all the three faults on the gravity profile, we first of all consider the principal fault. The effect of the upper block of thickness z_2-z_1 and density contrast

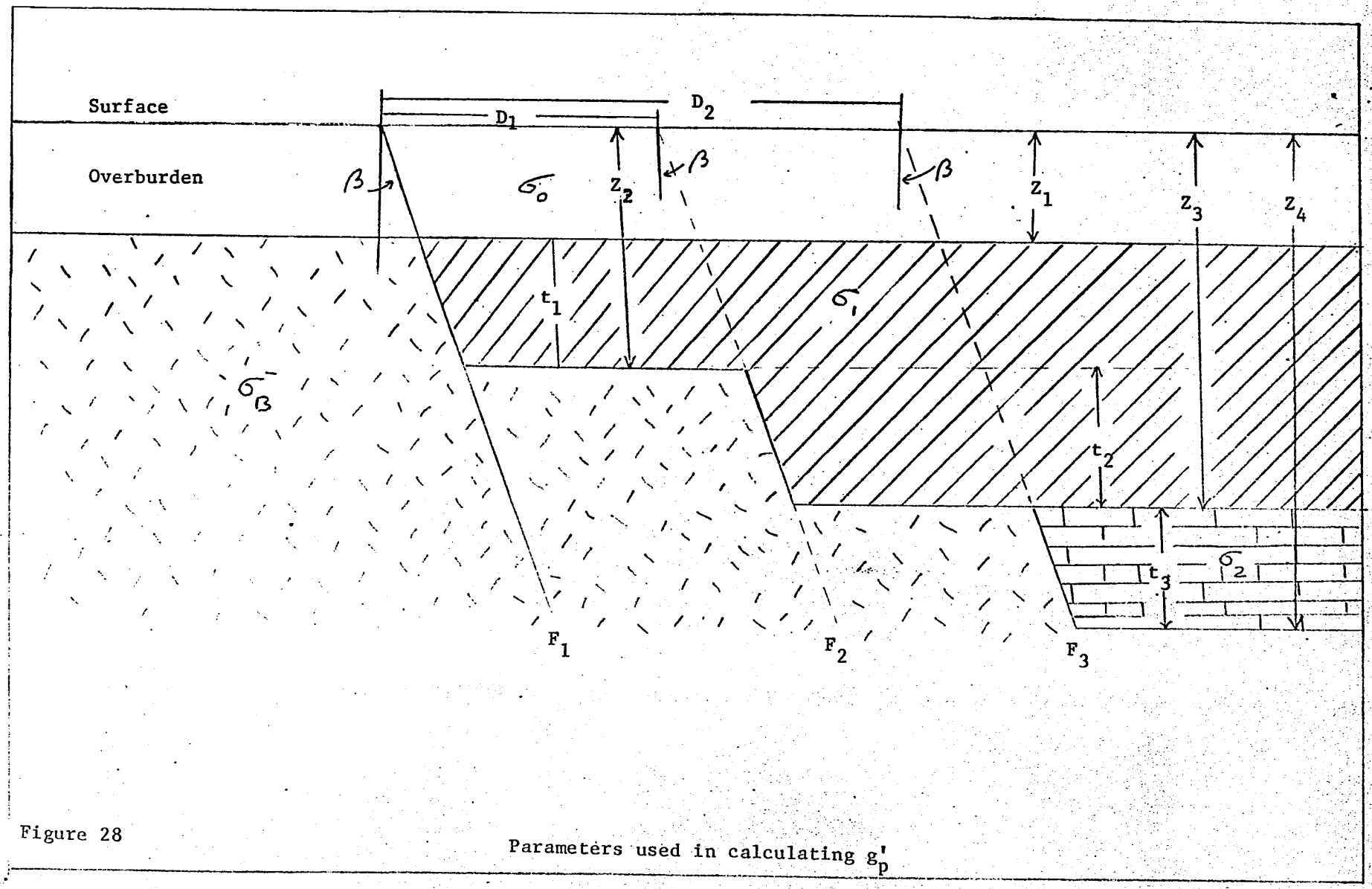

Figure 28

Parameters used in calculating g_p'

$\rho_1 = \sigma_B - \sigma_1$ can be obtained from Formula (1) and is given by

$$f_1 = x\rho_1 \cos^2\beta(L_2 - L_1)$$

The functions L_1 and L_2 are defined in the case of a fault cutting a series of beds.

In order to find the superimposed effect of the second fault upon the principal fault we consider the gravity anomaly of the block of thickness $z_3 - z_2$ and density contrast ρ_1. The effect of this block, however, has to be displaced to the right by an amount D_1 before adding to the effect of the principal fault, since the fault trace of the principal fault is at a distance D_1 to the left of the secondary fault. Hence, using Formula (1) the effect of this block, after displacing by D_1, is given by

$$f_2 = (x - D_1)\rho_1 \cos^2\beta(G_3 - G_2)$$

The functions G_3 and G_2 are similar to the functions L_i in the case of a fault cutting a series of beds, excepting that in G_2 and G_3 the distance x is replaced by $(x - D_1)$. The effect of the third fault can, similarly, be obtained by finding the effect of the block of thickness $z_4 - z_3$ and density contrast $\rho_2 = \sigma_B - \sigma_2$ and displacing it by an amount D_2. From Formula (1), the effect of the third fault on the gravity anomaly is given by

$$f_3 = (x - D_2)\rho_2 \cos^2\beta(H_4 - H_3)$$

The functions H_4 and H_3 are the same as the functions L_i for the case

of a fault cutting a series of beds excepting that in H_4 and H_3 the distance x is replaced by $(x-D_2)$.

The total observed gravity anomaly on the surface of the earth is merely the sum of the effects of all the three faults and is given by

$$g_p' = f_1 + f_2 + f_3 \qquad \ldots\ldots\ldots\ldots (4)$$

where f_1, f_2 and f_3 are as defined previously.

It can be shown that when x is positive and very large with respect to D_1 and D_2 the limiting value of g_p' is given by

$$g_p' = 2G\alpha(\rho_1 t_1 + \rho_1 t_2 + \rho_2 t_3)$$

Similarly, for very large negative values of x the limiting value of g_p' is given by

$$g_p' = 2G(\alpha-\pi)(\rho_1 t_1 + \rho_1 t_2 + \rho_2 t_3)$$

Hence the total change in gravity due to the three faults is equal to

$$2\pi G(\rho_1 t_1 + \rho_1 t_2 + \rho_2 t_3)$$

Figure 29 shows three curves based upon equation (4). In curve (1) the parameters of the different geological horizons are as follows:

$z_1 = 25$ ft , $z_2 = 325$ ft , $z_3 = 925$ ft , $z_4 = 2325$ ft.

$D_1 = 1{,}500$ ft , $D_2 = 3{,}000$ ft.

$\sigma_B = 2.85$ gm/c.c., $\sigma_1 = 2.67$ gm/c.c., $\sigma_2 = 2.47$ gm/c.c.

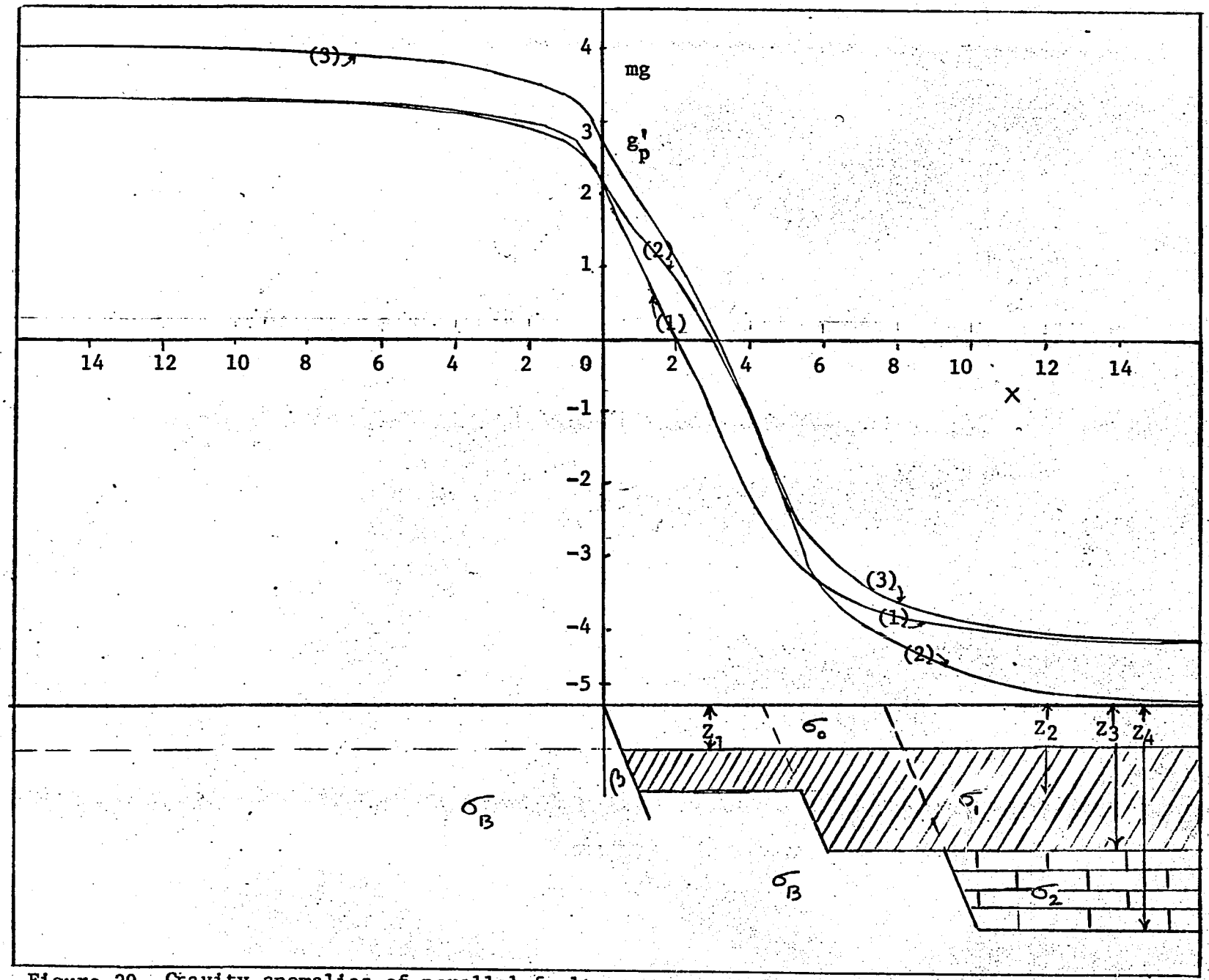

Figure 29 Gravity anomalies of parallel faults

Curve (1) resembles the curve over a single fault and does not indicate the presence of the secondary faults. The small variations in the gravity anomaly could not be detected because the widths of the two steps D_1 and D_2 are much too small. The effect of the secondary faults, however, are clearly observed in curve (2) which corresponds to the same three parallel faults as in curve (1) except that D_1, D_2 and z_2 have been increased to 2,000, 4,000 and 525 ft respectively. In curve (2) the effect of the first step is more pronounced than the effect of the second step because the former is much shallower than the latter. In curve (3) the parameters of the three parallel faults are identical with those in curve (2) excepting that the thickness of the deepest bed, t_3, has been increased from 1,400 to 1,800 ft. The effect of this increased thickness is to reduce the variations in gravity near the faults compared with those of the thinner bed.

Gravity Anomaly Of A Dike

The expression for the vertical component of gravity due to a single block may be used to calculate the gravity effect of the dike ABCD shown in Figure 30. The gravity anomaly due to ABDC is obtained by subtracting the effect of the semi-infinite block CDEF from that of the semi-infinite block ABEF.

If we measure the anomaly from the center of the dike, the expression for the gravity anomaly of the dike may be put in a slightly different manner. If $g_{\prime}(x)$ and $g_{\prime\prime}(x)$ represent the gravity anomalies of the blocks ABEF and CDEF when the anomaly is measured from the block traces O' and O'' respectively, then the gravity anomaly g_d of the dike when measured from O is given by:

$$g_d(x) = g_{\prime}(x + x_o) - g_{\prime\prime}(x - x_o)$$

Using equation (1) the function $g_d(x)$ is given by:

$$g_d = \cos^2\beta\left[(x + x_o)(F'_{2d} - F'_{1d}) - (x - x_o)(F_{2d} - F_{1d})\right] \quad \ldots\ldots (5)$$

where $F_{id} = 2G\rho(\psi_{id} \cot \psi_{id} - \log \sin \psi_{id})$

$$\psi_{id} = \theta_{id} - \beta \; ; \quad \tan \theta_{id} = \tan \beta + \frac{x - x_o}{z_i}$$

$$F'_{id} = 2G\rho(\psi'_{id} \cot \psi'_{id} - \log \sin \psi'_{id})$$

$$\psi'_{id} = \theta'_{id} - \beta \; ; \quad \tan \theta'_{id} = \tan \beta + \frac{x + x_o}{z_i}$$

$$i = 1, 2.$$

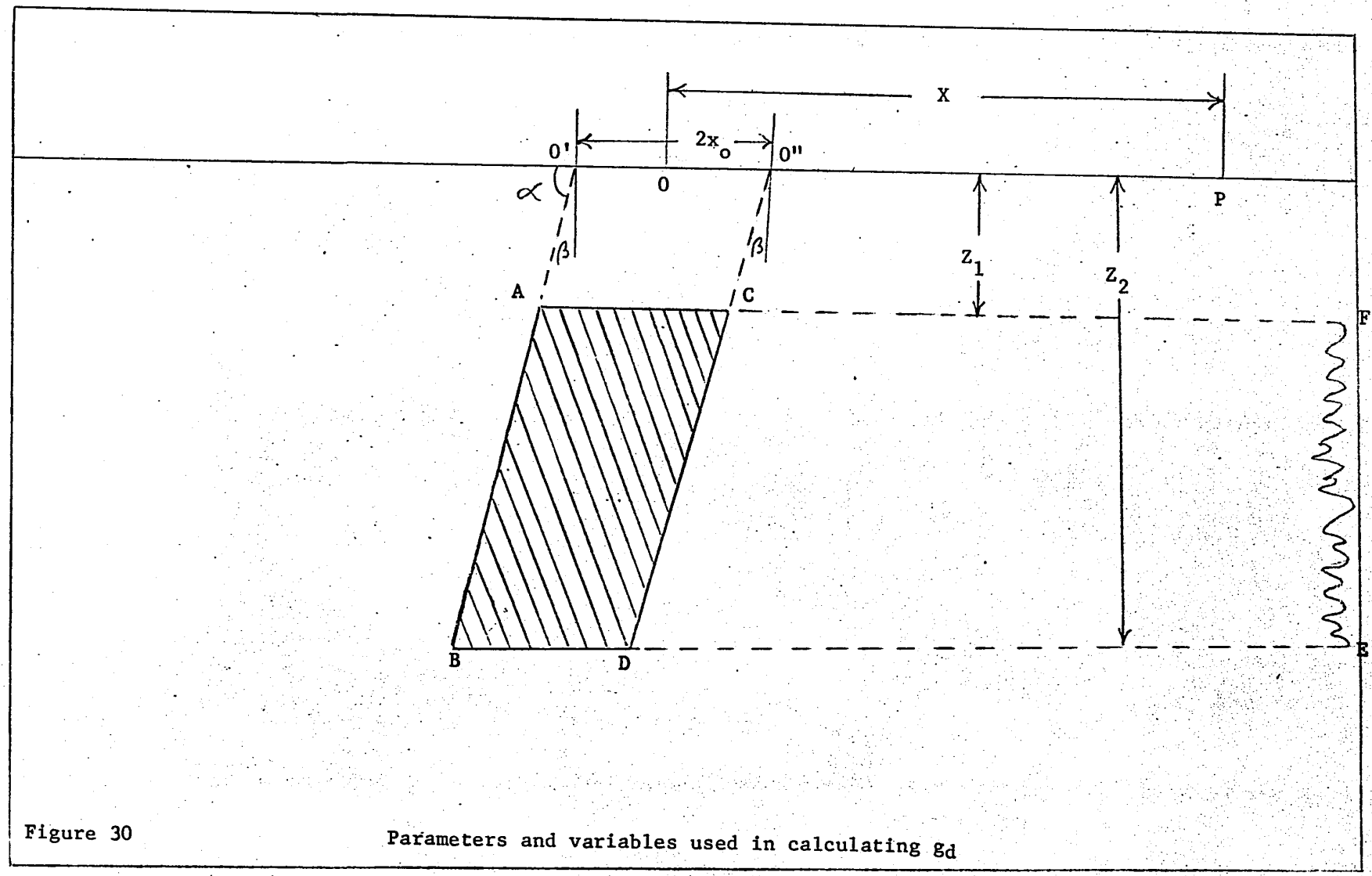

Figure 30 Parameters and variables used in calculating g_d

The limiting values of the function g_d for large positive and negative values of x may be obtained following the same procedure as in the case of a single block. For very large positive values of x, ψ_i approaches the value α, the inclination of the dike from the horizontal. For the first term within the bracket in equation (5), when $(x - x_o)$ is positive and much larger than z_i,

$$\psi_i \doteqdot \alpha - z_i/(x - x_o)$$

$$\psi_i \cot \psi_i \doteqdot \alpha \cot \alpha + (\alpha \csc^2\alpha - \cot \alpha)z_i/(x - x_o)$$

$$\text{Log}(\sin \psi_{2d}/\sin \psi_{id}) \doteqdot \{- t/(x - x_o)\} \cot \alpha$$

Hence the limiting value of the first term is $2G\rho\alpha t$. A similar analysis for the second term within the bracket for very large values of x in the positive direction also gives the limiting value of $2G\rho\alpha t$. Therefore as x becomes large, g_d approaches zero. For very large negative values of x, the limiting values of each term within the bracket is zero hence the limiting value of the function g_d is again zero.

As x approaches zero, the function g_d does not reduce to a simple form for an arbitrary angle of inclination β of the dike. However, for a vertical dike ($\beta = 0$) the expression at $x = 0$ reduces to

$$g_d = 4G\rho x_o \left[\frac{z_2}{x_o} \tan^{-1} \frac{x_o}{z_2} - \frac{z_1}{x_o} \tan^{-1} \frac{x_o}{z_1} - 1/2 \log\left(\frac{x_o^2 + z_1^2}{x_o^2 + z_2^2}\right)\right]$$

when the vertical extent of a dike is much greater than the width, the quantity x_o/z_2 is very small and $\tan^{-1} \frac{x_o}{z_2}$ is approximately equal to $\frac{x_o}{z_2}$. Hence the expression for a vertical dike at $x = 0$ becomes

$$g_d \doteqdot 4G\rho x_o \left[1 - \frac{z_1}{x_o} \tan^{-1} \frac{x_o}{z_1} - 1/2 \log\left(\frac{x_o^2 + z_1^2}{x_o^2 + z_2^2}\right) \right] \quad \ldots\ldots (5a)$$

When the dike reaches the surface, $z_1 = 0$, $\tan^{-1}(x_o/z_1) = \frac{\pi}{2}$, and

$$g_d \doteqdot 4G\rho x_o \left[1 + 1/2 \log\left(1 + \frac{z_2^2}{x_o^2}\right) \right] \quad \ldots\ldots (5b)$$

$$\doteqdot 4G\rho x_o \log\left(\frac{z_2}{x_o}\right) \text{ when } \quad z_2 >> x_o \quad \ldots\ldots (5c)$$

When the depth of burial, z_1, is much greater than x_o,

$$\tan^{-1} \frac{x_o}{z_1} \doteqdot \frac{x_o}{z_1} \ , \ \frac{z_1}{x_o} \tan^{-1} \frac{x_o}{z_1} = 1 \text{ , hence}$$

$$g_d \doteqdot 4G\rho x_o \log\left(\frac{z_2}{z_1}\right) \quad \ldots\ldots (5d)$$

Figure 31 shows curves for four vertical dikes, one having a vertical extent of 5 units (the dashed curve) and the others a vertical extent of 2 units. Comparing the dashed curve with that for the dike extending from 0.01 to 2.01, we see that the increase in vertical extent increases the maximum value and broadens the anomaly considerably. Comparison of the curves for the dike with vertical extent 2 units shows that increasing the depth to the top from 0.01 to 0.1 unit has a small effect on the anomaly while increasing the depth to 1.0 unit has a marked effect on the peak values.

Figure 32 shows the effect of varying the width of a vertical dike from 0.03 unit to 1.0 unit, z_1 and z_2 being kept fixed at 0.01 and 4.01 units. The anomaly for the dike of width 0.03 unit is very small; it has a small peak near the center of the dike and the anomaly

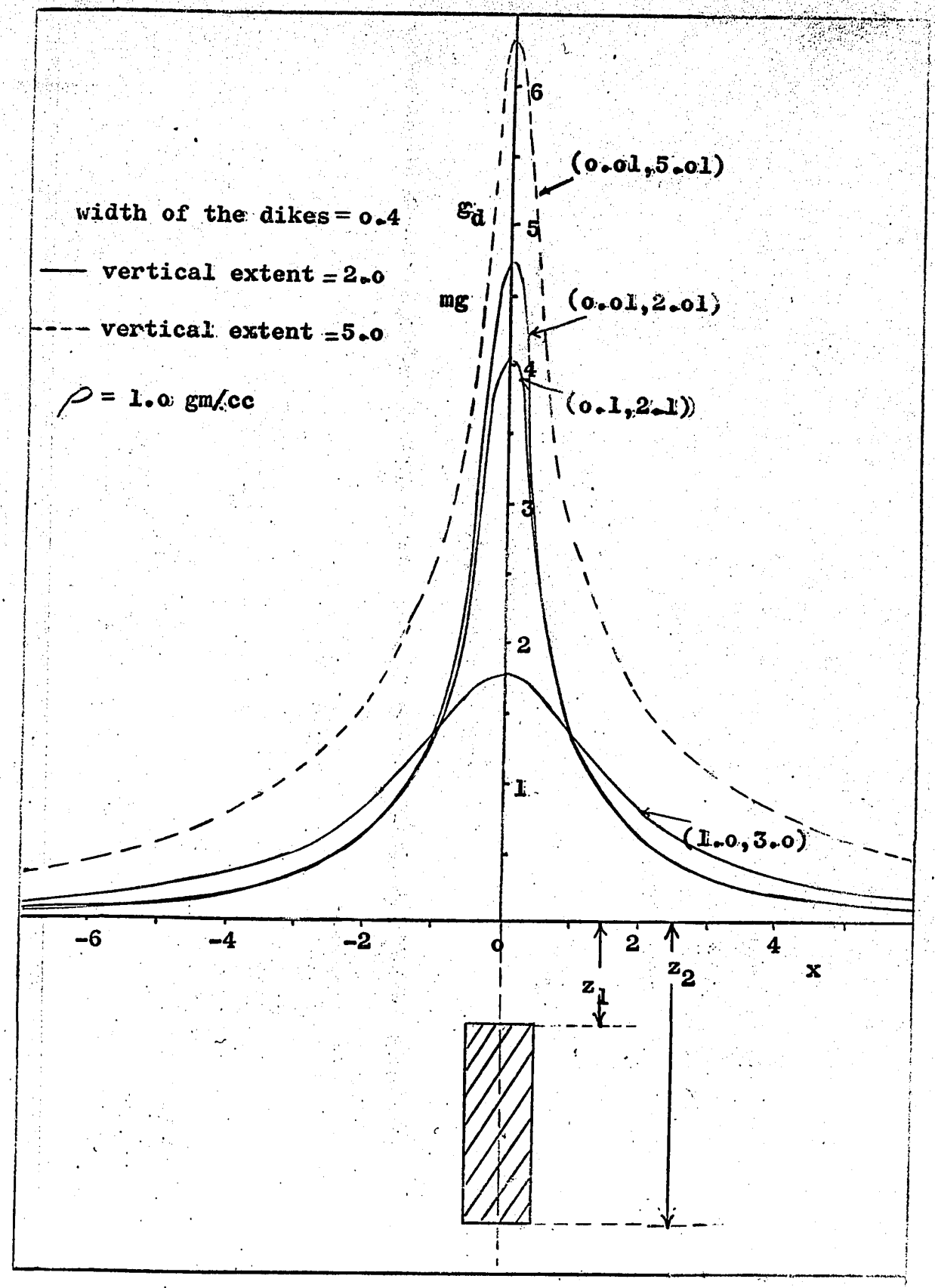

FIG 31. Relation between g_d and z_1 for a vertical dike

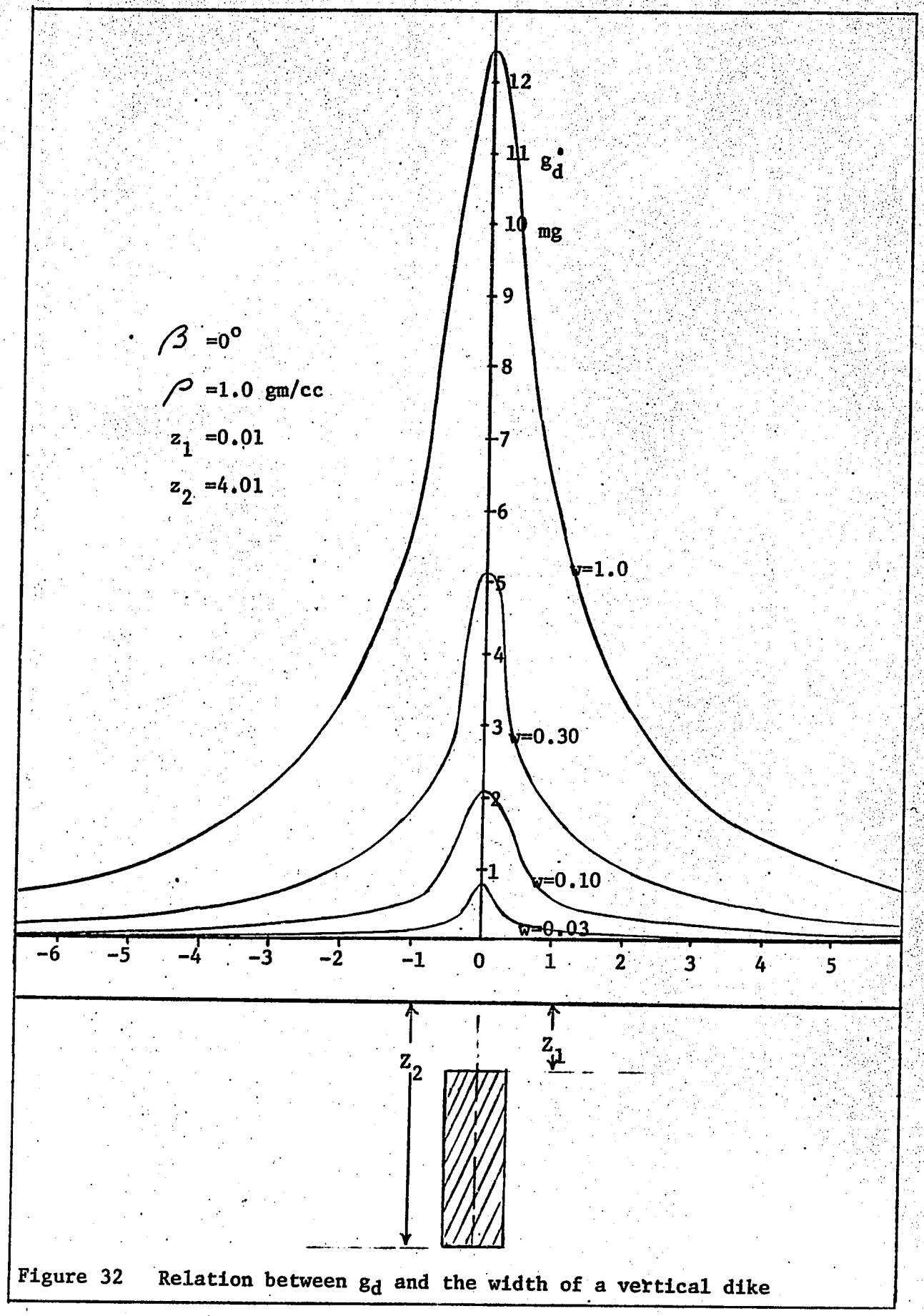

Figure 32 Relation between g_d and the width of a vertical dike

decreases very slowly for distances greater than 1 unit on either side of the center of the dike. As the width of the dike increases, the anomaly increases very sharply and the horizontal gradient of the anomaly at a given distance from the center of the dike is larger than for the thinner dikes.

The curves in Figure 33 show the effect of varying the angle of inclination of a dike. The solid-line curves in Figure 33 are gravity anomalies of dikes of width 0.05 unit and vertical extent 4.0 units whose angles of inclination have been varied from 0° to 80° from the vertical. As the inclination changes from the vertical the curves become asymmetrical about the center of the dike, the anomaly decreasing more quickly away from the direction of inclination of the dike than in the opposite direction. As the angle of inclination increases, the asymmetry increases until, for an angle of inclination of 80°, the curve resembles the characteristic curve for a single block or a step.

The effect of changing the width and depth of a dike inclined at 60° is shown by the dashed curve in Figure 33. As the width is increased from 0.05 to 0.2 unit, keeping $z_1 = 0.1, \beta = 60^{\circ}$, the anomaly increases from 0.33 to 1.35, a four-fold increase; however, the general shape of the two curves continues to be quite similar. For a dike inclined at 60° the effect of increasing the depth to the top from 0.01 to 0.20 unit can be seen by comparing the dashed curve with the dash-dot curve. It is interesting to note that the change in the anomaly resulting from the increase in depth is very slight in the direction of inclination of the dike but is large in the opposite direction.

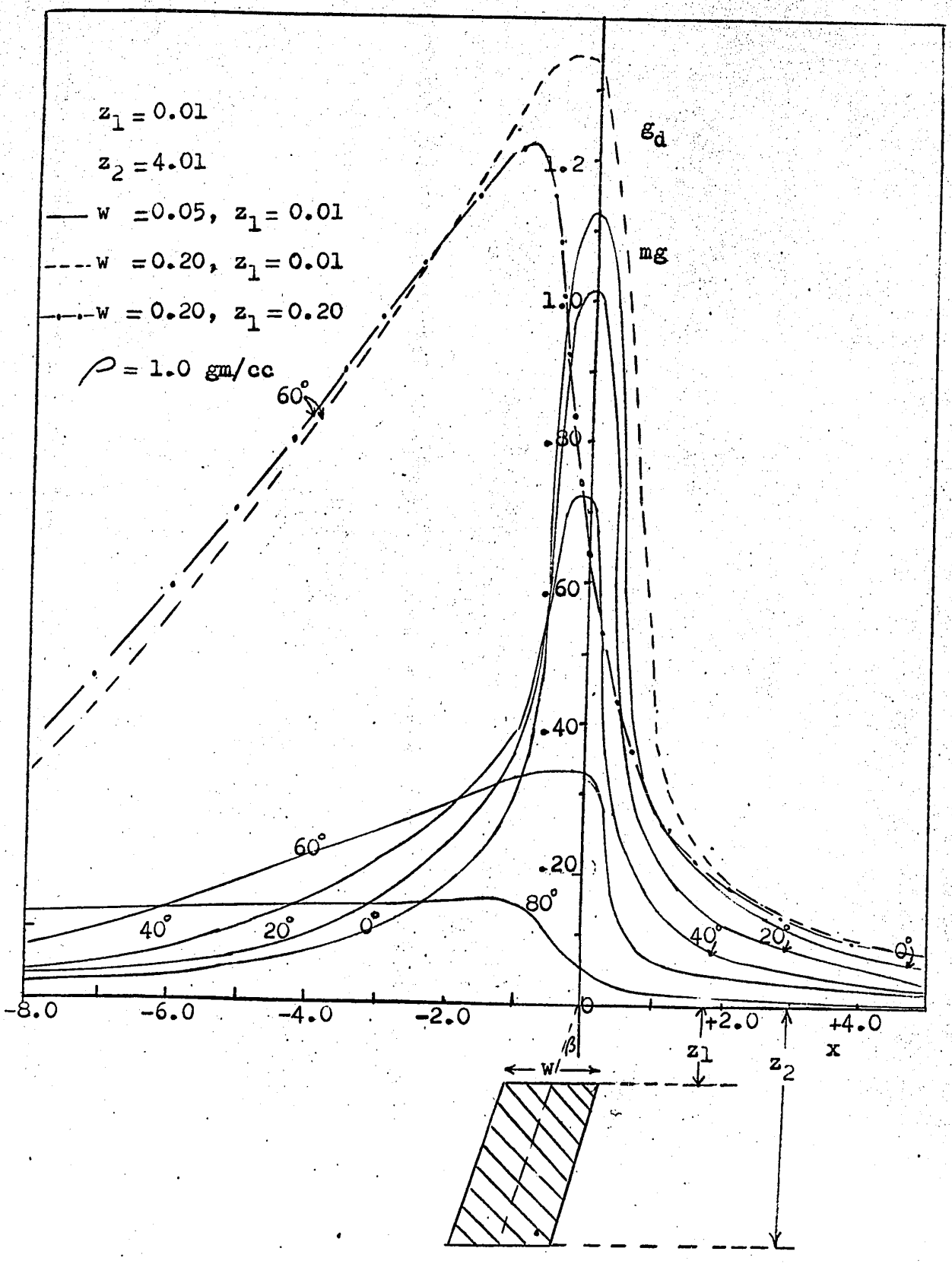

FIG 33. Variation of g_d with dip.

CHAPTER III

DERIVATIVES OF THE GRAVITY ANOMALIES

General: Since the expressions giving the gravity anomalies of the two-dimensional faults and dikes are functions of the space coordinates, x and z, these expressions can be differentiated with respect to x and z to give the two derivatives of the gravitational field.

For two-dimensional bodies, the derivatives with respect to y is zero since the body is assumed to extend to infinity without change in the y-direction. The derivative of the gravity field with respect to the variable x is called the horizontal derivative of gravity, or more commonly the gradient. The derivative with respect to z is known as the vertical gradient.

The gradient of the gravitational field may be defined as the rate of change of the vertical component of gravity in the horizontal direction. If g_1 and g_2 represent the gravity values at two points in the horizontal plane situated a distance Δx apart, then the horizontal derivative H is given by

$$H = \lim_{\Delta x \to o} \frac{g_1 - g_2}{\Delta x} = \frac{\partial g}{\partial x}$$

Since the gravitational field is conservative, the force of gravity may be expressed as the negative gradient of a scalar potential function U, that is,

$$g_T = - \nabla U$$

where g_T is the total gravitational field. The vertical component of gravity is then

$$g = -\frac{\partial U}{\partial z} ;$$

hence the horizontal derivatives of the vertical component of gravity are given by

$$\frac{\partial g}{\partial x} = U_{xz} = \frac{-\partial^2 U}{\partial x \partial z} , \text{ and } \frac{\partial g}{\partial y} = U_{yz} = -\frac{\partial^2 U}{\partial y \partial z}$$

As mentioned earlier, the horizontal gradient U_{yz} is zero for a two-dimensional body.

The gradient was of fundamental importance in the older torsion balance technique since it is one of the two quantities directly measurable by the torsion balance. The other was the horizontal directive tendency (H.D.T.), or the differential curvature as it is called by some authors. The differential curvature gives a measure of the distortion of the equipotential surface due to the disturbing mass; it is equal to the difference between the reciprocals of the minimum and the maximum radii of curvature of the equipotential surface at a point multiplied by the value of gravity at the same point. Thus, the differential curvature, R, is

$$R = g\left(\frac{1}{\rho_1} - \frac{1}{\rho_2}\right)$$

where ρ_2 and ρ_1 are the maximum and minimum radii of curvature of the equipotential surface.

The quantities measured by the torsion balance are U_Δ and

U_{xy} where

$$U_{\Delta} = \frac{\partial^2 U}{\partial y^2} - \frac{\partial^2 U}{\partial x^2} \quad , \quad U_{xy} = \frac{\partial^2 U}{\partial x \partial y}$$

U being the gravitational potential. It can be shown that

$$U_{\Delta} = -R \cos \lambda, \quad \frac{2U_{xy}}{U_{\Delta}} = \tan 2\lambda$$

Differentiating the gradient with respect to x we obtain higher order horizontal derivatives. One of these higher order derivatives, the second horizontal derivative, is of particular importance to us; it is denoted as

$$H_{xx} = -\frac{\partial^2 g}{\partial x^2} = \frac{\partial^3 U}{\partial x^2 \partial z}$$

Differentiation of the gravity anomaly function with respect to z gives the vertical derivatives of gravity. In general, the vertical derivatives are distinct from the horizontal derivatives and have entirely different properties. The first vertical derivative of gravity or the vertical gradient as it is sometimes called, is defined as the rate of change in the vertical direction of the acceleration due to gravity. If g_1 and g_2 are the gravity effects due to an anomalous body at two points, one of which is a distance Δz vertically above the other, the vertical gradient of gravity is defined as

$$\text{vertical gradient} = \lim_{\Delta z \to o} \frac{g_1 - g_2}{\Delta z} = \frac{\partial g}{\partial z}$$

In terms of the gravitational potential the vertical gradient of gravity is given by

$$\frac{\partial g}{\partial z} = -\frac{\partial^2 U}{\partial z^2}$$

Differentiating the above expression with respect to z, we obtain the higher order vertical derivatives. One commonly used higher order vertical derivative is the second vertical derivative of gravity obtained by differentiating the gravity field twice with respect to z or by differentiating the expression for the gravitational potential three times with respect to z. The second vertical derivative of gravity is denoted as

$$H_{zz} = \frac{\partial^2 g}{\partial z^2} = -\frac{\partial^3 U}{\partial z^3}$$

Since the gravitational field satisfies Laplace's equation, we have for a two-dimensional body

$$\frac{\partial^2 g}{\partial x^2} + \frac{\partial^2 g}{\partial z^2} = 0.$$

Therefore, for a two-dimensional body the second horizontal derivative is identical with the second vertical derivative except for algebraic sign. It is of interest to note that for a two-dimensional body (except for a change in the sign) the first vertical derivative is identical with the differential curvature. This follows from the fact that the gravitational potential also satisfies Laplace's equation, hence

$$\frac{\partial^2 U}{\partial x^2} + \frac{\partial^2 U}{\partial z^2} = 0$$

Since the derivatives with respect to y are zero, the differential curvature is merely $\frac{\partial^2 U}{\partial x^2}$.

Thus, differential curvature $= \frac{\partial^2 U}{\partial x^2} = -\frac{\partial^2 U}{\partial z^2} = -\frac{\partial g}{\partial z}$

The use of the derivatives of gravity in the interpretation of gravity maps have been discussed by several authors. A complete gravity map of an area contains, in principle, all of the information needed to describe the gravity field and all of its spatial derivatives. The calculation of the vertical derivatives of gravity is very useful if we want to emphasize the effect of small shallow structures at the expense of the larger and deeper structures.

Consider the simple example of two identical spheres, one of which is located at a depth twice that of the other below the surface of the earth. The gravity anomaly due to one of the spheres is given by

$$g = G\frac{mz}{r^3}$$

where m is the mass of the sphere,

z is the depth to the center of the sphere,

x the horizontal distance of the point of observation from the point on the surface directly above the center of the sphere, and $r^2 = x^2 + z^2$.

If we differentiate the expression for the gravity anomaly with respect to z, we get the first and second vertical derivatives of gravity,

$$\frac{\partial g}{\partial z} = Gm\frac{(x^2 - 2z^2)}{r^5}$$

and

$$\frac{\partial^2 g}{\partial z^2} = 3Gmz\frac{(2z^2 - 3x^2)}{r^7}$$

The above expressions have the following maxima:

$$\text{at } x = 0 \,, \quad g_{max} = \frac{Gm}{z^2}$$

$$\text{at } x = \pm 2z \,, \left(\frac{\partial g}{\partial z}\right)_{max} = \frac{2Gm}{25\sqrt{5}\, z^3}$$

$$\text{at } x = \pm \frac{2}{\sqrt{3}} z \,, \left(\frac{\partial^2 g}{\partial z^2}\right)_{max} = -\frac{162}{343}\sqrt{\frac{3}{7}}\,\frac{Gm}{z^4}$$

Thus, the maximum values of g, $\frac{\partial g}{\partial z}$ and $\frac{\partial^2 g}{\partial z^2}$ vary inversely as the second, third and fourth powers of the depth.

The effect of taking the successive derivatives is, therefore, to accentuate greatly the effect of shallower structures compared to those at greater depths. This is very useful in many situations in gravity interpretation where it is found that the effect of small anomalies at shallow depths are completely masked by larger and deeper features.

Another advantage of the derivatives of the anomaly, g, in comparison with g itself is that they have a higher resolving power, that is, they can distinguish between two masses much closer together than can gravity. Elkins and Hammer (1938) have given an analytical treatment to the problem of resolving buried masses by gravity and its derivatives. We will follow their approach to show for the case of a sphere the superior resolving power of the derivatives of gravity over gravity.

Let the effect (gravity or its derivatives) of each one of the two identical spherical bodies 1 and 2 (Figure 34) be denoted by $\Phi(x)$. Since the body 2 is situated at a distance 'a' to the right of the

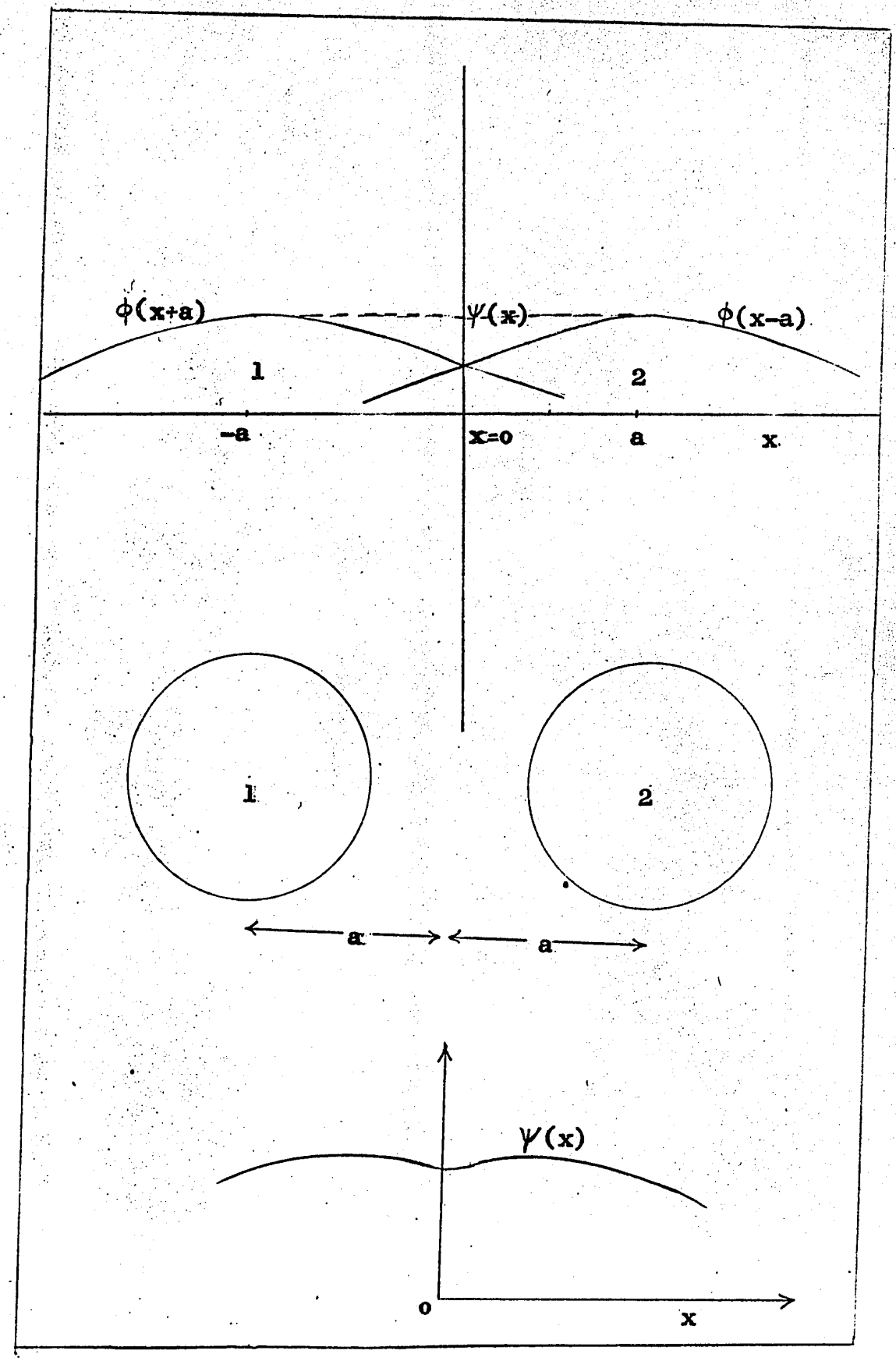

FIG 34. Resolving power of gravity and the second vertical derivative of gravity

origin its effect will be represented by $\Phi(x - a)$ and similarly the effect of the other body 1 will be represented by $\Phi(x + a)$. The anomaly observed at the surface is the combined effect of the two bodies, that is, $\psi(x) = \Phi(x + a) + \Phi(x - a)$. Assuming that $\Phi(x + a)$ and $\Phi(x - a)$ are analytical in the neighborhood of the point $x = a$, then the derivatives of each of these functions with respect to x may be expanded in a Taylor's series. Writing $f(x) = \frac{d\Phi(x)}{dx}$, we obtain

$$f(x + a) = f(a) + xf'(a) + \frac{x^2}{2} f''(a) + \frac{x^3}{6} f'''(a) + \ldots .$$

$$f(x - a) = - f(a - x) = - f(a) + xf'(a) - \frac{x^2}{2} f''(a) + \frac{x^3}{6} f'''(a) + \ldots .$$

The relationship between the first two expressions in the last line follows from the symmetry of $\Phi(x)$.

$$\psi'(x) = f(x + a) + f(x - a)$$

$$= 2 x f'(a) + \frac{x^3}{3} f'''(a) + \ldots .$$

The curve $\psi(x)$ reaches the resolution limit when a depression just begins to form on the graph of $\psi(x)$ at the origin (Figure 34). Geometrically, this condition is satisfied when a triple tangent occurs to the graph of $\psi(x)$ at $x = 0$ or $\psi'(x)$ has roots $x = 0$ three times. This condition will be satisfied if $f'(a) = 0$. Hence the condition on the parameters for the limiting case of resolution is $f'(a) = 0$ or $\Phi''(a) = 0$.

Thus in order to find the required condition on the parameters, we should find the second derivative of the function $\Phi(x)$ and then equate

it to zero at $x = a$. In Figure 34 are shown two identical spheres situated at a distance '2a' apart. We wish to find the minimum distance '2a' between the two spheres at which the combined effect of the two spheres gives the indication of the presence of two separate masses. The vertical component of gravity due to a sphere is given by

$$g = Gmz/r^3$$

Taking $\phi(x) = g$ and differentiating twice gives

$$\phi''(x) = 3Gmz(4x^2 - z^2)/r^7$$

Substituting $x = a$ and equating the expression to zero, we have $a/z = \pm 1/2$. Hence the minimum distance at which they can be resolved by gravity is

$$2a = z$$

In order to find the resolving power by the second vertical derivative we have the function $\phi(x) = \frac{3Gmz(2z^2 - 3x^2)}{r^7}$. Differentiating this equation twice with respect to x and then equating it to zero at $x = a$, we obtain the result $2a/z = 0.64$. Thus we see that the second vertical derivative has a higher resolving power than gravity itself.

The Horizontal Derivative Of Gravity Due To A Single Block

The expression for the horizontal derivative of gravity due to a single block is derived in Appendix A, the result being

$$\frac{dg_s}{dx} = \cos^2\beta(F_2-F_1) + \frac{2G\rho}{x}(z_1\psi_1 - z_2\psi_2) \qquad \ldots\ldots (6)$$

Figure 35 shows the plot of the horizontal derivative of gravity due to a normal fault dipping at 30° and cutting a horizontal bed with upper and lower surfaces at depths of 1.0 and 2.0 units. This curve was obtained from the gravity profile by taking the difference between two gravity values at two closely spaced points along the profile and dividing the difference by the distance between the two points. The gradient curve of Figure 35 attains its maximum value vertically above the inclined face of the block. To locate the maximum, we differentiate the expression for the gradient with respect to x and then equate the result to zero. Writing x_m for the value of x corresponding to the maximum gradient, we find

$$\frac{d}{dx}\left(\frac{dg_s}{dx}\right) = 0 = -\frac{G\rho}{x}(\cos 2\theta_2 - \cos 2\theta_1)$$

hence $\cos 2\theta_2 = \cos 2\theta_1$

Therefore, $\theta_2 = \theta_1$ or $\theta_2 = -\theta_1$.

Since $\tan\theta_i = \tan\beta + \frac{x}{z_i}$

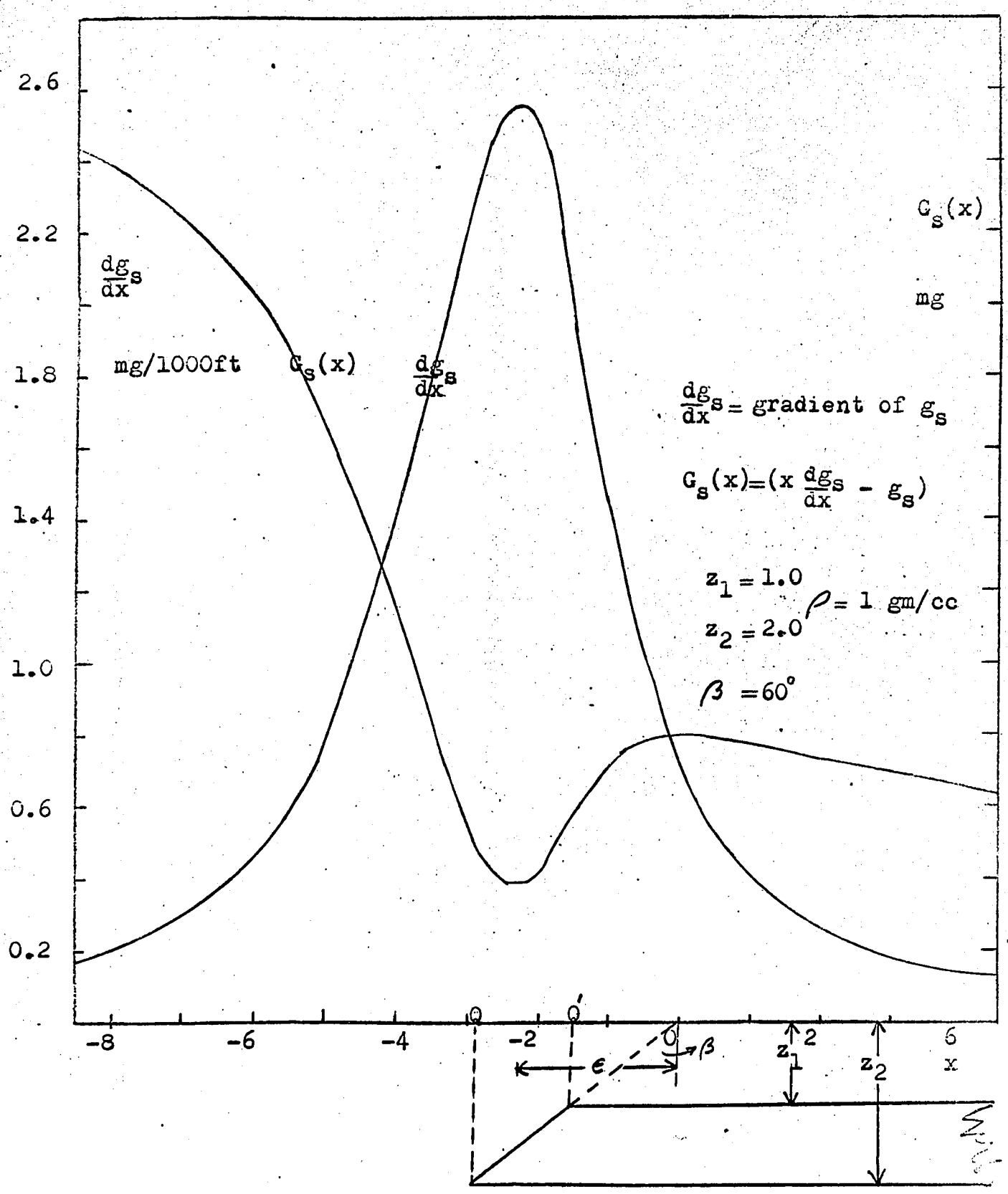

FIG 35. Graphs of $\frac{dg_s}{dx}$ and $G_s(x)$ for a single block

we must have $x = 0$ if $\theta_1 = \theta_2$; this value of x gives $\frac{0}{0}$ for $\frac{d}{dx}\left(\frac{dg_s}{dx}\right)$ but the limit of the indeterminate ratio is not zero. Thus, for a maximum we must have

$$\theta_2 = -\theta_1, \text{ that is, } \tan\theta_2 = -\tan\theta_1$$

hence, $$\left(\tan\beta + \frac{x_m}{z_2}\right) = -\left(\tan\beta + \frac{x_m}{z_1}\right)$$

or $$x_m = -2\tan\beta\left(\frac{z_1 z_2}{z_1 + z_2}\right)$$

The maximum gradient is located at a point in between Q and Q' in Figure 35 since the coordinates of Q and Q' are $(-z_1 \tan\beta)$ and $(-z_2 \tan\beta)$ respectively, and

$$z_1 \tan\beta < \frac{2z_1 z_2}{z_1 + z_2} \tan\beta < z_2 \tan\beta .$$

We therefore conclude that no matter what the inclination of the fault may be, a vertical hole drilled at the point of the maximum gradient of gravity will always intersect the faulted face of the bed.

It is shown in Appendix A that the gradient for a single block at $x = 0$ is given by

$$\frac{dg_s}{dx} = 2G\rho\cos^2\beta \log(1 + t/z_1)$$

For a given block the gradient at $x = 0$ is a maximum when the block is vertical ($\beta = 0$). As the dip of the fault plane is changed, the gravity curve is displaced laterally without any appreciable change in the shape. A method has been discussed earlier for finding the dip of the

fault plane of such a block by comparing the observed curve with the given theoretical curves, provided the location of the fault trace on the surface of the earth is known.

If an approximate position of the fault trace is known, the following procedure may be adopted to find a rough value of the dip of the fault plane. The gradient over a single block is given by

$$\frac{dg_s}{dx} = \cos^2\beta \ (F_2-F_1) + \frac{2G\rho}{x} (z_1\psi_1 - z_2\psi_2)$$

Multiplying both sides of the above equation by x and transferring the first term on the right side to the left of the equation, we have

$$x\frac{dg_s}{dx} - x\cos^2\beta \ (F_2-F_1) = 2G\rho(z_1\psi_1 - z_2\psi_2)$$

Since $x\cos^2\beta \ (F_2-F_1)$ is equal to the gravity anomaly of the block, the above equation becomes

$$x\frac{dg_s}{dx} - g_s = 2G\rho(z_1\psi_1 - z_2\psi_2)$$

If we denote the left side of the above equation by $G_s(x)$, a new function of x, we can obtain the value of the new function at any point along the profile by multiplying the gradient at the point by the distance from the fault trace, then subtracting the value of gravity at that point. The limiting value of $G_s(x)$ at certain points on the x-axis may be used to obtain information about the dip of the block.

We have, since $\psi_i = \theta_i - \beta$,

$$G_s(x) = 2G\rho(z_1\psi_1 - z_2\psi_2) = 2G\rho(z_1\theta_1 - z_2\theta_2) + 2G\rho\beta t$$

As $x \longrightarrow 0$, θ_1 and θ_2 both approach β so that

$$\lim_{x \longrightarrow 0} G_s(x) = 0$$

As $x \longrightarrow +\infty$, θ_1 and θ_2 both approach $\pi/2$ so that

$$\lim_{x \longrightarrow \infty} G_s(x) = -\pi G\rho t + 2G\rho\beta t = 2G\rho t(\beta - \pi/2) = -2G\rho\alpha t.$$

As $x \longrightarrow -\infty$, θ_1 and θ_2 both approach $-\pi/2$ so that

$$\lim_{x \longrightarrow -\infty} G_s(x) = \pi G\rho t + 2G\rho\beta t = 2G\rho t(\beta + \pi/2) = 2G\rho(\pi - \alpha)t$$

Besides the origin, there is a second point where $G_s(x) = 0$. This point may be found by equating the right side of the above equation for $G_s(x)$ to zero. We thus have,

$$G_s(x) = 2G\rho(z_1\theta_1 - z_2\theta_2) + 2G\rho\beta t = 0$$

or, since $t = z_2 - z_1$, $z_1(\theta_1 - \beta) = z_2(\theta_2 - \beta)$

hence $$z_1 \left\{ \tan^{-1}(\tan\beta - \frac{x}{z_1}) - \beta \right\} = z_2 \left\{ \tan^{-1}(\tan\beta - \frac{x}{z_2}) - \beta \right\}$$

that is,

$$z_2 \tan^{-1}(\tan\beta - \frac{x}{z_2}) - z_1 \tan^{-1}(\tan\beta - \frac{x}{z_1}) = \beta(z_2 - z_1)$$

The last equation shows that by noting where $G_s(x)$ becomes zero we can find one of the three unknown quantities (β, z_1, and z_2), provided the other two are known.

As mentioned earlier, the function $G_s(x)$ approaches the values $2G\rho(\beta - \frac{\pi}{2})$ and $2G\rho(\beta + \frac{\pi}{2})$ for very large values of x in the positive and negative directions. Hence the sum and difference of these two values of $G_s(x)$ gives $4G\rho\beta t$ and $2\pi G\rho t$.

Figure 35 shows the graph of $G_s(x)$ calculated from the gradient curve in the same diagram. Since the graph of $G_s(x)$ was not extended to large enough distances on either side of the fault plane, the curve does not attain the limiting values which are of interest to us. The theoretical limiting values are 10.6 and -2.15 and these are reached approximately when $x = \pm 20$.

The Horizontal Derivative For A Fault Cutting A Single Bed

The horizontal derivative of gravity due to a fault truncating a single bed is given by (see Appendix A)

$$\frac{dg_f}{dx} = \cos^2\beta\left\{(F_2-F_1) - (F_4-F_3)\right\} + \left(\frac{2G\rho}{x}\right)(z_1\psi_1 - z_2\psi_2 - z_3\psi_3 + z_4\psi_4)$$

where $\psi_i = \theta_i - \beta$; $i = 1, 2, 3$ and 4.

Multiplying both sides of the above equation by x we have

$$x\frac{dg_f}{dx} = x\cos^2\beta\left\{(F_2-F_1) - (F_4-F_3)\right\} + 2G\rho(z_1\psi_1 - z_2\psi_2 - z_3\psi_3 + z_4\psi_4)$$

Since $x\cos^2\beta(F_2-F_1-F_4+F_3) = g_f$, transferring the first term on the right side of the above equation to the left of the equation gives

$$G_f(x) = x\frac{dg_f}{dx} - g_f = 2G\rho(z_1\psi_1 - z_2\psi_2 - z_3\psi_3 + z_4\psi_4).$$

Since $\psi_i = \theta_i - \beta$, and $(z_2-z_1) = (z_4-z_3) = t$, the thickness of the bed, we get

$$G_f(x) = 2G\rho(z_1\theta_1 - z_2\theta_2 - z_3\theta_3 + z_4\theta_4)$$

The limiting values of the angles θ_1, θ_2, θ_3 and θ_4 as x approaches zero is β. Hence the limiting value of $G_f(x)$ at $x = 0$ is zero. As x approaches $+\infty$ or $-\infty$, the limiting values of the angles θ_1, θ_2, θ_3 and θ_4 are $\pi/2$ or $-\pi/2$ respectively. Hence the limiting value of the function $G_f(x)$ is also zero for very large positive and negative values of x.

The Horizontal Derivative For A Fault Cutting A Series Of Beds

The horizontal derivative of gravity for a fault truncating a series of beds may be obtained following the same procedure as in the case of the single block. The gravity anomaly of the fault shown in Figure 24 is given by (see equation 3)

$$g_m = x \cos^2\beta\Big[(\sigma_o-\sigma_1)(L_1-L_1') + (\sigma_1-\sigma_2)(L_2-L_2') + \ldots + (\sigma_N-\sigma_r)(L_{N+1}-L_{N+1}')\Big]$$

The horizontal derivative of g_m then becomes

$$\frac{dg_m}{dx} = \frac{g_m}{x} + \frac{2G}{x}\Big[(\sigma_o-\sigma_1)(z_1'\psi_1' - z_1\psi_1) + \ldots + (\sigma_N-\sigma_r)(z_{N+1}'\psi_{N+1}' - z_{N+1}\psi_{N+1})\Big]$$

Since $\psi_i = \theta_i - \beta$ and $\psi_i' = \theta_i' - \beta$,

$$\frac{dg_m}{dx} - \frac{g_m}{x} = \frac{2G}{x}\Big[(\sigma_o-\sigma_1)(z_1'\theta_1' - z_1\theta_1) + \ldots + (\sigma_N-\sigma_r)(z_{N+1}'\theta_{N+1}' - z_{N+1}\theta_{N+1})\Big] - \frac{2G\beta\delta(\sigma_o-\sigma_r)}{x}$$

where $\delta = z_i' - z_i$

Multiplying both sides of the above equation by x we obtain the function, $G_m(x)$, given by

$$G_m(x) = x\frac{dg_m}{dx} - g_m = 2G\left[(\sigma_o-\sigma_1)(z_1'\theta_1' - z_1\theta_1) + \ldots\right.$$

$$\left. + (\sigma_N-\sigma_r)(z_{N+1}'\theta_{N+1}' - z_{N+1}\theta_{N+1})\right] - 2G\beta\delta(\sigma_o-\sigma_r)$$

As x approaches zero, each of the angles θ_1, θ_2 ..... θ_{N+1}, θ_1' ..... θ_{N+1}' approaches β. Hence, as x approaches zero,

$$\lim_{x \to o} G_m(x) = 0$$

As x approaches $+\infty$ or $-\infty$ the limiting values of the angles θ_1, θ_2 .....θ_{N+1}, θ_1', θ_2' .....θ_{N+1}' are $\pi/2$ or $-\pi/2$ respectively. Hence,

$$\lim_{x \to \infty} G_m(x) = 2G\,\frac{\pi}{2}\delta(\sigma_o-\sigma_r) - 2G\beta\delta(\sigma_o-\sigma_r)$$

$$= 2G\delta(\sigma_o-\sigma_r)(\frac{\pi}{2} - \beta)$$

and

$$\lim_{x \to -\infty} G_m(x) = -2G\,\frac{\pi}{2}\delta(\sigma_o-\sigma_r) - 2G\beta\delta(\sigma_o-\sigma_r)$$

$$= -2G\delta(\sigma_o-\sigma_r)(\beta + \frac{\pi}{2})$$

Thus, the limiting values of $G_m(x)$ depend upon the fault displacement, δ, the angle of the fault plane, β, and the density contrast between the topmost bed and the bed below the Nth one. The sum and difference of the limiting values of $G_m(x)$ for very large positive and negative values of x is $-4G\beta\delta(\sigma_o-\sigma_r)$ and $2\pi G\delta(\sigma_o-\sigma_r)$ respectively. If the density contrast $(\sigma_o-\sigma_r)$ is known, the displace-

ment of the fault, δ , and the dip of the fault plane, $(\pi/2 - \beta)$, can be found.

The Second Derivative Due To A Single Block

The horizontal derivative of gravity due to a single block is given by (see Appendix A)

$$\frac{dg_s}{dx} = \frac{g_s}{x} + \frac{2G\rho}{x}(z_1\psi_1 - z_2\psi_2)$$

The second horizontal derivative of gravity due to a single block is also derived in Appendix A, the result being

$$\frac{d^2g_s}{dx^2} = -\frac{G\rho}{x}(\cos 2\theta_2 - \cos 2\theta_1) \qquad \ldots\ldots (7)$$

$$= -\frac{d^2g_s}{dz^2}$$

Limiting values of $\frac{d^2g_s}{dx^2}$

(a) Limiting values of $\frac{d^2g_s}{dx^2}$ as $z_1 \longrightarrow 0$.

Since $\tan\theta_1 = \tan\beta + \frac{x}{z_1}$,

as $z_1 \longrightarrow 0$, $\tan\theta_1 \longrightarrow \pm\infty$ and $\theta_1 \longrightarrow \frac{\pi}{2}$

and $\cos 2\theta_1 \longrightarrow \cos\pi = -1$

Hence $$\left(\frac{d^2g_s}{dx^2}\right)_{z_1=0} = -\frac{G\rho}{x}(1 + \cos 2\theta_2) = -\frac{2G\rho}{x}\cos^2\theta_2$$

(b) Limiting values of $\frac{d^2 g_s}{dx^2}$ as $x \longrightarrow 0$.

We have $\lim_{x \to o} \left(\frac{d^2 g_s}{dx^2}\right) = \lim_{x \to o} \left[- \frac{G\rho}{x} (\cos 2\theta_2 - \cos 2\theta_1) \right]$

$$= \lim_{x \to o} \left[- \frac{G\rho}{x} \left\{ \frac{1 - \tan^2 \theta_2}{1 + \tan^2 \theta_2} - \frac{1 - \tan^2 \theta_1}{1 + \tan^2 \theta_1} \right\} \right]$$

$$= \lim_{x \to o} \left[\frac{G\rho}{x} \left\{ \frac{2(\tan^2 \theta_2 - (\tan^2 \theta_1)}{(1+\tan^2\theta_1)(1+\tan^2 \theta_2)} \right\} \right]$$

As $x \longrightarrow 0 \quad \theta_i \longrightarrow \beta$, since

$$\tan \theta_i = \tan\beta + \frac{x}{z_i}$$

Therefore, $\tan^2 \theta_i = \tan^2\beta \left(1 + \frac{2x}{z_i \tan\beta}\right)$,

Hence

$$\lim_{x \to o} \left(\frac{d^2 g_s}{dx^2}\right) = \lim_{x \to o} \left(\frac{4G\rho}{x}\right) \frac{x \tan\beta \left(\frac{1}{z_2} - \frac{1}{z_1}\right)}{(1 + \tan^2\beta)^2}$$

$$= - 2G\rho t \left(\frac{\sin 2\beta \cos^2\beta}{z_1 z_2}\right)$$

Figure 36 shows the second vertical derivative of gravity over a 200 ft thick block cut by a vertical fault for various values of the depth of the block. For a vertical fault the maximum and the minimum are of equal amplitude and occur at equal distance from the fault trace. When the block is at the surface, the second derivative is infinite at $x = 0$, but the maximum value diminishes rapidly as the

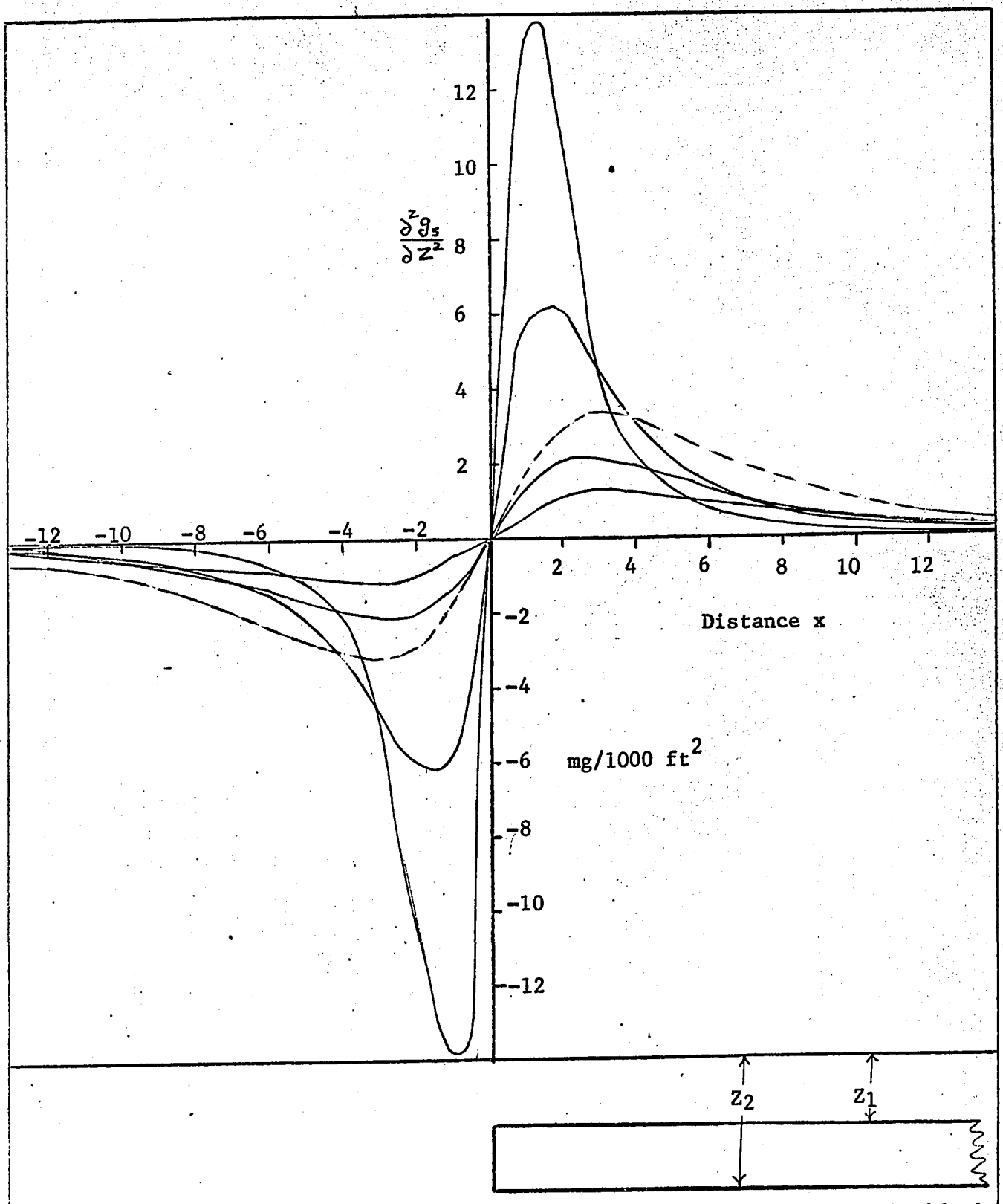

Figure 36 Effect on the second derivative of depth & thickness of the block.

depth of burial is increased. The dashed line curve in the same figure shows the effect of increasing the thickness of the block.

Figure 37 shows the effect on the second derivative of changing angle of inclination of the fault. The maximum and minimum are no longer equal and they occur at different distances from the fault trace.

It was shown earlier that the distance from the fault trace to the zero value of the second derivative (for positive β) is given by

$$x = -2 \tan\beta \frac{z_1 z_2}{z_1 + z_2}$$

To find the points where the maximum and minimum of the second derivative occur on the x-axis we differentiate the expression for the second derivative with respect to x and equate the result to zero.

Thus

$$\frac{d}{dx}\left(\frac{d^2 g_s}{dx^2}\right) = 0 = \frac{d}{dx}\left(\frac{\cos 2\theta_2}{x} - \frac{\cos 2\theta_1}{x}\right)$$

that is,

$$\frac{d}{dx}\left(\frac{\cos 2\theta_2}{x}\right) = \frac{d}{dx}\left(\frac{\cos 2\theta_1}{x}\right)$$

We have

$$\frac{d}{dx}\left(\frac{\cos 2\theta_i}{x}\right) = -\frac{1}{x^2}\cos 2\theta_i - \frac{2}{x}\sin 2\theta_i \frac{d\theta_i}{dx}$$

Now,

$$\tan \theta_i = \tan\beta + \frac{x}{z_i}$$

and

$$\frac{d\theta_i}{dx} = \frac{\cos^2\theta_i}{z_2}$$

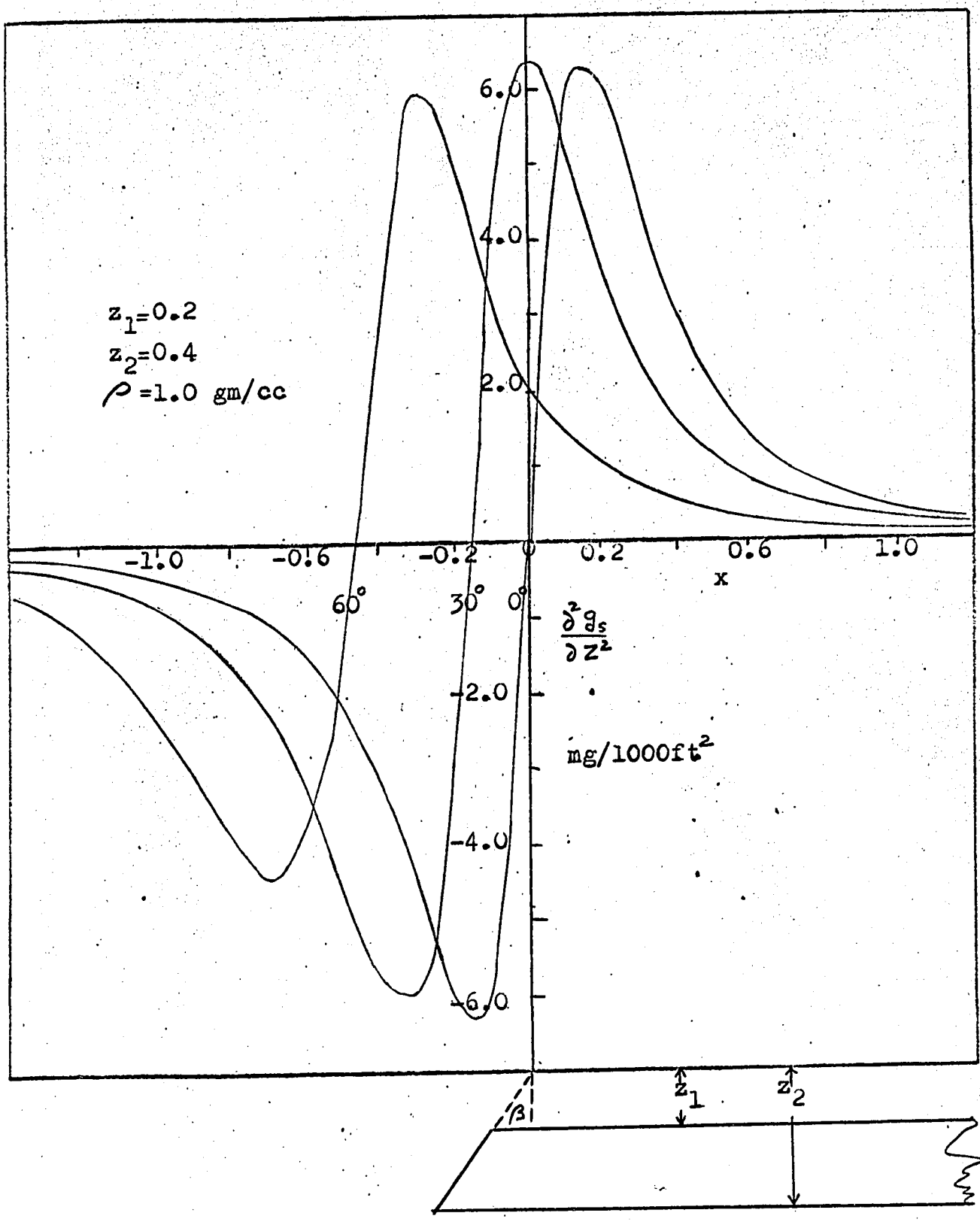

FIG 37. Variation of the second derivative with dip

Hence $$\frac{d}{dx}\left(\frac{\cos 2\theta_2}{x}\right) = -\frac{1}{x^2}\left(\cos 2\theta_2 + 2x \sin 2\theta_2 \frac{\cos^2\theta_2}{z_2}\right)$$

Therefore,

$$\cos 2\theta_2 + 2x \sin 2\theta_2 \frac{\cos^2\theta_2}{z_2} = \cos 2\theta_1 + 2x \sin 2\theta_1 \frac{\cos^2\theta_1}{z_1}$$

or

$$\cos 2\theta_2 + 2x \sin 2\theta_2 \frac{\cos^2\theta_2}{z_2} + 1 = \cos 2\theta_1 + 2x \sin 2\theta_1 \frac{\cos^2\theta_1}{z_1} + 1$$

Writing $\frac{x}{z_1} = q_1$, $\frac{x}{z_2} = q_2$, $\tan\theta_i = \tan\beta + q_i$, we have

$$\cos 2\theta_i = \frac{1 - \tan^2\theta_i}{1 + \tan^2\theta_i} = \frac{1 - (\tan\beta + q_i)^2}{1 + (\tan\beta + q_i)^2},$$

$$\frac{2x \sin 2\theta_i \cos^2\theta_i}{z_i} = 4q_i \tan\theta_i \cos^4\theta_i = \frac{4q_i \tan\theta_i}{(1 + \tan^2\theta_i)^2}$$

$$= \frac{4q_i(\tan\beta + q_i)}{\left\{1 + (\tan\beta + q_i)^2\right\}^2}$$

Then,

$$E_i = \frac{\cos 2\theta_i + 2x \sin 2\theta_i \cos^2\theta_i}{z_i} + 1$$

$$= \frac{1 - (\tan\beta + q_i)^4 + 4q_i(\tan\beta + q_i) + \left\{1 + (\tan\beta + q_i)^2\right\}^2}{\left\{1 + (\tan\beta + q_i)^2\right\}^2}$$

$$= \frac{2\left\{1 + (\tan\beta + q_i)(\tan\beta + 3q_i)\right\}}{\left\{1 + (\tan\beta + q_i)^2\right\}^2}$$

$$= \frac{2(\sec^2\beta + 4q_i\tan\beta + 3q_i^2)}{(\sec^2\beta + 2q_i\tan\beta + q_i^2)^2}$$

Thus, to find the points where $\frac{d^2 g_s}{dx^2}$ is a maximum or minimum, we must solve the equation

$$E_1 = E_2 ,$$

By cross multiplying and collecting like powers of x in the above equation, we obtain a polynomial of the fourth degree in x of the form

$$ax^4 + bx^3 + cx^2 + dx + e = 0$$

where the coefficients a, b, c, d and e are given by

$$a = 6(z_1^2 - z_2^2)$$

$$b = 8 \tan\beta \, (z_1 - z_2)\left[z_1^2 + z_2^2 + 4z_1 z_2 \right]$$

$$c = 2(z_1^2 - z_2^2) \left\{(z_1^2 + 16 z_1 z_2 + z_2^2) \tan^2\beta + (z_1^2 + z_2^2)\right\}$$

$$d = 8 z_1 z_2 (z_1 - z_2) \tan\beta \left\{(z_1^2 + 4 z_1 z_2 + z_2^2) \tan^2\beta + (z_1^2 + z_2^2)\right\}$$

$$e = (z_1^2 - z_2^2) \ (z_1^2 z_2^2) \sec^2\beta \ (6 \sec^2\beta - 8)$$

The above polynomial in x has at least two real roots. These give the distances of the maximum and minimum of the second derivative from the fault trace.

The calculation of the roots of the polynomial is a long and tedious process. The problem, however, can be solved very easily in a digital computer. A computer program has been written which calculates the coefficients of the polynomial from given values of β, z_1 and z_2 and

then finds the roots of the polynomial to any degree of accuracy desired.

It is seen in Figure 37 that the amplitude of the minimum is very sensitive to change in the inclination of the block. Calculations of the position and amplitude of the minimum of the second derivative curve, therefore, will be very useful in determining the inclination of the fault plane.

The great amplifying effect of the second derivative on shallow structures is seen in Figure 36. Hence sharp maxima and minima of large amplitude are clear indications of a shallow structure.

Separate curves showing the positions and the magnitudes of the maximum and minimum due to a single block were not drawn since it will be seen later that the curves for a single block will approach very closely the curves due to a fault truncating a single bed when the lower block is at great depth. Hence these curves for large values of z_3 will be a very good approximation to curves for the second derivative for the upper block alone (see Figures 40-44).

The Second Horizontal Derivative Due To A Fault Truncating A Single Bed

The horizontal derivative of the gravity anomaly due to a fault truncating a single bed may be obtained by combining the effect of two individual beds on either side of the fault plane. Following the same procedure as in the case of the single block, therefore, the second derivative over such a fault is given by

$$\frac{d^2 g_f}{dx^2} = \frac{-G\rho}{x} (\cos 2\theta_2 - \cos 2\theta_1 + \cos 2\theta_3 - \cos 2\theta_4) \quad \ldots . \quad (8)$$

Limiting values of $\frac{d^2 g_f}{dx^2}$

Limiting value as $z_1 \longrightarrow 0$

Since $\tan \theta_1 = \tan\beta + \frac{x}{z_1}$,

at $z_1 = 0$, $\tan \theta_1 = \infty$, $\theta_1 = \frac{\pi}{2}$ hence

$$\cos 2\theta_1 = \cos \pi = -1$$

Hence

$$\lim_{z_1 \longrightarrow o} \frac{d^2 g_f}{dx^2} = \frac{-G\rho}{x} (1 + \cos 2\theta_2 + \cos 2\theta_3 - \cos 2\theta_4)$$

Limiting value as $x \longrightarrow 0$

We have

$$\lim_{x \longrightarrow o} \frac{d^2 g_f}{dx^2} = -\lim_{x \longrightarrow o} \frac{G\rho}{x} (\cos 2\theta_2 - \cos 2\theta_1 + \cos 2\theta_3 - \cos 2\theta_4)$$

Substituting $\cos 2\theta_i = \dfrac{1 - \tan^2\theta_i}{1 + \tan^2\theta_i}$, $\tan\theta_i = \tan\beta + \dfrac{x}{z_i}$,

We have

$$\lim_{x \longrightarrow o} \frac{d^2 g_f}{dx^2} = -\lim_{x \longrightarrow o} \left[\frac{2G\rho}{x} \frac{2x\tan\beta\left(\frac{1}{z_1} - \frac{1}{z_2}\right) + x^2\left(\frac{1}{z_1^2} - \frac{1}{z_2^2}\right)}{\left(\sec^2\beta + \frac{x^2}{z_1^2} + 2\tan\beta\,\frac{x}{z_1}\right)\left(\sec^2\beta + \frac{x^2}{z_2^2} + 2\tan\beta\,\frac{x}{z_2}\right)} \right.$$

$$\left. - \frac{2G\rho}{x} \frac{2x\tan\beta\left(\frac{1}{z_3} - \frac{1}{z_4}\right) + x^2\left(\frac{1}{z_3^2} - \frac{1}{z_4^2}\right)}{\left(\sec^2\beta + \frac{x^2}{z_3^2} + 2\tan\beta\,\frac{x}{z_3}\right)\left(\sec^2\beta + \frac{x^2}{z_4^2} + 2\tan\beta\,\frac{x}{z_4}\right)} \right]$$

$$= \frac{-4G\rho\tan\beta}{\sec^4\beta}\left(\frac{1}{z_1} - \frac{1}{z_2} - \frac{1}{z_3} + \frac{1}{z_4}\right)$$

If the displacement is very large in the above expression, z_3 and z_4 are large compared with z_1 and z_2, hence $\dfrac{1}{z_3}$ and $\dfrac{1}{z_4}$ can be neglected. Therefore, for a fault with large displacement, the limiting value of the second derivative at $x = 0$, is given by

$$\lim_{x \to o} \frac{d^2 g_f}{dx^2} = -2G\rho t \sin 2\beta \cos^2\beta \left(\frac{1}{z_1 z_2}\right)$$

This is the same expression as the limiting value of the second derivative over a single block at x = 0.

Points on the x-axis where $\frac{d^2 g_f}{dx^2} = 0$

Equating the expression for the second derivative to zero, we obtain

$$\frac{d^2 g_f}{dx^2} = \frac{-G\rho}{x}(\cos 2\theta_2 - \cos 2\theta_1 + \cos 2\theta_3 - \cos 2\theta_4) = 0$$

Thus at the point where the second derivative vanishes, we must have

$$\cos 2\theta_2 - \cos 2\theta_1 = \cos 2\theta_4 - \cos 2\theta_3$$

Substituting for $\cos 2\theta_i$ in terms of x, z_i and β in the above expression and writing $q_i = x/z_i$ where i = 1, 2, 3, 4, we have

$$\cos 2\theta_2 - \cos 2\theta_1 = (\cos 2\theta_2 + 1) - (\cos 2\theta_1 + 1)$$

$$= 2\left(\frac{1}{1 + \tan^2\theta_2} - \frac{1}{1 + \tan^2\theta_1}\right)$$

$$= 2\left[\frac{(\tan\beta + q_1)^2 - (\tan\beta + q_2)^2}{\left\{1 + (\tan\beta + q_2)^2\right\}\left\{1 + (\tan\beta + q_1)^2\right\}}\right]$$

$$= 2\left[\frac{(q_1^2 - q_2^2) + 2(q_1 - q_2)\tan\beta}{\sec^4\beta + (q_1^2 + q_2^2)\sec^2\beta + 2(q_1 + q_2)\tan\beta\sec^2\beta + 2q_1q_2\tan^2\beta + 2q_1q_2(q_1 + q_2)\tan\beta + q_1^2q_2^2}\right]$$

$$= D(q_1, q_2)$$

At the point where the second derivative vanishes we must have

$$D(q_1 , q_2) = D(q_3 , q_4)$$

By cross-multiplying the above expression on either side of the equal sign and collecting like powers of x we obtain a polynomial of the 5th degree in x of the form

$$ax^5 + bx^4 + cx^3 + dx^2 + ex + f = 0$$

where the coefficients a, b, c, d, e and f are given by

$$a = 2(z_2 - z_1)(z_1 - z_3)$$

$$b = 2(z_2 - z_1)(z_1 z_2 - z_3 z_4)\tan\beta$$

$$c = 2(z_2^2 z_3^2 - z_1^2 z_4^2)\sec^2\beta$$

$$d = 4(z_1 + z_4)(z_3^2 z_2^2 - z_1^2 z_4^2)\tan\beta\sec^2\beta$$

$$e = (z_2 - z_1)\Big\{ z_3^2 z_4^2 (z_1 + z_2) - z_1^2 z_2^2 (z_3 + z_4) + 8 z_1 z_2 z_3 z_4 (z_2 z_3 - z_1 z_4)\tan^2\beta\sec^2\beta \Big\}\sec^4\beta$$

$$f = 2(z_2 - z_1)(z_1 z_2 z_3 z_4)(z_3 z_4 - z_1 z_2)\tan\beta\sec^4\beta$$

The above polynomial has at least one real root which gives the position on the x-axis where the second derivative becomes zero. A program was written which first calculates the five coefficients from the given values of z_1 , z_2 , z_3 , z_4 and β , then calculated the roots of the polynomial by the Newton-Raphson method.

Figure 38 shows the second derivative graph over a fault which

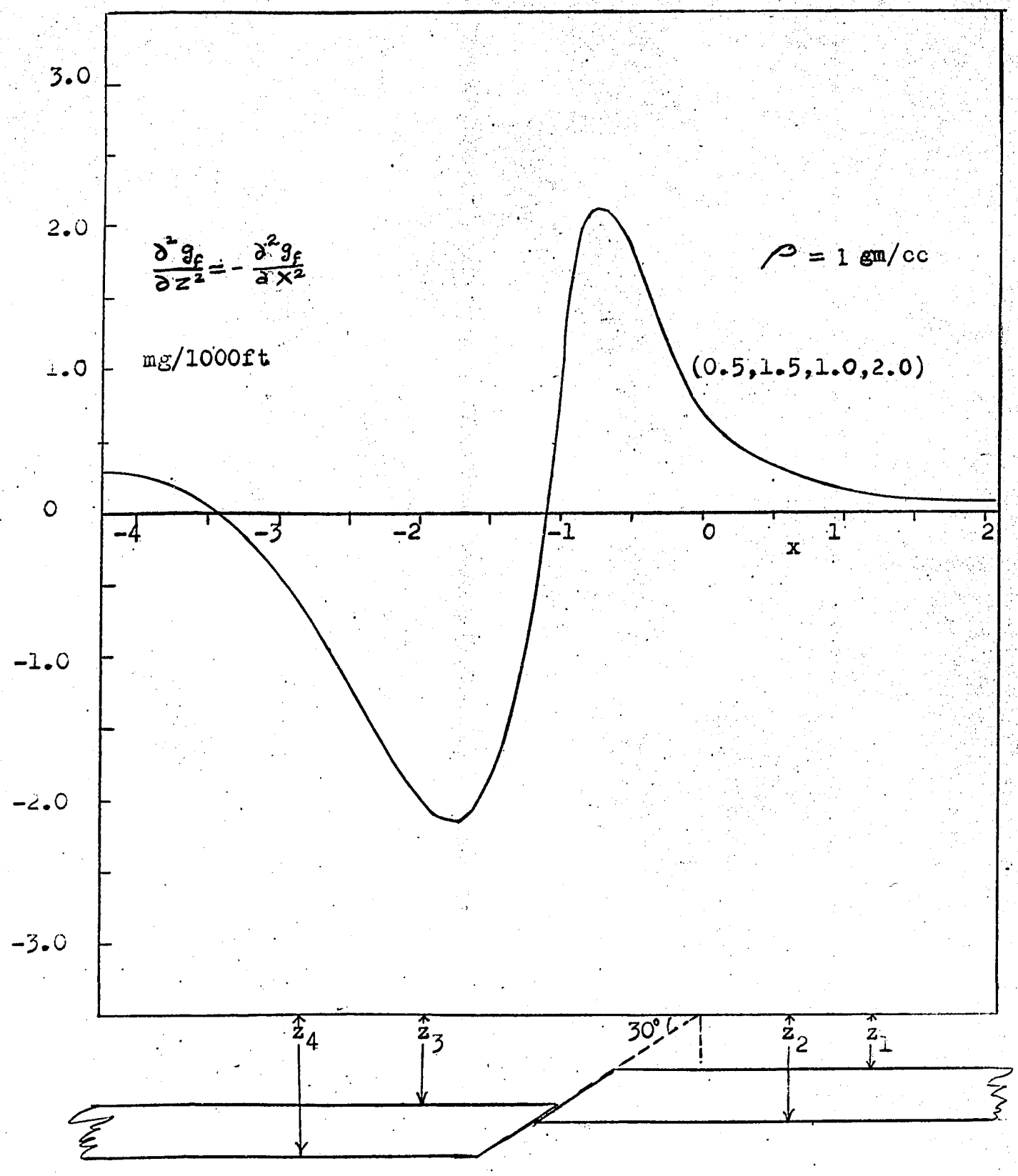

FIG 38. Effect of dip on the second derivative over a fault

cuts a single bed, the plane of the fault making an angle of 60° with the vertical. The depths from the surface to the four horizons z_1, z_2, z_3, and z_4 are 0.5, 1.0, 1.5 and 2.0 units. The second derivative graph shows two zero points - the first one close to the fault trace and the second one further away on the down-thrown side of the fault. On opposite sides of the first zero point there is a maximum and a minimum located at the points $x = -0.7$ and $x = -1.75$. The magnitudes of the two extrema are almost the same, the minimum being slightly higher than the maximum.

Maxima and Minima of $\frac{d^2g_f}{dx^2}$: To find the distance of the minimum and maximum from the fault trace, we solve the equation $\frac{d}{dx}\left(\frac{d^2g_f}{dx^2}\right) = 0$ by the Newton-Raphson method as mentioned above.

The Newton-Raphson method is based on the assumption that the curve has no inflexion point along QP (see Figure 39). The function f(x), whose roots we are interested in finding, has an inflexion point which is near the point x_o where $\frac{d^2g_f}{dx^2}$ is zero. After finding x_o, we choose two starting points, one $(x_o + \Delta x)$ and the other $(x_o - \Delta x)$ where Δx is a small quantity which keeps the starting points of the Newton-Raphson calculations away from the inflexion point of f(x). The quantity Δx is obtained by trial and error. In this way, after a few iterations, two roots of f(x) may be obtained giving x_{max} and x_{min}, the abscissae of the maximum and minimum of the second derivative. After calculating the roots of the equation, the computer calculates the values of the

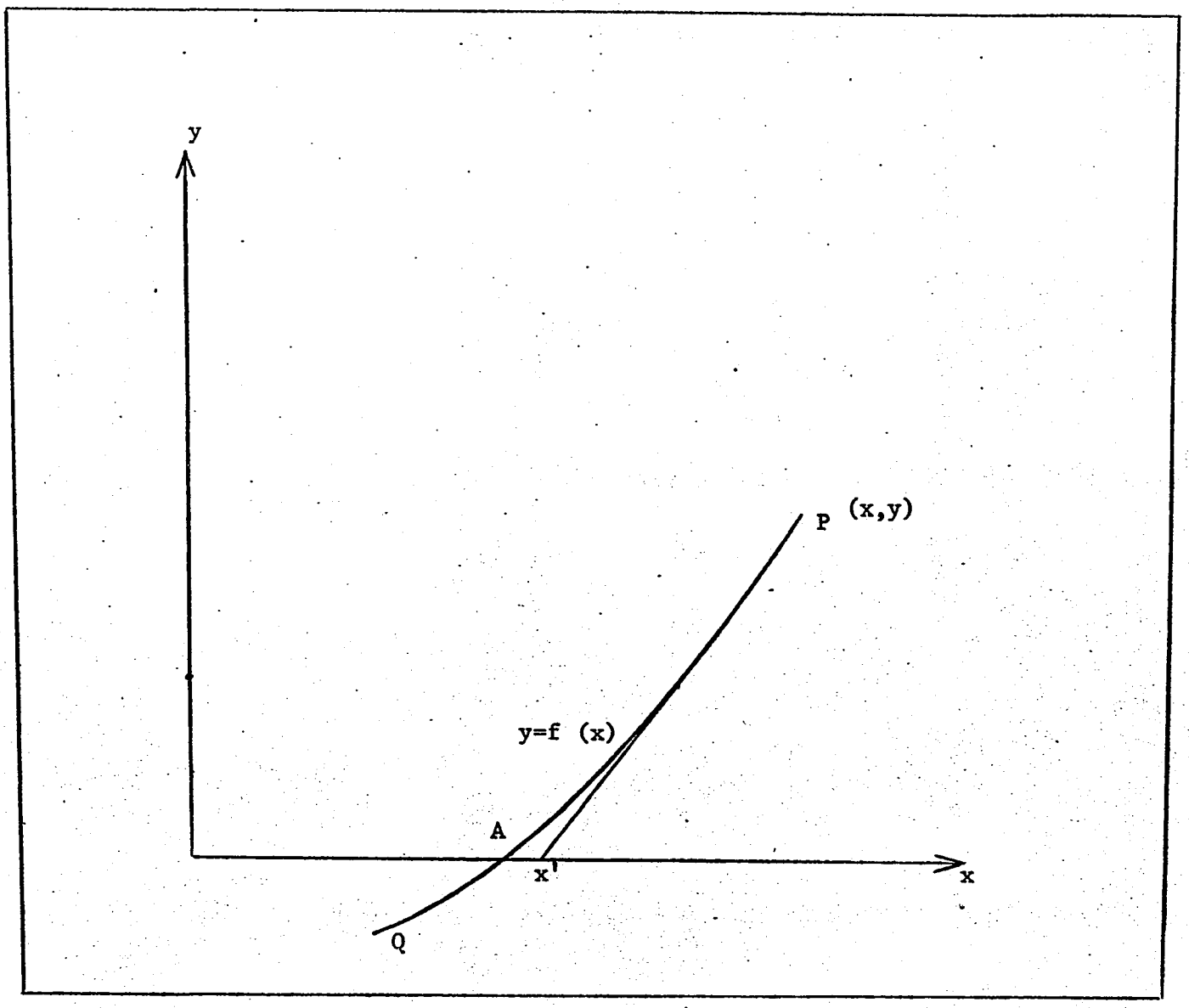

Figure 39. Calculation of roots of a polynomial by the Newton-Raphson method

of the second derivative at these points, thus giving the maximum and the minimum values of the second derivative. The equation $\frac{d}{dx}\left(\frac{d^2 g_f}{dx^2}\right)$ whose roots are obtained by the Newton-Raphson method to get x''_{max} and x''_{min} is derived in Appendix C.

Figures 40-44 show the graphs of the amplitude versus abscissae of the second derivative maximum and minimum. Figure 40 refers to a vertical fault. Since for a vertical fault the two extrema are equal in amplitude and symmetrical about the fault trace, the curve corresponds to both the maximum and minimum second derivative. In this figure, z_1, the depth to the upper block of the faulted bed, is kept fixed, while the lower block is moved downwards in successive steps to a maximum depth of 32 units. The two numbers at the ends and to the left of each curve refer to the minimum and maximum values of z_3. It is seen in Figure 40 that, for small values of z_1, the magnitude of the second derivative increases much more rapidly than does its position as z_3 is increased, while for large values of z_1, the magnitude and position of the second derivative change equally rapidly as z_3 changes. Furthermore, as z_3 is increased keeping z_1 fixed, a condition is eventually reached where any further increase in z_3 produces very little change either in the magnitude or position of the second derivative extrema. Points in these curves for the largest value of z_3, therefore, will give a good approximation to the position and magnitude of the second derivative extrema for a single faulted block of thickness one unit whose upper surface is at a depth as shown in the curves.

Figures 41 and 42 are the plots of the amplitude of the second

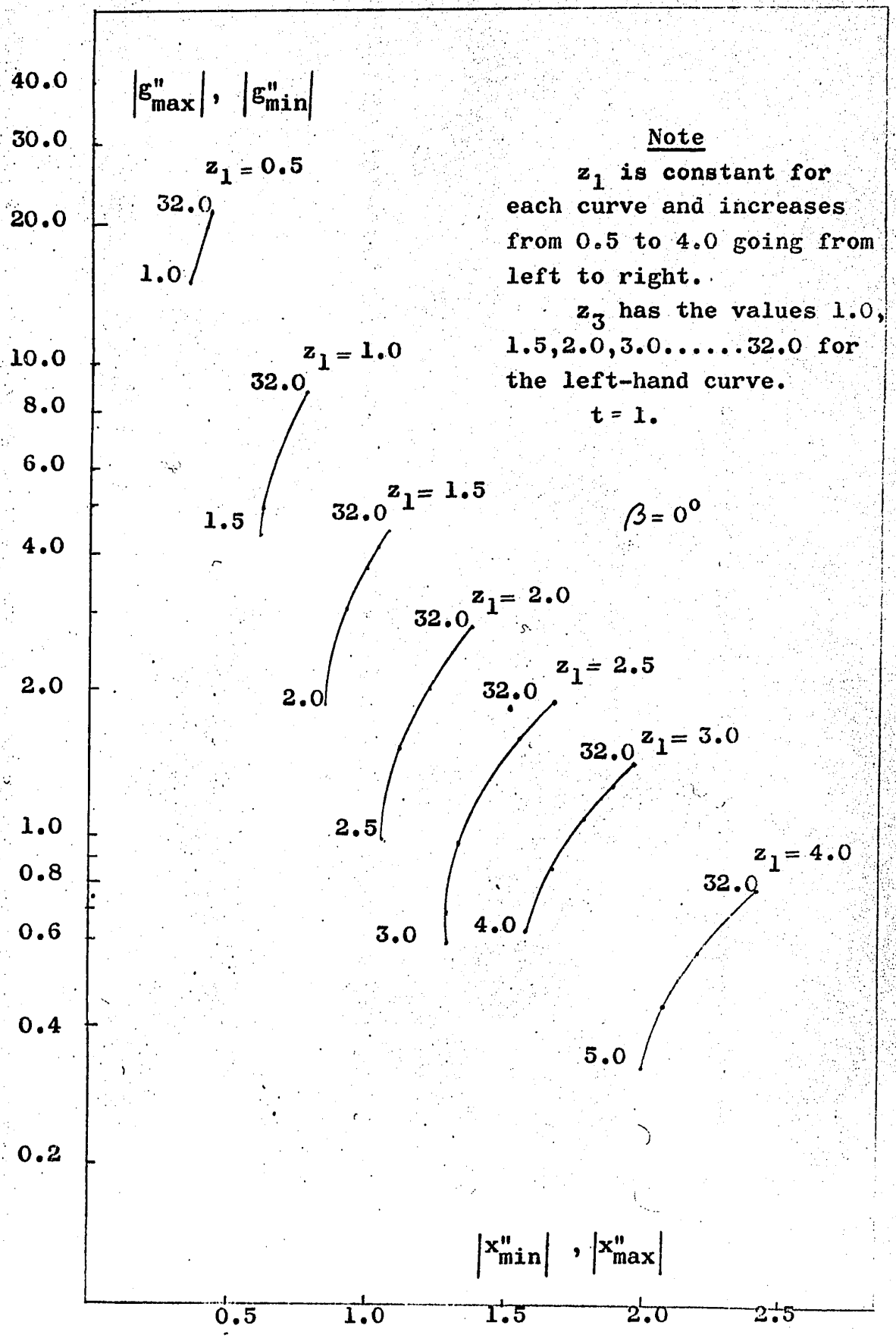

FIG 40. Variation of size and position of second derivative maxima or minima with z_1 and z_3 for a vertical fault.

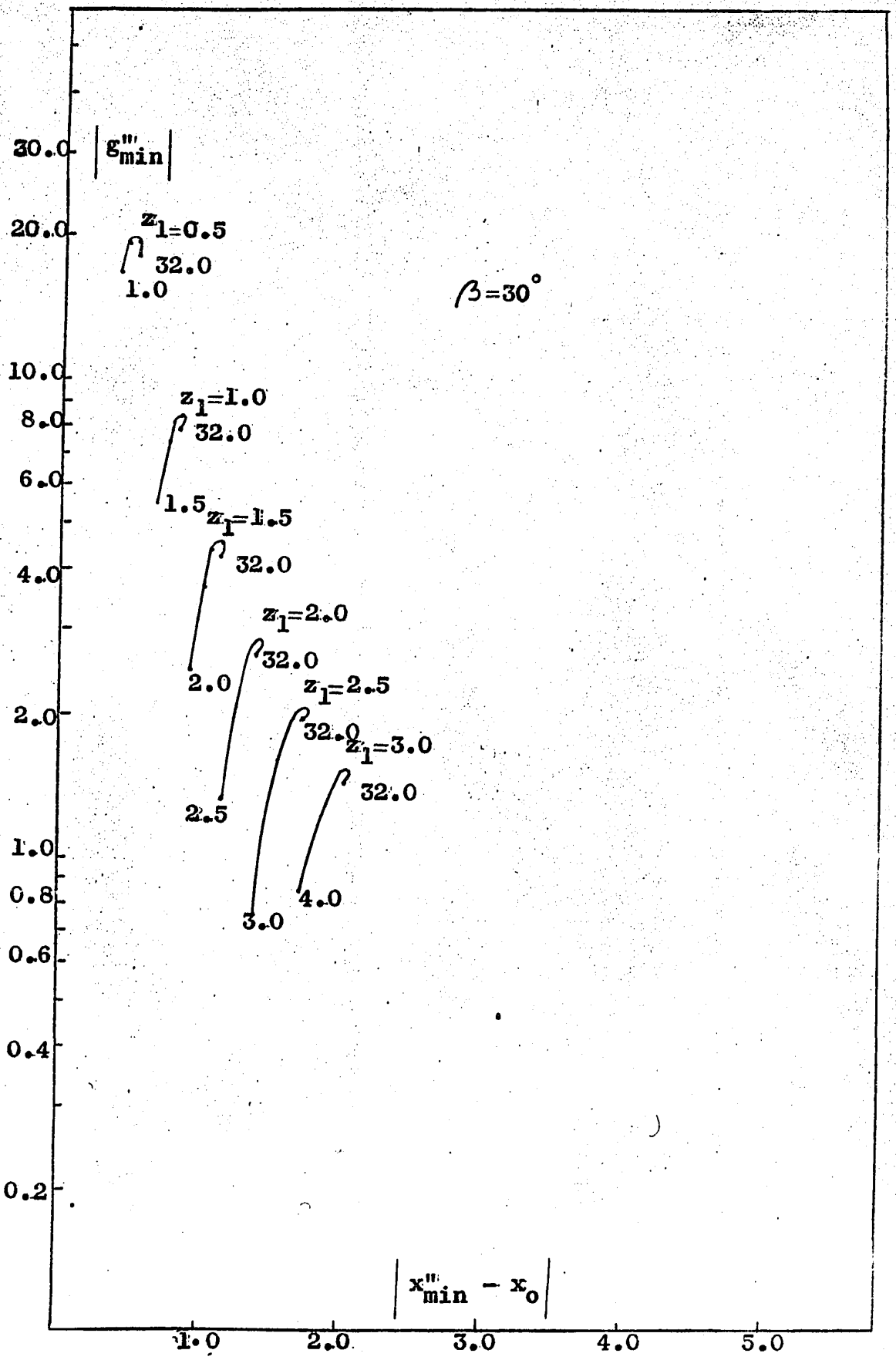

FIG 41. Variation of size and position of second derivative minimum with z_1 and z_3 for $\beta = 30^\circ$.

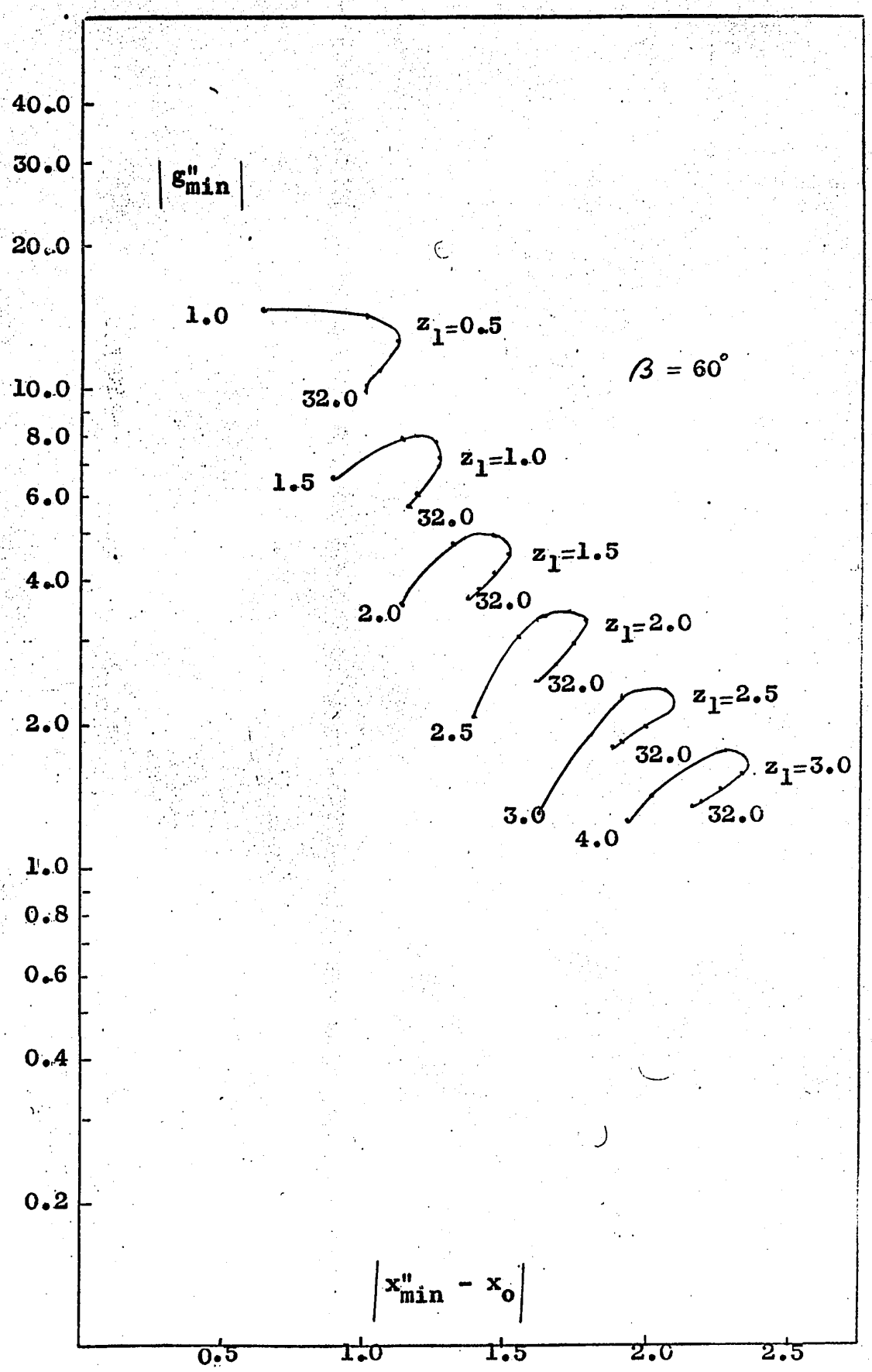

FIG 42. Variation of size and position of second derivative minimum with z_1 and z_3 for $\beta = 60^\circ$.

derivative minimum due to a fault dipping at 30° and 60°. The abscissae in these curves, however, are not x''_{min} but $(x''_{min} - x_o)$ (this quantity is the distance between the minimum and the point where the second derivative vanishes, hence can be obtained from the observed data whereas to find x''_{min} we must know the location of the fault trace). The numbers beside each curve have the same meaning as in Figure 40. Unlike the curves for the vertical fault, the curves in these two figures show that, as z_3 is increased keeping z_1 fixed, the amplitude of the second derivative minimum attains a maximum value, then swings around and decreases slowly, so that further increase in z_3 does not produce large changes either in g''_{min} or x''_{min}.

The curves in Figures 43 and 44 show the amplitudes of the maximum second derivative plotted as a function of $(x''_{max} - x_o)$ for the same series of faults as in the case of the minimum. For the range of values of the parameters chosen for these curves, the maximum second derivative does not show any turning point and it appears to be a curve with slowly varying slope.

The curves in Figures 40-44 are for the same series of faults as those in Figures 18-23 which give the position and size of the gravity maximum and minimum. In Figures 40-44 the faults at zero depths have been omitted since, when the upper block reaches the surface of the earth, the second derivative extrema become infinitely large at $x = 0$.

Figure 45 shows three profiles across a fault cutting a bed of thickness 0.5 unit, the upper block of the faulted bed being at the

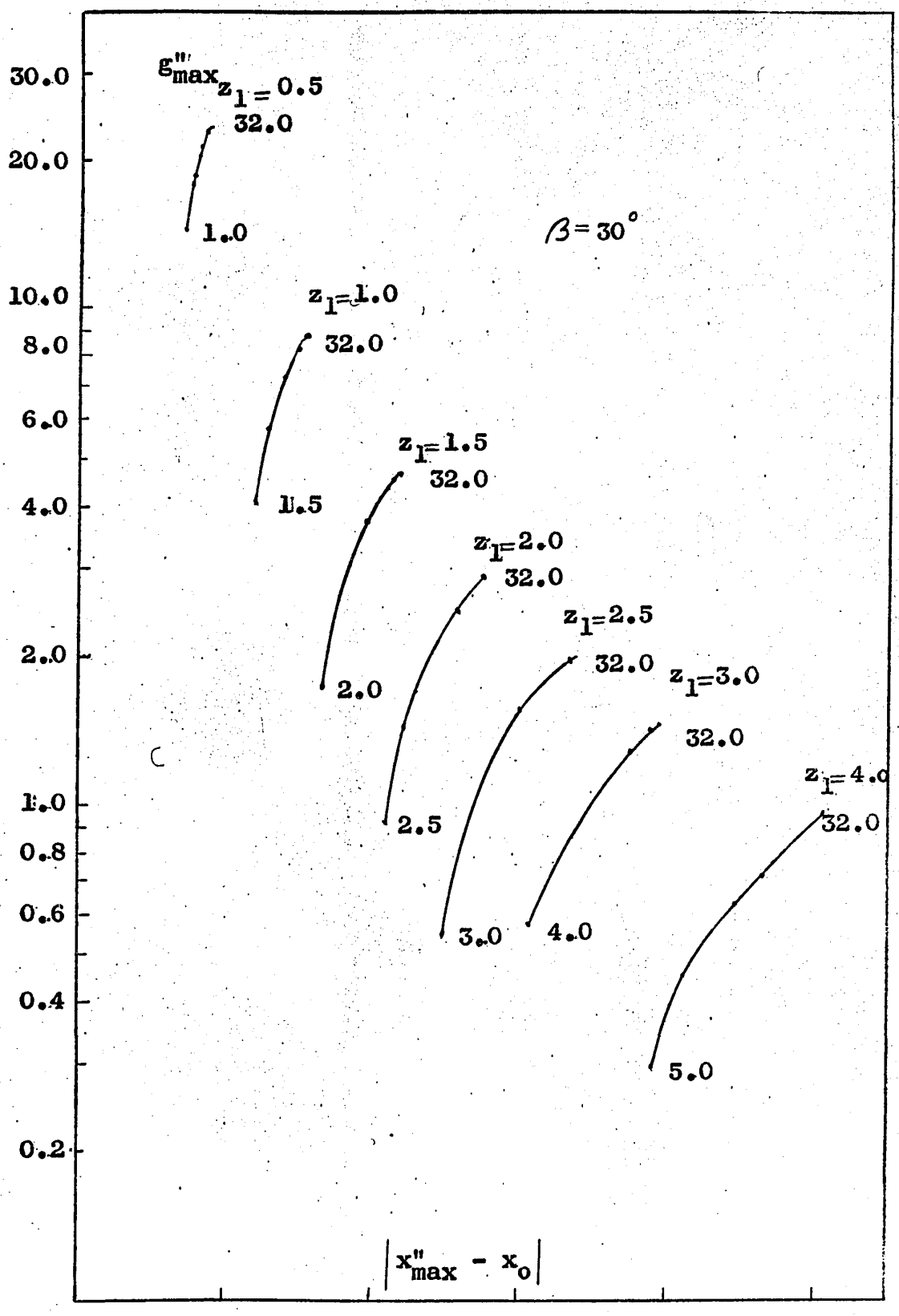

FIG 43. Variation of size and position of second derivative maximum with z_1 and z_3 for $\beta = 30^\circ$.

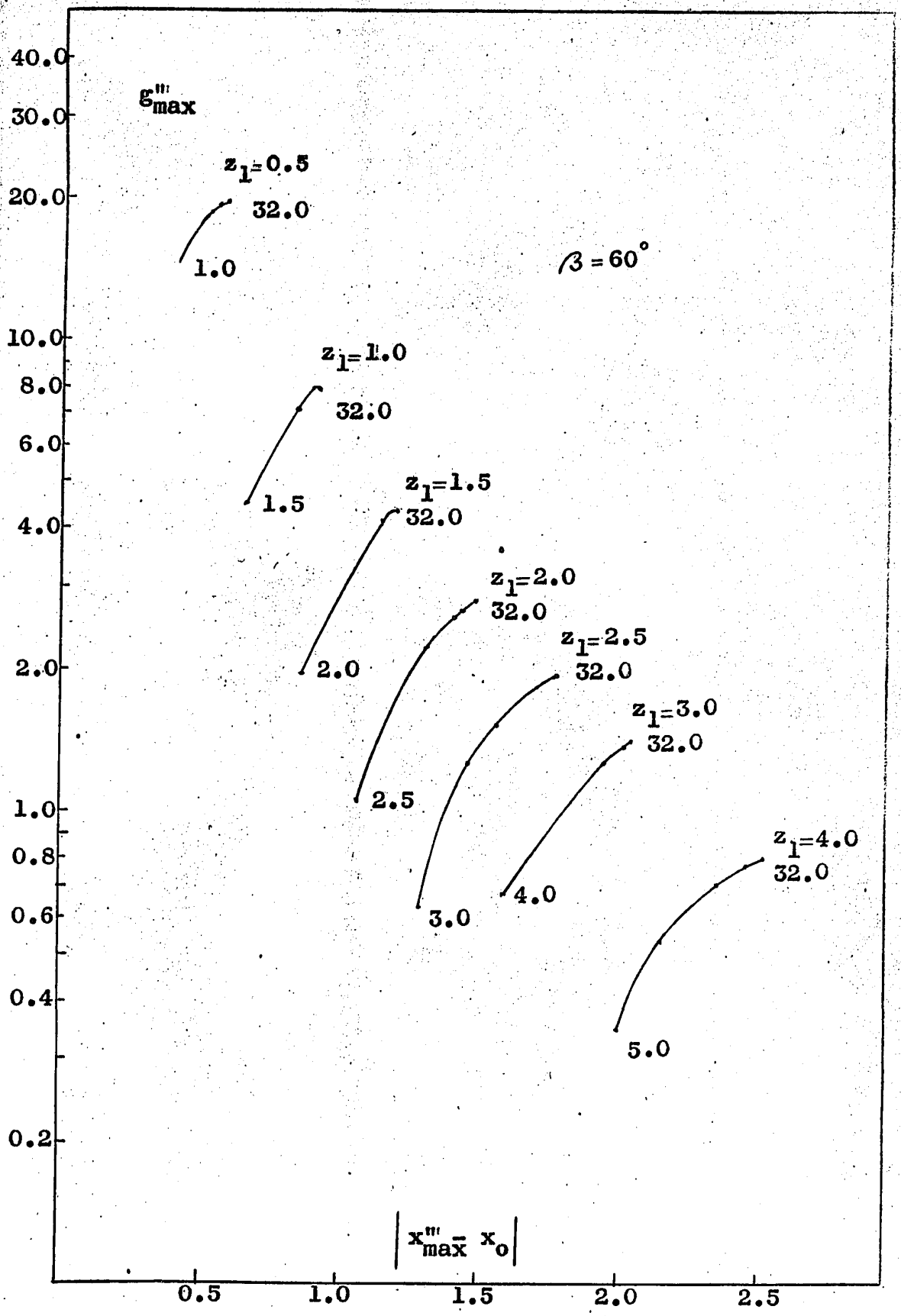

FIG 44. Variation of size and position of second derivative maximum with z_1 and z_3 for $\beta = 60°$.

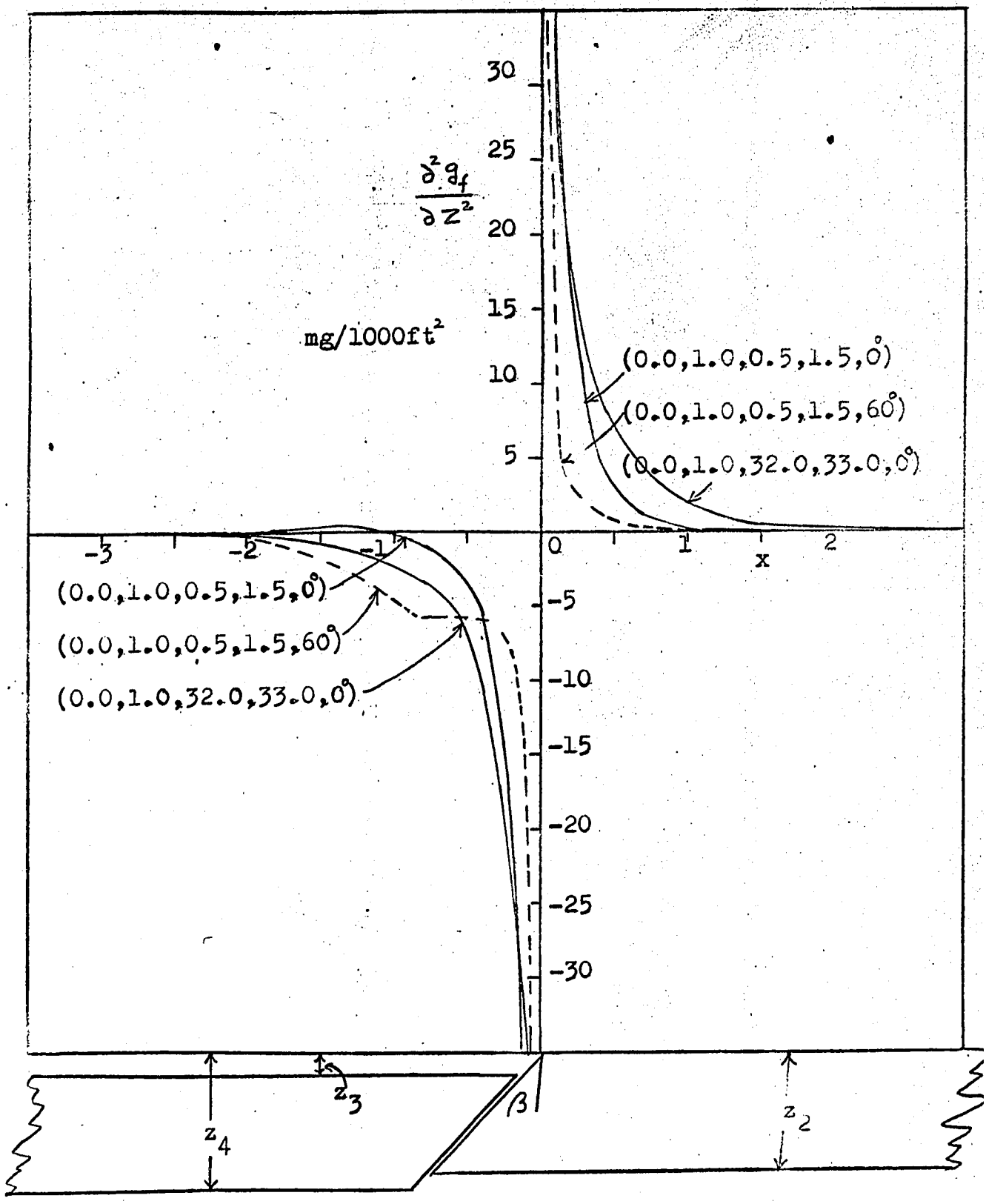

FIG 45 The second derivative over faults when the upper block reaches the surface

surface of the earth. The second derivative becomes infinitely large at $x = 0$ but decreases very rapidly as we go away from the trace and is essentially zero at distances of 2 units or more. The effect on the second derivative of lowering the second block to a depth of 32 units is shown by curve (2) of Figure 45. The general shape of this curve is the same as curve (1) but the decrease in the second derivative as we go away from the fault trace is not as rapid.

In curve (3) the fault has a dip of 30°. The dip causes some changes in the second derivative values near the inclined face of the fault, but the dominant features of this curve are the same as those of the other two curves.

The Vertical Gradient Of Gravity

(a) The vertical gradient of gravity due to a single block and a fault:

The expression for the vertical gradient of gravity due to a single block is derived in Appendix D, the result being

$$\frac{\partial g_s}{\partial z} = -2G\rho\cos^2\beta\left\{\frac{1}{2}\tan\beta\,\log\left(\frac{q_2^2\cos^2\beta + q_2\sin 2\beta + 1}{q_1^2\cos^2\beta + q_1\sin 2\beta + 1}\right)\right.$$

$$\left. + \tan^{-1}\left(\frac{q_2\tan\beta + \sec^2\beta}{q_2}\right) - \tan^{-1}\left(\frac{q_1\tan\beta + \sec^2\beta}{q_1}\right)\right\} \quad \ldots\ldots (9)$$

where $q_i = \frac{x}{z_i}$ as before.

The vertical gradient of gravity due to a fault cutting a single bed is also derived in Appendix D and is given by

$$\frac{\partial g_f}{\partial z} = (-2G\rho\cos^2\beta)\left[\frac{1}{2}\tan\beta\,\log\left\{\left(\frac{q_2^2\cos^2\beta + q_2\sin 2\beta + 1}{q_1^2\cos^2\beta + q_1\sin 2\beta + 1}\right)\left(\frac{q_3^2\cos^2\beta + q_3\sin 2\beta + 1}{q_4^2\cos^2\beta + q_4\sin 2\beta + 1}\right)\right\}\right.$$

$$+ \tan^{-1}\left(\frac{q_2\tan\beta + \sec^2\beta}{q_2}\right) - \tan^{-1}\left(\frac{q_1\tan\beta + \sec^2\beta}{q_1}\right)$$

$$\left. + \tan^{-1}\left(\frac{q_3\tan\beta + \sec^2\beta}{q_3}\right) - \tan^{-1}\left(\frac{q_4\tan\beta + \sec^2\beta}{q_4}\right)\right] \quad \ldots\ldots (10)$$

Figure 46 shows the curves of the vertical gradient of gravity for several single blocks and faults. The solid line curves of Figure 46 correspond to vertical faults while the dashed line curves are for faults dipping at 30°. It is evident that the shallower blocks have much greater vertical gradient anomalies than the deeper blocks showing that vertical gradient accentuates shallow structures. Comparing the curves in Figure 46 with those in Figure 36, page 83, for the second derivative effect over single blocks, it is seen that the second derivative effect is confined to a small region near the fault plane while the vertical gradient effect extends to far greater distances. Furthermore, as the depth of burial of the anomalous mass varies, the change in the second derivative is much larger than that of the vertical gradient.

The dashed line curve in Figure 46 shows that as the angle of dip of the fault plane increases towards 90°, the maximum and the minimum of the vertical gradient are shifted towards the inclined faces of the fault plane.

The limiting value of the vertical gradient as x approaches zero is derived in Appendix D and is given by:

$$\left(\frac{\partial g_s}{\partial z}\right)_{x=o} = G\rho \sin 2\beta \log\left(\frac{z_2}{z_1}\right)$$

and

$$\left(\frac{\partial g_f}{\partial z}\right)_{x=o} = G\rho \sin 2\beta \log \frac{z_2 z_3}{z_1 z_4}$$

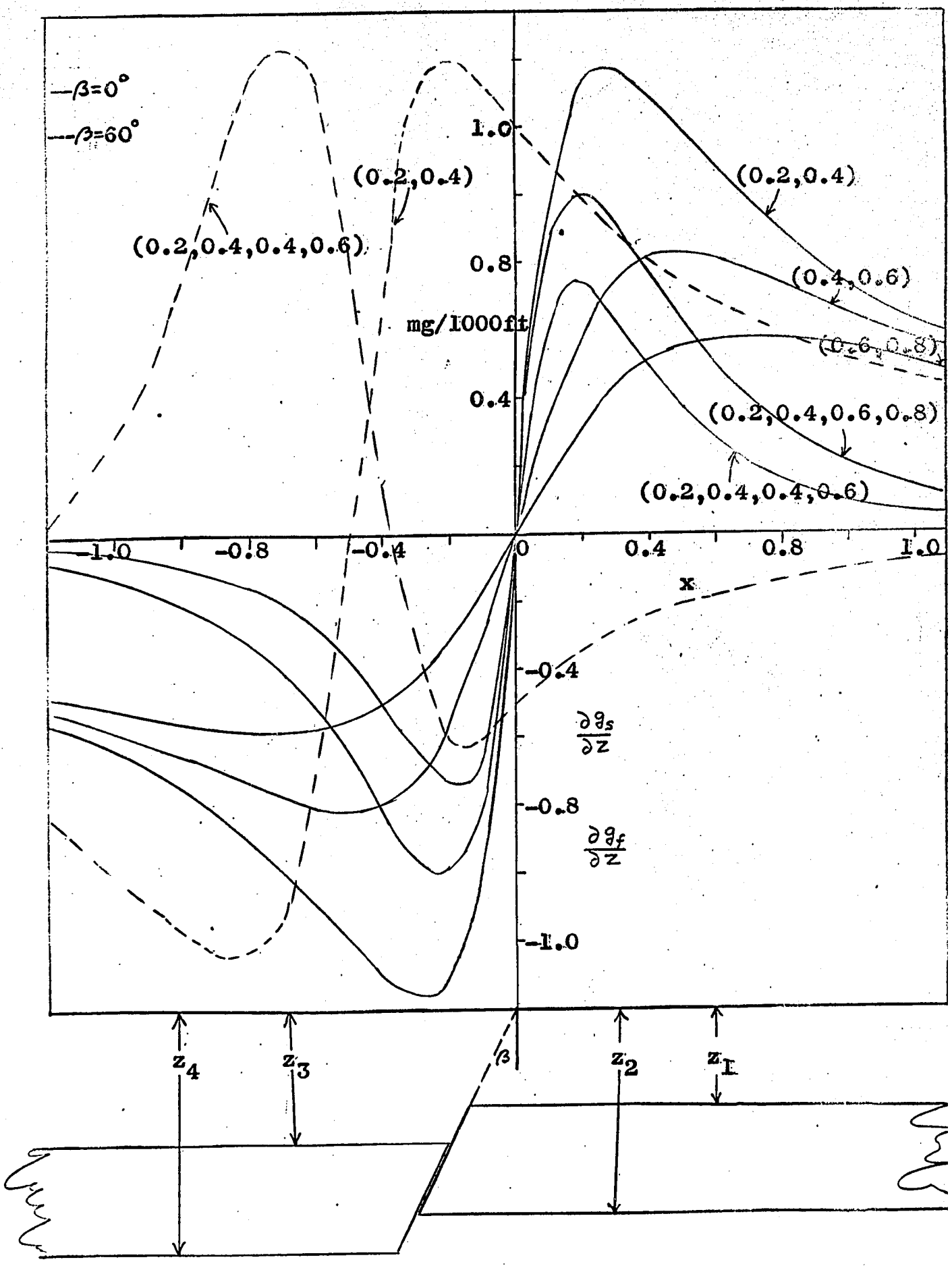

FIG 46. The vertical gradient of gravity over single blocks

This shows that, knowing the vertical gradient of gravity directly over the fault trace, we can obtain information about the angle of inclination of the fault plane and the depths to the different geologic horizons from the surface of the earth.

Equations 9 and 10 giving the vertical gradient of gravity for a single block and a fault are more complicated than the corresponding equations 7 and 8 giving the second derivative effect over a single block and a fault. Since the properties of the vertical gradient are not greatly different from those of the second derivatives, the use of the vertical gradient for interpreting faults will not be discussed further.

CHAPTER IV

The Fourier Transform Of Gravity Data

General: For a two-dimensional body, the gravity anomaly is usually expressed as a function of the distance, x. By making a Fourier transformation, the gravity anomaly can be transformed from the original distance domain, x, into the frequency domain, ω. If we transform the data into the frequency domain, then carry out the interpretation, we obtain certain advantages over interpretation based on the raw data; firstly, in transforming into the frequency domain, an entirely new function is obtained which is more easily handled than the original function; secondly, in calculating the Fourier transform, all available gravity data are used so that none of the gravity data are rejected in the interpretation.

Odegard and Berg (1965) have made frequency analysis of gravitational fields of several bodies of simple geometric shapes, such as the cylinder, the sphere, the single block with a vertical edge, and have shown how the depth and size of the causative body may be obtained from the Fourier transform of the gravity data.

The basic transform formula discussed in this section is the transform of equation (1). The Fourier transform of the right-hand side of (1) is not readily calculable; however, we can calculate the transform of the second derivative, and from this transform we can easily obtain the transform of g.

Fourier transforms: The Fourier transform of the function f(x) is defined by the relation

$$F(\omega) = \int_{-\infty}^{\infty} f(x)e^{-j\omega x}dx \qquad \ldots\ldots (11)$$

provided the integral exists for all real values of ω. The Fourier transform, $F(\omega)$, is in general a complex quantity, that is,

$$F(\omega) = R(\omega) + jX(\omega) = A(\omega)e^{j\phi(\omega)},$$

$R(\omega)$, $X(\omega)$, $A(\omega)$ and $\phi(\omega)$ being real functions of ω. $A(\omega)$ and $\phi(\omega)$ are called the Fourier spectrum and phase of f(x). The function f(x) can be obtained from the transform, $F(\omega)$, through the formula

$$f(x) = \frac{1}{2\pi}\int_{-\infty}^{\infty} F(\omega)e^{j\omega x}d\omega \qquad \ldots\ldots (12)$$

The notation $f(x) \longleftrightarrow F(\omega)$ is used to indicate that f(x) and $F(\omega)$ are transform pairs. The Fourier transform of f(x) will also be written in the operator form $F\{f(x)\}$ on occasion.

By differentiating both sides of equation (12) with respect to x, it will be seen that

$$\frac{d^n}{dx^n} f(x) \longleftrightarrow (j\omega)^n F(\omega) \qquad \ldots\ldots (13)$$

Fourier transform of $\dfrac{d^2 g_s}{dx^2}$

As mentioned earlier, the Fourier transform of the right side of

(1) is difficult to obtain. We shall, therefore, calculate the transform of the second derivative, $\frac{d^2 g_s}{dx^2}$, and use (13) to obtain the transform of g.

Writing K for (Gρ), the expression given in Appendix A for the second derivative of g_s can be written

$$\frac{d^2 g_s}{dx^2} = \frac{-K}{x}(\cos 2\theta_2 - \cos 2\theta_1)$$

$$= \frac{-K}{x}\left\{(1 + \cos 2\theta_2) - (1 + \cos 2\theta_1)\right\}$$

$$= \frac{-2K}{x}\left\{(1 + \tan^2\theta_2)^{-1} + (1 + \tan^2\theta_1)^{-1}\right\}$$

$$= \frac{-2K}{x}(H_2 - H_1) \qquad \ldots\ldots (14)$$

where $H_i = (1 + \xi_i^2)^{-1}$; $\xi_i = \tan\theta_i = a + \frac{x}{z_i}$, $a = \tan\beta$, $i = 1, 2$.

If we write $F_{2s}(\omega)$ for the Fourier transform of the expression in (14), then we have the following transform pairs:

$$\frac{d^2 g_s}{dx^2} \longleftrightarrow F_{2s}(\omega)$$

$$\frac{dg_s}{dx} \longleftrightarrow \frac{F_{2s}(\omega)}{j\omega} \qquad \ldots\ldots (15)$$

$$g_s \longleftrightarrow \frac{F_{2s}(\omega)}{(j\omega)^2}$$

When calculating $F_{2s}(\omega)$, the constant term $2G\rho(\pi - \alpha)t$ does not enter into the calculations, hence it will not appear in the transform for g_s.

The Fourier transform of the function $\frac{d^2g_s}{dx^2}$ is derived in Appendix E where it is shown that the real and imaginary parts of the transform $F_{2s}(\omega)$ for a single block are given by

$$R_{2s}(\omega) = c\ Me^{-\omega z_1}\sin(h_1 + \phi) \quad \ldots\ldots (16a)$$

$$X_{2s}(\omega) = -c\ Me^{-\omega z_1}\cos(h_1 + \phi) \quad \ldots\ldots (16b)$$

where $M = \{1 - 2e^{-\omega T}\cos(\omega aT) + e^{-2\omega T}\}^{1/2}$

$$\tan\phi = \frac{\sin(\omega aT)}{\cos(\omega aT) - e^{\omega T}}$$

$T = z_2 - z_1$ = Thickness of the bed

$h_1 = \omega z_1 a + \beta$

Fourier transform of $\frac{d^2g_f}{dx^2}$

The real and imaginary parts of the transform for a fault cutting a single bed are also given in Appendix E and are equal to

$$R_{2f}(\omega) = c\ MNe^{-\omega z_1}\sin(h_1 + \phi + \eta) \quad \ldots\ldots (17a)$$

$$X_{2f}(\omega) = -c\ MNe^{-\omega z_1}\cos(h_1 + \phi + \eta) \quad \ldots\ldots (17b)$$

where $N = \{1 - 2e^{-\omega\delta}\cos(\omega a\delta) + e^{-2\omega\delta}\}^{1/2}$

$$\tan\eta = \frac{\sin(\omega a\delta)}{\cos(\omega a\delta) - e^{\omega\delta}}$$

$\delta = z_3 - z_1$ = Vertical displacement of the fault.

In the above expression of the Fourier transform of a fault, it we let δ go to infinity, the transforms* $R_{2f}(\omega)$ and $X_{2f}(\omega)$ will approach the transform of the anomaly due to the upper block alone. Hence transforms for single blocks may be obtained from the transforms for a fault by assuming the fault to have infinite displacement.

Fourier spectrum $A_{2f}(\omega)$

The Fourier spectrum $A_{2f}(\omega)$ of the fault anomaly may be written as

$$A_{2f}(\omega) = \left\{ R_{2f}^2(\omega) + X_{2f}^2(\omega) \right\}^{1/2}$$

$$= c\, MNe^{-\omega z_1} \qquad \ldots\ldots \quad (18a)$$

$$\text{Hence Log } A_{2f}(\omega) = \text{Log } c - \omega z_1 + \frac{1}{2} \text{Log} \left\{ 1 + e^{-2\omega T} - 2e^{-\omega T} \cos(\omega a T) \right\}$$

$$+ \frac{1}{2} \text{Log} \left\{ 1 + e^{-2\omega\delta} - 2e^{-\omega\delta} \cos(\omega a \delta) \right\}$$

$$\ldots\ldots \quad (18b)$$

If $\omega >> T$ and $\omega >> \delta$, the graph of $\log A_{2f}(\omega)$ versus ω is approximately a straight line. Hence for sufficiently large values of ω ,

---

* Strictly speaking, $R(\omega)$ and $X(\omega)$ are not transforms but merely the real and imaginary parts of a transform; however, it is convenient to refer to them as transforms and this practice will be followed in subsequent pages.

$$\text{Log } A_{2f}(\omega) = \text{Log } c - \omega z_1$$

$$z_1 = \frac{d}{d\omega} \text{Log } A_{2f}(\omega)$$

Also the intercept of the straight line at $\omega = 0$ gives the result $A_{2f}(0) = c = 2\pi G\rho\cos\beta$. Thus, from the graph of log $A_{2f}(\omega)$ for large values of ω, we can find z_1 from the slope and β from the intercept, the latter requiring a knowledge of ρ as well.

Fourier transform of $\frac{d^2 g_m}{dx^2}$

From equation (3) it can be seen that the gravity anomaly, g_m, of a fault truncating a series of N beds is equivalent to the combined gravity anomaly due to N + 1 single blocks each of thickness δ, the blocks being at depths $z_1, z_2, \ldots\ldots z_{N+1}$ and having density contrasts $(\sigma_1 - \sigma_0), (\sigma_2 - \sigma_1), \ldots\ldots (\sigma_r - \sigma_N)$ respectively. Formulas (16a) and (16b) can be used to calculate the Fourier transform of each block individually and then the real and imaginary parts of the N + 1 blocks can be added up separately to give and real and imaginary parts of the transform of $\frac{d^2 g_m}{dx^2}$.

Consequently, the real and the imaginary parts of the transform of $\frac{d^2 g_m}{dx^2}$ are given by

$$R_{2m}(\omega) = cR\Big\{\rho_1 e^{-\omega z_1}\sin(h_1+\phi) + \rho_2 e^{-\omega z_2}\sin(h_2+\phi) + \ldots\ldots + \rho_{N+1} e^{-\omega z_{N+1}}\sin(h_{N+1}+\phi)\Big\} \quad \ldots\ldots \text{(19a)}$$

$$X_{2m}(\omega) = -cR\Big\{\rho_1 e^{-\omega z_1}\cos(h_1+\phi) + \rho_2 e^{-\omega z_2}\cos(h_2+\phi) + \ldots\ldots + \rho_{N+1} e^{-\omega z_{N+1}}\cos(h_{N+1}+\phi)\Big\} \quad \ldots\ldots \text{(19b)}$$

where $R = \left\{1 - 2e^{-\omega\delta}\cos(\omega\delta\tan\beta) + e^{-2\omega\delta}\right\}^{1/2}$

$$\tan\phi = \frac{\sin(\omega\delta\tan\beta)}{\cos(\omega\delta\tan\beta) - e^{\omega\delta}} \; ; \quad h_i = (\omega z_i \tan\beta + \beta)$$

$$\rho_1 = \sigma_1 - \sigma_o \, , \quad \rho_2 = \sigma_2 - \sigma_1 \ldots\ldots \rho_{N+1} = \sigma_r - \sigma_N \, .$$

The amplitude spectrum of the transform of g_m is a complicated function and it is doubtful that any useful information can be obtained from it.

Determination of $R_2(\omega)$ And $X_2(\omega)$ From The Field Data

In order to find $A_2(\omega)$ as a function of ω we must find $R_2(\omega)$ and $X_2(\omega)$ as functions of ω. This can be done by making a harmonic analysis of the observed gravity data.

A function f(x) which is periodic with period 2L and which satisfies certain conditions of continuity can be represented by the complex Fourier series

$$f(x) = \sum_{n=-\infty}^{\infty} \alpha_n e^{+jn\omega_o x} \qquad \ldots\ldots (20)$$

the complex coefficients, α_n, being given by

$$\alpha_n = \frac{1}{2L}\int_{-L}^{L} f(x)e^{-jn\omega_o x}dx\,, \quad \omega_o = \frac{\pi}{L}\,.$$

Obviously α_n is the conjugate complex of α_{-n}.

The function f(x) can also be represented by the real Fourier series

$$f(x) = \frac{a_o}{2} + \sum_{n=1}^{\infty} (a_n \cos n\omega_o x + b_n \sin n\omega_o x) \qquad \ldots\ldots (21)$$

where the coefficients are given by the expressions

$$a_n = \frac{1}{L}\int_{-L}^{L} f(x)\cos n\omega_o x dx$$

$$b_n = \frac{1}{L}\int_{-L}^{L} f(x)\sin n\omega_o x dx.$$

The two sets of coefficients are related as follows:

$$a_n = \alpha_n + \alpha_{-n} = 2\mathrm{Re}\{\alpha_n\}, \quad b_n = j(\alpha_n - \alpha_{-n}),$$

$$= -2\mathrm{Im}\{\alpha_n\},$$

Re { } and Im { } denoting the 'real part of' and the 'imaginary part of' respectively.

Assume that the observed gravity anomaly, g(x), has been represented by a Fourier series similar to equation (21), the interval (-L, L) being sufficiently large that

$$g(x) \doteq 0, \quad x^2 \geq L^2.$$

The Fourier series will represent the gravity anomaly as accurately as desired within the interval (-L, L); outside this interval, however, g(x) vanishes while the series reproduces the gravity anomaly in each interval (c, c + 2L), c being an arbitrary constant.

The complex Fourier coefficient in the series representing g(x) is closely related to F(ω), the Fourier transform of g(x). Thus, we have

$$\alpha_n = \frac{1}{2L}\int_{-L}^{L} g(x)e^{-jn\omega_o x}dx = \frac{1}{2L}\int_{-\infty}^{\infty} g(x)e^{-jn\omega_o x}dx$$

$$= \frac{1}{2L}F(n\omega_o)$$

Therefore,

$$\left.\begin{aligned} a_n &= \frac{1}{L}\,\mathrm{Re}\{\,F(n\omega_o)\,\} = \frac{1}{L}\,R(n\omega_o) \\ b_n &= -\frac{1}{L}\,\mathrm{Im}\{\,F(n\omega_o)\,\} = -\frac{1}{L}\,X(n\omega_o) \end{aligned}\right\} \quad \ldots\ldots (22)$$

Thus, by analyzing the field data to find a_n and b_n, we can obtain the values of $R(n\omega_o)$ and $X(n\omega_o)$ with an accuracy which theoretically can be made as high as we wish by increasing L sufficiently.

If we write

$$f'(x) = \sum_{n=1}^{\infty} (a_{n1}\cos n\omega_o x + b_{n1}\sin n\omega_o x)$$

and

$$f''(x) = \sum_{n=1}^{\infty} (a_{n2}\cos n\omega_o x + b_{n2}\sin n\omega_o x)\ ,$$

the values of the coefficients a_{n1}, b_{n1}, a_{n2} and b_{n2} can be found by differentiating equation (21). The results are

$$\left.\begin{aligned} a_{n2} &= (n\omega_o)b_{n1} = (-n^2\omega_o{}^2)a_n \\ b_{n2} &= (-n\omega_o)a_{n1} = (-n^2\omega_o{}^2)b_n \end{aligned}\right\} \quad \ldots\ldots (23)$$

For very large values of x in the positive and negative directions from the fault trace, the function g_f is approximately equal to zero, hence by choosing L very large, the coefficients a_n and b_n in the Fourier series representing g_f should be approximately equal to $R_{2f}(n\omega_o)$ and $X_{2f}(n\omega_o)$.

The gravity anomaly due to a single block as well as the anomaly

due to a fault truncating a series of beds for certain combinations of density, do not approach zero for large positive and negative values of x, hence the method described above is not directly applicable to the calculation of transforms of such anomalies. However we can use one of the following methods to find transforms of anomalies which do not approach zero values for large positive and negative values of x.

Method No. 1

Let g(x) in Figure 47 be the gravity anomaly due to a single block or a fault truncating a series of beds. The first derivative of g(x), g'(x), shown in Figure 47, is a well-behaved function in that it rapidly goes to zero for large positive and negative values of x. A Fourier analysis performed on g'(x) will give the coefficients a_{n1} and b_{n1}. The Fourier coefficients a_{n1} and b_{n1} are related to $R(n\omega_o)$ and $X(n\omega_o)$ as follows:

$$a_{n1} = \frac{R_1}{L}(n\omega_o) = jn\omega_o \frac{R(n\omega_o)}{L}$$

$$b_{n1} = \frac{X_1}{L}(n\omega_o) = -jn\omega_o \frac{X(n\omega_o)}{L}$$

Thus, once we have the transforms $R_1(n\omega_o)$ and $X_1(n\omega_o)$, the transforms $R(n\omega_o)$ and $X(n\omega_o)$ can be readily calculated, thus giving the transforms of g(x).

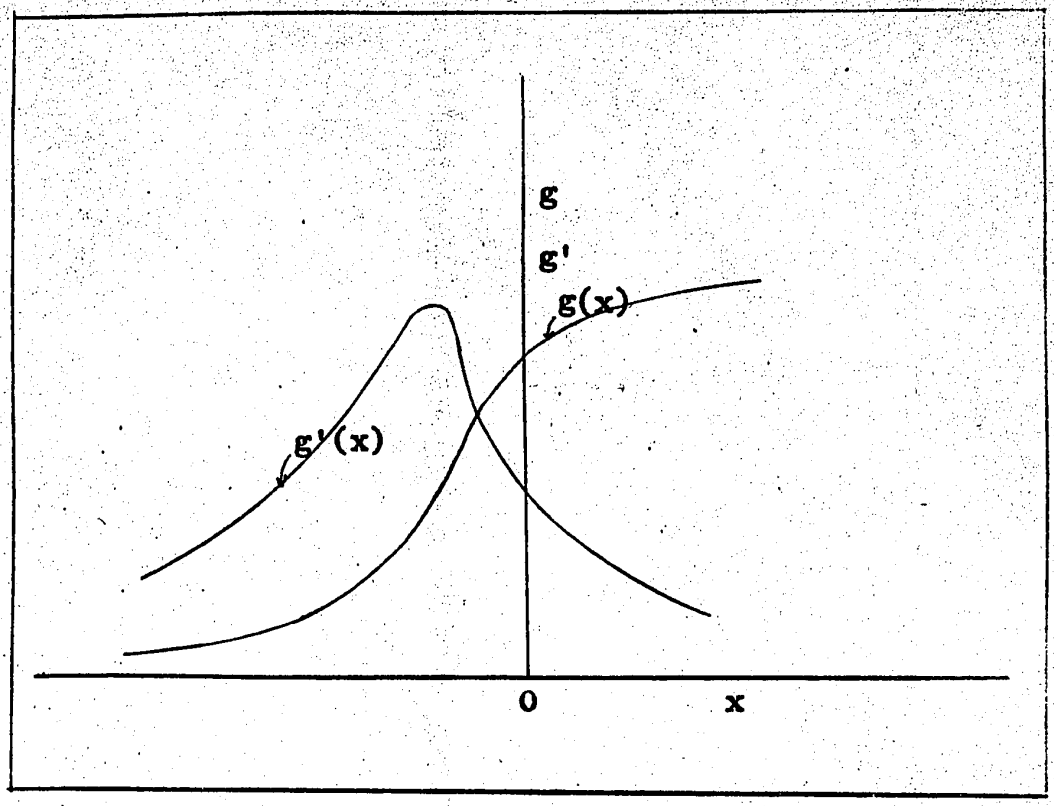

FIG 47.

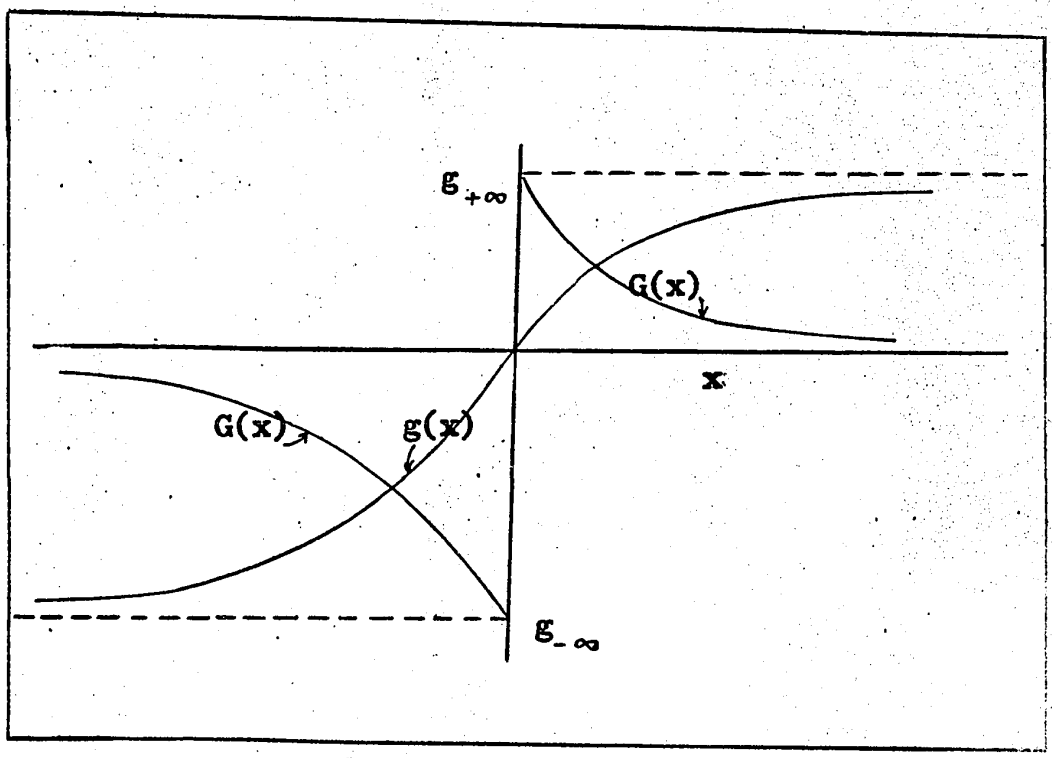

FIG 48.

Method No. 2

Let $g_{+\infty}$ and $-g_{-\infty}$ be the limiting values of $g(x)$ as x approaches $\pm \infty$. Then we define a new function g_L such that

$$g_L = g_{+\infty} \qquad x \geq 0$$

$$= -g_{-\infty} \qquad x \leq 0$$

Then the function $G(x)$ defined by the equation

$$G(x) = g_L - g(x)$$

approaches zero as x approaches $\pm \infty$.

The Fourier transform of g_L can be obtained by finding the Fourier transforms of the two step functions of amplitudes $g_{+\infty}$ and $-g_{-\infty}$ separately and then adding the two results to give the Fourier transform of g_L. Thus, if $g_1(\omega)$ be the Fourier transform of the step of amplitude $g_{+\infty}$, we have,

$$g_1(\omega) = \int_{-\infty}^{\infty} g_{+\infty} e^{-j\omega x} dx$$

$$= g_{+\infty} \lim_{\varepsilon \to 0} \int_{0}^{\infty} e^{-j\varepsilon t - j\omega t} dt$$

$$= g_{+\infty} \lim_{\varepsilon \to 0} \frac{1}{j(\varepsilon + \omega)}$$

$$= g_{+\infty} \left[\pi\delta(\omega) + \frac{1}{j\omega} \right] *$$

where $\delta(\omega)$ is the Dirac 'δ' function or the unit impulse function, defined by

$$\delta(\omega) = \infty \text{ at } \omega = 0$$
$$= 0 \qquad \omega \neq 0$$

and $$\int_{-\infty}^{\infty} \delta(\omega) d\omega = 1$$

Similarly, the transform $g_2(\omega)$ of the step of height $-g_{-\infty}$ is given by

$$g_2(\omega) = -g_{-\infty} \left[\pi\delta(\omega) - \frac{1}{j\omega} \right]$$

Hence the Fourier transform of g_L is $g_1(\omega) + g_2(\omega)$

$$= \pi(g_{+\infty} - g_{-\infty})\, \delta(\omega) + \frac{(g_{+\infty} + g_{-\infty})}{j\omega}$$

Except for the point $\omega = 0$, the real part of the transform of g_L is zero. There will, however, be a contribution from the imaginary part of the transform of g_L for every ω equal to $-\frac{(g_{+\infty} + g_{-\infty})}{\omega}$.

To fine the Fourier transform of $g(x)$, therefore, we first calculate the Fourier coefficients of the function $G(x) = \{g_L - g(x)\}$ in the usual manner. If a_n' and b_n' be these coefficients, the real

---

* See Papoulis, 1962.

and imaginary parts of the transform of g(x) is given by

$$\left.\begin{aligned} \frac{R}{L} &\doteq a_n' \\ \frac{X}{L} &\doteq \left(b_n' + \frac{g_{+\infty} + g_{-\infty}}{Ln\omega_o}\right) \end{aligned}\right\} \quad \ldots\ldots (24)$$

Theoretical examples

Example No. 1: In this section we use equations (2) and (8) to calculate the anomaly and its derivatives, then analyze these data as though they had been obtained in the field. The calculations listed below were made for a fault with the following parameters:

$$z_1 = 0.5 \quad z_2 = 1.5 \quad z_3 = 1.0 \quad z_4 = 2.0$$

$$\rho = 1.0 \quad \beta = 60^\circ \quad L = 12.4$$

(a) g(x) and g''(x) were calculated,

(b) harmonic analysis of the results in (a) gave the two sets of coefficients, (a_n, b_n) and (a_{n2}, b_{n2}), as functions of $(n\omega_o)$, that is, as functions of n, since ω_o was the same for all calculations,

(c) values of (a_{n2}, b_{n2}) were calculated from the values of (a_n, b_n) using equation (23),

(d) $R_{2f}(n\omega_o)$ and $X_{2f}(n\omega_o)$ were calculated as functions of n using equations (17a) and (17b), after which equation (22) gave a_{n2}, b_{n2},

(e) $R_f(n\omega_o)$ and $X_f(n\omega_o)$ were obtained from the results in (d) using equation (15), after which equation (22) gave a_n, b_n.

If we regard the values of g(x) obtained in (a) as representing field data obtained under perfect field conditions, then the coefficients obtained in (b) and (c) are based upon field data while the coefficients obtained in (d) and (e) represent true values. The two sets of coefficients are compared in various ways in Figures 49-53.

Figure 49 compares a_n obtained in (b) above with (1/L) $R_f(n\omega_o)$ obtained in (e). The agreement between the two sets of values is exact within the accuracy of plotting so that the two curves merge into one. Figure 50 shows the relation between b_n and -(1/L) $X_f(n\omega_o)$; the latter gives a smooth curve about which the curve of b_n oscillates with decreasing amplitude.

Figures 51 and 52 compare values of (1/L) $R_{2f}(n\omega_o)$ and -(1/L) $X_{2f}(n\omega_o)$ with (a_{n2}, b_{n2}) obtained in (b) and (c). In Figure 51, the three curves coincide within the plotting error, whereas in Figure 52, -(1/L) $X_{2f}(n\omega_o)$ and b_{n2} obtained in (b) coincide to give a smooth curve about which the b_{n2} values obtained in (c) oscillate with an amplitude which seems to increase slowly with increasing n.

The disparity between Figures 49 and 51 on the one hand and Figures 50 and 52 on the other is striking. The two curves which deviate from the smooth theoretical curves representing the transforms -(1/L) $X_f(n\omega_o)$ and -(1/L) $X_{2f}(n\omega_o)$ are curves of b_n obtained in (b) and b_{n2} obtained from b_n (procedure (c)). Both of these curves depend upon the harmonic analysis of the gravity anomaly, and further study shows that the oscillatory nature of these curves is due to neglect of the tails of

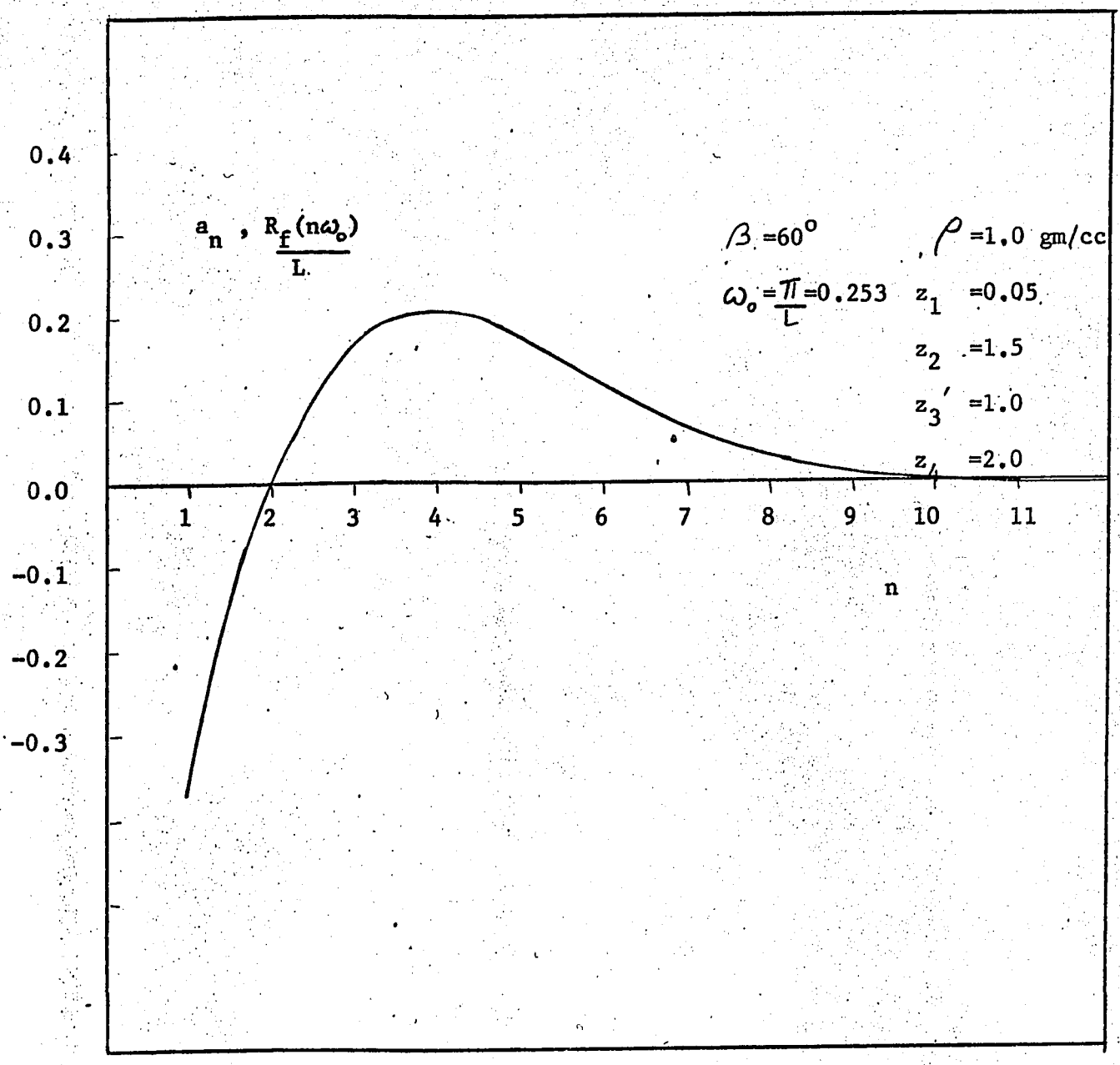

FIG 49. Comparison of a_n and $\frac{R_f(n\omega_o)}{L}$

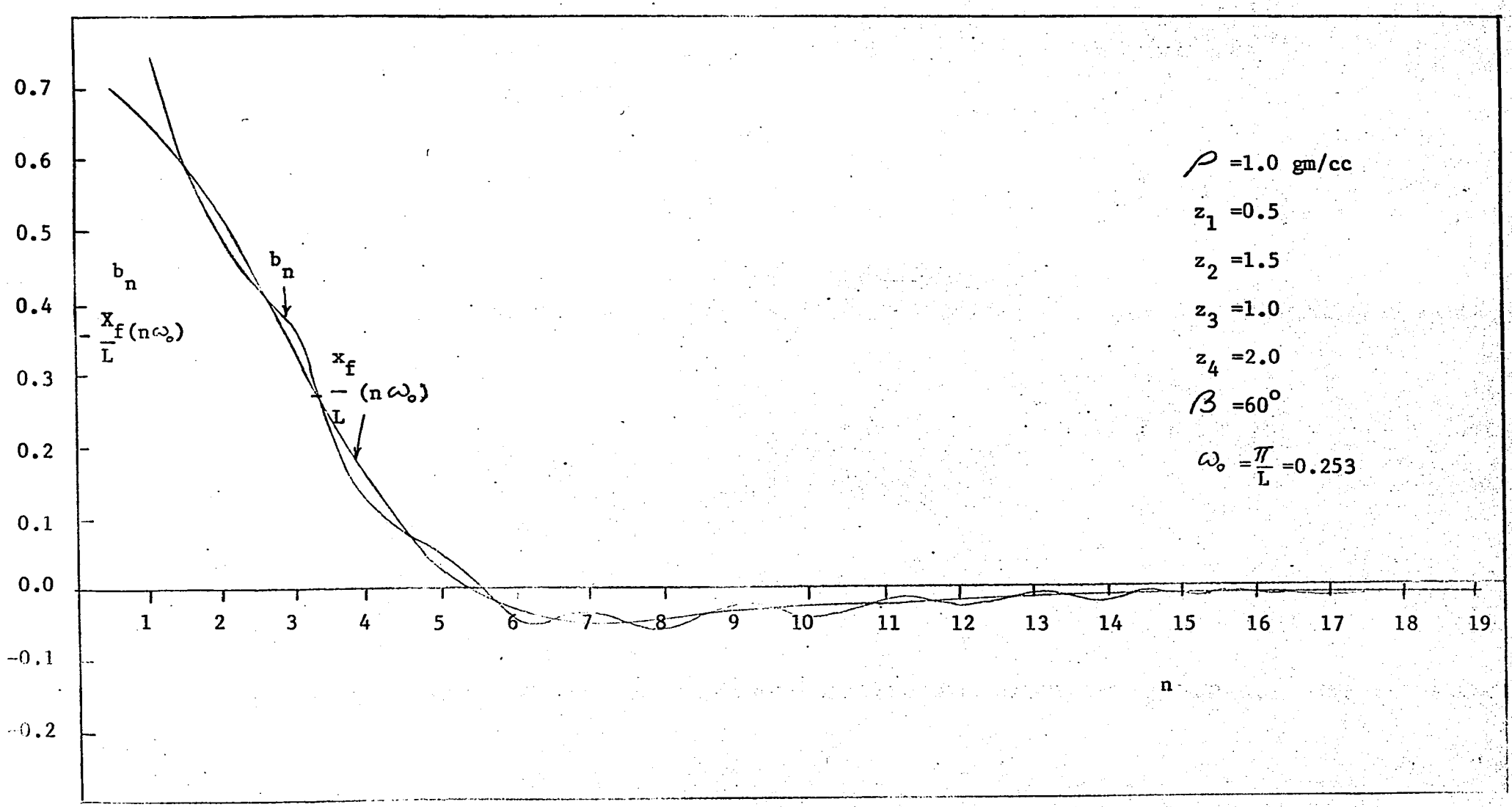

FIG 50 Comparison of b_n and $-\frac{X_f(n\omega_o)}{L}$

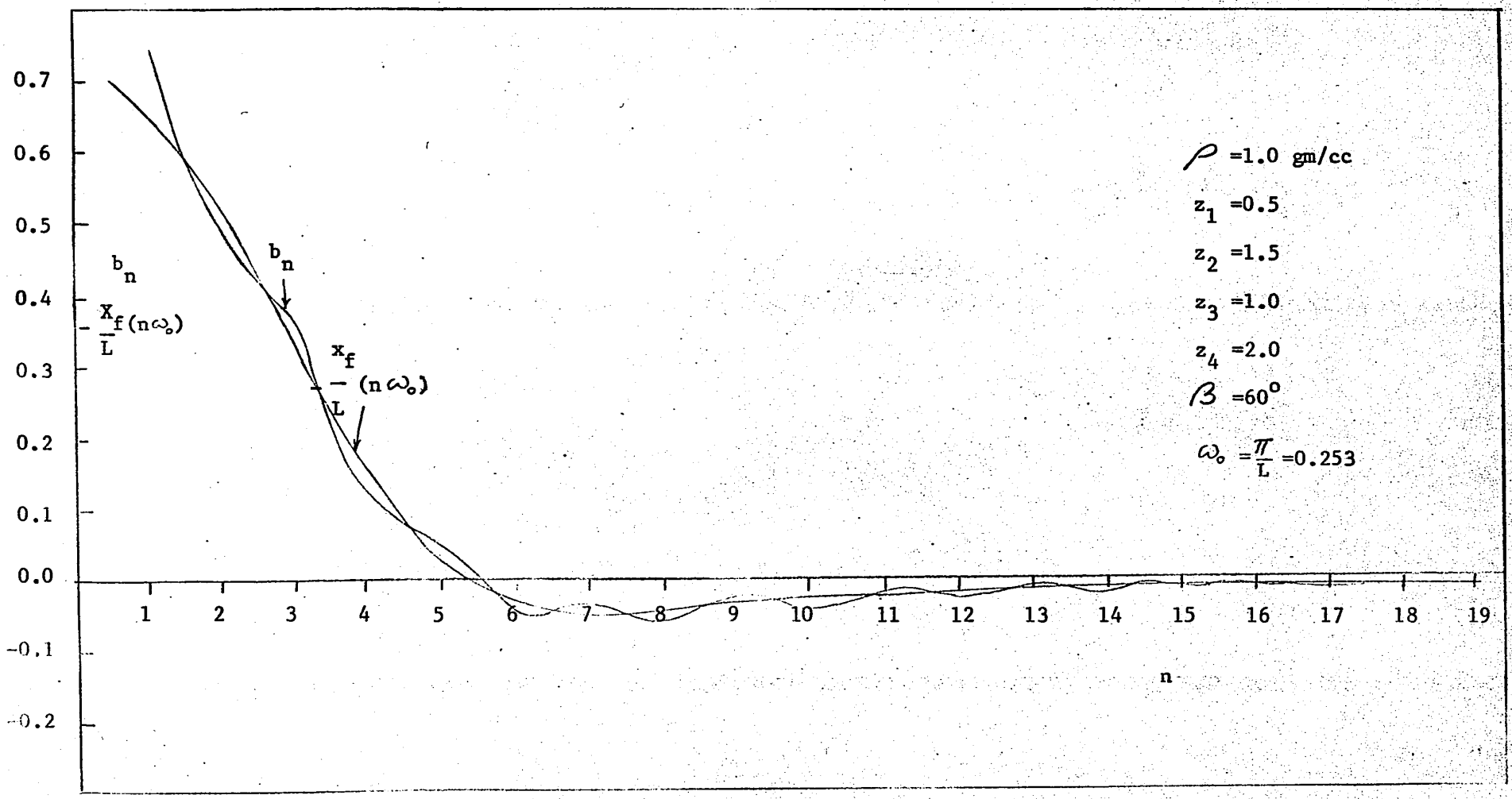

FIG 50 Comparison of b_n and $-\frac{X_f(n\omega_o)}{L}$

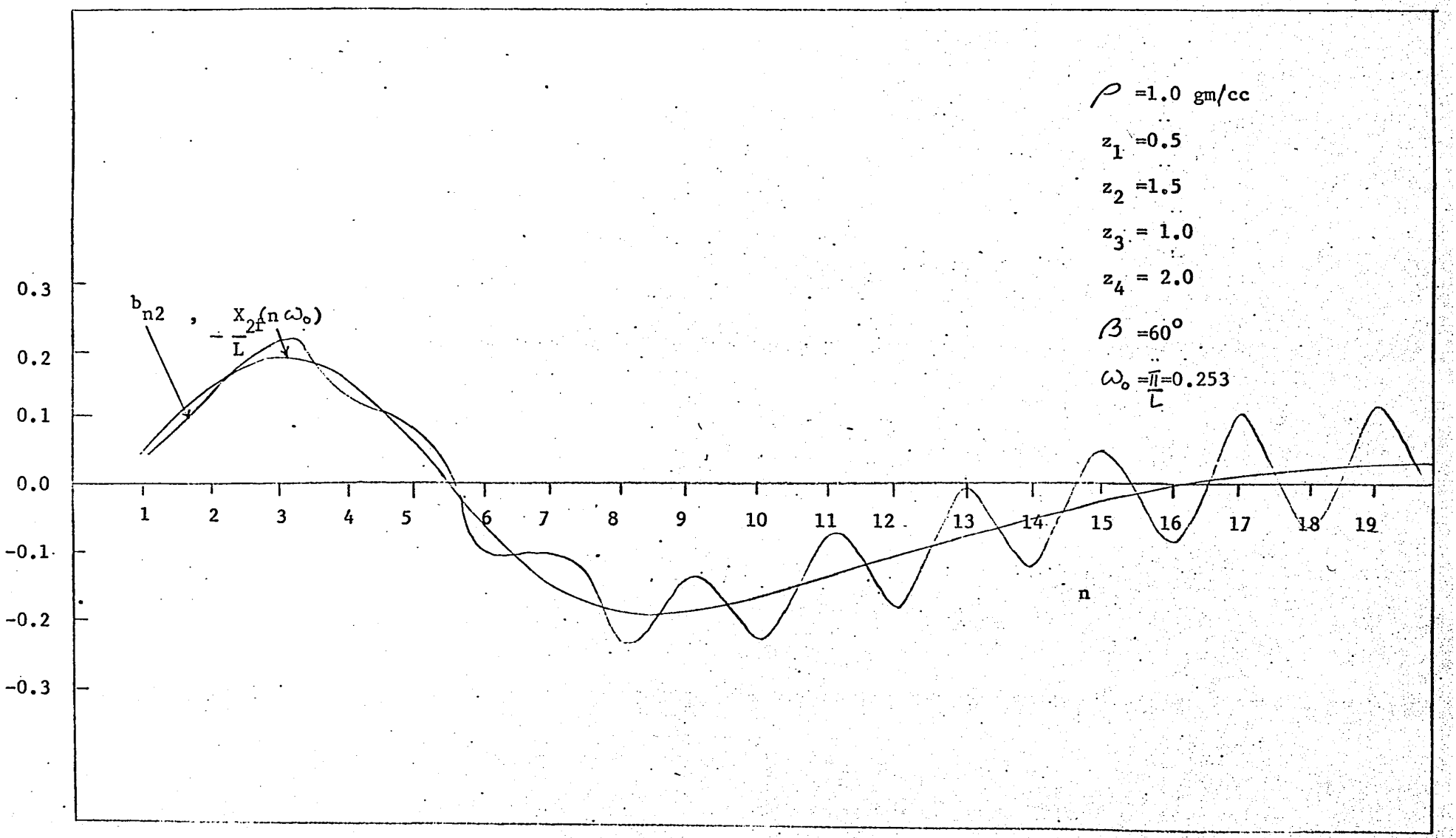

FIG 52 Comparison of b_{n2} and $-\frac{X_{2f}(n\omega_o)}{L}$

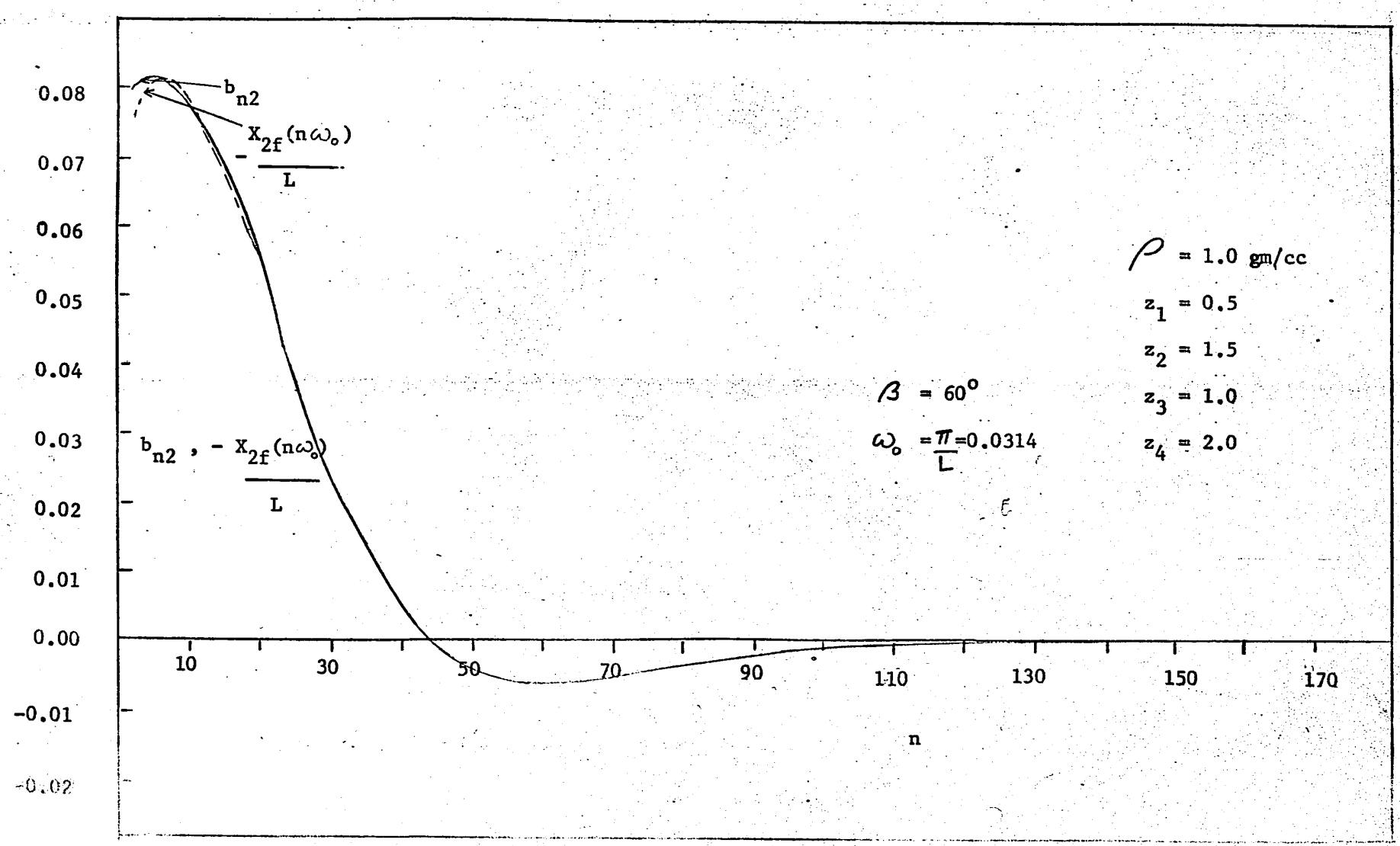

FIG 53. Comparison of b_{n2} and $-\frac{X_{2f}(n\omega_o)}{L}$ for large value of L

the anomaly beyond the points $x = \pm L$. The effect of reducing these tails by increasing L from 12.4 to 100 can be seen by comparing Figures 52 and 53; the latter shows almost perfect agreement between b_{n2} and $-(1/L)\, X_{2f}(n\omega_o)$ except for low values of n. Thus, provided L is taken sufficiently large, b_n and b_{n2} agree very closely with the theoretical values given by the imaginary parts of the Fourier transform. However, even when L is much less than this value, acceptable values of the transforms can be obtained by smoothing the curves of b_n and b_{n2} to remove the oscillatory part.

In order to find the amplitude spectrum, $A_{2f}(n\omega_o)$, it is not necessary to carry out a Fourier analysis of the second derivative of the gravity anomaly. $A_{2f}(n\omega_o)$ can be obtained directly from the Fourier coefficients, a_n and b_n, obtained by Fourier analysis of the gravity anomaly as shown below:

The second derivative spectrum can be written as

$$A_{2f}(n\omega_o) = \sqrt{R_{2f}^2(n\omega_o) + X_{2f}^2(n\omega_o)}$$

$$= (n\omega_o)^2 \sqrt{R_f^2(n\omega_o) + X_f^2(n\omega_o)}\ ,$$

since $R_{2f} = (jn\omega_o)^2 R_f$

and $X_{2f} = (jn\omega_o)^2 X_f$.

Dividing both sides of the above equation by L, and using the relations $a_n = \frac{1}{L} R(n\omega_o)$, $b_n = -\frac{1}{L} X(n\omega_o)$, we obtain,

$$\frac{A_{2f(n\omega)}}{L} = (n\omega_o)^2 \sqrt{a_n^2 + b_n^2}$$

and $$\text{Log}\left\{\frac{A_{2f}(n\omega_o)}{L}\right\} = 2\,\text{Log}(n\omega_o) + \frac{1}{2}\,\text{Log}\left(a_n^2 + b_n^2\right).$$

Hence $A_{2f}(n\,\omega_o)$ may be obtained from the Fourier coefficients, a_n and b_n. The above equation was used to plot the curve in Figure 54. The slope of the amplitude spectrum in the linear region gives $z_1 = 0.5$ and the intercept corresponding to the straight line portion of the curve gives $\beta = 60^\circ$.

Example No. 2: Using equation (1), the gravity anomaly, g_s, was calculated for a single block having the following parameters:

$$z_1 = 1.0, \quad z_2 = 2.0, \quad \beta = 60^\circ, \quad \rho = 1.0 \text{ gm/c.c.}$$

In order to calculate the Fourier transform of the above anomaly, method No. 2 on page 121 was used. A Fourier analysis was performed on the function $(g_L - g_s)$, obtained by subtracting the anomaly from $-g_{-\infty}$ for negative values of x, from $g_{+\infty}$ for positive values of x. If a_n' and b_n' are the Fourier coefficients of the function $(g_L - g_s)$ and a_n and b_n the Fourier coefficients of the function g_s, then

$$a_n = a_n' \text{ except at } \omega = 0$$

$$b_n = b_n' + \frac{(g_{+\infty} + g_{-\infty})}{Ln\omega_o}$$

Figure 55 shows that, except for small values of ω, the agreement between a_n and $\frac{R_s(n\omega_o)}{L}$ is very good. In Figure 56, the

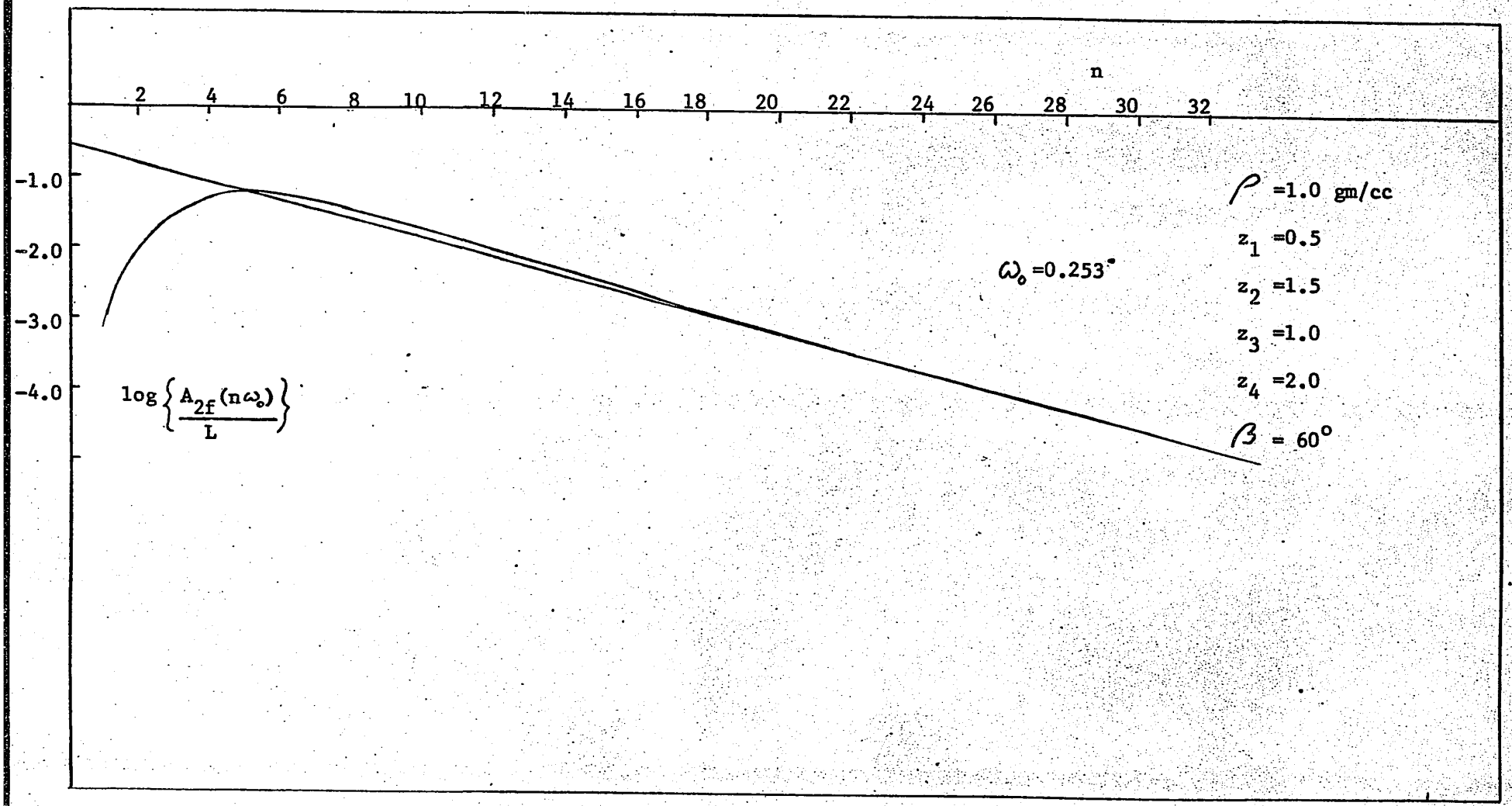

FIG 54 Amplitude spectrum as a function of n

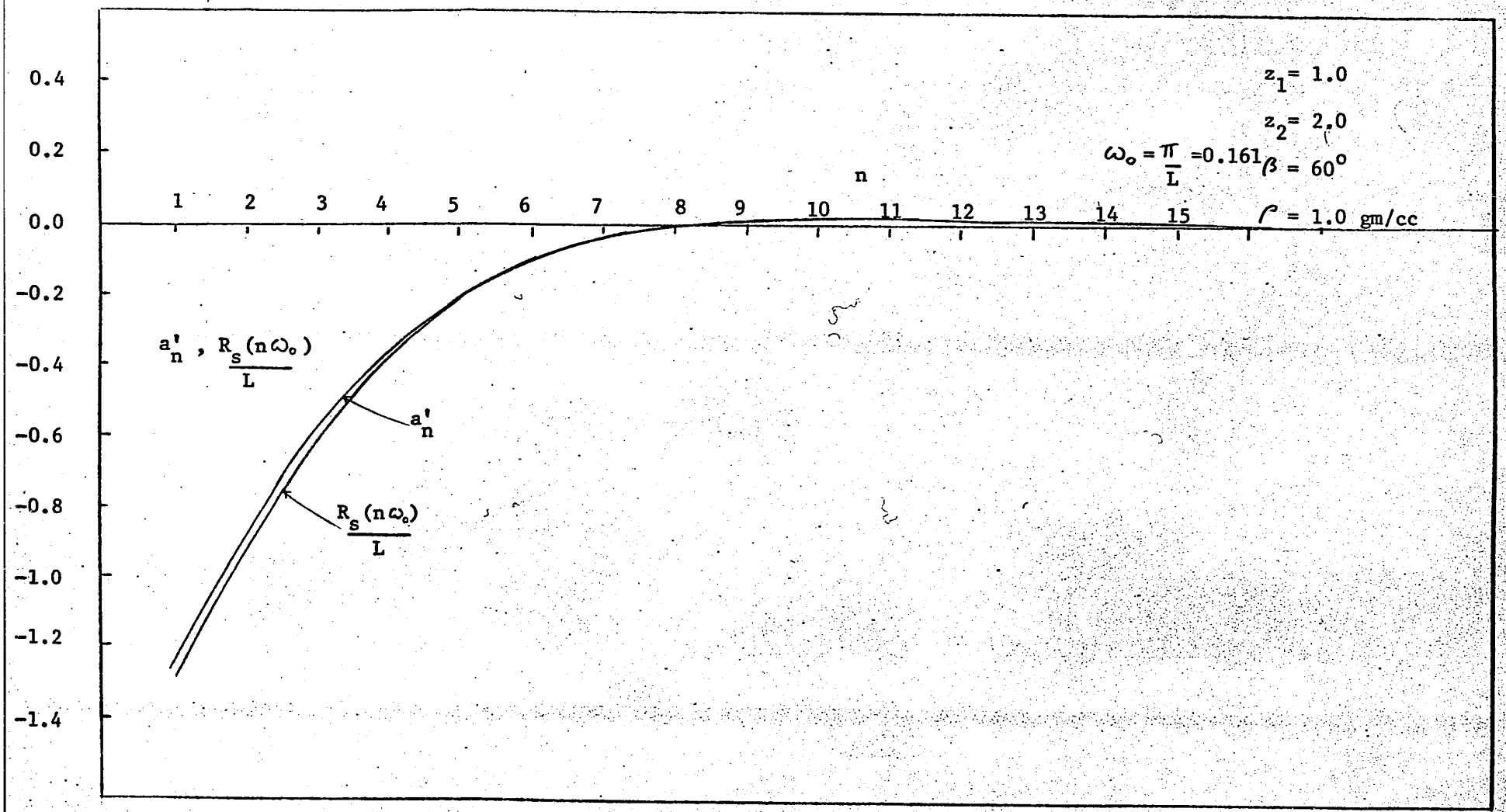

FIG 55. Comparison of a'_n and $\frac{R_s(n\omega_o)}{L}$ for a single block

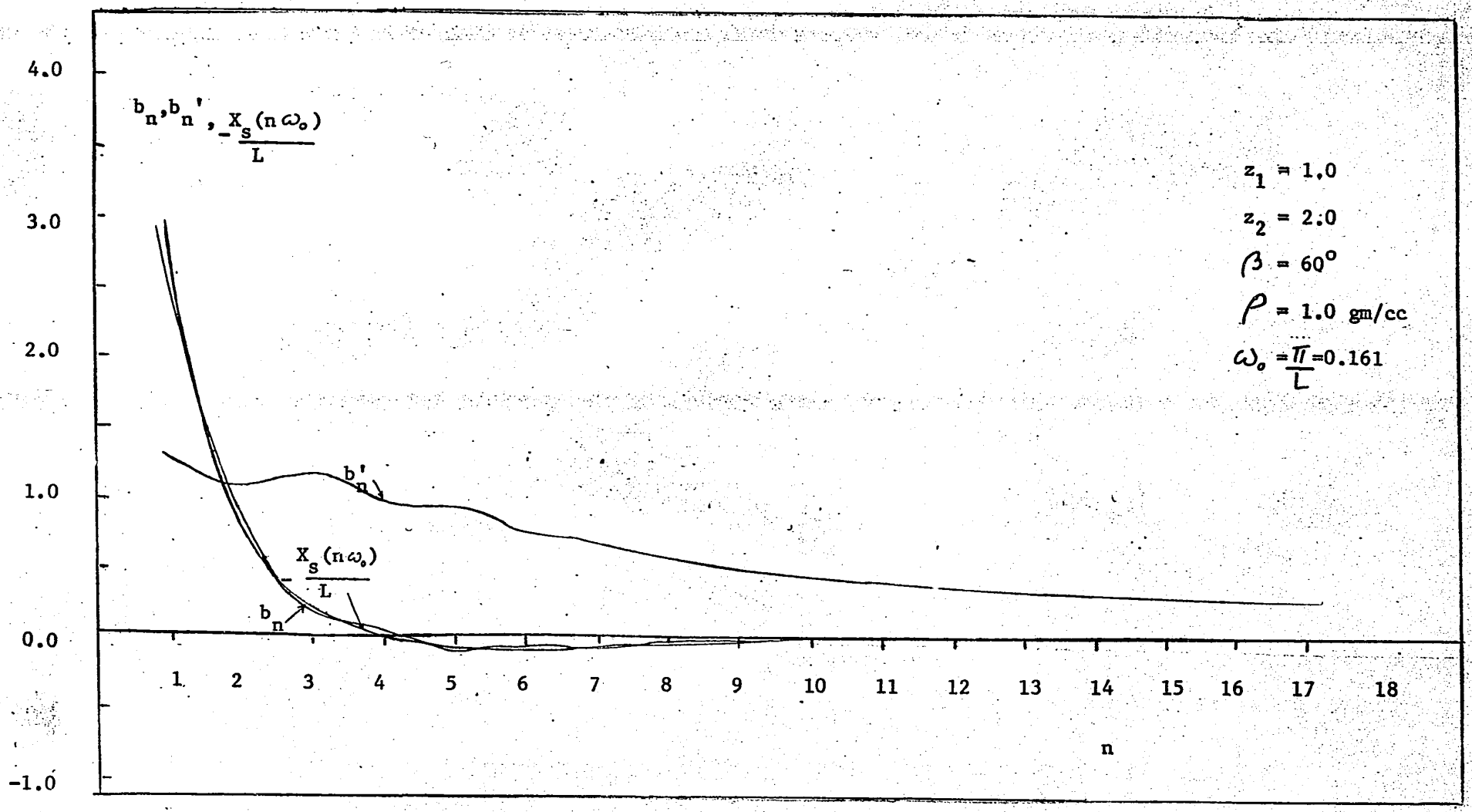

FIG 56. Comparison of b_n and $-\frac{X_s(n\omega_o)}{L}$ for a single block

theoretical values of $\frac{X_s(n\omega_o)}{L}$ are compared with the Fourier coefficients b_n and b_n'; as in the case of the fault, the b_n coefficients oscillate about the theoretical graph and acceptable values of the transform can be obtained by smoothing out the coefficient graph.

The amplitude spectrum, $A_{2s}(n\omega_o)$, for the transform of the second derivative of g_s is shown in Figure 57, plotted as a function of the order of the Fourier harmonic, n. The slope of the amplitude graph in the linear part gives $z_1 = 1.1$ and intercept of the linear part gives $\beta = 56^\circ$.

Determination of fault parameters: Certain geometrical properties of the fault can be expressed in terms of the Fourier coefficients. Let us define S and S' according to the relations

$$S = \frac{1}{\pi}\int_o^\infty R_2(\omega)d\omega , \quad S' = \frac{1}{\pi}\int_o^\infty X_2(\omega)d\omega.$$

Referring to equations (16a') and (16b') in Appendix E, the typical terms in the expressions for S and S' due to a single block are given by

$$I = \int_o^\infty e^{-\omega z}\sinh d\omega , \quad I' = \int_o^\infty e^{-\omega z}\cosh d\omega , \quad h = \omega z\tan\beta + \beta$$

Integrating by parts twice and solving for I and I' gives

$$I = \cos\beta \sin 2\beta/z \qquad I' = \cos\beta\cos 2\beta/z$$

Substituting these results in equations (16a') and (16b'), we find for a single block

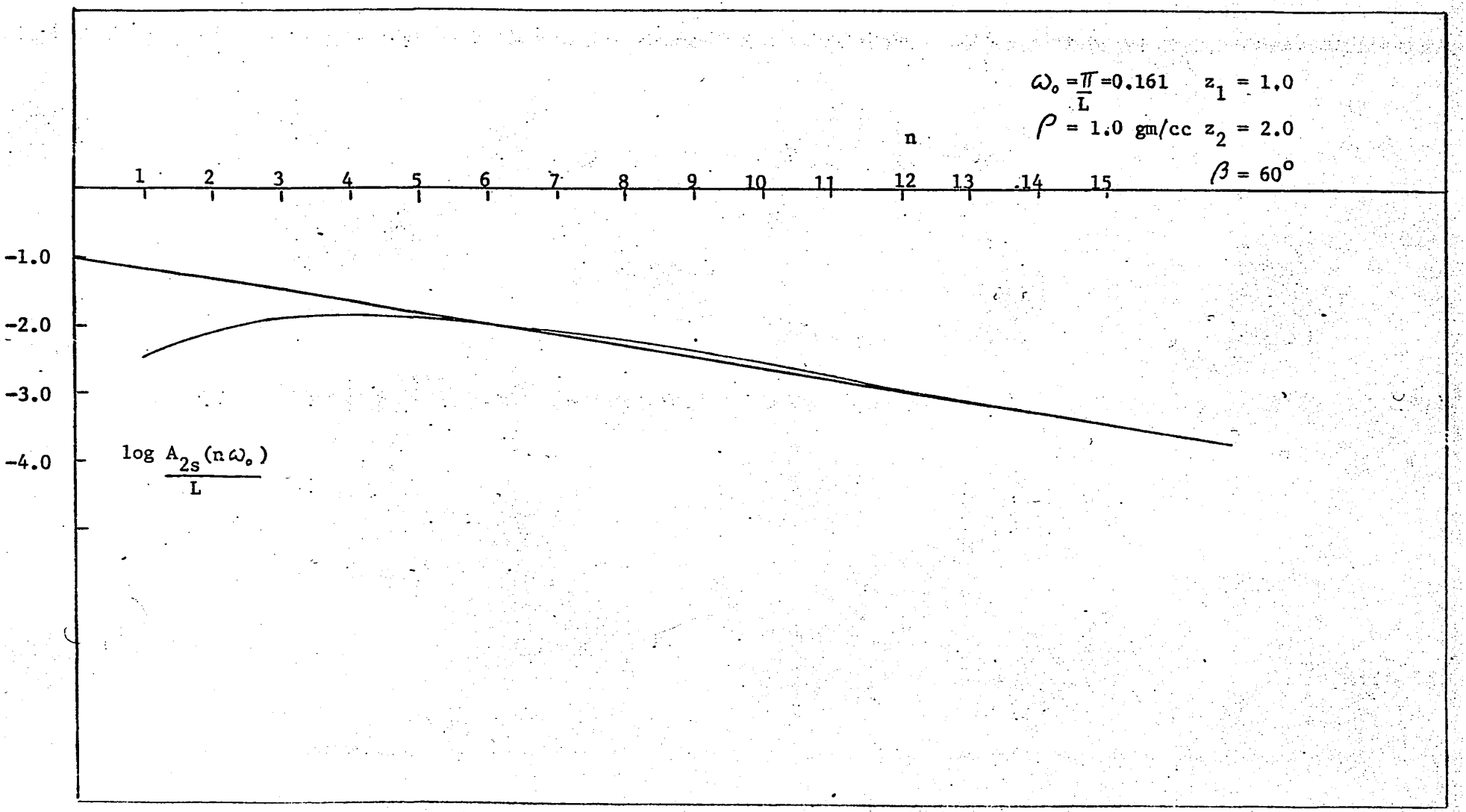

FIG 57. Amplitude spectrum for a single block as a function of n

$$S_s = 2K \cos^2\beta \sin 2\beta \left(\frac{1}{z_2} - \frac{1}{z_1}\right)$$

$$S_s' = -2K\cos^2\beta \cos 2\beta \left(\frac{1}{z_2} - \frac{1}{z_1}\right)$$

Similarly, for a fault cutting a single bed, the corresponding functions, S_f and S_f', are given by

$$S_f = 2K \cos^2\beta \sin 2\beta \left(\frac{1}{z_2} - \frac{1}{z_1} + \frac{1}{z_3} - \frac{1}{z_4}\right)$$

$$S_f' = -2K\cos^2\beta \cos 2\beta \left(\frac{1}{z_2} \quad \frac{1}{z_1} \quad \frac{1}{z_3} \quad \frac{1}{z_4}\right)$$

Referring to equations (19a) and (19b), we find that S_m and S_m' for a fault cutting a series of beds are given by

$$S_m = 2G\delta \cos^2\beta \sin 2\beta \left(\frac{\rho_1}{z_1 z_1'} + \frac{\rho_2}{z_2 z_2'} + \cdots \frac{\rho_{N+1}}{z_{N+1} z_{N+1}'}\right)$$

$$S_m' = -2G\delta \cos^2\beta \cos 2\beta \left(\frac{\rho_1}{z_1 z_1'} + \frac{\rho_2}{z_2 z_2'} + \cdots \frac{\rho_{N+1}}{z_{N+1} z_{N+1}'}\right)$$

where δ = Displacement of the fault

$$z_i' = z_i + \delta, \quad i = 1, 2, \ldots\ldots N+1$$

The functions S and S' are related to the Fourier coefficients a_{n2} and b_{n2} as follows:

$$S = \frac{1}{\pi}\int_0^\infty R_2(\omega)d\omega = \frac{L}{\pi}\int_0^\infty a_{n2}d\omega = \left(\frac{L}{\pi}\right)\sum_{n=1}^{\infty} a_{n2}\,\Delta\omega$$

However, $a_{n2}\,\Delta\omega = a_{n2}\left\{n\left(\frac{2\pi}{2L}\right) - (n-1)\left(\frac{2\pi}{2L}\right)\right\} = \frac{\pi}{L}a_{n2}$, so that

$$S = \sum_{n=1}^{\infty} a_{n2} = -\omega_o^2 \sum_{n=1}^{\infty} n^2 a_n ;$$

Similarly $$S' = \sum_{n=1}^{\infty} b_{n2} = \omega_o^2 \sum_{n=1}^{\infty} n^2 b_n$$

Hence the functions S and S' may be found by summing the Fourier coefficients a_{n2} and b_{n2}, or a_n and b_n.

After S and S' have been found, we can obtain β by taking the ratio of S and S'; thus

$$\tan 2\beta = - S/S'$$

In obtaining values of S and S' from the coefficients a_{n2} and b_{n2}, it is found that the sums of the coefficients converge very slowly to S and S' when z_1 is small, hence a large number of coefficients are necessary to get a good estimate of S and S'.

Limiting Values Of The Transforms As $\omega \longrightarrow 0$

Useful information about the parameters of two-dimensional faults can be obtained by taking the limits of the Fourier transform functions as ω approaches zero. Expressions for the limiting values of the transforms of a single block, a fault cutting a single bed and a fault cutting a series of beds are derived in Appendix F. These limiting values are

Single block:

$$\text{(a)} \lim_{\omega \longrightarrow 0} R_s(\omega) = \pi G\rho T \tan\beta \, (z_1 + z_2) \qquad \ldots\ldots (25a)$$

$$\text{(b)} \lim_{\omega \longrightarrow 0} X_s(\omega) = 2\pi G\rho \left[\frac{T}{2}(z_1 + z_2) - T \lim_{\omega \longrightarrow 0} \left(\frac{1}{\omega}\right) \right] \qquad \ldots\ldots (25b)$$

$$= -\infty$$

Fault cutting a single bed:

$$\text{(c)} \lim_{\omega \longrightarrow 0} R_f(\omega) = -2\pi G\rho T\delta \tan\beta \qquad \ldots\ldots (25c)$$

$$\text{(d)} \lim_{\omega \longrightarrow 0} X_f(\omega) = -2\pi G\rho T\delta \qquad \ldots\ldots (25d)$$

Fault cutting a series of beds:

$$\text{(e)} \lim_{\omega \longrightarrow 0} R_m(\omega) = \pi G\delta \tan\beta \left[2z_{N+1}(\sigma_r - \bar{\sigma}) + \delta(\sigma_r - \sigma_o) \right] \qquad \ldots\ldots (25e)$$

$$\text{(f)} \lim_{\omega \longrightarrow 0} X_m(\omega) = \pi G\delta \left[2z_{N+1}(\sigma_r - \bar{\sigma}) + \delta(\sigma_r - \sigma_o) - \lim_{\omega \longrightarrow 0} \frac{2\delta(N+1)(\sigma_r - \sigma_o)}{\omega} \right] \qquad \ldots\ldots (25f)$$

where $\bar{\sigma} = \dfrac{\sigma_o z_1 + \sum_{i=1}^{N} \sigma_i t_i}{z_{N+1}}$

Thus by extrapolating curves for $R(\omega)$ and $X(\omega)$ to $\omega = 0$ we can find certain parameters of two-dimensional structures. As an example, in Figure 55, the graphs of the coefficients a_n' and the transform $\frac{R_s}{L}(n\omega_o)$ have the same limiting value 1.7 at $\omega = 0$. Such extrapolation is possible only if the curves are approximately straight lines near $\omega = 0$. By plotting a large number of theoretical curves for a fault it is found that the slope near $\omega = 0$ changes quite rapidly for $|\beta| > 45^\circ$ hence the results obtained by extrapolation will not be very accurate for faults dipping less than 45°.

Approximate Values Of T And δ

For a fault cutting a single bed an approximate value of the thickness T can be found when z_1 and β are known and when it is assumed (or known) that T is small and δ is large. In the same way, δ can be found when it is small and T is large. In practice this means that the one to be found is less than about 3,000 feet while the other is greater than about 4,000 feet.

The amplitude spectrum of the transform of the gravity anomaly due to a fault cutting a single bed can be obtained by a combination of equations (18a) and (15). Thus, the amplitude spectrum A_f is given by,

$$A_f(\omega) \doteq \left(\frac{ce^{-\omega z_1}}{\omega^2}\right)\left\{1 - 2e^{-\omega T}\cos(\omega T\tan\beta + e^{-2\omega T}\right\}^{1/2}$$

$$\left\{1 - 2e^{-\omega\delta}\cos(\omega\delta\tan\beta) + e^{-2\omega\delta}\right\}^{1/2}$$

where $c = 2\pi G\rho\cos\beta$.

Let us assume that T is large while δ is relatively small. Then as ω increases, the bracket involving terms in T approaches unity much more quickly than terms in δ, hence for moderately large values of ω the above expression reduces to

$$A_f(\omega) \doteq \frac{ce^{-\omega z_1}}{\omega^2}\left\{1 - 2e^{-\omega\delta}\cos(\omega\delta\tan\beta) + e^{-2\omega\delta}\right\}^{1/2}$$

To solve for δ, we take two values of ω, say ω_1 and ω_2, and determine the ratio $\tau = \frac{A_f(\omega_1)}{A_f(\omega_2)}$. Since β, z_1, ω_1 and ω_2 are known, τ is a

function of δ only; thus

$$\frac{1 - 2e^{-\omega_1\delta}\cos(\omega_1\delta\tan\beta) + e^{-2\omega_1\delta}}{1 - 2e^{-\omega_2\delta}\cos(\omega_2\delta\tan\beta) + e^{-2\omega_2\delta}} = \tau^2\left(\frac{\omega_1}{\omega_2}\right)^4 e^{(\omega_1-\omega_2)z_1} \quad \ldots\ldots (26)$$

'δ' is the only unknown in this equation, hence it can be found by numerical methods of solving the equation.

The Fourier Transform Of The Dike Anomaly

From equation (5), the gravity anomaly of a dike is given by

$$g_d = \cos^2\beta \left[(x + x_o)(F'_{2d} - F'_{1d}) - (x - x_o)(F_{2d} - F_{1d}) \right]$$

To find the Fourier transform of the right-hand side of the above expression, we note from the shift theorem of the Fourier transform that, given

$$f(x) \longleftrightarrow F\{\omega\},$$

then $$f(x - x_o) \longleftrightarrow e^{-j\omega x_o} F(\omega).$$

Using equation (15) and the above formula, the Fourier transform of the dike anomaly may be written as

$$g_d \longleftrightarrow \frac{e^{+j\omega x_o} F_{2s}(\omega) - e^{-j\omega x_o} F_{2s}(\omega)}{(j\omega)^2}$$

where $F_{2s}(\omega)$ is the Fourier transform of the second derivative $\frac{d^2 g_s}{dx^2}$ of the gravity anomaly g_s due to a single block (see equations (16a) and (16b)).

Writing $F_d(\omega)$ for the right-hand side of the last expression, we have

$$F_d(\omega) = -\frac{2j\sin\omega x_o \; F_{2s}(\omega)}{\omega^2} \qquad \ldots\ldots (27)$$

$$= R_d(\omega) + jX_d(\omega)$$

The Fourier transform $F_{2s}(\omega)$ of the function $\frac{d^2 g_s}{dx^2}$ is derived in Appendix E. Substituting for $F_{2s}(\omega)$ in equation (27) we obtain

$$F_d(\omega) = -2jcM\sin\omega x_o \frac{e^{-\omega z_1}}{\omega^2}\left\{\sin(h_1 + \phi) - j\cos(h_1 + \phi)\right\} \quad \ldots\ldots (28)$$

where c, M, T, ϕ are defined in the same way as in equations (16a) and (16b).

The amplitude spectrum $A_d(\omega)$ of the dike anomaly may now be written as

$$A_d(\omega) = \left\{R_d^2(\omega) + X_d^2(\omega)\right\}^{1/2}$$

$$= \frac{2c\sin\omega x_o e^{-\omega z_1}\left\{1 + e^{-2\omega T} - 2e^{-\omega T}\cos(\omega T\tan\beta)\right\}^{1/2}}{\omega^2} \quad \ldots\ldots (29)$$

From equation (28),

$$R_d(\omega) = \frac{-2c\sin\omega x_o M e^{-\omega z_1}\cos(h_1 + \phi)}{\omega^2} \quad \ldots\ldots (30a)$$

and

$$X_d(\omega) = \frac{-2c\sin\omega x_o M e^{-\omega z_1}\sin(h_1 + \phi)}{\omega^2} \quad \ldots\ldots (30b)$$

Taking the logarithm of the expression in (29) we obtain

$$\text{Log } A_d(\omega) = \text{Log } (2c) + \text{Log } (\sin\omega x_o) - \omega z_1 - 2 \text{ Log } \omega + \frac{1}{2}\text{ Log}\left\{1 + e^{-2\omega T} - 2e^{-\omega T}\cos(\omega T\tan\beta)\right\} \quad \ldots\ldots (31)$$

T is usually fairly large for a dike, hence we assume that the last term in the above expression is unity.

Furthermore, for $(\omega x_o)^2 < \pi^2$, log $(\sin\omega x_o)$ can be expanded in a Taylor's series, so that

$$\text{Log } (\sin\omega x_o) = \text{Log } (\omega x_o) - \frac{(\omega x_o)^2}{6} - \frac{(\omega x_o)^4}{180} - \frac{(\omega x_o)^6}{2835} \quad \ldots\ldots (32)$$

The quantity x_o for a dike is usually very small (of the order of 0.2 or less); for $\omega x_o \leq 1$ all the terms excepting the first in equation (32) are negligible. With these simplifications equation (31) may be written as

$$\text{Log } A_d(\omega) = \text{Log } (2c) + \text{Log } (\omega x_o) - \omega z_1 - 2 \text{ Log } \omega$$

$$= \text{Log}\left(\frac{2cx_o}{\omega}\right) - \omega z_1$$

We define a new function $B(\omega)$ given by

$$B(\omega) = \omega A_d(\omega)$$

Hence $\log B(\omega) = \log A_d(\omega) + \log \omega$

$$= \log (2cx_o) - \omega z_1 \quad \ldots\ldots (33)$$

Then the slope of the above equation gives z_1 and the intercept at $\omega = 0$ gives us the value of $\log (2cx_o) = \log (4\pi G\rho\, x_o \cos\beta)$. Thus, knowing ρ, the density contrast and x_o, the half-width of the dike, β can be obtained. Alternatively, knowing ρ and β, x_o can be obtained.

In order to calculate $B(\omega)$, we must first find $R_d(\omega)$ and $X_d(\omega)$. The procedure is exactly the same as that outlined in the section on fault interpretation, pages 116-118, hence further discussion here is unnecessary.

Theoretical Example

In this section we calculate the Fourier coefficients obtained from the gravity expression of the dike anomaly given by equation (5). We then compare the Fourier coefficients with the transforms $\frac{R_d(n\omega_o)}{L}$, $-\frac{X_d(n\omega_o)}{L}$. The calculations were made for a dike with the following parameters:

$$z_1 = 0.5, \quad z_2 = 2.5, \quad x_o = 0.2, \quad \beta = 60^o,$$

$$\rho = 1.0, \quad \omega_o = \frac{\pi}{L} = 0.291, \quad L = 10.8$$

a_n and $\frac{R_d}{L}(n\omega_o)$ are compared in Figure 58. Within the accuracy of plotting the two graphs are indistinguishable and so the graph of the transform merges into the graph of a_n. Similarly, in Figure 59, we see that the graph of b_n also merges into the graph of $-\frac{X_d}{L}(n\omega_o)$ so that the two are indistinguishable. Figure 60 shows the graph of $\log \{B(n\omega_o)/L\}$ versus n. The slope of this graph in the linear region gives $z_1 = 0.49$ and the intercept at $n = 0$ gives $\beta = 61^o$.

Limiting Values Of $R_d(\omega)$ And $X_d(\omega)$

The limiting values of the functions $R_d(\omega)$ and $X_d(\omega)$ as $\omega \longrightarrow o$ are of interest.

From equation (30a), page 144,

$$R_d(\omega) = -\left(\frac{2c}{\omega^2}\right)\sin\omega x_o \, M e^{-\omega z_1}\cos(h_1 + \phi)$$

Substituting $$M = \left\{1 + e^{-2\omega T} - 2e^{-\omega T}\cos(\omega T\tan\beta)\right\}^{1/2},$$

$$h_1 = \omega z_1 \tan\beta + \beta,$$

and $$\tan\phi = \frac{\sin(\omega T\tan\beta)}{\cos(\omega T\tan\beta) - e^{\omega T}},$$

in the above expression, we have,

$$R_d(\omega) = -\left(\frac{2c}{2}\sin\omega x_o\right)\left[e^{-\omega z_2}\cos(\omega z_2\tan\beta + \beta) - e^{-\omega z_1}\cos(\omega z_1\tan\beta + \beta)\right] \quad \ldots\ldots (34)$$

Taking a typical term in the above expression, we can write

$$\lim_{\omega \longrightarrow o} -\left(\frac{2c}{\omega^2}\sin\omega x_o\right) e^{-\omega z}\cos(\omega z\tan\beta + \beta)$$

$$= -\lim_{\omega \longrightarrow o} \frac{(2c\omega x_o)}{\omega^2}\left[(1 - \omega z)\cos\beta - \sin\beta\,(\omega z\tan\beta)\right]$$

$$= -\lim_{\omega \longrightarrow o} \frac{(2cx_o)}{\omega}\left[\cos\beta - \omega z\cos\beta - \omega z\,\frac{\sin^2\beta}{\cos\beta}\right]$$

$$= -\lim_{\omega \longrightarrow o} \frac{2cx_o}{\omega}\cos\beta(1 - \omega z\sec^2\beta).$$

If we take into consideration both terms within the square bracket in equation (34), we obtain

$$\lim_{\omega \to 0} R_d(\omega) = -\lim_{\omega \to 0} \frac{2cx_o}{\omega} \cos\beta \sec^2\beta(\omega z_1 - \omega z_2)$$

$$= 2cx_o T \sec\beta$$

$$= 4\pi G \rho x_o T \qquad \ldots\ldots (35)$$

A similar analysis for the imaginary part gives

$$\lim_{\omega \to 0} X_d(\omega) = 0$$

Provided the slope of the a_n versus n curve does not change very rapidly near the origin, we can extrapolate the curve to $\omega = 0$ and so find the value of the product $x_o T$, provided ρ is known.

In Figure 58, the intercept obtained by extrapolating the curve to $\omega = 0$ is 0.92. The calculated value is 0.94.

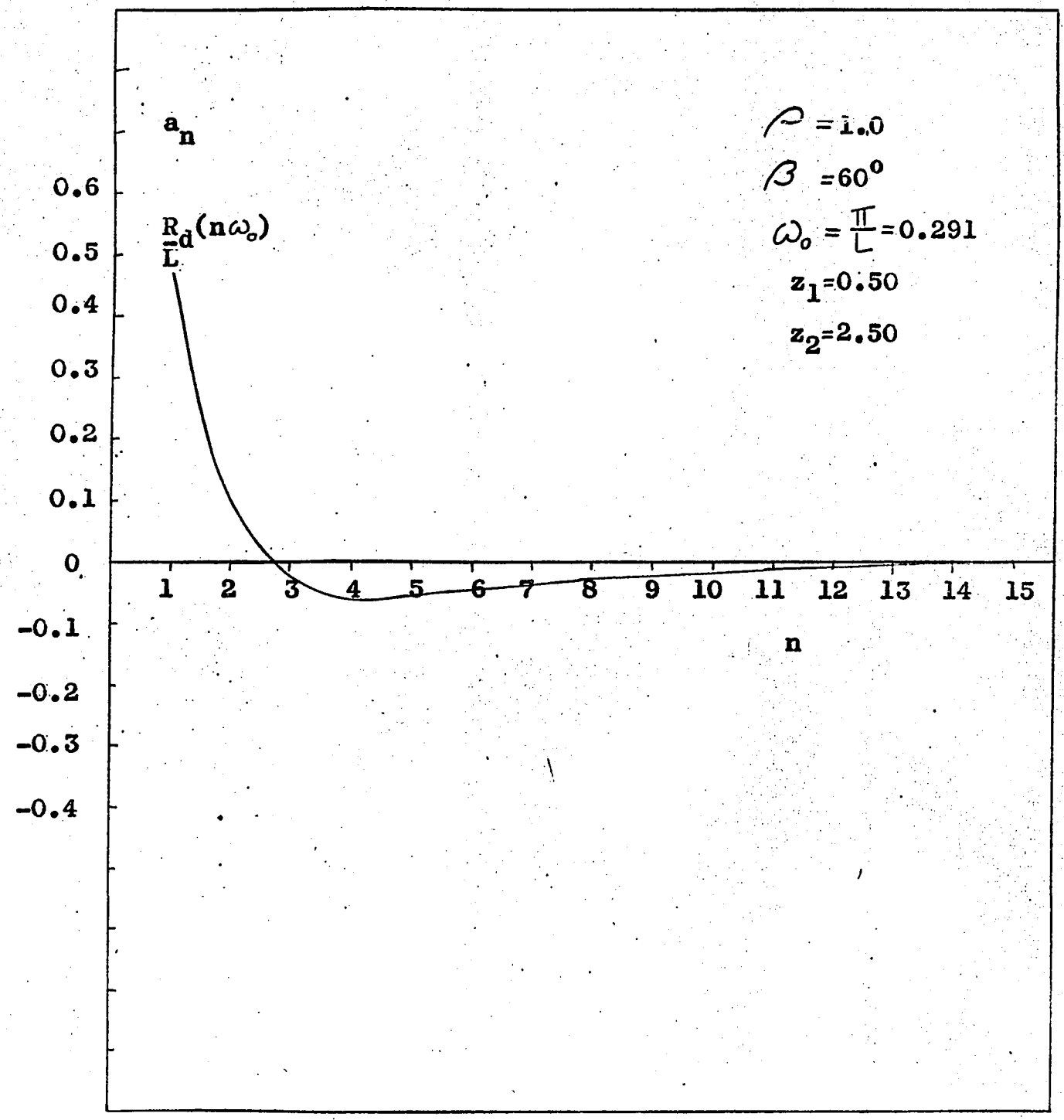

FIG 58. Comparison of a_n and $\frac{R_d(n\omega_o)}{L}$

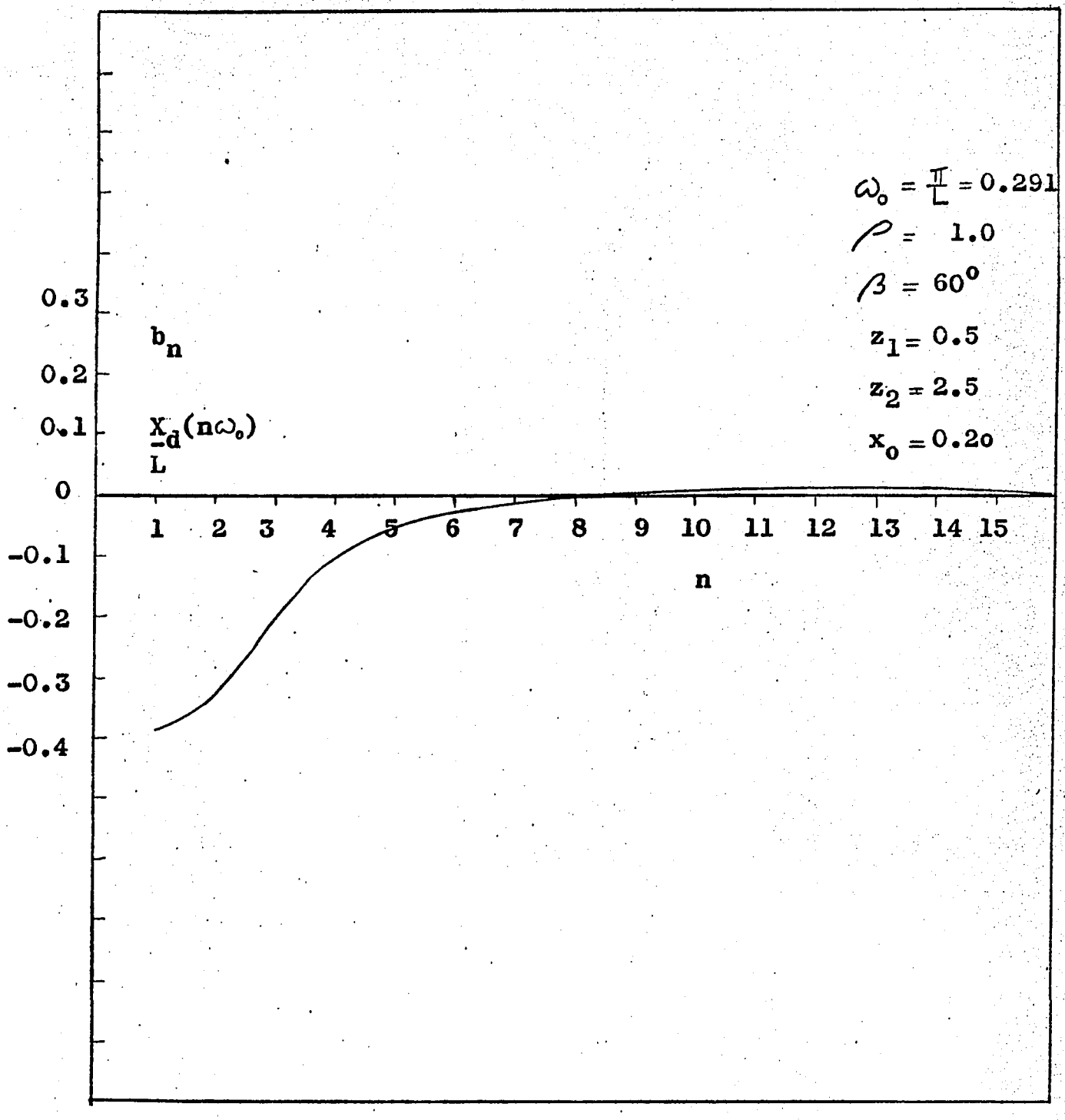

FIG 59. Comparison of b_n and $\frac{X_d}{L}(n\omega_o)$

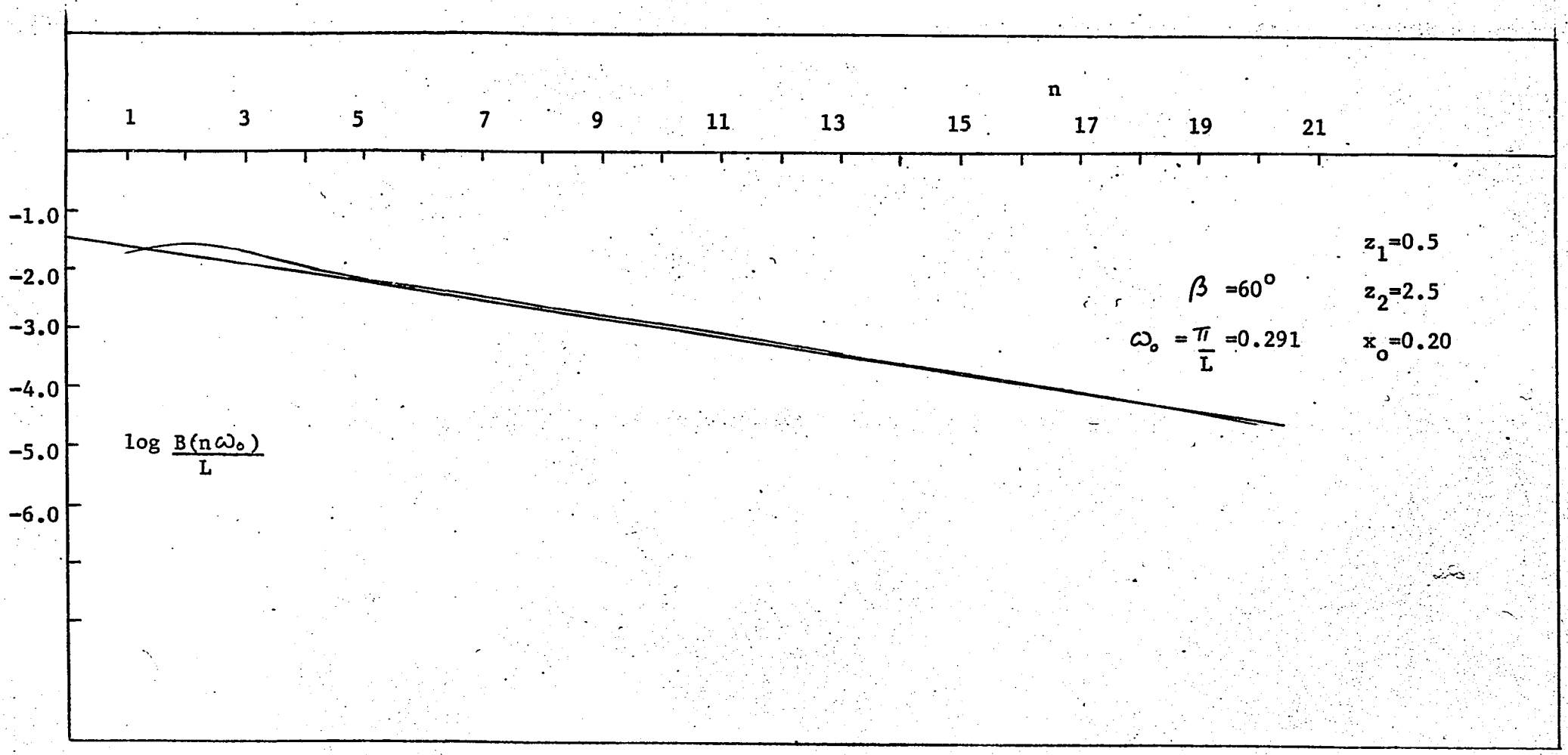

FIG 60. Amplitude spectrum for a dike as a function of n

CHAPTER V

Field Examples

General: In order to test the validity of some of the formulas derived earlier, several gravity surveys were made over known faults and dikes during the summers of 1965 and 1966. Each survey is described separately in the following sections.

The elevation measurements at the stations were made with a quick-set Zeiss surveying level capable of giving readings accurate to the nearest 0.01 foot within a horizontal range of 400 feet or less.

The pressure in the vacuum chamber of the gravimeter was checked and the gravimeter recalibrated before the start of the survey. The performance of the gravimeter was excellent during most of the survey with drifts rarely exceeding 0.02 mgls/hr. There were, however, a few days when the gravimeter drifted by as much as 0.1 mgls/hr. This comparatively large drift of the gravimeter is believed to be a temperature effect because it invariably occurred on very hot, humid days. In order to correct for the gravimeter drift, the base station was revisited every hour or so. The drift was found to vary almost linearly with time, hence readings of all stations occupied in between two readings at the same base station were corrected by assuming linear drift.

The Worden gravimeter used was model No. 506 with a dial

constant of 0.1071 mgl/Div and a sensitivity of 0.01 milligals.

The locations of the various gravity surveys are shown in the index map of the St. Lawrence Lowlands in Figure 61.

Delson Fault Area

Introduction: A detailed gravity survey over the Delson fault area near Montreal was carried out in 1965 for the purpose of determining some of the fault parameters by the application of some of the formulas derived earlier. The geology of the area is comparatively well known so that interpretation based on these formulas may be directly compared with the geology of the area.

The Delson fault area is situated about fifteen miles to the southeast of Montreal and covers the area between Latitudes $45^{\circ}19'6''$ and $45^{\circ}24'8''$, Longitudes $73^{\circ}36'$W and $73^{\circ}30'$ W. Five profiles were taken at right angles to the strike of the fault, as indicated on the geologic map of the area (Clark, 1955). There are several roads crossing the area so that gravity surveys in most cases could be carried out along these roads.

The topography of the area is smooth with elevations of most stations ranging between 100 and 200 feet above sea level. The lack of large relief renders it unnecessary to make topographic corrections.

The rate of change of gravity with latitude is equal to $1.307 \sin 2\phi$ mg/mile where ϕ is the Latitude of the station. Since the present area of survey is located very near to the 45° Latitude, the variation in gravity due to change in Latitude may be taken to be linear and equal to 1.307 mg/mile. The free air and Bouguer corrections were applied in the usual manner assuming a density of 2.0 gm/c.c.

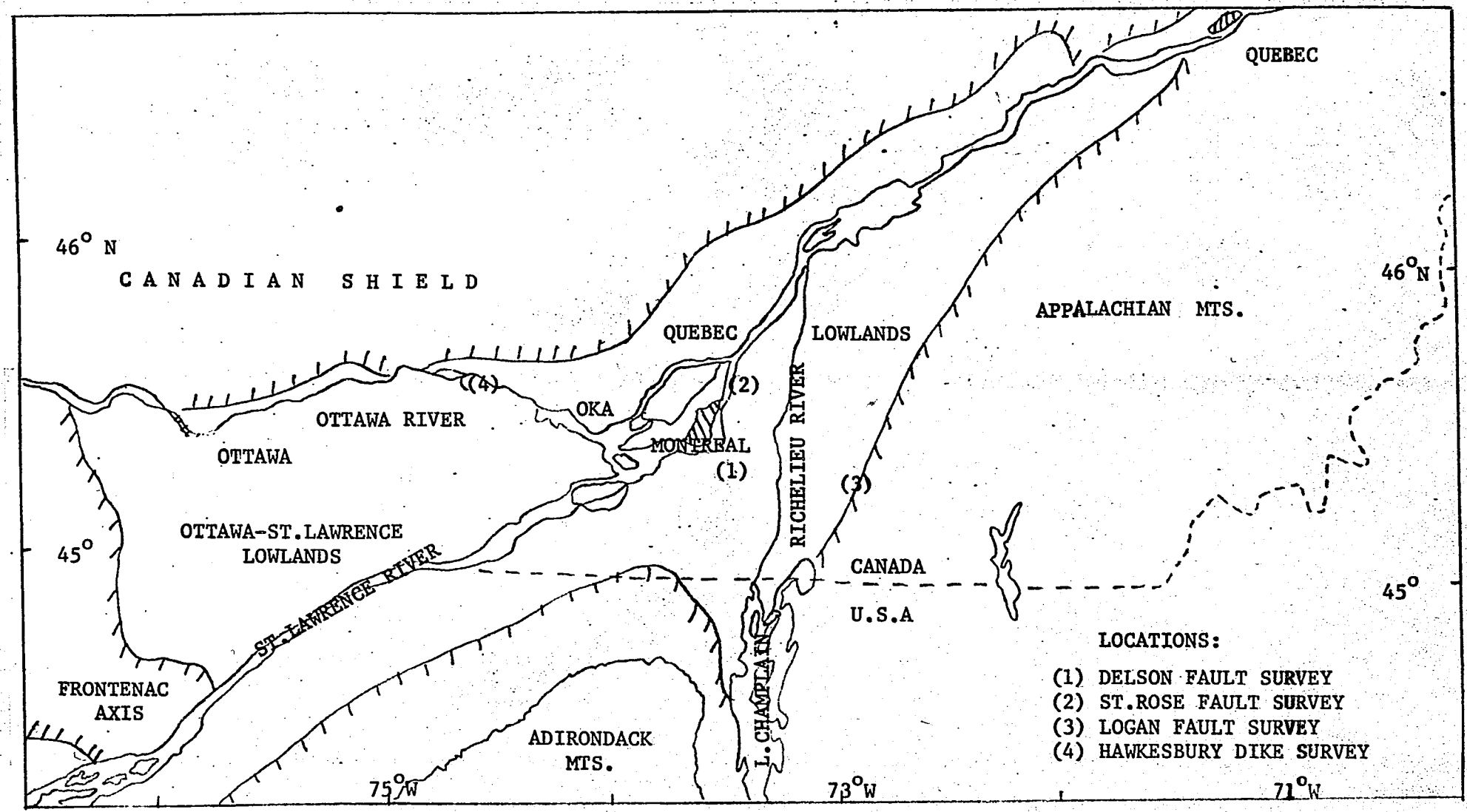

FIG 61. Index map showing the locations of various gravity surveys

for the overburden.

The first gravity survey of the area was made by R.J. Uffen of the Dominion Observatory of Ottawa in 1954. The results of Uffen's survey were published by Thomson and Garland (1957). Uffen's work was in the nature of a very broad regional survey with station spacing between 2-10 miles. D. McDonald carried out a gravity survey of the St. Lawrence Lowlands in 1964 for his Master's thesis in the Department of Mining Engineering and Applied Geophysics, McGill University.

The geology of the Delson fault area has been dealt with quite exhaustively by T.H. Clark in his Department of Mines (Quebec) reports of the Montreal area (Clark, 1952). The formations present in the area, according to Clark, are flat lying with dips rarely exceeding five degrees. The entire area is covered with glacial drift of average thickness 50 feet. Below this overburden are disposed sedimentary rocks of Ordovician age belonging to different groups, such as the Chazy limestones, the Trenton limestones, the Utica shales and the Lorraine shales. The occurrence of the Potsdam sandstone of the upper Cambrian series underlying the Ordovician is postulated because of the outcrop of Potsdam sandstone in the Laval and Lachine areas. Further, as reported by Clark, a well drilled just north of the village of St. Hubert reached Potsdam sandstone at a depth of 3,965 feet. Since drilling was discontinued after penetrating only five feet of sandstone, the actual thickness of the formation is uncertain: however, it is reasonable to expect that the Potsdam formation extends over the entire St. Jean-Beloeil areas. Pre-cambrian basement rocks are believed to underlie the Cambrian.

The presence of glacial drift makes it almost impossible to observe the Delson fault at the surface. The evidence for the existence of the fault is the fact that in the Delson area, flat lying Utica beds are observed at the surface, while in the Caughnawaga area just to the west the surface beds are flat lying Chazy beds. The attitude of the Chazy and the Utica cannot be reconciled without postulating a major dislocation striking approximately east-west. Moreover, at St. Jean, which is in the eastern extremity of the present area, the succession is Trenton, Black River and Chazy whereas two miles to the north of this occurrence there is exposure of Utica at Delson. The Delson fault has been used to explain these breaks in stratigraphy. The strike direction of the Delson fault as postulated by following the outcrops of the Chazy and the Utica is fairly well established and is shown by the line xx' in the Bouguer anomaly map in Figure 62.

Thicknesses of the various sedimentary formations in the St. Jean-Beloeil areas are given by Clark (1955), based upon various well logs and also from measurements of exposed rocks wherever available. An approximate section through the Delson fault is shown in Figure 63 as deduced from Clark's report.

From geological evidence the Delson fault is believed to be vertical with a throw of about 900 feet down to the north.

The density figures of the different formations of Figure 63 are based on measurements made by McDonald (1964) and Saxov (1956).

FIGURE 62 . Please see folder at the back of the thesis.

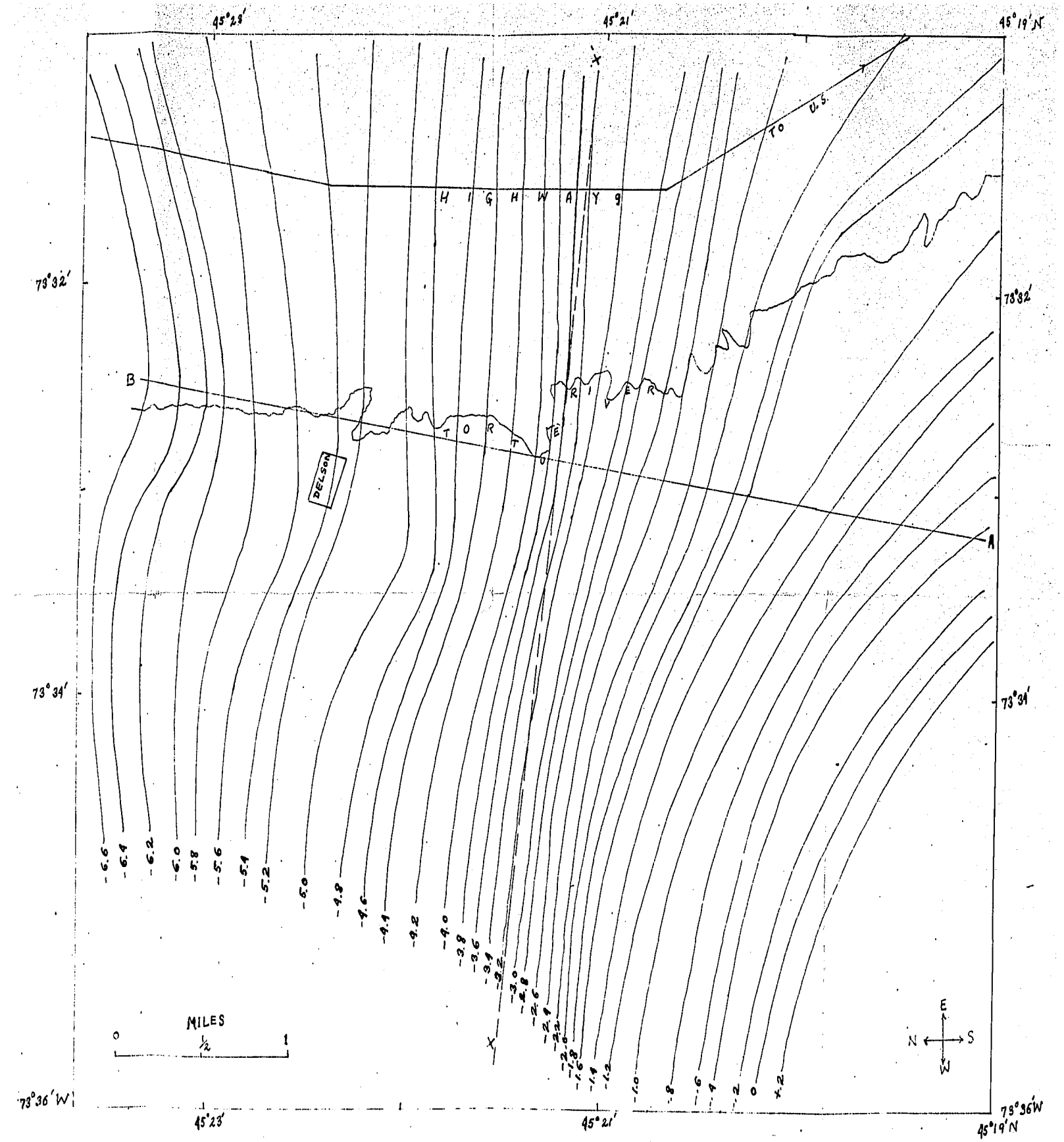

FIG 62 BOUGUER ANOMALY MAP OF THE DELSON FAULT AREA

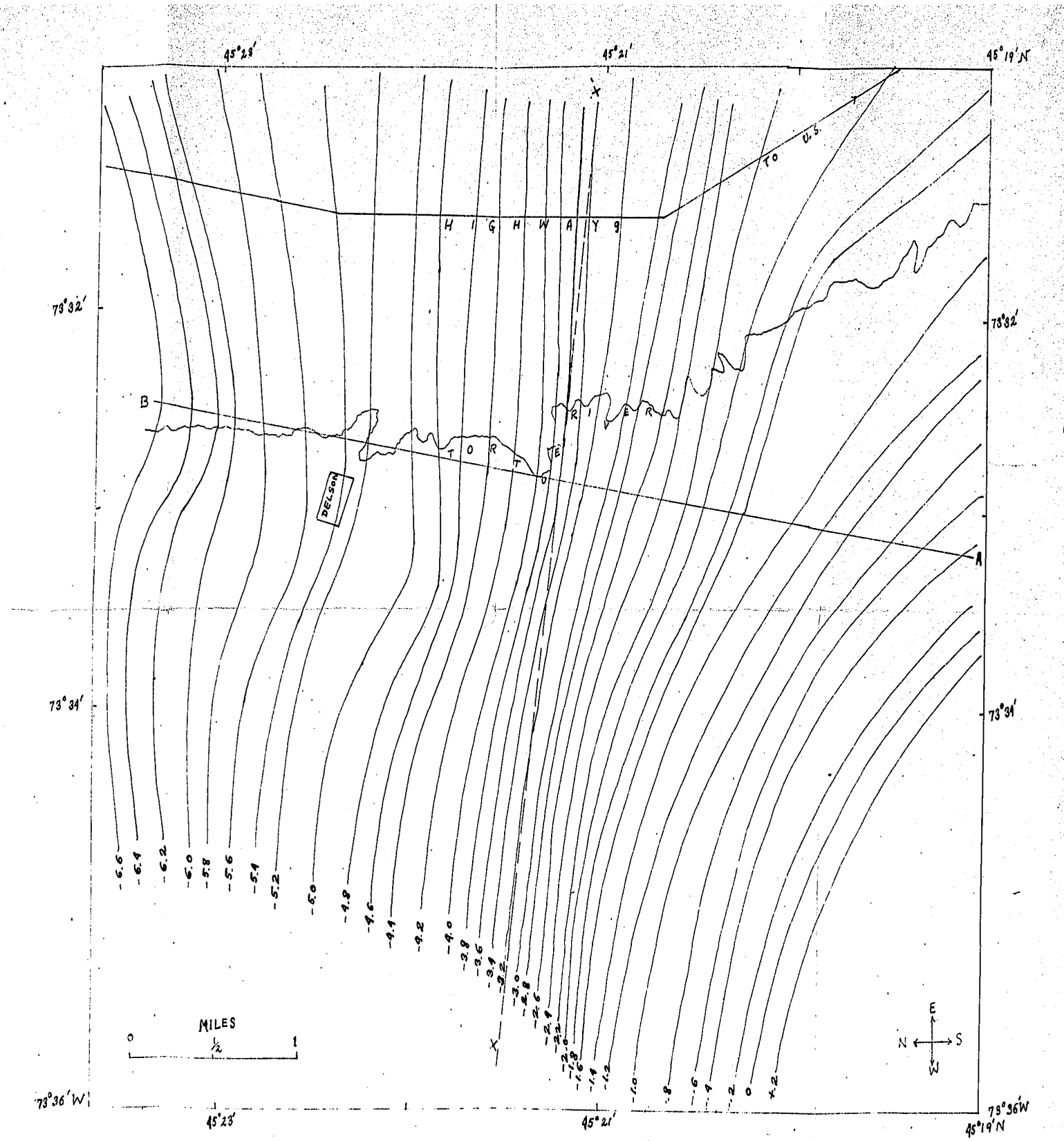

FIG 62 BOUGUER ANOMALY MAP OF THE DELSON FAULT AREA

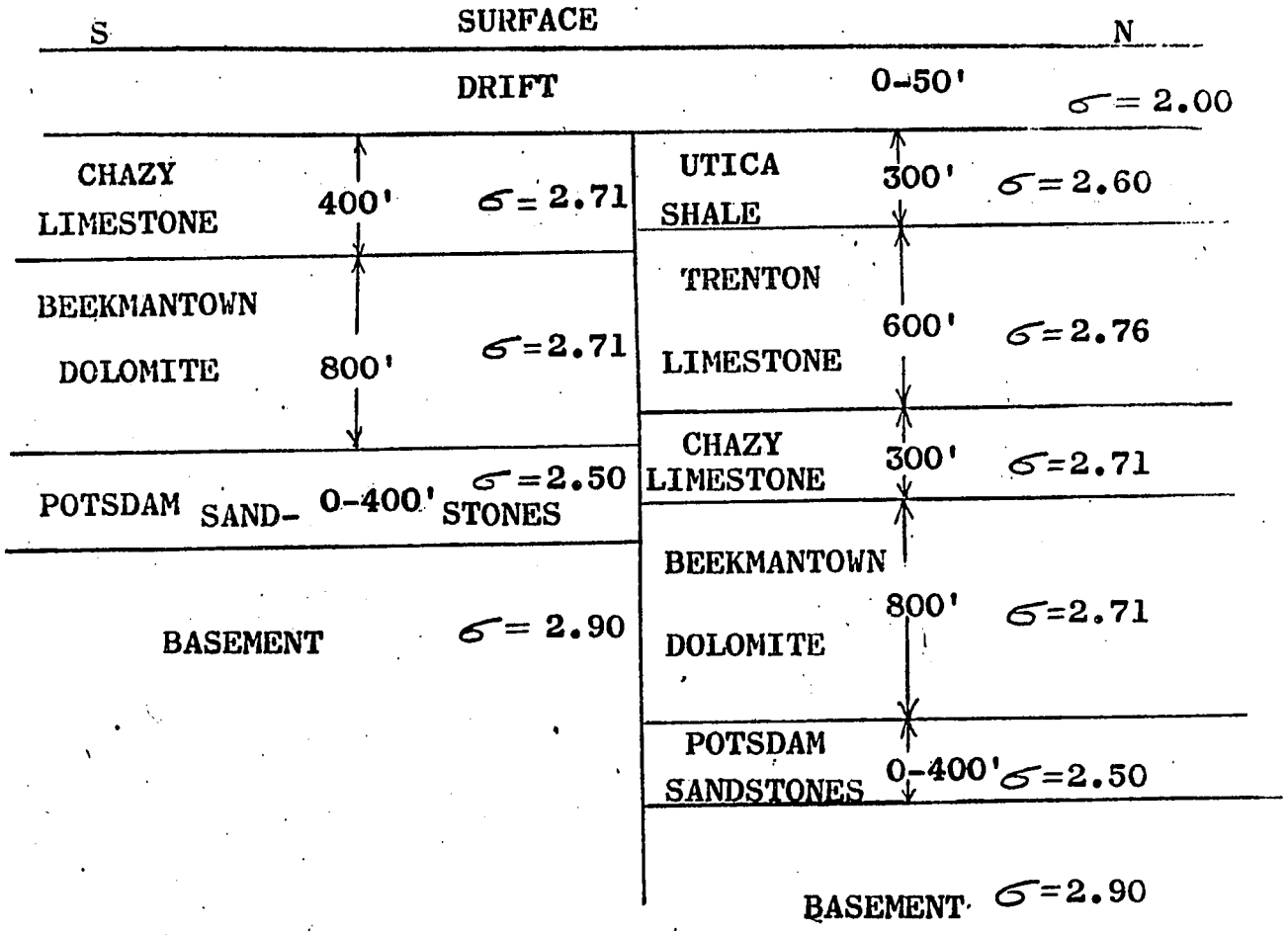

FIG 63. Section through the Delson fault

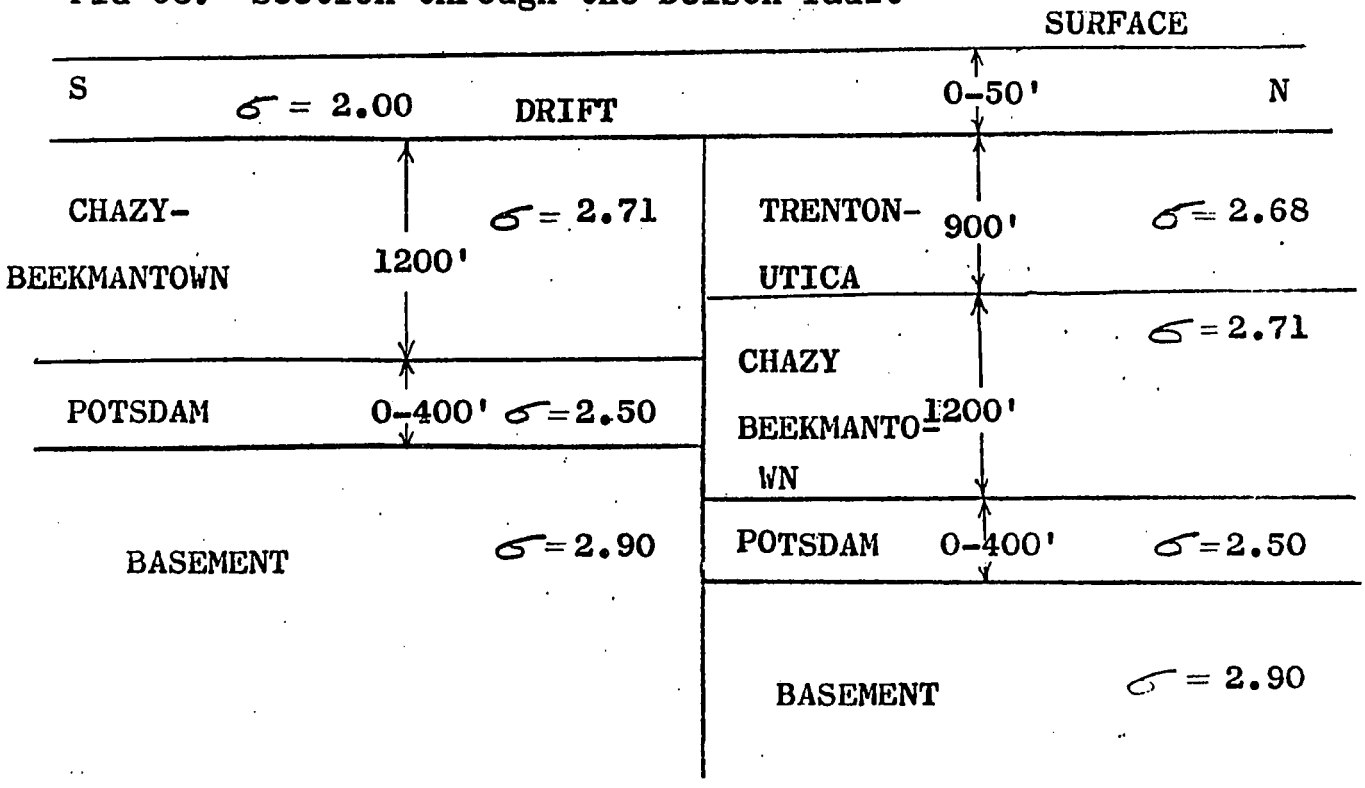

FIG 64. Simplified section through the Delson fault

Observations: Figure 62 shows the Bouguer gravity anomaly map of the Delson area. Altogether, 202 stations were occupied along five profiles perpendicular to the strike direction of the fault. Station spacings in most cases were 400 feet but this was reduced to 300 feet in certain parts of the profile. The contour interval in Figure 62 is 0.2 milligals.

The general pattern of the gravity anomaly contours in Figure 62 shows that the gravity decreases from the south to the north. The spacings between contours is a minimum at the center of the map and becomes wider at the southern and the northern parts of the map and the contours bend down quite sharply at the south-east corner of the map. This bending of the contours is believed to be due to the influence of a second fault, the so-called Tracy Brook fault, which strikes in the north-south direction.

Profile A-B is drawn perpendicular to the contours of the Bouguer anomaly as shown in Figure 62. Since the gravity anomaly contours are fairly regular at the central part of the map the influence of the Tracy Brook fault on profile A-B may be considered negligible and whatever anomaly is obtained, may be attributed to the Delson fault.

The gravity anomaly across the Delson fault along profile A-B (Figure 65) resembles the characteristic gravity profile across a single block or of a fault truncating a series of beds. The total change in the gravity due to the Delson fault as measured from profile A-B is 2.3 milligals. If this change is entirely due to the density difference

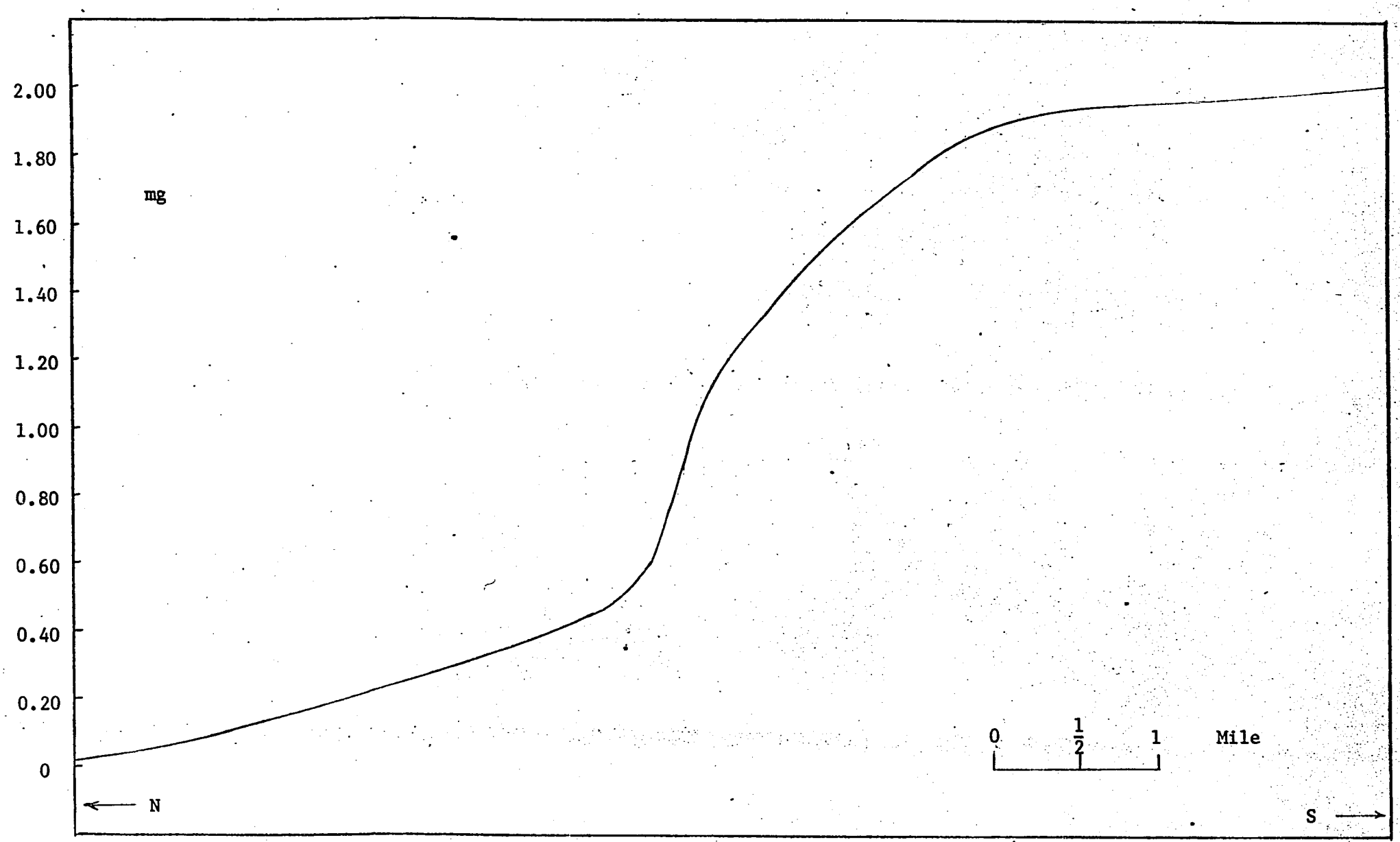

FIG 65. Gravity anomaly across Delson fault along profile A-B

between the Chazy and the Utica beds, then we have approximately,

$$g_1 = 2\pi G(\sigma_1 - \sigma_2)t$$

where g_1 = Total change in gravity due to the Delson fault.

σ_1 = Density of the Chazy beds.

σ_2 = Density of the Utica beds.

t = Thickness of the Utica beds.

The density of the Utica shale is about 2.60 gm/c.c. and of the Chazy limestone beds 2.71 gm/c.c., and the Utica is about 300 feet thick. Hence, the total change in the gravity is 0.4 mgls. This is far too small to explain the 2.3 milligals obtained from the field data. The possibility that the other Paleozoic beds below the Chazy formation may add significantly to the anomaly is ruled out since the Beekmantown beds below the Chazy beds have virtually the same density as the Chazy beds and the low density Potsdam beds below the Beekmantown will have a negative effect, thereby reducing the total anomaly. To account for the large gravity anomaly, therefore, we must look for some other sources of high density rocks besides the Paleozoic. The Precambrian rocks have a high density and are believed to underlie the whole of this area. The contribution of these high density rocks to the gravity anomaly therefore can account for the comparatively large gravity anomaly of the Delson fault.

In order to apply the gravity formula to a fault truncating the series of Paleozoic formations and the basement, the section through the Delson fault was simplified as shown in Figure 64. The Utica and

the Trenton beds in the above figure are assigned the density of 2.68 gm/c.c. We, therefore, have a fault truncating a series of beds and the basement. The total change in gravity due to such a fault, from equation (3a) is

$$g_m = 2\pi G(\sigma_r - \sigma_o)$$

where g_m is the total change in gravity due to the fault

σ_o is the average density of the Utica and the Trenton beds

σ_r is the density of the basement.

Substituting the respective values of the densities the total change in gravity due to the Delson fault is given by

$$g_m = 2\pi G(2.90 - 2.68)\delta = 2.3$$

From above, the displacement 'δ' of the Delson fault is 820 feet. This value for the displacement of the Delson fault agrees very closely with the value estimated by Clark which is 900 feet at the Mercier Bridge (about 8 miles to the north-west of the present area) and 800 feet at the Menard corner (about 10 miles to the south-east of the present area).

Figure 66 shows the gradient profile across the Delson fault. This gradient curve was obtained from the gravity profile A-B by taking the difference in the observed gravity values between two closely spaced points and dividing this difference by the distance separating the two points. The gradient attains the maximum value of 0.47 milligals per 1000 feet near $x = -0.3$. Thus the position of the maximum

gradient is very close to the fault trace, indicating that the Delson fault is very nearly vertical. However, for a vertical fault, the maximum gradient occurs directly over the fault trace and the gradient curve is perfectly symmetrical about the fault trace. The gradient curve of Figure 66 is not perfectly symmetrical, the gradient decreasing slightly more rapidly on the north side than on the south side. This shows that the Delson fault dips very steeply to the north. In order to obtain an approximate value of the inclination of the fault plane, we calculate the following function:

$$G_m(x) = x \frac{dg_m}{dx} - g_m$$

where g_m is the gravity anomaly of the Delson fault.
It is shown earlier that the limiting values of $G_m(x)$ for very large values of x in the positive and negative directions have the values $2G\delta(\sigma_o - \sigma_r)(\frac{\pi}{2} - \beta)$ and $-2G\delta(\sigma_o - \sigma_r)(\frac{\pi}{2} + \beta)$ respectively. Hence the sum of the limiting values of $G_m(x)$ in the positive and negative directions has the value $4G\beta\delta(\sigma_r - \sigma_o)$. Thus, knowing the limiting values of $G_m(x)$ and δ, an approximate value of β may be obtained.

Figure 66 shows the function $G_m(x)$ calculated for the Delson fault from the gradient and the gravity profile over the fault. The limiting value of $G_m(x)$ from Figure 66 appears to be about 1.0 and -0.8 milligals so that the sum of the two limiting values is about 0.2 milligals. Substituting $\delta = 0.9$, $(\sigma_r - \sigma_o) = 0.22$ gives $\beta = 0.12$ radians or 7 degrees. We thus conclude that the Delson fault is a high angle normal fault whose fault plane dips about 83° towards the north.

To find the depth to the basement we use the value of the maximum gradient. It was shown earlier that for a single fault the horizontal gradient is given by

$$\frac{dg_s}{dx} = 2G\rho\sin^2\alpha \, \mathrm{Log}(1 + \frac{t}{z_1})$$

For a fault truncating a series of N beds the expression for the horizontal gradient at x = 0 is derived in Appendix B (see equation 3b) and is given by

$$\frac{dg_m}{dx} = 2G\cos^2\beta \left\{ \rho_1 \, \mathrm{Log}(1 + \frac{\delta}{z_1}) + \rho_2 \, \mathrm{Log}(1 + \frac{\delta}{z_2}) \right.$$

$$\left. + \ldots . \; \rho_{N+1} \, \mathrm{Log}(1 + \frac{\delta}{z_{N+1}}) \right\}$$

$$\rho_i = (\rho_i - \rho_{i-1}); \quad i = 1, 2, \ldots . N$$

and $\rho_{N+1} = (\sigma_r - \sigma_N)$.

From above it is clear that in order to calculate the depth to the basement, z_{N+1}, we require the knowledge of the depths from the surface to the top of each bed and also the densities of each bed. Since the depths are unknown, an approximate solution may be obtained by giving a uniform density to the Paleozoic sediments and assuming that the entire gradient is due to the basement step at depth z_{N+1}.

It was shown earlier that the maximum slope of the gravity curve for any value of α is very nearly equal to the maximum slope for $\alpha = 90^\circ$. Hence the formula for the maximum gradient of the basement step becomes

$$\frac{dg_m}{dx} = 2G(\sigma_r - \bar{\sigma}) \text{ Log}(1 + \frac{\delta}{z_{N+1}})$$

where σ_r is the density of the basement rocks.

$\bar{\sigma}$ is the average density of the Paleozoic sediments.

z_{N+1} is the depth to the basement on the south side of the fault.

Substituting in the above equation the values obtained earlier for the maximum gradient and the displacement δ, and taking $\sigma_r = 2.90$ gm/c.c., $\bar{\sigma} = 2.68$ gm/c.c., we find the value 1300 feet for the depth to the basement on the south side of the Delson fault. From geological considerations, the actual depth to the basement should be somewhat greater, probably about 1500-1800 feet.

Interpretation: The gravity anomaly of the Delson fault does not approach zero values for large positive and negative values of x on either side of the fault trace. The first derivative of the anomaly, however, approaches zero values as shown in Figure 66. In order to obtain the transform of the gravity anomaly of the Delson fault, therefore, we perform a Fourier analysis of the first derivative of the gravity anomaly. As mentioned in the last chapter, the Fourier coefficients, a_{n1} and b_{n1}, of the first derivative of the anomaly will be proportional to the Fourier transforms, $R_1(n\omega_o)$ and $X_1(n\omega_o)$ respectively. Having obtained $R_1(n\omega_o)$ and $X_1(n\omega_o)$, the Fourier transforms, $R(n\omega_o)$ and $X(n\omega_o)$, of the gravity anomaly or the transforms, $R_2(n\omega_o)$ and $X_2(n\omega_o)$, of the second derivative of the anomaly can be obtained as discussed in the last chapter.

The fundamental wavelength (2L) chosen for Fourier analysis of the gravity data is 21.21 units. This interval was divided into 100 equal increments, $\Delta x = 0.2121$ units. The first derivative was obtained by taking the gravity difference across each increment, Δx, and then dividing the difference by 0.2121. The ratio is approximately equal to the derivative at the mid-point of each increment. The Fourier coefficients, a_{n1} and b_{n1}, of the first derivative, $g'(x)$, of the gravity anomaly are obtained by carrying out the following summations

$$a_{n1} = \frac{1}{L} \sum_{x=-L}^{x=L} g'_1(x)\cos(n\omega_o x)\Delta x$$

$$b_{n1} = \frac{1}{L} \sum_{x=-L}^{x=L} g'_1(x)\sin(n\omega_o x)\Delta x$$

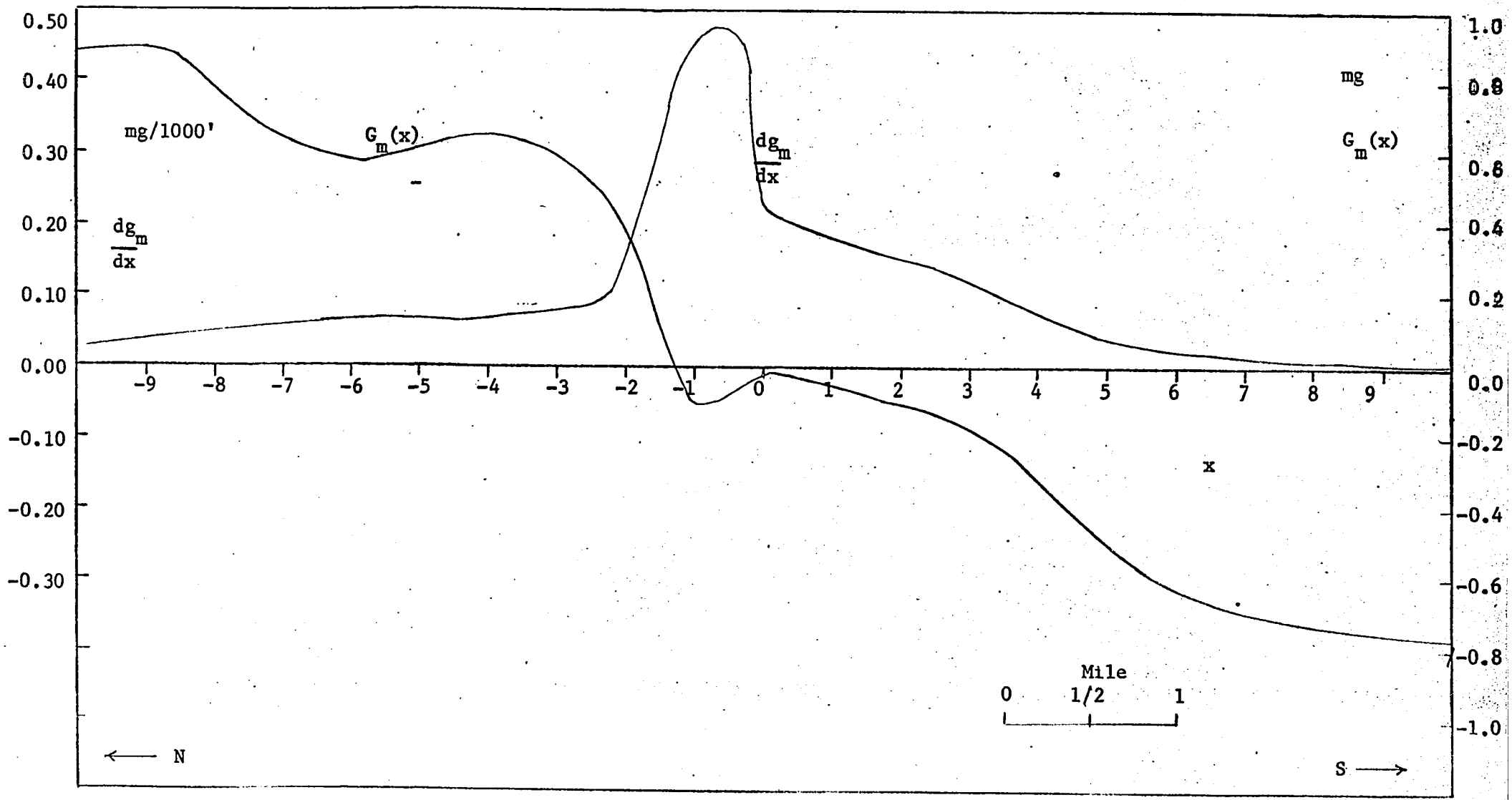

FIG 66 Graphs of $\frac{dg_m}{dx}$ and $G_m(x)$ for Delson fault

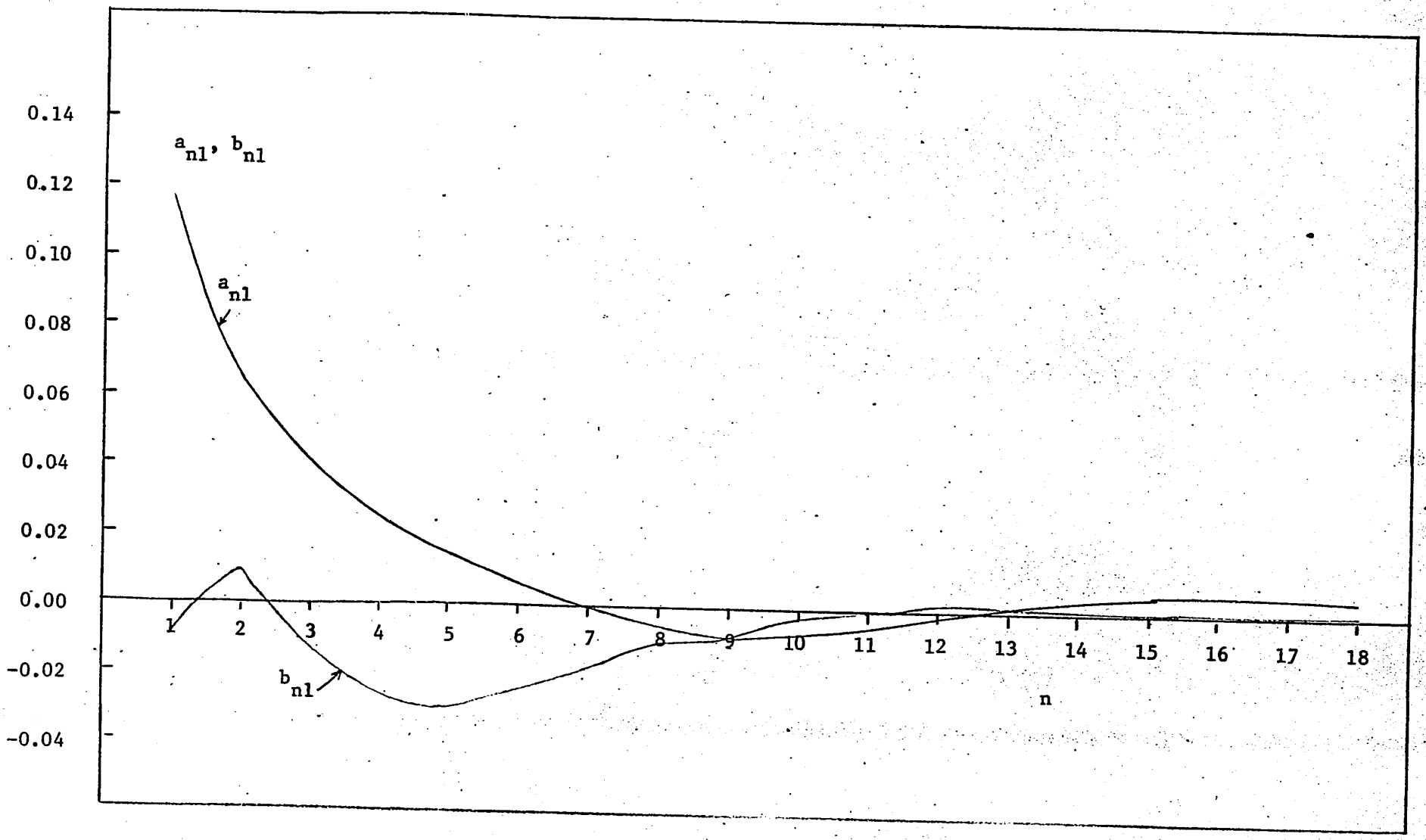

FIG 67 Coefficients a_{n1} and b_{n1} obtained from Fourier analysis of the gradient of the Delson fault anomaly

where ω_o = Fundamental wavelength = $\frac{2\pi}{2L} = \frac{6.2832}{21.21} = 0.3022$

The entire operation for the calculation of the coefficients was performed on the IBM 7044 computer. The data fed into the computer comprised values of L, ω_o and the 101 gravity values at the beginning and end of each of the 100 equal increments. The computer first calculates the derivative and then carries out the summations to give the Fourier coefficients, a_{n1} and b_{n1}.

The resulting Fourier coefficients, a_{n1} and b_{n1}, are shown in Figure 67. For a perfectly vertical fault, the coefficients b_{n1} should all be zero. Since the b_{n1} coefficients obtained from the field data are not all zero but have small values, we can conclude that the Delson fault instead of being vertical, is slightly inclined.

As ω approaches zero, the limiting values of $R_1(\omega)$ and $X_1(\omega)$ are given by (see Appendix F)

$$R_1(\omega) = 2\pi G\delta(\sigma_r - \sigma_o),$$

$$X_1(\omega) = 0$$

Producing the curve a_{n1} backwards, it is seen that at n = 0, it has the value 0.22. Therefore, we have

$$\frac{R_1(0)}{L} = 0.22 = \frac{2\pi G\delta}{L}(\sigma_r - \sigma_o)$$

$$\text{or } R_1(0) = 2\pi G\delta(\sigma_r - \sigma_o) = 2.33.$$

This corresponds to δ = 820 feet. From equation (3a), the total change

in gravity, g_m, due to a fault cutting a series of beds is $2\pi G\delta(\sigma_r - \sigma_o)$, hence we find

$$g_m = 2\pi G\delta(\sigma_r - \sigma_o) = R_1(0)$$

As discussed in the last chapter, a second method of obtaining the Fourier transform of the gravity anomaly, g(x), is by making a Fourier analysis of the function G(x). The function G(x) is obtained by subtracting g(x) from $g_{+\infty}$ when x is positive and by subtracting g(x) from $-g_{-\infty}$ when x is negative. The coefficients, a_n' and b_n', obtained by a Fourier analysis on G(x), are shown in Figure 68. It is shown in Appendix F that for very small values of ω, the coefficients a_n' and b_n' are approximately given by

$$a_n' \doteqdot \frac{\pi G\delta \tan\beta}{L}\left\{2z_{N+1}(\bar{\sigma} - \sigma_r) + \delta(\sigma_o - \sigma_r)\right\} \quad \ldots\ldots (39a)$$

$$b_n' \doteqdot \frac{\pi G\delta}{L}\left\{2z_{N+1}(\bar{\sigma} - \sigma_r) + \delta(\sigma_o - \sigma_r)\right\} \quad \ldots\ldots (39b)$$

Hence the dip of the fault plane can be obtained from the relation $\tan\beta = \frac{a_n'}{b_n'}$.

From Figure 68 the limiting values of a_n' and b_n' at n = 1 are -0.02 and -0.18 respectively. Hence it follows that $\tan\beta = 0.11$ and $\beta \doteqdot 6^\circ$.

Equation (39b) can also be used to find an approximate value for the depth to the basement if the displacement of the fault δ, the average density $\bar{\sigma}$ of the sedimentary rocks, the density of the basement σ_r, and the density of the rocks immediately above the first bed on the downthrown

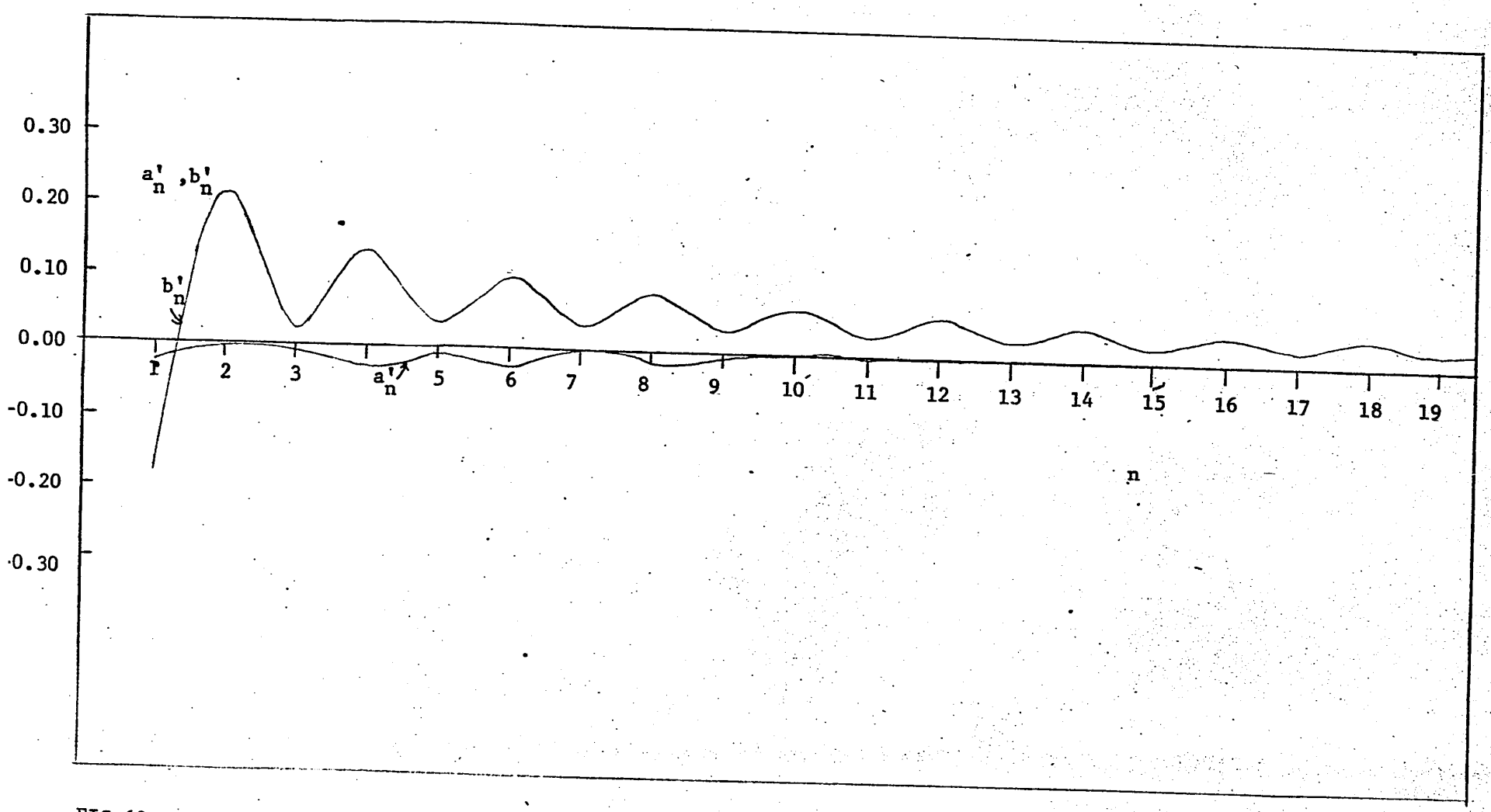

FIG 68 Coefficients a'_n and b'_n obtained from Fourier analysis of gravity data over Delson fault

side, σ_r, are known. Substituting $\delta = 0.82$ (obtained previously) and $\bar{\sigma}$, σ_r and σ_o respectively equal to 2.71, 2.90 and 2.68 gm/c.c. in equation (39b), the depth to the basement z_{N+1} on the south side of the Delson fault is found to be 1400 feet. The depth estimated on the basis of geological information is around 1500-1800 feet.

The St. Rose Fault

Introduction: The St. Rose fault, which strikes almost exactly east-west, is located around Latitude 45°40' N. The area surveyed was about 15 miles to the north-east of Montreal. Several profiles were taken at right angles to the strike of the fault.

Previous gravity surveys in the St. Rose fault area by Uffen (1957) and Hosain (1965) indicate that the anomaly of the St. Rose fault is small, of the order of a milligal or so. Therefore, gravity stations were established at intervals of 300 feet or less at most places.

The general topography of the area is flat with elevations of most stations around 100 feet above sea level. The large intrusives in the St. Lawrence Lowlands, such as Mt. Royal, Mt. Bruno and Mt. St. Hilaire, are too far away from the present area of survey to have appreciable gravitational effect.

The St. Rose fault area is underlain throughout by sedimentary rocks of Cambrian, Ordovician and Silurian ages. Pre-cambrian basement rocks are believed to underlie the entire area. The sedimentary rocks are very flat lying with dips rarely exceeding 2°.

There is no surface evidence of the St. Rose fault in the entire area. In order to explain the juxtaposition of the flat lying sedimentary beds at certain places, however, it is necessary to postulate a dislocation in the form of a fault (Clark, 1952).

Deep well logs are not available in the area of survey. Some

information about the general stratigraphy of the area can be obtained from the St. Hubert No. 1 well at St. Hubert airport (about 12 miles to the south of the area) and the Mallet test hole No. 1 at St. Therese (about 22 miles to the west of the area).

Based upon data from the above two wells and also the Department of Mines (Quebec) geologic reports of Clark (1952), the section through the St. Rose fault appears to be approximately as shown in Figure 69. The thickness of the Potsdam sandstone overlying the Precambrian varies widely from place to place. It is believed that the downthrow of the St. Rose fault is about 500 feet and the dip of the fault plane almost vertical.

The density information in Figure 69 was obtained from density measurements made by Saxov (1956), McDonald (1964) and Hosain (1965).

Observations: The observed and residual gravity profiles across the St. Rose fault are shown in Figure 71. The total amplitude of the anomaly from peak to peak is just over a milligal. If the observed gravity anomaly is due solely to the density difference between the limestone and the shale beds, then theoretically, the total change in gravity from the single block formula is $2\pi G\rho t$. Since the density contrast between the limestone and the shale beds is about 0.20 gm/c.c. and the thickness of the shale beds 400 feet, the total change in gravity due to the shale-limestone contact is 1.02 mg. This value for the total change in gravity for the shale-limestone contact agrees closely with the change in the observed gravity anomaly over the St. Rose fault. However, the distinct

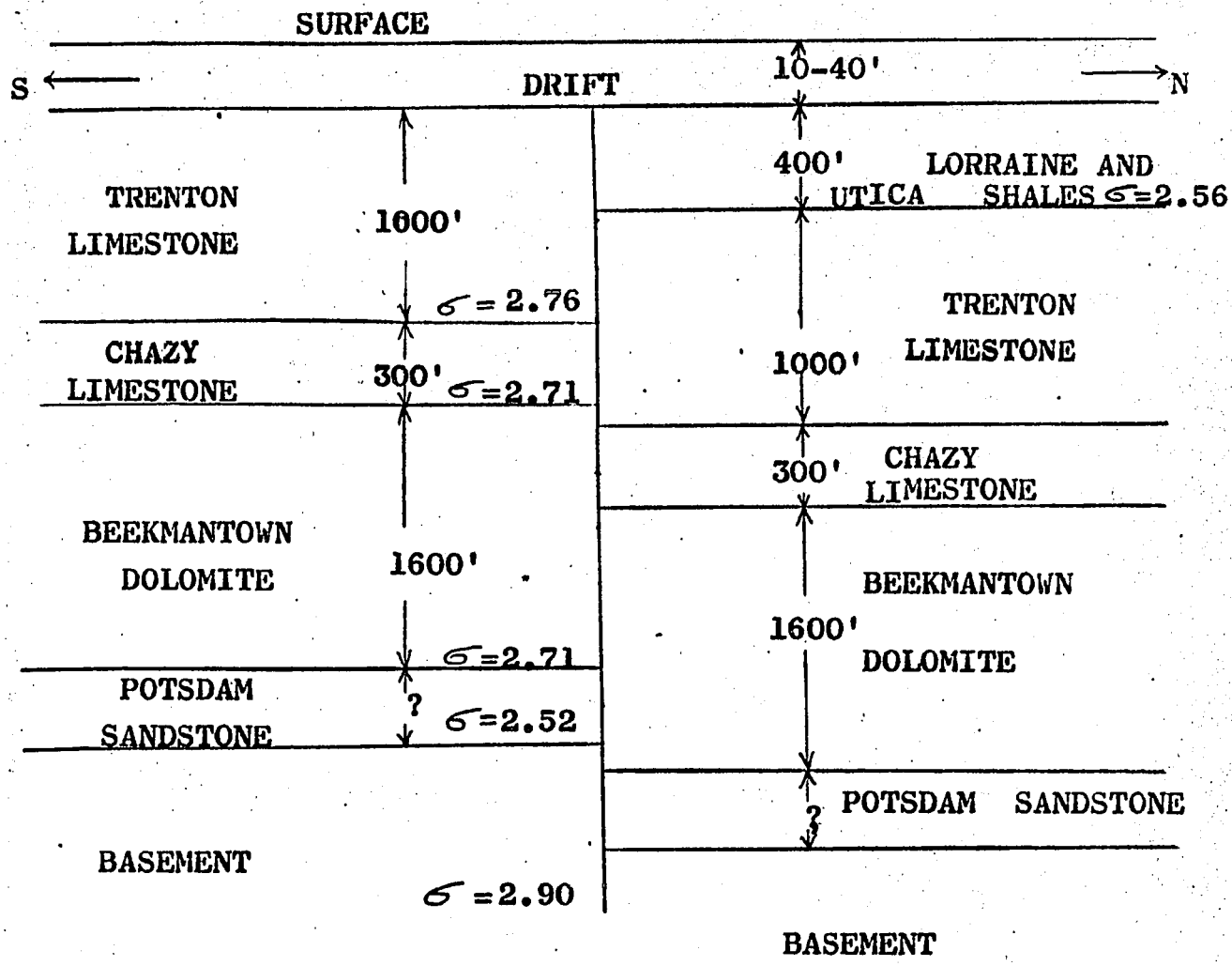

FIG 69. Section through the St.Rose fault area

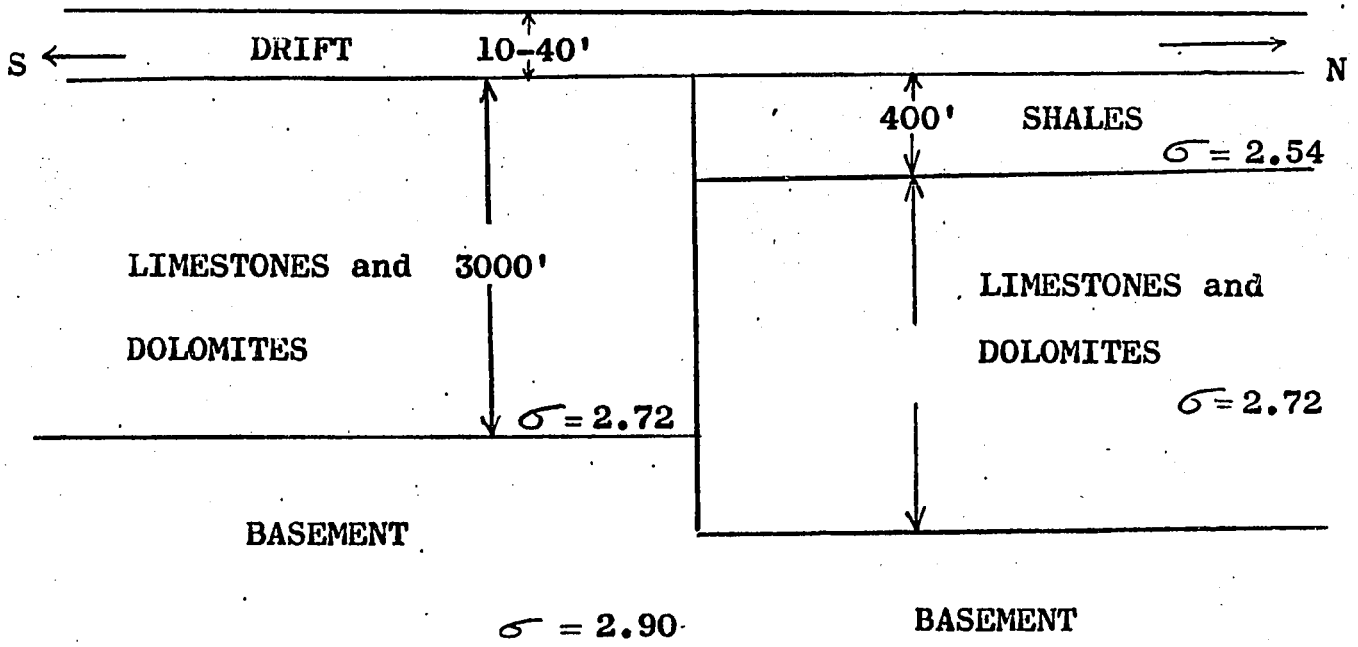

FIG 70. Simplified section for the St.Rose fault area

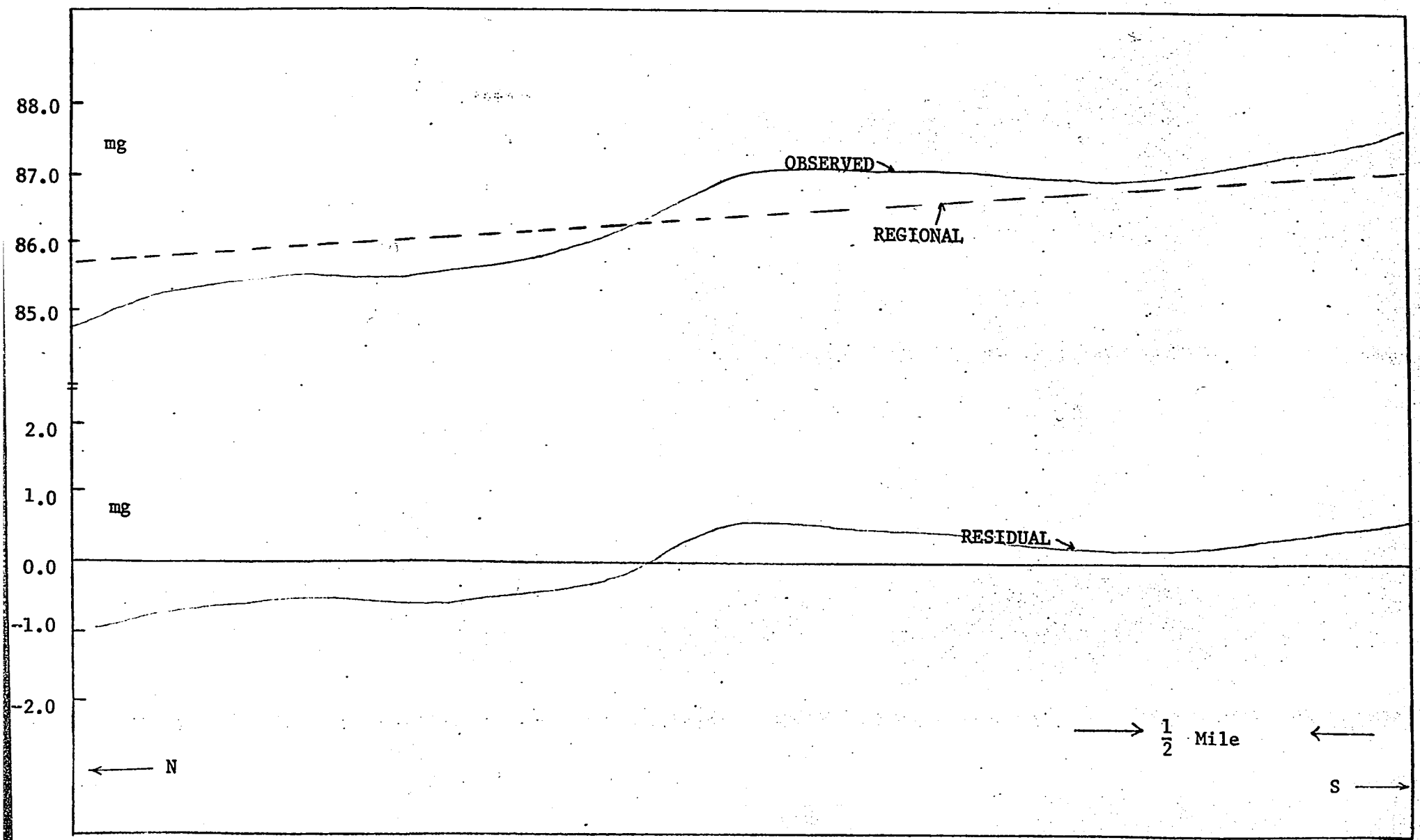

FIG 71 Observed and residual gravity anomaly across the St.Rose fault

maximum and the minimum suggest that the observed anomaly cannot be due to a single block alone. The possibility that the sedimentary beds are folded or that intrusives produce the gravity maximum and minimum can be ruled out since, from the known geology of the area, the sedimentary beds are very gently dipping and there is no evidence of any intrusives in the area. Formula (3), giving the gravity anomaly of a fault truncating a series of beds was used to calculate the gravity anomaly of the St. Rose fault from the known densities and thicknesses of the different beds as given in Figure 69. If the basement is also faulted and contributes to the observed anomaly, then the calculations show that the basement density must be about 2.7 gm/c.c. in order that the gravity anomaly have a maximum and a minimum. While the density of the basement is known to vary widely, the most probable range of basement density is between 2.80 to 2.96 gm/c.c. Considering variations of the section shown in Figure 69, it was concluded that no reasonable combination of bed thicknesses and densities resulted in a gravity anomaly exhibiting a maximum and a minimum wherever the basement density is in the range 2.80 to 2.96 gm/c.c. Moreover, the maximum and minimum can be explained if we assume that the faulting is confined to the sedimentary rocks above the basement so that the deepest faulted bed is the low density Potsdam sandstone (average density 2.50 gm/c.c.).

A simplified section through the St. Rose fault is shown in Figure 70. In this section the limestones and dolomites are lumped as a single bed of density 2.72 gm/c.c. The only other beds in this section with different density are the shale beds at the top and the

sandstone beds at the bottom, both of these having densities of about 2.54 gm/c.c. The above section through the St. Rose fault, therefore, approximates the case of a fault truncating a single bed of density contrast 0.18 gm/c.c. and thickness 3,000 feet.

Interpretation: The graphs of the coefficient a_n and b_n obtained from a Fourier analysis of the gravity anomaly over the St. Rose fault are shown in Figure 72. The ratio a_n/b_n at $n = 1$ is about 0.18. Hence $\tan\beta \doteqdot -0.18$, showing that the fault plane of the St. Rose fault has a dip of about 80°. The approximate equality of the amplitudes of the gravity maximum and minimum is further confirmation that the fault plane of the St. Rose fault is nearly vertical.

Figure 72 shows the graph of $\mathrm{Log}\left\{\frac{A_2(n\omega_o)}{L}\right\}$ calculated from the coefficient sets (a_n, b_n). For large values of n the slope of $\mathrm{Log}\left\{\frac{A_2(n\omega_o)}{L}\right\}$ approaches zero, showing that the depth to the first block is very small. This is confirmed by observations in the field which show that the glacial drift overlying the fault is about 20 feet thick.

An approximate value of the product $T\delta$ can also be obtained from the values of a_n and b_n at $n = 0$. The smoothed-out curve of b_n, when extrapolated backwards, intersects the y-axis at about 0.52. From Appendix F, at $n = 0$, we have

$$\left(b_n\right)_{n=0} \doteqdot \frac{2\pi G\rho T\delta}{L}$$

Substituting $b_n = 0.52$ and $\rho = 0.18$ in the above equation, we find that $T\delta \doteqdot 2.1$. With this value of $T\delta$, equation (2) was used to calculate the gravity anomaly of a fault. A series of curves were drawn varying δ from 0.1 to 1.0 and the resulting curves were then compared with the observed gravity anomaly. It was found that the best fit with the observed gravity anomaly can be obtained with a fault having the following

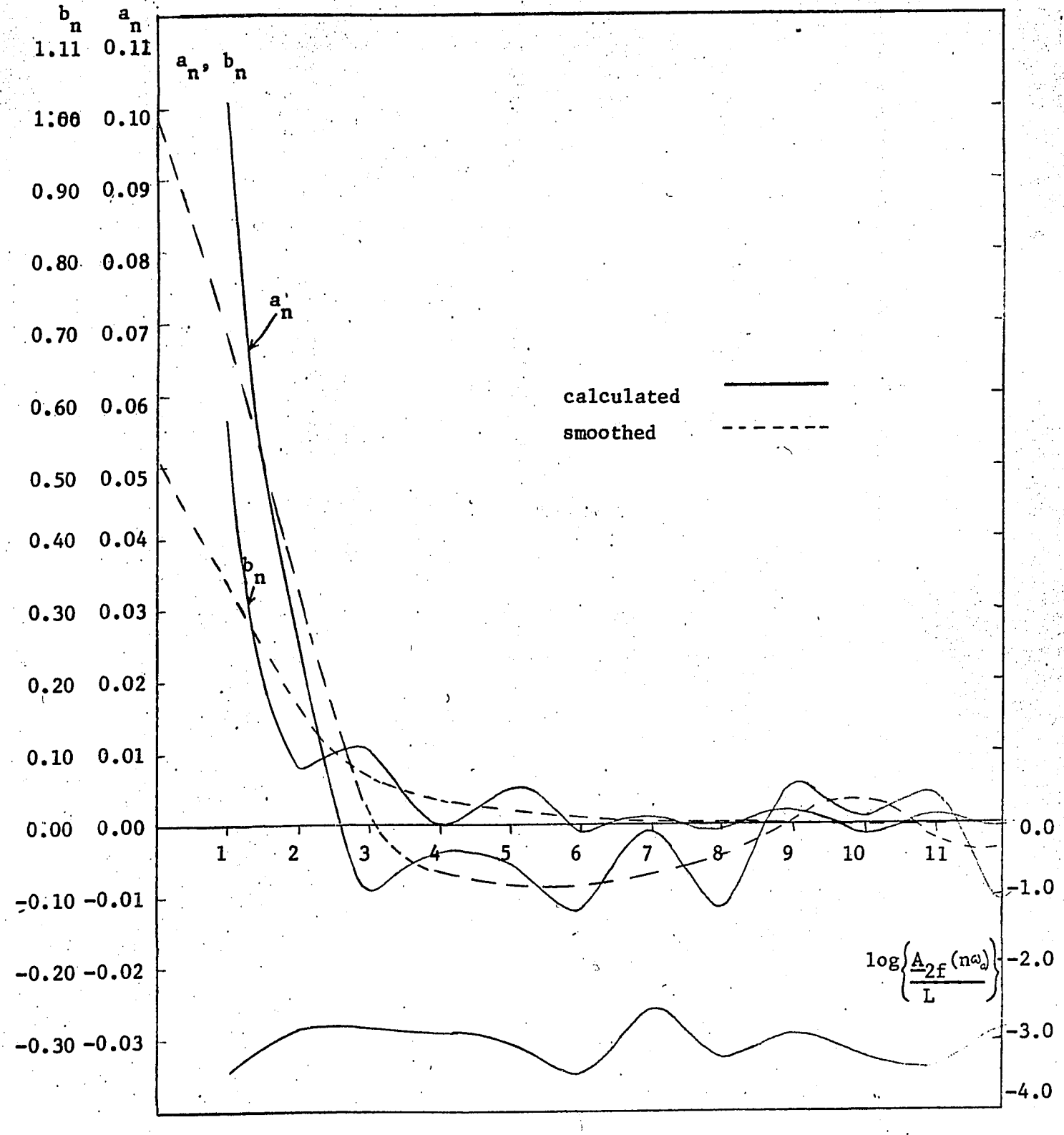

FIG 72 Fourier coefficients and the amplitude spectrum for the gravity anomaly across the St.Rose fault

parameters:

$z_1 = 0.03$ $\quad \beta = -10^{\circ}$

$z_2 = 3.52$ $\quad \rho =$ Density contrast $= 0.18$

$z_3 = 0.65$ $\quad T = 3.5$

$z_4 = 4.14$ $\quad \delta = 0.6$

Figure 73 affords a comparison between the observed gravity anomaly and the theoretical anomaly due to the above fault.

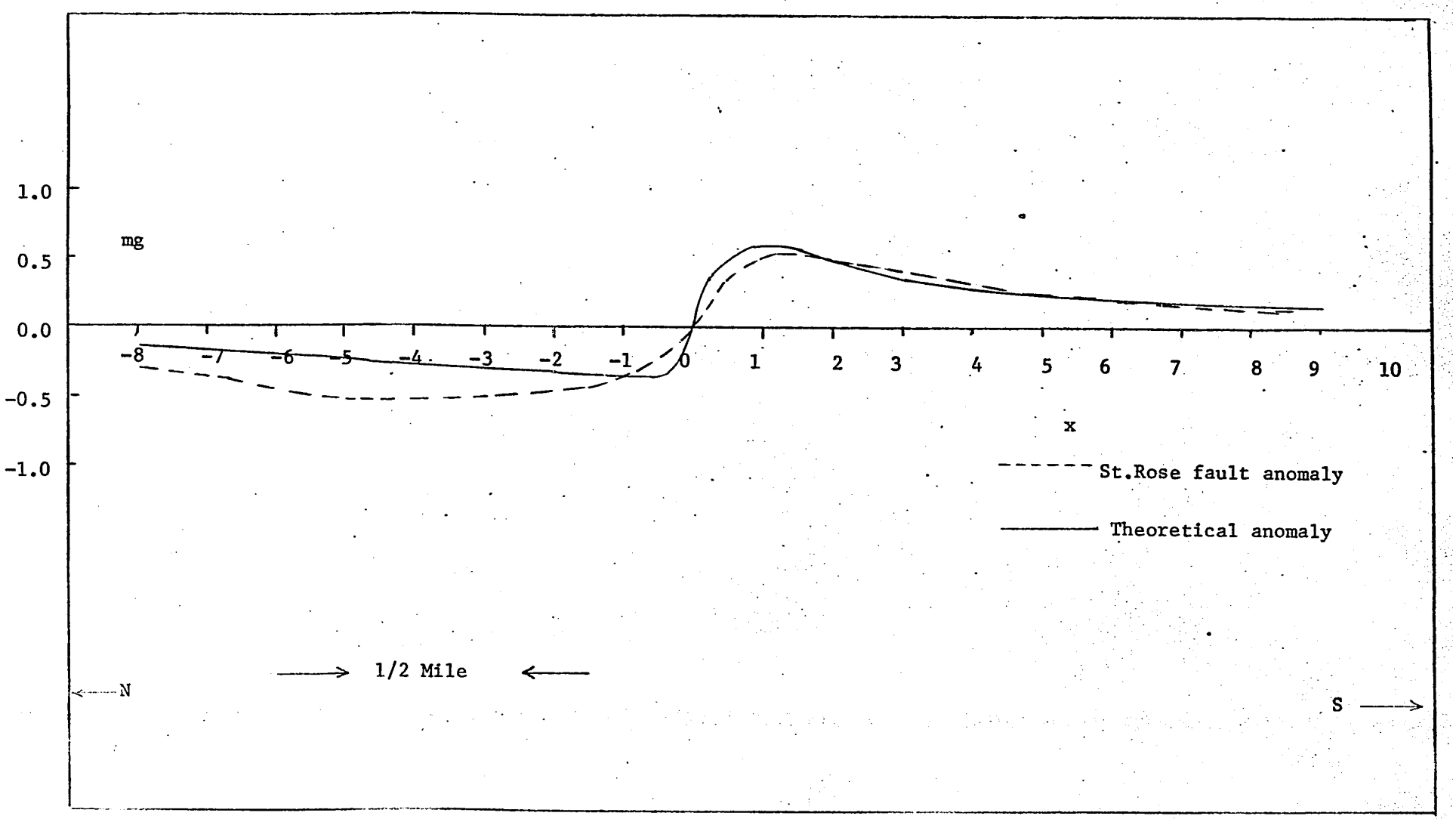

FIG 73 Comparison of the St.Rose fault anomaly with the theoretical anomaly

The Logan Fault

Introduction: The survey area is situated about 70 miles to the east of Montreal. 'Logan's Line' is the name given to the zone of dislocation separating the St. Lawrence and the Champlain valleys from the Appalachian highlands. This zone of dislocation extends in a north-easterly direction from Lake Champlain to a point about 100 km south of Quebec City. Logan's Line has been drawn principally to explain several stratigraphic peculiarities, and the precise nature of the faulting, if any exists, is not known.

Logan's fault is believed to be a high angle thrust, the older Sillerian formation (interbedded shales and sandstones) being thrust up with respect to the younger and more dense St. Germain complex (shales and calcareous limestones). The density contrast is about 0.04 gm/c.c. (based on several well cores in the area).

Observations: The reduced Bouguer anomaly curve is shown in Figure 74. Figure 75 shows the residual Bouguer anomaly curve after removing the regional. This curve has a prominent maximum and minimum and resembles the curves due to a fault cutting a single bed. The subsequent interpretation by the Fourier transforms is, therefore, based on the assumption of a fault cutting a single bed.

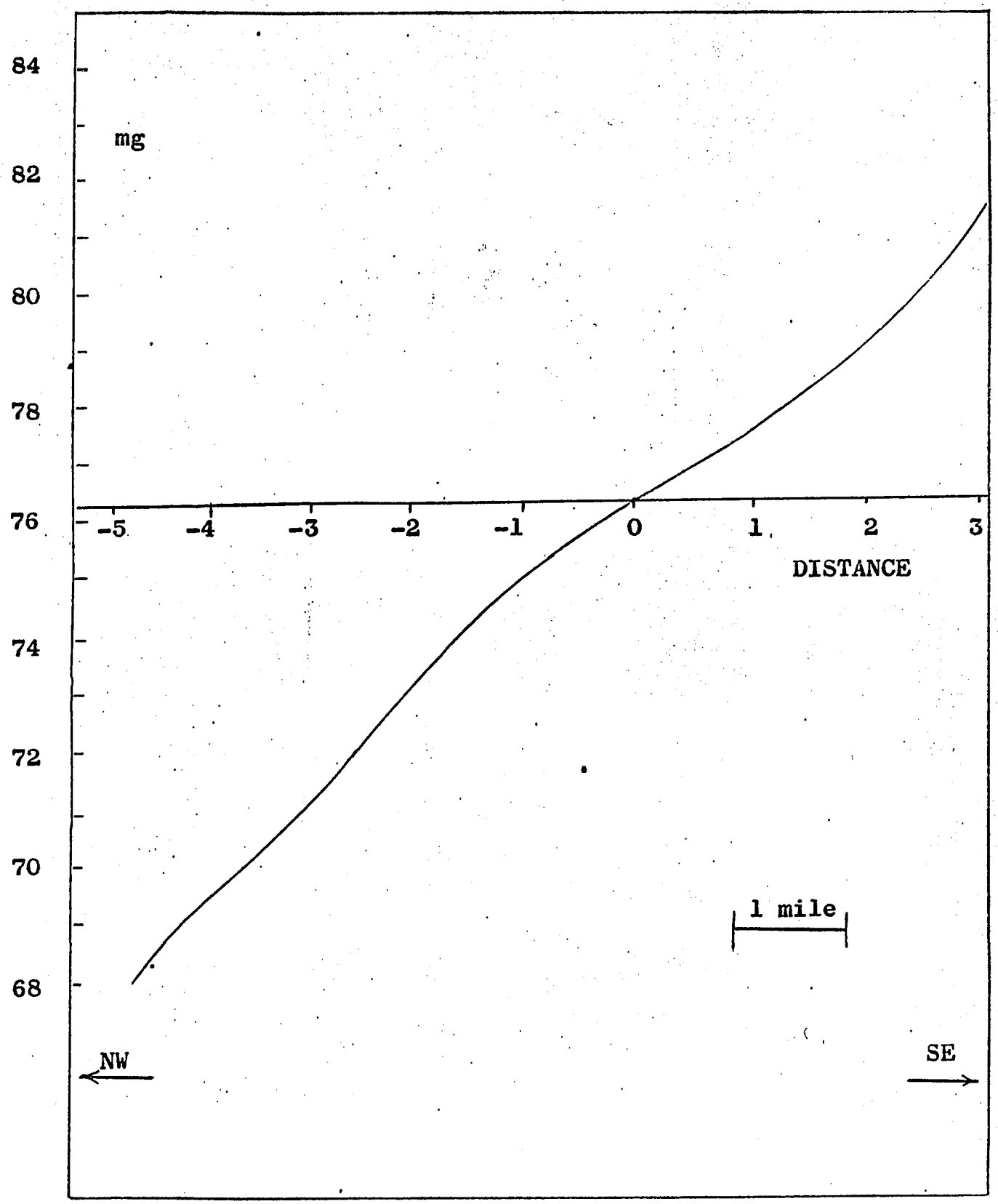

FIG 74. Gravity profile across Logan fault

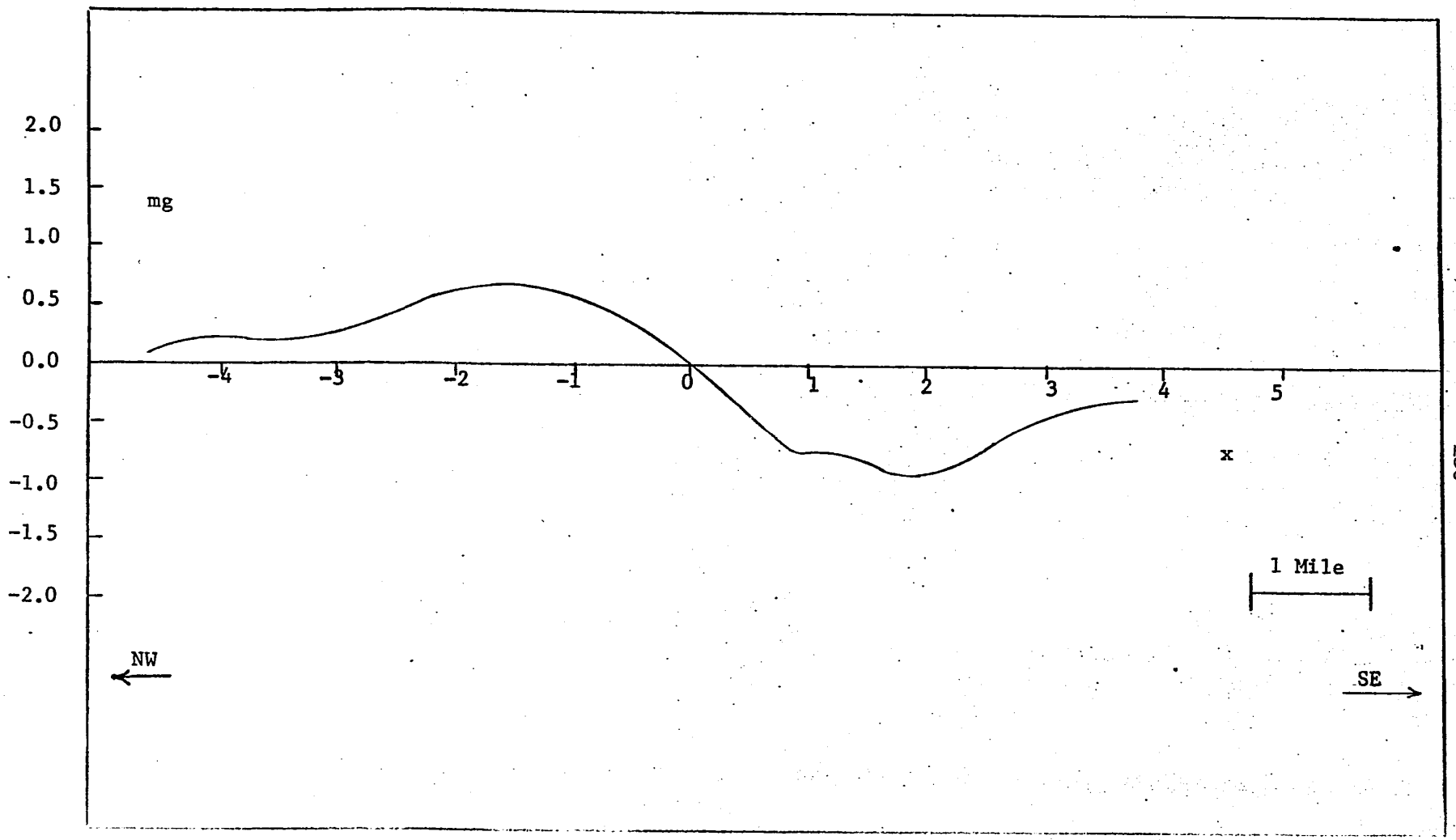

FIG 75 Residual gravity anomaly across Logan fault

Interpretation: Figure 76 shows the plot of a_n, b_n and $\log\left\{\frac{A_2(n\omega_o)}{L}\right\}$ from the gravity data. From the $\log\left\{\frac{A_2(n\omega_o)}{L}\right\}$ curve we get $\beta = 65^o$ for $\rho = 0.04$ gm/c.c. and $\beta = 70^o$ for $\rho = 0.05$ gm/c.c. The smoothed graph of $\log \frac{A_2(n\omega_o)}{L}$ (shown by dotted line in Figure 76) for large values of n is almost horizontal which shows that z_1 is practically zero. This agrees with the observation in the field where it is found that the Sillerian outcrops in the vicinity of the fault.

Seismic evidence shows that the thickness of the Sillerian bed is greater than 6,000 feet. Equation (26) was used, therefore, to obtain values of 'δ' for a series of values (ω_1, ω_2). The mean value of 'δ' obtained in this way is 2,500 feet.

In Figure 77 is shown the theoretically calculated graphs of a_n, b_n and $\log\left\{\frac{A_2(n\omega_o)}{L}\right\}$ for the anomaly over a fault having approximately the same parameters as those estimated for the Logan fault. The general shapes of the three graphs in Figure 77 agree well with the graphs of the corresponding quantities in Figure 76.

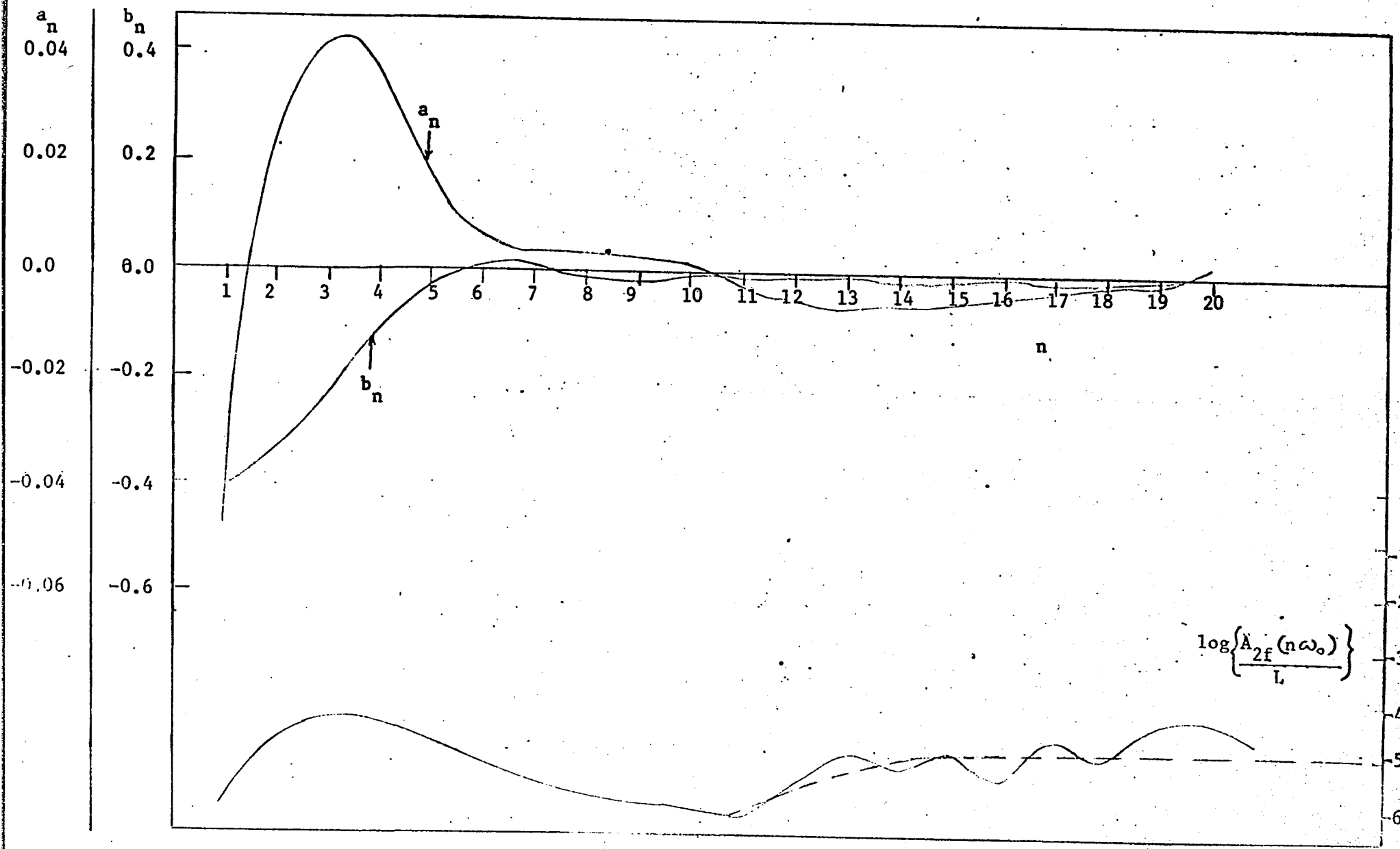

FIG 76 Graphs of a_n, b_n and $\log\left\{\frac{A_{2f}(n\omega_o)}{L}\right\}$ for gravity data in Figure 75

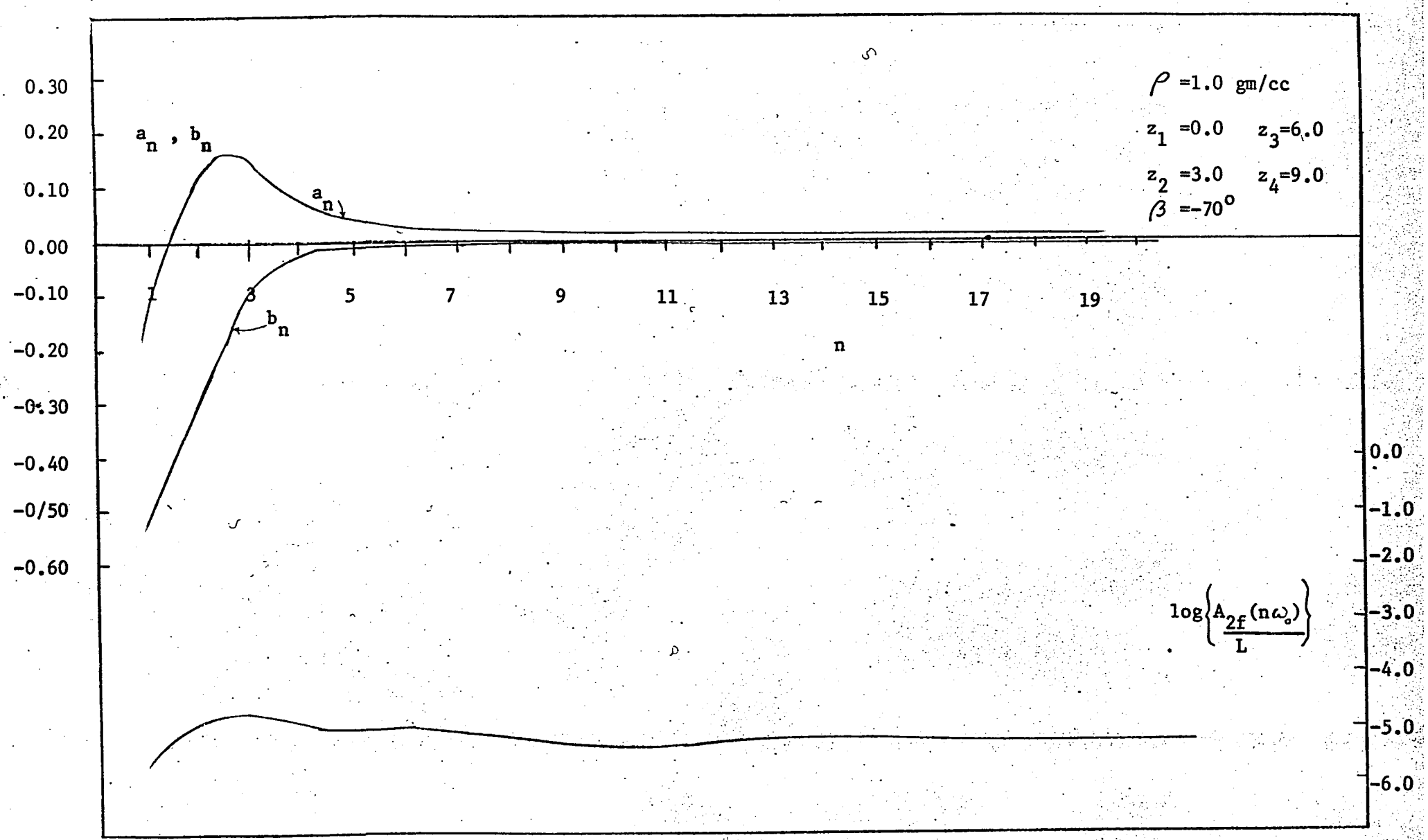

FIG 77. Graphs of a_n, b_n, and $\log\left\{\frac{A_{2f}(n\omega_o)}{L}\right\}$ for the theoretical anomaly

Diabase Dike in Grenville Township

Introduction: A gravity survey was carried out to investigate a diabase dike in Grenville township, the survey area being about seventy miles west of Montreal.

Philpotts (1961) in his geological report of Grenville township has given the results of detailed mapping in this area. Grenville township lies north of the faulted contact between the Precambrian rocks of the shield and the Paleozoic formation of the St. Lawrence Lowlands. The area is believed to be underlain by Precambrian basement rocks.

The diabase dikes in Grenville township are Precambrian rocks intruded into the older Grenville and Morin series. The older formations are mostly quartzites, quartzofeldspathic gneisses and crystalline limestones. The rocks in the vicinity of the particular dike investigated in this thesis are mostly crystalline limestones.

Like most dikes in this area, the dike surveyed strikes almost exactly east-west. The dike reached the surface, and therefore its outline can be observed in the field. The width of the dike is about 200 feet and it dips almost vertically.

Observations: Two gravity profiles taken across the strike of the dike are shown in Figure 78. Gravity readings were taken at intervals of thirty feet along these profiles. In Figure 79 is shown a gravity profile taken perpendicular to the gravity contours of Figure 78. This gravity profile appears to be almost symmetrical about the center of the dike; however, a closer examination of the profile reveals that the anomaly

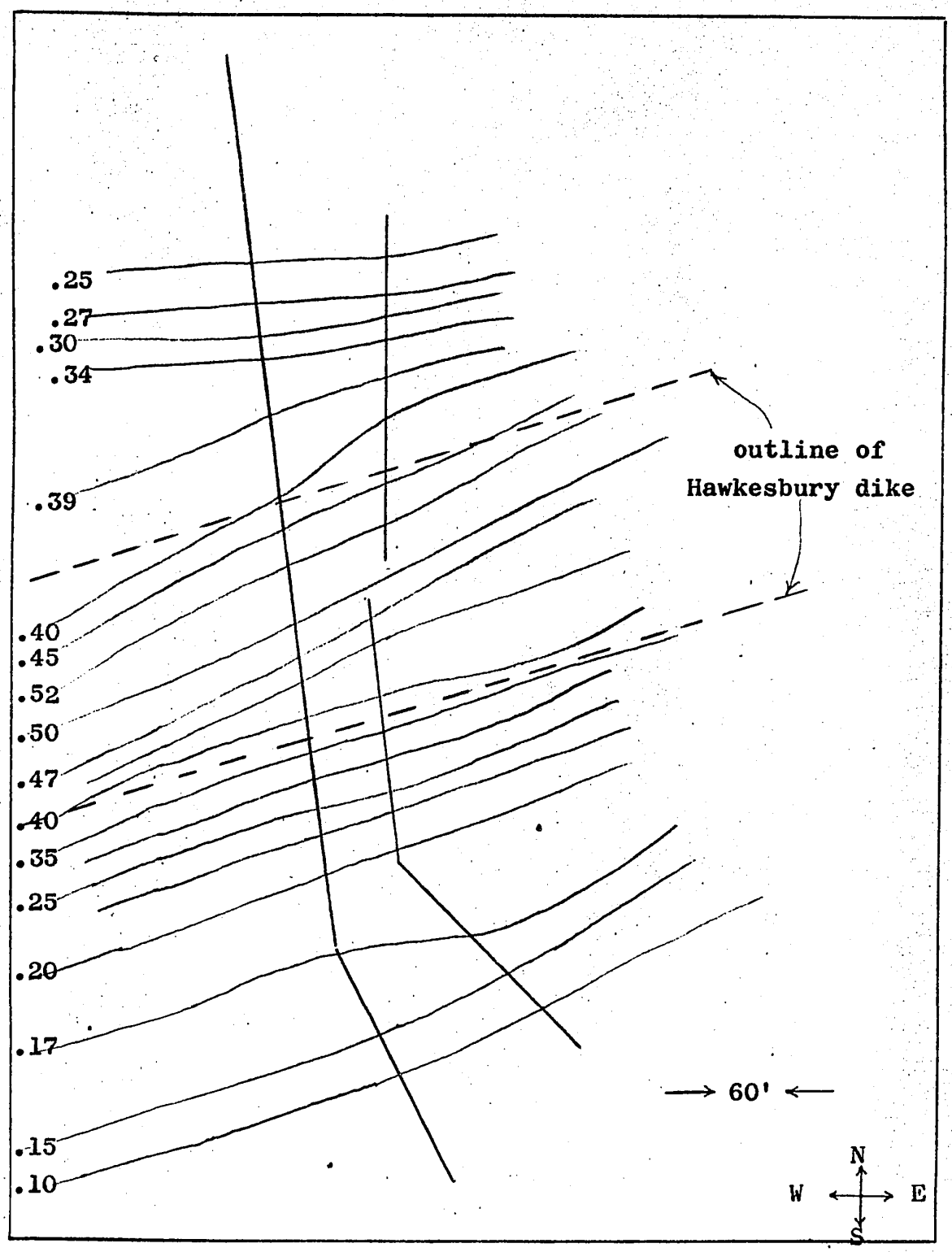

FIG 78. Bouguer anomaly map over the Hawkesbury dike

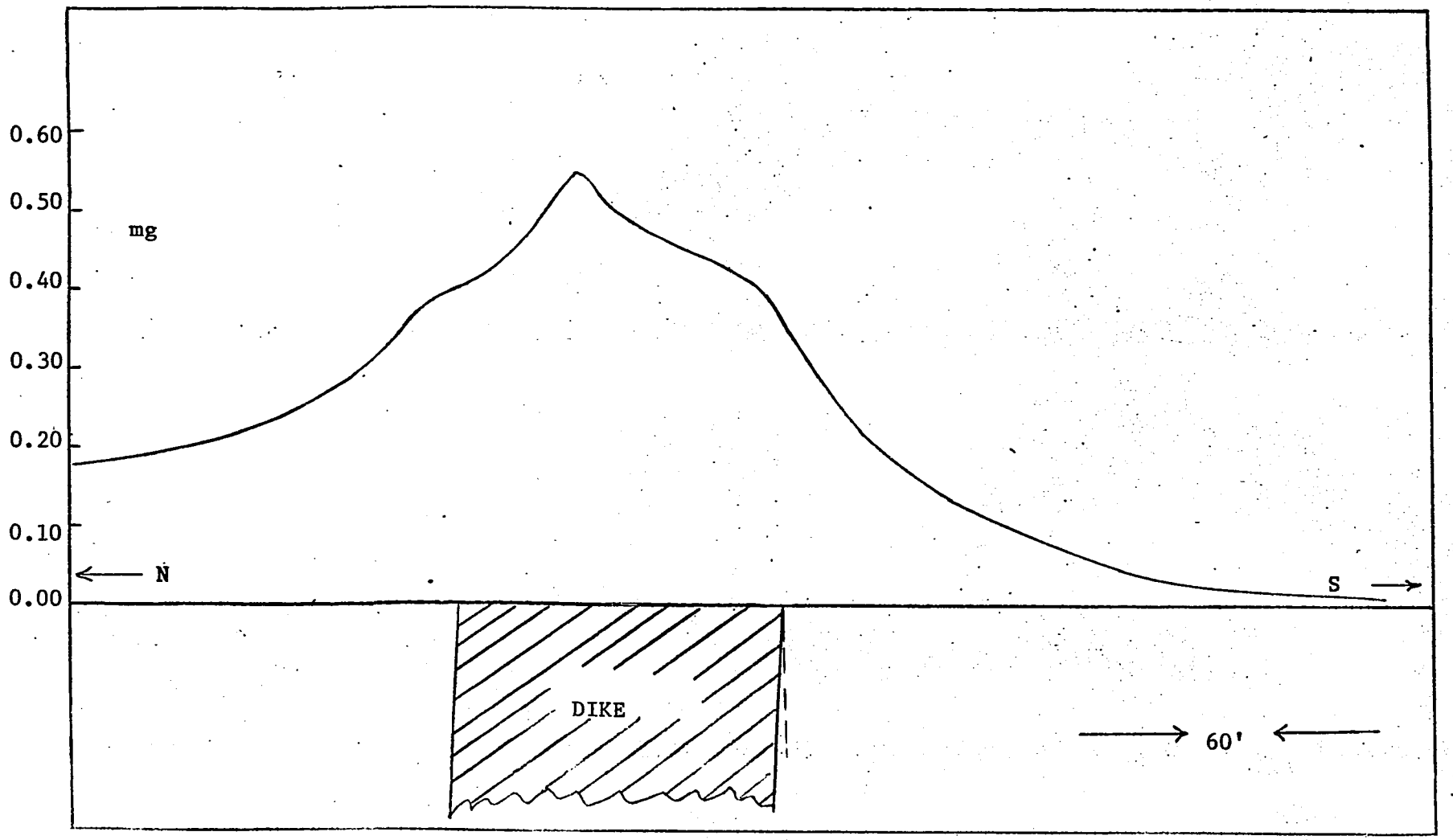

FIG 79 Gravity anomaly across the Hawkesbury dike

drops off a little faster towards the south than towards the north. This shows that the dike is dipping north at an angle slightly less than 90°.

Interpretation: It was shown in an earlier chapter that for a vertical dike the maximum anomaly always occurs over the center of the vertical dike and if the dike reaches the surface of the earth, the maximum anomaly over the center of a vertical dike is given by (see equation (5b) p. 57)

$$4G\rho x_o \left[1 + \frac{1}{2} \log\left\{1 + \left(\frac{z_2}{x_o}\right)^2\right\}\right]$$

Assuming our dike to be vertical, a value for the vertical extent of the dike can be obtained, since ρ and x_o are known approximately. The measured density contrast between the diabase and the crystalline limestone is 0.2 gm/c.c. and from field observation x_o is about 0.1; the maximum anomaly is about 0.54 mg, hence the vertical extent of the dike is about 900 feet.

A Fourier analysis performed on the gravity data of Figure 79 gave the Fourier coefficients a_n and b_n shown in Figure 80. It was shown earlier that extrapolating the coefficient graphs, a_n and b_n, to $n = 0$ gives the following results:

$$(a_n)_{n=0} \doteq \frac{4\pi}{L} G\rho x_o T$$

$$(b_n)_{n=0} \doteq 0$$

It can be seen in Figure 80 that extrapolation of a_n to $n = 0$ is difficult. A second difference extrapolation formula applied to the coefficient graph gave the value of a_n at $n = 0$ of 0.44. This gives a value of 600 feet for the vertical extent of the dike.

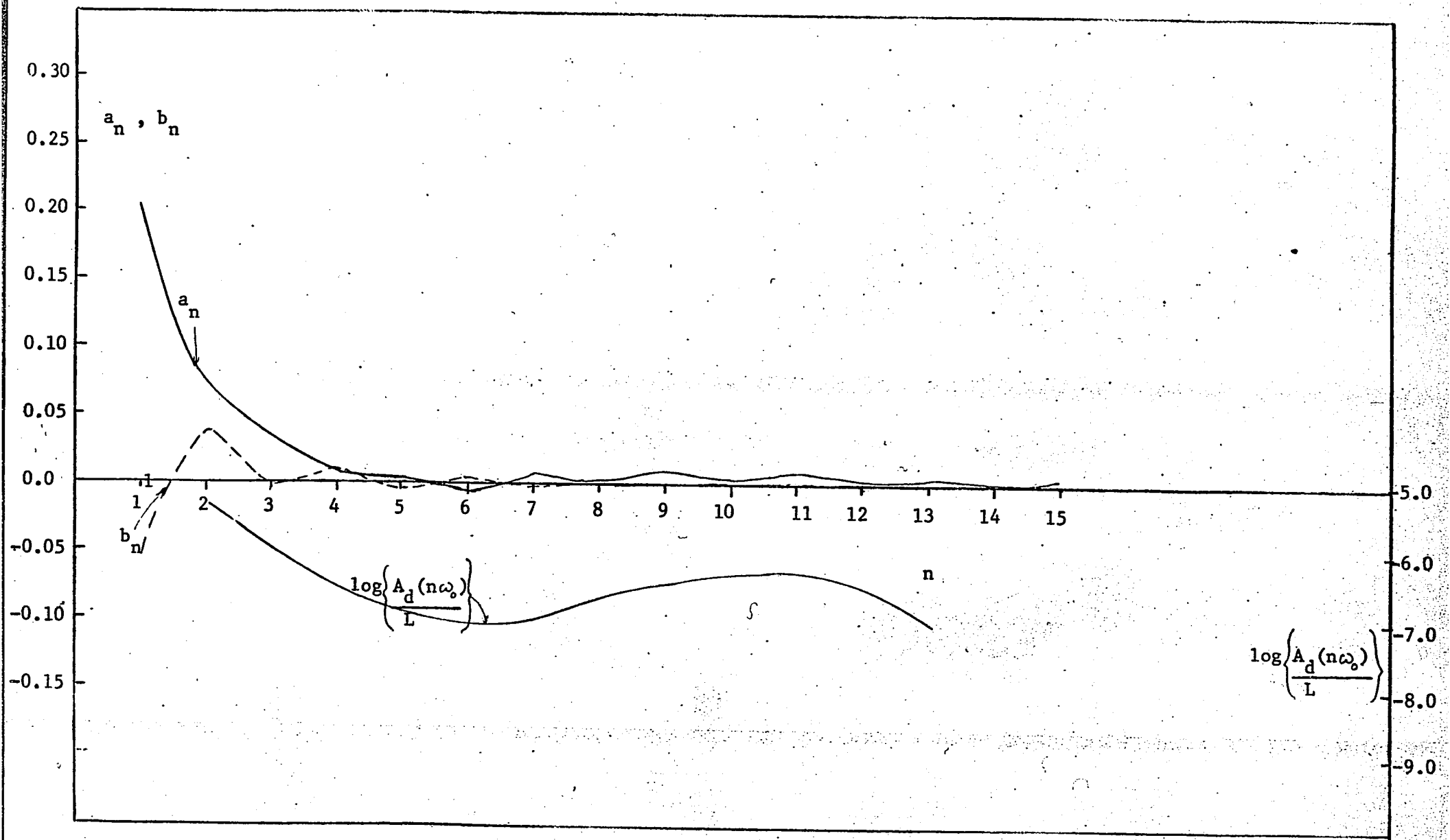

FIG 80. Graphs of a_n, b_n and $\log\left\{\frac{A_d(n\omega_o)}{L}\right\}$ obtained from gravity data in Figure 79

From the coefficient graphs the function $\log\left\{\frac{A_d}{L}(n\omega_o)\right\}$ was calculated and plotted in Figure 80. Further analysis of this graph was not attempted because the curve does not show any definite trend for large values of n.

DISCUSSION

The gravity anomalies of two-dimensional faults and dikes discussed in this thesis are based upon the expression for the gravity anomaly of a single block terminated by a fault at an arbitrary angle of inclination. Although this single block formula is gratifyingly simple and is easily adaptable for calculating the gravity anomalies of a large number of other two-dimensional structures, certain simplifying assumptions were made in deriving this formula. The first principal assumption is, of course, that the faults are two-dimensional, whereas in actual situation they are three-dimensional. This, probably, is a minor source of error in cases where the fault runs to a considerable extent in the strike direction. The second assumption made in the single block formula is that the faulted beds are all horizontal although in actual situation the beds are usually dipping in some direction. The application of the single block formula to the case of beds which are not horizontal is bound to introduce some errors which will increase as the dip of the beds increase from the horizontal. In most cases it will be seen that the effect of steeply dipping or severely folded beds will be reflected on the gravity anomaly itself, so that necessary caution may be applied in such situations. The third simplifying assumption is that the fault plane is a plane surface with a constant dip. Usually, however, the fault plane is a curved surface and the curvature of the fault plane may change quite rapidly with depth. Again, the rocks in the vicinity of the fault plane are usually highly fractured and this zone of fracture, called the 'fault-

zone', may be quite extensive so that assumption of a sharp density contrast across the fault plane may not always be strictly valid. Corrections for some of these assumptions may be possible; but the resulting equations would be so complicated that it is doubtful whether they would have any practical utility. The case of a single block dipping at an angle from the horizontal is treated in Appendix A but the resulting equation is much more complicated than the corresponding equation of a horizontal block so that no further investigation was made with the dipping block formula. It may be mentioned that the limitations of the single block formula discussed so far are present in all the single block formulas previously published, so that no easy method is available at the moment of getting around them.

Coupled with the inherent limitations of the single block formula, there are some peculiar difficulties posed by the fault problem. Probably the most serious of these problems is the isolation of the fault anomaly from the influence of the neighbouring masses. Since the observed gravity anomaly on the surface is the combined effect of all the subterranean masses, the success of the methods will depend to a large extent upon how accurately the effect of the neighbouring masses can be removed from that of the fault anomaly. The problem of isolating the gravity anomaly of a dike may also be serious when the dike occurs with other stratigraphic features.

The other difficulty that one faces in interpretating the fault or the dike anomaly, a difficulty which is common to all gravity problems,

is the proper choice of densities for the overburden and the subterranean masses. In many new areas of investigation, the density information may be non-existent or very scanty. Also, laboratory measurements of densities of core samples may not be truly representative of densities at depths. Wherever feasible, methods are given in this thesis which will enable us to obtain information about some parameters of the underground structure without any density information. As an example, the ratios of the amplitudes of the gravity anomaly of a fault cutting a single bed and also the ratio of the amplitude of the second derivative of the anomaly are independent of any density considerations and the dip of the fault plane is shown to be strongly dependent upon these ratios.

Due to its inherent weaknesses, the gravity method has so far been used principally as a reconnaissance tool prior to more detailed survey by other methods. An attempt is made in this thesis to show that when geological situations are favorable, gravity can be more than a mere reconnaissance tool and it can give quantitative information about the parameters of the two-dimensional structures. For the field examples given in this thesis, the calculated values for the parameters all seem to lie within about 10 percent of the values estimated from the geological information. It should be mentioned, however, that the field examples chosen were more or less ideal structures from the point of view of application of the formulas. The sedimentary beds were almost perfectly horizontal, the regional trend was fairly well established and the general topography was very flat lying. The simplifying assumptions made in the derivation of the formulas and the interpretation techniques are, therefore, more or less valid. For a successful application of the methods,

therefore, all available geological, drill-hole and other pertinent information must be taken into consideration.

In some cases, more than one method is given in this thesis for calculating the same quantity. The reason for this is that although the different methods are not entirely independent of each other, some of the methods are more objective than the others. When a situation warrants a very accurate estimation of a parameter of the two-dimensional structure, it will be interesting to find out if the same quantity calculated by the two different methods agree. As an example, it is shown that the throw of a fault cutting a series of beds can be obtained very easily from the total change in the gravity anomaly due to such a structure provided the density contrast between rocks in the overburden and the basement is known. The same quantity can also be obtained by calculating the Fourier transform of the first derivative of the anomaly and taking the limit of the real part of the transform as ω tends to zero. While calculations by both the methods should give identical results, the second method is more objective while the first method has the virtue of simplicity and ease of comprehension. The throw of the Delson fault calculated by both these methods gives the same result which in turn agrees very well with the geological estimate.

In situations where a precise estimation of the parameters is not necessary, a qualitative idea about the geological structure may be obtained from the large number of curves given in this thesis. As an example, an approximate idea about the manner in which the gravity anomaly of a dike changes with the change in the parameters can be obtained from

Figures 31-33 showing the gravity anomaly of a dike as its parameters are varied. Situations may also arise when more curves are needed to interpret a given anomaly than those given in this thesis. In such situations, a desk calculator can be used or some of the formulas can be programmed in a digital computer after approximate values of the parameters have been obtained.

The accuracy of interpretation by the Fourier transform method depends to a large extent upon the choice of the value of L, the half-wavelength, used in calculating the Fourier coefficients. Since the accuracy increases as L increases, it is of great importance that we have gravity data at as large a distance as possible from the fault trace. The situation in the case of the dike is not as serious, since the width of a dike is usually small and the gravity anomaly becomes very small at a relatively short distance from the dike. The grid interval chosen for calculating the Fourier coefficients depends upon the gradient of the gravity anomaly itself. If the anomaly changes slowly, i.e. it has a small gradient, the grid spacing may be relatively large. On the other hand, if the anomaly has large gradients at some parts of the curve, the grid interval must be so chosen that no part of the anomaly with a large gradient is neglected. The grid spacings also determine the highest harmonic that we can obtain from the Fourier analysis of the gravity data. The wavelength of the highest harmonic obtainable is equal to twice the grid spacing chosen.

Calculations involved in obtaining the Fourier transforms of the gravity data are long and tedious. An IBM 7044 digital computer has

been used to make all the calculations in this thesis. In order that the method of interpretation by the Fourier transforms may be readily usable, a comprehensive scheme for obtaining the Fourier transforms from the gravity data will be very useful and needs further investigation.

CONTRIBUTIONS TO KNOWLEDGE

The formulas for the gravity anomaly of a single block and for a fault cutting a single bed are given by Geldart et al. (1966). The original contributions to knowledge claimed in this thesis are as follows:

1) Derivation of a formula giving the gravity anomaly of a fault cutting any number of beds having any density distribution and thickness of the different beds.

2) Derivation of a formula giving the gravity anomaly of several parallel faults cutting a bed.

3) Derivation of the formula giving the gravity anomaly of a dike inclined at an arbitrary angle and having any vertical extent.

4) From a combination of the gradient and the gravity anomaly profiles across a fault, simple expressions are obtained which give information about the parameters of the two-dimensional fault such as the dip of the fault plane and the throw of the fault.

5) Expressions are obtained in a polynomial form for the positions of the zero, the maximum and the minimum of the second derivative profile across a fault.

6) Expressions are obtained for the vertical gradient of gravity across a block and a fault cutting a single bed.

7) The Fourier transform formulas are obtained for the gravity anomalies across a single block, a fault cutting a single bed, and a fault cutting a series of beds and a dike.

8) Expressions are obtained for the Fourier spectrum of the gravity anomalies across a fault and a dike. The Fourier spectrum is shown to contain information about the depth and the inclination of the anomalous structures. Under suitable circumstances, valuable information about the throw and the thickness of the faulted bed can also be obtained from the Fourier spectrum.

9) Simple expressions are obtained for the limiting values of all the Fourier transform formulas for very small values of ω. These limiting values are of particular interest because these can give quick and reliable information about some parameters of the two-dimensional structures.

10) A method is given for obtaining the Fourier transforms of the field data by making a Fourier analysis of the data. By slight adjustments, this method can be used for obtaining the Fourier transforms of all types of two-dimensional structures discussed in this thesis.

11) The suitability of the new formulas and the applicability of the interpretation techniques are tested on the gravity anomalies across three faults and a dike. The results obtained by the new methods are, in most cases, in very good agreement with the known geology of the surveyed areas.

APPENDIX A

Gravity Anomaly of a Semi-infinite Bed

The attraction of an infinitely long straight line of density ρ per unit length is $2G\rho/r$, G being the gravitational constant, r the distance from the given point to the line. Starting from this expression, the vertical component of gravity at the point P in Figure 81 for the semi-infinite plane corresponding to the positive half of the XY plane is

$$g = 2G\rho\int_{o}^{\infty} \cos\xi \, dy/r$$

$$= 2G\rho\int_{-\theta}^{\pi/2} d\xi$$

$$= 2G\rho(1/2\pi + \theta).$$

When a is infinite or b zero, θ equals $1/2\pi$ and $g = 2\pi G\rho$, the familiar result for an infinite plane. When the quantity 'a' is negative, the point P is left of the x-axis and θ is negative.

Figure 82 shows a horizontal bed of thickness t truncated by a plane dipping at an angle α. The vertical component of gravity at P is given by

$$g_s = 2G\rho\int_{z_1}^{z_2} (1/2\pi + \theta)dz$$

$$= G\rho(\pi t + 2\int_{z_1}^{z_2} \theta dz.)$$

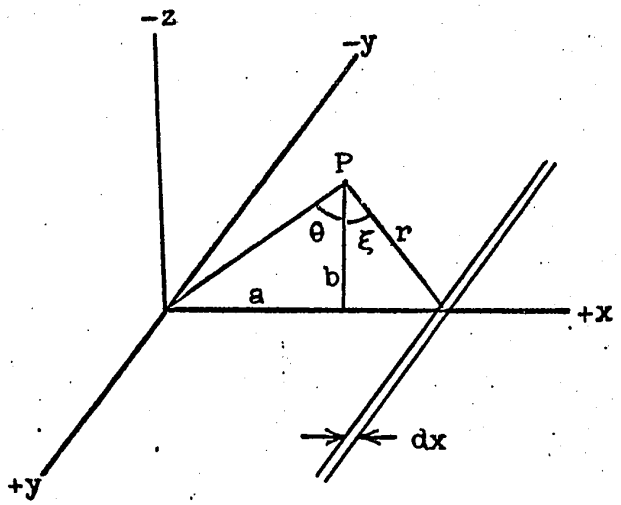

FIG 81. Calculation of attraction of a semi-infinite horizontal plane

$$\text{Since } \tan\theta = \tan\beta + x/z,$$

$$\text{therefore} \qquad dz = -x\cos^2\beta \csc^2(\theta - \beta)d\theta,$$

$$\text{and} \qquad \int\theta dz = -x\cos^2\beta\left[\int\theta\csc^2(\theta - \beta)d\theta\right]$$

$$= x\cos^2\beta\left[\theta\cot(\theta - \beta) - \log\sin(\theta - \beta)\right].$$

$$\text{Writing} \quad \psi_i = (\theta_i - \beta), \quad i = 1, 2, \text{ and}$$

$$F_i = 2G\rho(\psi_i\cot\psi_i - \log\sin\psi_i),$$

and noting that

$$(\cot\psi_2 - \cot\psi_1) = (AC\text{-}BC)/CP \text{ in Figure 82,}$$

the final result can be written

$$g_s = 2G\rho(1/2\pi + \beta)t + x\cos^2\beta(F_2 - F_1) \quad \ldots\ (1')$$

$$= 2G\rho(\pi - \alpha)t + x\sin^2\alpha(F_2 - F_1) \quad \ldots\ (1)$$

The quantities x, α, β, θ_1, θ_2, ψ_1, ψ_2 are positive as shown in Figure 82. Thus, x is positive when P is to the right of the fault trace, β and θ_i are positive when measured in a clockwise direction from the vertical, α and ψ_i are positive when measured in a clockwise direction from the fault plane. If α is greater than $1/2\pi$, β is negative and the fault dips downward to the right.

The term $\log\sin\psi_i$ is meaningless if $\sin\psi_i$ is negative. However, the quantity F_i always appears in pairs, such as $(F_2 - F_1)$, representing the effects of the upper and lower surfaces of a bed. In these expressions the two values of ψ_i always have the same sign, hence the expression $(F_2 - F_1)$ contains the term $\log(\sin\psi_2/\sin\psi_1)$ where the ratio of the sines is always positive. Also, the quantity, $\psi_i\cot\psi_i$, is always positive. Therefore F_i can be regarded as an even function of

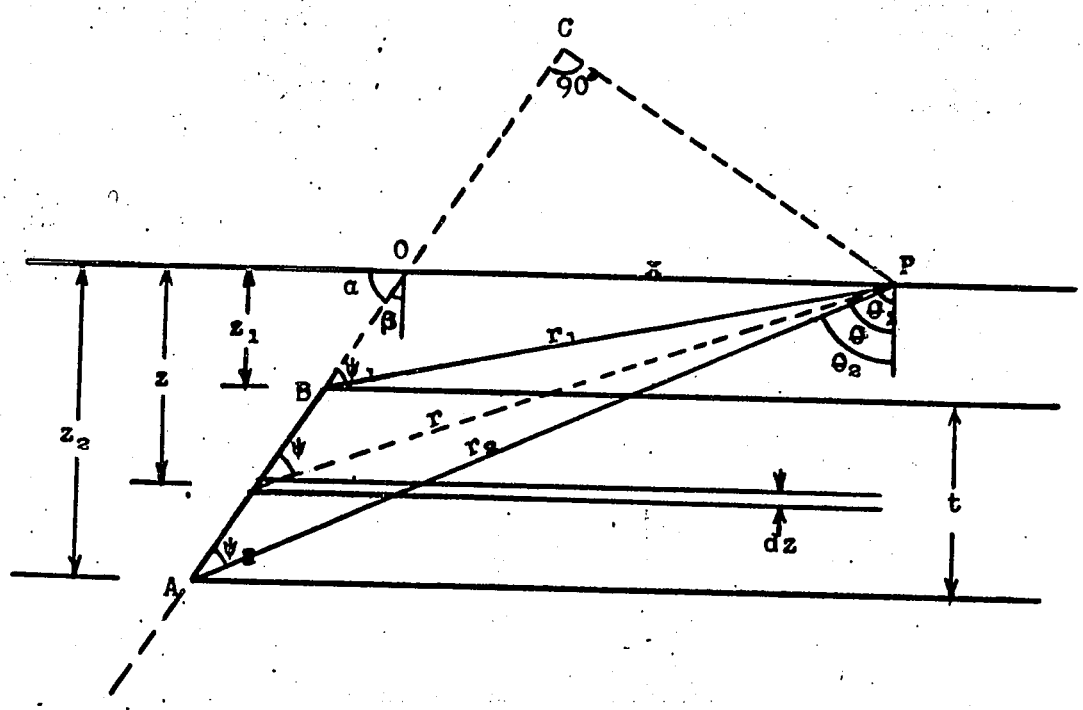

FIG 82. Calculation of g_s for a semi-infinite truncated block

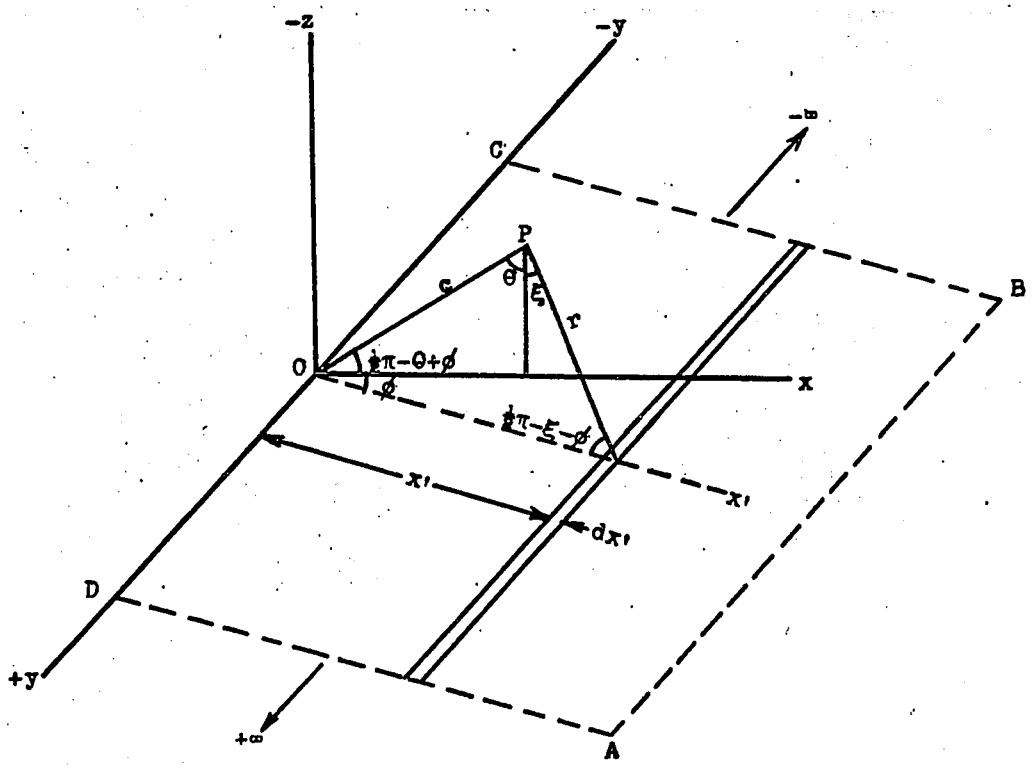

FIG 83. Calculation of g for a dipping plane

ψ_i having the same value regardless of the algebraic sign of ψ_i.

To obtain the gravity effect of a truncated bed lying to the left of the fault plane, the effect of an infinite bed is added to the effect of a truncated bed to the right of the fault plane, the latter having a negative density. The result is

$$g_s' = 2G\rho\alpha t - x \sin^2\alpha(F_2 - F_1) \quad \ldots\ldots (1'')$$

$$= 2G\rho(1/2\pi - \beta)t - x \cos^2\beta(F_2 - F_1) \quad \ldots\ldots (1''')$$

Also, $$g_s + g_s' = 2\pi G\rho t.$$

Limiting values of g_s: g_s depends upon several parameters as well as the variable x, and the limiting values of g_s in certain cases are important.

(a) x approaches $\pm\infty$. As x becomes very large, ψ_i approaches the value α or $(\alpha - \pi)$, according as x is positive or negative. When x is positive and much larger than z_i,

$$\psi_i \doteq (\alpha - z_i/x)$$

$$\psi_i \cot \psi_i \doteq \alpha\cot\alpha + (\alpha \csc^2\alpha - \cot\alpha)z_i/x,$$

$$\log(\sin\psi_2/\sin\psi_1) \doteq -(t/x)\cot\alpha,$$

and $$g_s \doteq 2\pi G\rho t.$$

In the same way it can be shown that g_s approaches zero as x approaches $-\infty$.

(b) x approaches zero. When $x = 0$, ψ_i is also zero, hence

$$x(\psi_i \cot \psi_i) = x(\psi_i/\tan\psi_i) = 0,$$

$$x \log(\sin \psi_2/\sin \psi_1) = x \log (r_1/r_2) = 0,$$

therefore, when $x = 0$,

$$g_s = 2G\rho(\pi - \alpha)t = 2G\rho(1/2\pi + \beta)t.$$

(c) α approaches 0 or π (β approaches $\pm 1/2\pi$). When β is equal to $\pm 1/2\pi$, θ_i also equals $\pm 1/2\pi$ and ψ_i vanishes. Therefore the term $(F_2 - F_1)$ reduces to $2G\rho \log(r_1/r_2)$, so that

$$g_s = 2\pi G\rho t \quad \text{when} \quad \alpha = 0, \text{ i.e.,} \quad \beta = +1/2\pi,$$
$$= 0 \quad \text{when} \quad \alpha = \pi, \text{ i.e.,} \quad \beta = -1/2\pi.$$

(d) Depth to the top of the bed approaches zero. As z_1 approaches zero, θ_1 approaches $\pm 1/2\pi$ according as x is positive or negative. Therefore, when $z_1 = 0$,

$$\psi_1 = \alpha = 1/2\pi - \beta \quad \text{when x is positive,}$$
$$= \alpha - \pi = -(1/2\pi + \beta) \quad \text{when x is negative.}$$

(e) Depth to the top of the bed approaches infinity. Writing $z_2 = z_1 + t$, and allowing z_1 to approach infinity, it will be seen that θ_i approaches β, hence in the limit ψ_i vanishes. Also

$$\sin \psi_2/\sin \psi_1 = r_1/r_2 = 1$$

when z_1 is infinite. Therefore $(F_2 - F_1)$ vanishes for z_1 infinite, and

$$g_s = 2G\rho(\pi - \alpha)t = 2G\rho(1/2\pi + \beta)t$$

when z_1 is infinite. This is the same value as that at $x = 0$ when z_1 is finite.

Derivative of g_s with respect to x: Omitting the constant term, we have

$$g_s = x \cos^2\beta(F_2 - F_1)$$

Then,

$$\frac{dg_s}{dx} = \cos^2\beta(F_2 - F_1) + x \cos^2\beta\left(\frac{dF_2}{dx} - \frac{dF_1}{dx}\right)$$

Since $F_i = 2G\rho(\psi_i \cot \psi_i - \log \sin \psi_i)$,

We have

$$\frac{dF_i}{dx} = 2G\rho(\cot \psi_i - \psi_i \csc^2\psi_i - \cot \psi_i)\frac{d\psi_i}{dx}$$

$$= -2G\rho\psi_i \csc^2 \psi_i \frac{d\theta_i}{dx}$$

$$= -2G\rho\psi_i \csc^2 \psi_i(\cos^2\theta_i/z_i)$$

Therefore,

$$\frac{dg_s}{dx} = \frac{g_s}{x} - 2G\rho\, x \cos^2\beta\left(\frac{\psi_2\cos^2\theta_2}{z_2\sin^2\psi_2} - \frac{\psi_1\cos^2\theta_1}{z_1\sin^2\psi_1}\right)$$

From Figure 82, we see that

$$\frac{x}{\sin\psi_i} = \frac{AP}{\cos\beta} = \frac{z_i}{\cos\beta\cos\theta_i} ,$$

hence $$\frac{dg_s}{dx} = \frac{g_s}{x} + \frac{2G\rho}{x}(z_1\psi_1 - z_2\psi_2) \qquad \ldots . (6)$$

When x = 0, the second term is indeterminate; however, on substituting

$$\psi_i = \theta_i - \beta = \tan \psi_i \doteq (x/z_i)\cos^2\beta,$$

the term reduces to zero for x = 0, hence, at x = 0,

$$\frac{dg_s}{dx} = 2G\rho \sin^2\alpha \log(r_2/r_1)$$

$$= 2G\rho \sin^2\alpha \log(1 + t/z_1)$$

$$= \infty \text{ when } z_1 = 0.$$

Second derivative of g_s with respect to x: Differentiating $\frac{dg_s}{dx}$ in (6), we have

$$\frac{d^2g_s}{dx^2} = -\frac{g_s}{x^2} + \frac{1}{x}\frac{dg_s}{dx} - \frac{2G\rho}{x^2}(z_1\psi_1 - z_2\psi_2) + \frac{2G\rho}{x}(z_1\frac{d\psi_1}{dx} - z_2\frac{d\psi_2}{dx})$$

$$= \frac{2G\rho}{x}(z_1\frac{d\theta_1}{dx} - z_2\frac{d\theta_2}{dx}) \text{ , using (6),}$$

$$= \frac{2G\rho}{x}(\cos^2\theta_1 - \cos^2\theta_2)$$

$$= \frac{G\rho}{x}(\cos 2\theta_1 - \cos 2\theta_2) \qquad \ldots . (7).$$

Formula for a dipping bed: To obtain the result for a dipping bed, it is necessary to return to the formula for the attraction of the infinite straight line and derive the formula for a dipping semi-infinite plane. Referring to Figure 83, ABCD represents a portion of a plane which is infinite in the +x and -x directions and which dips downward to the right at an angle ϕ. Taking the y'-axis as the projection of the y-axis onto this plane, the vertical component of gravity at P is

$$g = 2G\rho \int_{o}^{y'} \cos \xi \, dy'/r.$$

But $y' = c \sin (\xi - \theta)/\cos (\xi + \phi)$,

$r = c \cos (\theta - \phi)/\cos (\xi + \phi)$,

so that

$$g = 2G\rho \int \cos \xi \, d\xi/\cos (\xi + \phi)$$

$$= 2G\rho \int \cos (\omega - \theta) \, d\omega/\cos \omega$$

where $\omega = \xi + \phi$, and the limits of the integral are $\omega_1 = \phi + \xi$, $\omega_o = \phi - \theta$. The final result is

$$g = 2G\rho \cos\phi \left[(\theta + \xi) + \tan \phi \log \{\cos (\phi - \theta)/\cos (\phi + \xi)\} \right]$$

$$= 2G\rho \cos\phi \left[(\theta + \xi) + \tan \phi \log (r/c) \right].$$

If the dipping plane goes to infinity in the down-dip direction, r is infinite and consequently g also becomes infinite. Therefore one must use beds of finite length in the direction of the dip. However, the resulting formula, equivalent to equation (1), is so complex that it is useless from a practical viewpoint.

APPENDIX B

Gravity Anomaly of a Dipping Fault

From Figure 7 it is evident that the gravity expression for a fault can be obtained by adding together equations (1) and (1") giving the result

$$g_f = 2\pi G\rho t + x \sin^2\alpha\left\{(F_2 - F_1) - (F_4 - F_3)\right\} \qquad \ldots . (2)$$

The first term on the right-hand side represents the effect of the unfaulted infinite bed, the second the effect of displacing part of this bed.

Limiting values of g_f: Limiting values are easily found by considering the limiting values for the two truncated beds making up the fault. The expression for g_f can be regarded as the sum of the effect of an infinite bed and the effects of two truncated beds which differ only in the sign of ρ and the depth to the upper surface of the bed. Hence, for those cases where the limiting value of g_s is independent of depth, the limiting value of g_f is $2\pi G\rho t$. These cases are:

(a) $x = \pm\infty$,

(b) $x = 0$,

(c) $\alpha = 0$ or $\alpha = \pi$.

As the displacement of the fault becomes very large, the effect of the lower bed approaches $2G\rho(\pi - \alpha)t$, that is, $(F_4 - F_3)$ approaches zero. Therefore, for infinite displacement,

$$g_f = 2\pi G\rho t + x \sin^2\alpha\ (F_2 - F_1).$$

Derivative of g_f with respect to x: Proceeding as for the single bed, one obtains

$$\frac{dg_f}{dx} = \sin^2\alpha\{(F_2-F_1) - (F_4-F_3)\} + (2G\rho/x)(z_1\psi_1-z_2\psi_2-z_3\psi_3+z_4\psi_4).$$

At $x = 0$, the last bracket on the right-hand side has a limiting value of zero, hence the slope becomes

$$\frac{dg_f}{dx} = 2G\rho \sin^2\alpha \log (z_2z_3/z_1z_4)$$

$$= 2G\rho \sin^2\alpha \log\{ (1 + a)(1 + b)/(1 + a + b)\}$$

where $a = t/z_1$, $b = 1 + d/z_1$, d being the displacement. For $z_1 = 0$, the slope at the origin is infinite. For large displacement the slope at the origin becomes

$$\frac{dg_f}{dx} = 2\ G\rho \sin^2\alpha \log (1 + a).$$

Derivative of g_m with respect to x: From equation (3) we have,

$$g_m = x \cos^2\beta \left[(\sigma_1 - \sigma_o)(L_1' - L_1) + (\sigma_2 - \sigma_1)(L_2' - L_2) + \ldots. \right.$$
$$\left. (\sigma_r - \sigma_N)(L_{N+1}'-L_{N+1})\right]$$

Differentiating each term within the brackets in the above expression and using equation (6), we have

$$\frac{dg_m}{dx} = \frac{g_m}{x} + \frac{2G}{x}\Big\{\rho_1(z_1\psi_1 - z_1'\psi_1') + \rho_2(z_2\psi_2 - z_2'\psi_2') + \ldots.$$
$$\rho_{N+1}(z_{N+1}\psi_{N+1} - z_{N+1}'\psi_{N+1}')\Big\}$$

where $\rho_i = \sigma_i - \sigma_{i-1}$; $i = 1, 2, \ldots N$

and $\rho_{N+1} = \sigma_r - \sigma_N$

At $x = 0$,

$$\frac{dg_m}{dx} = 2G\cos^2\beta\left\{\rho_1 \log\left(1 + \frac{\delta}{z_1}\right) + \rho_2 \log\left(1 + \frac{\delta}{z_2}\right)\right.$$

$$\left. + \ldots\ldots \rho_{N+1} \log\left(1 + \frac{\delta}{z_{N+1}}\right)\right\} \qquad \ldots\ldots (3b)$$

APPENDIX C

Roots of the Equation $\frac{d}{dx}\left(\frac{d^2g_f}{dx^2}\right) = 0$

Equation (8), p.89 gives

$$\frac{d^2g_f}{dx^2} = -\frac{G\rho}{x}(\cos 2\theta_2 - \cos 2\theta_1 + \cos 2\theta_3 + \cos 2\theta_4)$$

Differentiating with respect to x and writing $q_i = \frac{x}{z_i}$, we find

$$f(x) = \frac{d}{dx}\left(\frac{d^2g_f}{dx^2}\right) = -\frac{G\rho}{x^2}(H_2 - H_1 + H_3 - H_4)$$

where

$$H_i = \frac{8q_i\tan\beta + 6q_i + 2\sec^2\beta}{\sec^2\beta + 2q_i\tan\beta + q_i^2}$$

The derivative of f(x) is given by

$$F'(x) = -\frac{2}{x}f(x) - (H_2' - H_1' + H_3' - H_4')$$

where
$$H_i' = \frac{1}{x^3}\left\{\frac{8q_i\tan\beta + 12q_i}{P} - \frac{A}{P^2}(4q_i^2 + 12q_i^2\tan^2\beta + \right.$$
$$\left. + 4q_i^4 + 4q_i\tan\beta\sec^2\beta + 12q_i^3\tan\beta)\right\}$$

where $A = 8q_i\tan\beta + 6q_i^2 + 2\sec^2\beta$

and $P = \sec^4\beta + q_i^4 + 6q_i^2\tan^2\beta + 2q_i^2 + 4q_i\tan\beta\sec^2\beta + 4q_i^3\tan\beta$

APPENDIX D

The Vertical Gradient of Gravity Over a Single Block

The vertical gradient of gravity due to a block may be obtained by differentiating g_s with respect to z. We shall, however, obtain the vertical gradient expression from first principles.

From Appendix A, the vertical component of gravity at the point P in Figure 82 for the semi-infinite plane corresponding to the positive half of the XY plane is

$$g = 2G\rho\int_0^\infty \frac{\cos\xi}{r}\,dx$$

Substituting $\cos\xi = z/r$ and differentiating the above expression with respect to z, we obtain for the vertical gradient of gravity at P for the semi-infinite plane

$$\frac{\partial g}{\partial z} = 2G\rho\int_0^\infty \frac{\partial}{\partial z}\left(\frac{z}{r^2}\right)dx$$

$$= 2G\rho\int_0^\infty \frac{1}{r^2}\left(1 - \frac{2z^2}{r^2}\right)dx$$

$$= -2G\rho\int_{-\theta}^{\pi/2} \frac{1}{z}\cos 2\xi\,dx$$

$$= -G\rho\,\frac{\sin 2\theta}{z}$$

To obtain the vertical gradient of gravity due to a block whose upper and lower surfaces are at depths z_1 and z_2, we integrate the above expression between the limits z_1 to z_2. Hence the vertical

gradient of gravity due to the block is

$$\frac{\partial g_s}{\partial z} = -G\rho\int_{z_1}^{z_2} \frac{\sin 2\theta}{z}\, dz = -2G\rho\int_{z_1}^{z_2} \frac{\sin\theta\cos\theta dz}{z}$$

Since $\tan\theta = \tan\beta + \frac{x}{z}$,

referring to Figure 84, we have

$$\cos\theta = \frac{1}{\sqrt{\sec^2\beta + 2\frac{x}{z}\tan\beta + x^2/z^2}}$$

and

$$\sin\theta = \frac{\tan\beta + x/z}{\sqrt{\sec^2\beta + 2\frac{x}{z}\tan\beta + x^2/z^2}}$$

Substituting these values of $\sin\theta$ and $\cos\theta$ in the integral, we have

$$\frac{\partial g_s}{\partial z} = -2G\rho\int_{z_1}^{z_2} \frac{x + z\tan\beta}{z^2\sec^2\beta + 2xz\tan\beta + x^2}$$

$$= (-2G\rho\cos^2\beta)\left[\frac{1}{2}\tan\beta \log\left(\frac{q_2^2\cos^2\beta + q_2\sin 2\beta + 1}{q_1^2\cos^2\beta + q_1\sin 2\beta + 1}\right)\right.$$

$$\left. + \cos^2\beta\left\{\tan^{-1}\frac{q_2\tan\beta + \sec^2\beta}{q_2} - \tan^{-1}\frac{q_1\tan\beta + \sec^2\beta}{q_1}\right\}\right] \quad \ldots\ (9)$$

The Vertical Gradient Over a Fault Truncating a Single Bed

To obtain the vertical gradient of gravity over a fault truncating a single bed, we subtract from equation (9) the effect of a similar second

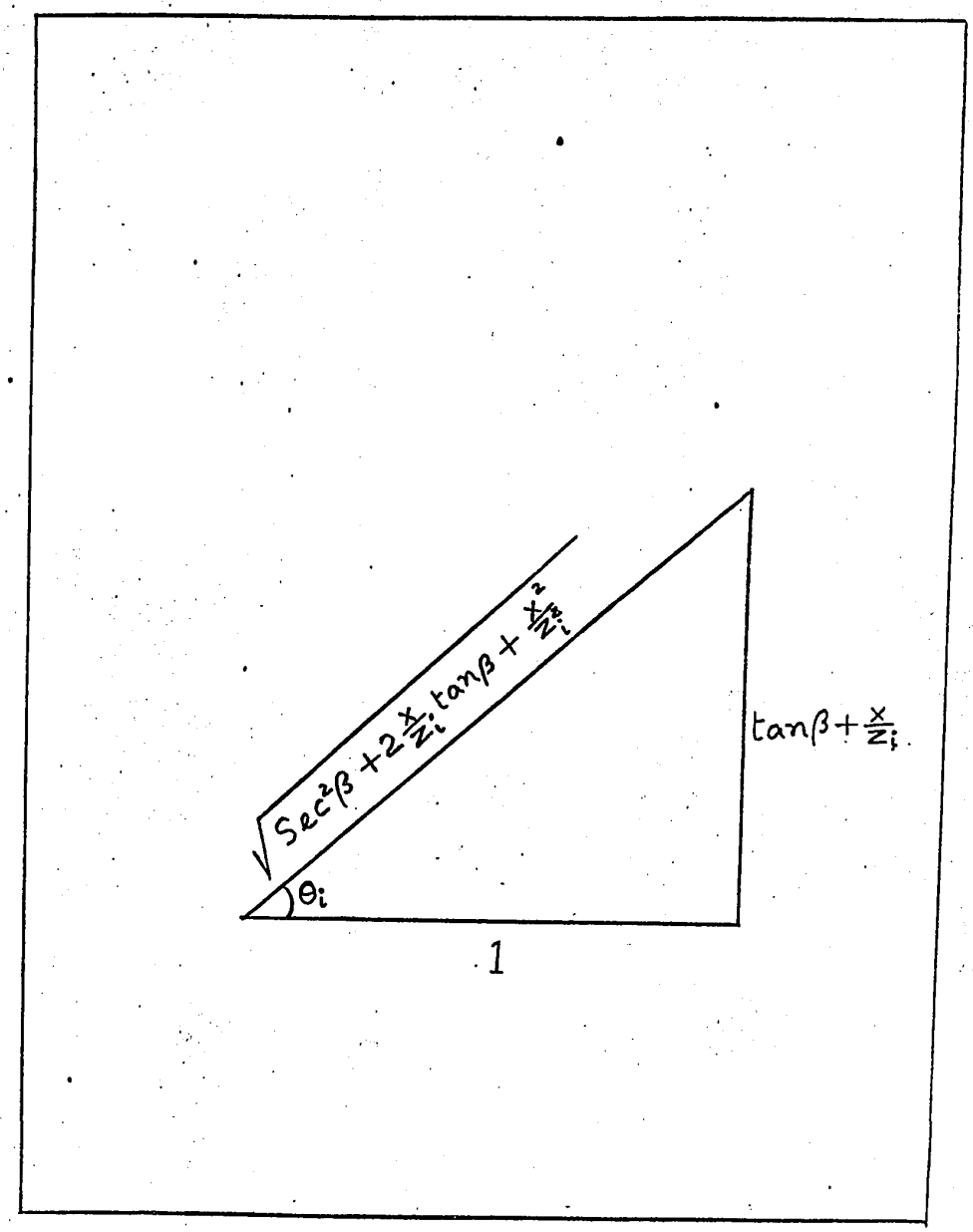
$\sqrt{\sec^2\beta + 2\frac{x}{z_i}\tan\beta + \frac{x^2}{z_i^2}}$
$\tan\beta + \frac{x}{z_i}$
θ_i
1

FIG 84.

block whose surfaces are at depths z_3 and z_4. The vertical gradient of gravity over such a fault is, therefore, given by

$$\frac{\partial g_f}{\partial z} = (-2G\rho)\left[\frac{\sin 2\beta}{4}\log\frac{(z_2^2\sec^2\beta + 2xz_2\tan\beta + x^2)(z_3^2\sec^2\beta + 2xz_3\tan\beta + x^2)}{(z_1^2\sec^2\beta + 2xz_1\tan\beta + x^2)(z_4^2\sec^2\beta + 2xz_4\tan\beta + x^2)}\right.$$

$$+ \cos^2\beta\left\{\tan^{-1}(\tan\beta + \frac{z_2}{x}\sec^2\beta) - \tan^{-1}(\tan\beta + \frac{z_1}{x}\sec^2\beta) + \tan^{-1}(\tan\beta + \right.$$

$$\left.\left.\frac{z_3}{x}\sec^2\beta) - \tan^{-1}(\tan\beta + \frac{z_4}{x}\sec^2\beta)\right\}\right] \qquad \ldots . \quad (10)$$

Limiting value of $\frac{\partial g_s}{\partial z}$ as $x \longrightarrow 0$

As x approaches zero the arguments of both inverse tangents in (9) approach ∞ and hence all the angles approach $\pi/2$ and cancel each other. Therefore,

$$\lim_{x \longrightarrow o}\left(\frac{\partial g_s}{\partial z}\right) = G\rho\sin 2\beta \log\left(\frac{z_2}{z_1}\right)$$

Limiting value of $\frac{dg_f}{dz}$ as $x \longrightarrow 0$

Applying the result for the single block, the limiting value of $\frac{\partial g_f}{\partial z}$ as $x \longrightarrow 0$ is given by

$$\frac{\partial g_f}{\partial z} = G\rho\sin 2\beta \log\frac{z_2 z_3}{z_1 z_4}$$

APPENDIX E

Fourier Transform of $\frac{d^2 g_s}{dx^2}$

From equation (14), we have

$$\frac{d^2 g_s}{dx^2} = -\frac{2K}{x}\left\{(1 + \tan^2\theta_2)^{-1} - (1 + \tan^2\theta_1)^{-1}\right\}$$

where $\tan\theta_i = \tan\beta + \frac{x}{z_i} = a + \frac{x}{z_i} = \xi_i$; $a = \tan\beta$, $i = 1, 2$.

The Fourier transform of the typical term in the above expression is given by

$$F_2(\omega) = -2K\int_{-\infty}^{\infty} \frac{e^{-j\omega x}}{x(1 + \xi^2)}\,dx$$

$$= -2Ke^{jma}\int_{-\infty}^{\infty} \frac{e^{-jm\xi}\,d\xi}{(\xi - a)(1 + \xi^2)} \quad \ldots (36)$$

where $m = \omega z$

Equation (36) can be evaluated by contour integration in the complex plane. Writing $z = x + jy$, so that z is the complex variable (instead of depth), and referring to Figure 85, the path of integration is along the real axis from A to C, then back to A along the semi-circle D whose radius R is large compared to unity. The point $z = a$ is avoided by making a small detour along the semi-circle B. Then,

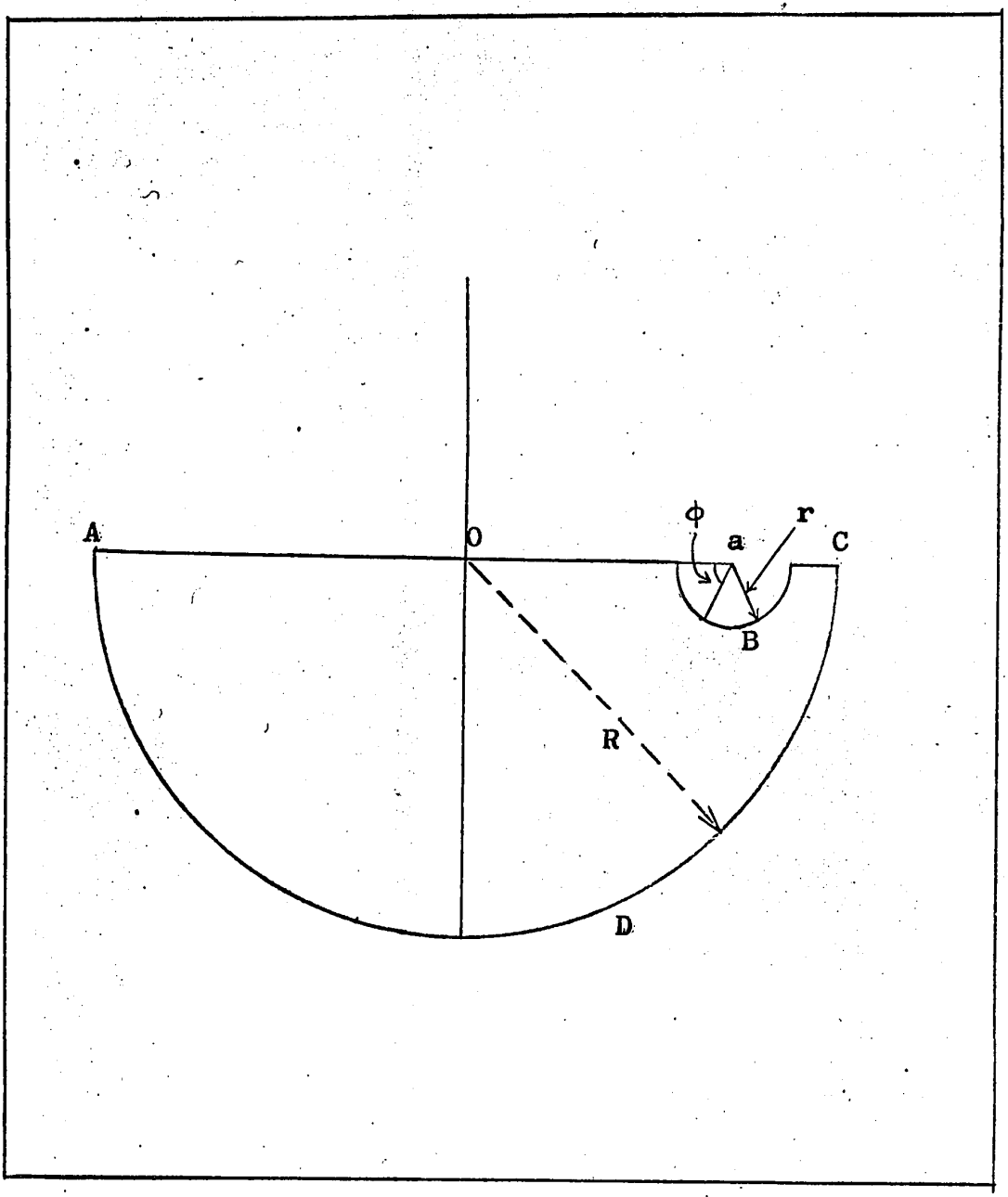

FIG 85. Contour integration in the complex plane

$$\oint \frac{e^{-jmz}dz}{(z-a)(1+z^2)} = \int_{-R}^{R} \frac{e^{-jmx}dx}{(x-a)(1+x^2)} + \int_{B} \frac{e^{-jmz}dz}{(z-a)(1+z^2)} + \int_{D} \frac{e^{-jmz}dz}{(z-a)(1+z^2)}$$

As R approaches infinity the last integral vanishes. Also, when the radius of B is small, $\frac{e^{-jmz}}{1+z^2} \doteq \frac{e^{-jma}}{1+a^2}$, $(z-a) = -r\cos\phi - jr\sin\phi = -re^{j\phi}$, $dz = -jre^{j\phi}d\phi$. Therefore,

$$\int_{D} \frac{e^{-jmz}dz}{(z-a)(1+z^2)} \doteq \frac{e^{-jma}}{1+z^2}\int_{o}^{\pi} jd\phi = \frac{j\pi e^{-jma}}{(1+a^2)}$$

Hence

$$\oint \frac{e^{-jmz}dz}{(z-a)(1+z^2)} \doteq \int_{-\infty}^{\infty} \frac{e^{-jmx}dx}{(x-a)(1+x^2)} + \frac{j\pi e^{-jma}}{(1+a^2)}$$

In the limit, when $r = 0$, the above equation is exact.

The left-hand side of the last equation equals $-2\pi j$ times the residue at $z = -j$, the only singularity enclosed by the path of integration. Therefore, the left-hand side equals

$$-2\pi j \lim_{z \to} -j\left\{\frac{(z+j)e^{-jmz}}{(z-a)(1+z^2)}\right\} = \frac{-\pi e^{-m}}{(a+j)}$$

so that

$$\frac{-\pi e^{-m}}{(a+j)} = \int_{-\infty}^{\infty} \frac{e^{-jmx}dx}{(x-a)(1+x^2)} + \frac{j\pi e^{-jma}}{(1+a^2)}$$

and we obtain finally

$$\int_{-\infty}^{\infty} \frac{e^{-jmx}dx}{(x-a)(1+x^2)} = \left(\frac{-\pi}{1+a^2}\right)\left\{(a-j)e^{-m} + je^{-jma}\right\}$$

Thus,

$$F_2(\omega) = \left(\frac{2\pi K}{1+a^2}\right)\left\{(a-j)e^{-m(1-ja)} + j\right\}$$

$$= \left(\frac{2\pi K}{1+a^2}\right)\left[e^{-m}(a\cos ma + \sin ma) + j\left\{e^{-m}(a\sin ma - \cos ma) + 1\right\}\right]$$

But $\frac{1}{(1+a^2)} = \frac{1}{(1+\tan^2\beta)} = \cos^2\beta$, and we can take out $\cos\beta$ inside the brackets and so obtain the result

$$F_2(\omega) = c\left[e^{-\omega z}\left\{\sinh - j\cosh\right\} + j\cos\beta\right]$$

Where $c = 2\pi K\cos\beta = 2\pi G\rho\cos\beta$,

$h = (ma + \beta) = (\omega z\tan\beta + \beta)$

Let $F_{2S}(\omega) = R_{2S}(\dot{\omega}) + jX_{2S}(\omega)$. Adding together the effects of the two interfaces, we obtain

$$R_{2S}(\omega) = c(e^{-\omega z_2}\sinh_2 - e^{-\omega z_1}\sinh_1) \qquad \ldots\ldots (16a')$$

$$X_{2S}(\omega) = -c(e^{-\omega z_2}\cosh_2 - e^{-\omega z_1}\cosh_1) \qquad \ldots\ldots (16b')$$

Also, $z_2 = z_1 + T$, hence

$$e^{-\omega z_2}\sinh_2 - e^{-\omega z_1}\sinh_1$$

$$= e^{-\omega z_1}\{e^{-\omega T}\sin(h_1 + \omega T\tan\beta) - \sinh_1\}$$

$$= Me^{-\omega z_1}\sin(h_1 + \phi)$$

and $$e^{-\omega z_2}\cosh_2 - e^{-\omega z_1}\cosh_1$$

$$= e^{-\omega z_1}\{e^{-\omega T}\cos(h_1 + \omega T\tan\beta) - \cosh_1\}$$

$$= Me^{-\omega z_1}\cos(h_1 + \phi)$$

where $\tan\phi = \dfrac{\sin(\omega T\tan\beta)}{\cos(\omega T\tan\beta) - e^{\omega T}}$; $M = \left\{1 + e^{-2\omega T} - 2e^{-\omega T}\cos(\omega T\tan\beta)\right\}^{1/2}$

Hence

$$R_{2S}(\omega) = cMe^{-\omega z_1}\sin(h_1 + \phi) \qquad \ldots\ldots (16a)$$

$$X_{2S}(\omega) = -cMe^{-\omega z_1}\cos(h_1 + \phi) \qquad \ldots\ldots (16b)$$

Considering next the case of a fault, we write

$T = z_2 - z_1 = z_4 - z_3$ = thickness of the bed,

$\delta = z_3 - z_1 = z_4 - z_2$ = displacement of the fault.

Then,

$$(e^{-\omega z_4}\sinh_4 - e^{-\omega z_3}\sinh_3) = Me^{-\omega z_3}\sin(h_3 + \phi)$$

so that

$$R_{2f}(\omega) = cM\{e^{-\omega z_1}\sin(h_1 + \phi) - e^{-\omega z_3}\sin(h_3 + \phi)\}$$

$$= cMNe^{-\omega z_1}\sin(h_1 + \phi + \eta)$$

Similarly we find

$$X_{2f}(\omega) = cMNe^{-\omega z_1}\cos(h_1 + \phi + \eta)$$

where $\tan\eta = \dfrac{\sin(\omega\delta\tan\beta)}{\cos(\omega\delta\tan\beta) - e^{\omega\delta}}$

$$N = \left\{1 + e^{-2\omega\delta} - 2e^{-\omega\delta}\cos(\omega\delta\tan\beta)\right\}^{1/2}$$

APPENDIX F

Limiting Values of the Fourier Transforms as $\omega \longrightarrow 0$

Limiting value of $R_S(\omega)$ as $\omega \longrightarrow 0$

We have from equations (16a') p. 225 and (15) p. 111,

$$R_S(\omega) = \frac{c}{(j\omega)^2}\left[e^{-\omega z_2}\sin(\omega z_2\tan\beta + \beta) - e^{-\omega z_1}\sin(\omega z_1\tan\beta + \beta)\right]$$

We shall first calculate the limiting value of the typical term in the above expression, that is,

$$\lim_{\omega \longrightarrow o}\left[\frac{ce^{-\omega z}\sin(\omega z\tan\beta + \beta)}{-\omega^2}\right]$$

Expanding the numerator in powers of ω and neglecting terms involving cubes and higher powers of ω, we obtain

$$c \lim_{\omega \longrightarrow o} \frac{(1 - \omega z + \frac{1}{2}\omega^2 z^2)}{-\omega^2}\left[\cos\beta(\omega z\tan\beta) + \sin\beta(1 - \omega^2 z^2\tan^2\beta)\right]$$

$$= c\sin\beta \lim_{\omega \longrightarrow o}\left\{(1 - \omega z + \tfrac{1}{2}\omega^2 z^2)(1 + \omega z - \tfrac{1}{2}\omega^2 z^2\tan^2\beta)\right\}$$

$$= \frac{c}{2}\sin\beta \lim_{\omega \longrightarrow o}\left(\frac{\omega^2 z^2\sec^2\beta - 2}{\omega^2}\right)$$

The limiting value of $R_S(\omega)$ may be obtained by adding together the effects of the two interfaces at z_1 and z_2

Hence $$\lim_{\omega \to o} R_S(\omega) = \frac{c}{2} \sin\beta \sec^2\beta (z_2^2 - z_1^2)$$

$$= \pi G\rho T \tan\beta (z_1 + z_2) \qquad \ldots . \text{(25a)}$$

In the same way, we find that

$$X_S(\omega) = -\frac{c}{(j\omega)^2} \left[e^{-\omega z_2} \cos(\omega z_2 \tan\beta + \beta) - e^{-\omega z_1} \cos(\omega z_1 \tan\beta + \beta) \right]$$

As before,

$$\lim_{\omega \to o} c \left\{ \frac{e^{-\omega z} \cos(\omega z \tan\beta + \beta)}{\omega^2} \right\}$$

$$= c \lim_{\omega \to o} \frac{(1 - \omega z + \frac{1}{2}\omega^2 z^2)}{\omega^2} \left[\cos\beta (1 - \tfrac{1}{2}\omega^2 z^2 \tan^2\beta) - \sin\beta (\omega z \tan\beta) \right]$$

$$= c \cos\beta \lim_{\omega \to o} \frac{(1 - \omega z + \frac{1}{2}\omega^2 z^2)}{\omega^2} (1 - \omega z \tan^2\beta - \tfrac{1}{2}\omega^2 z^2 \tan^2\beta)$$

$$= c \cos\beta \lim_{\omega \to o} \frac{1}{\omega^2} (1 - \omega z \sec^2\beta + \tfrac{1}{2}\omega^2 z^2 \sec^2\beta)$$

hence, $$\lim_{\omega \to o} X_S(\omega) = c \sec\beta \lim_{\omega \to o} \left[\frac{\omega^2/2(z_2^2 - z_1^2) - \omega(z_2 - z_1)}{\omega^2} \right]$$

$$= 2\pi G\rho \left[\frac{T}{2} (z_1 + z_2) - T \lim_{\omega \to o} (\tfrac{1}{\omega}) \right]$$

$$\ldots . \text{(25b)}$$

The limiting value of $R_f(\omega)$ can be obtained by adding to the above result for $R_S(\omega)$ the effect of the interfaces at depths z_3 and z_4.

Thus, $$\lim_{\omega \to o} R_f(\omega) = \pi G\rho T \tan\beta (z_2 + z_1 - z_3 - z_4)$$

$$= -2\pi G\rho T \delta \tan\beta \qquad \ldots . \text{(25c)}$$

Similarly, we have

$$\lim_{\omega \to 0} X_f(\omega) = cT\sec\beta \lim_{\omega \to 0} \left\{ \frac{\omega^2(z_1 + z_2 - z_3 - z_4)}{2\omega^2} \right\}$$

$$= \frac{-2c\delta T\sec\beta}{2}$$

$$= -2\pi G\rho\delta T \qquad \ldots\ldots (25d)$$

Limiting values of $R_m(\omega)$ and $X_m(\omega)$ as $\omega \to 0$

From equations (19a), p. 115 and (15), p. 111, we have

$$R_m(\omega) = \frac{cR}{(j\omega)^2}\left\{ \rho_1 e^{-\omega z_1}\sin(h_1 + \phi) + \rho_2 e^{-\omega z_2}\sin(h_2 + \phi) + \right.$$

$$\left. + \ldots\ldots \rho_{N+1} e^{-\omega z_{N+1}}\sin(h_{N+1} + \phi) \right\}$$

The above equation is equivalent to the sum of the transforms of the gravity anomalies of N + 1 single blocks. The limiting value or $R_m(\omega)$ can be obtained by finding the limiting value of the transform for each block separately by the use of equation (25a) and then summing the effect of all the (N + 1) blocks. Since $z_i' = z_i + \delta$, we thus have

$$\lim_{\omega \to 0} R_m(\omega) = \pi G\delta\tan\beta\left\{ \rho_1(z_1 + z_1') + \rho_2(z_2 + z_2') + \ldots\ldots \right.$$

$$\left. \ldots\ldots \rho_{N+1}(z_{N+1} + z_{N+1}') \right\}$$

$$= \pi G\delta\tan\beta\left\{ 2(\rho_1 z_1 + \rho_2 z_2 + \ldots\ldots \rho_{N+1} z_{N+1}) \right.$$

$$\left. + \delta(\sigma_r - \sigma_o) \right\}$$

Now,

$$\rho_1 z_1 + \rho_2 z_2 + \ldots\ldots \rho_{N+1} z_{N+1}$$

$$= z_1(\sigma_1 - \sigma_o) + z_2(\sigma_2 - \sigma_1) + \ldots\ldots z_{N+1}(\sigma_r - \sigma_N)$$

$$= -(\sigma_o z_1 + \sigma_1 t_1 + \sigma_2 t_2 + \ldots\ldots \sigma_N t_N) + \sigma_r z_{N+1}$$

$$= \sigma_r z_{N+1} - \bar{\sigma} z_{N+1} = z_{N+1}(\sigma_r - \bar{\sigma})$$

Where $\bar{\sigma} = \dfrac{\sigma_o z_1 + \sigma_1 t_1 + \ldots\ldots \sigma_N t_N}{z_{N+1}}$

= Mean density of the top (N + 1) beds.

Hence

$$\lim_{\omega \to o} R_m(\omega) = \pi G \delta \tan\beta \left\{ 2z_{N+1}(\sigma_r - \bar{\sigma}) + \delta(\sigma_r - \sigma_o) \right\} \quad \ldots \quad (25e)$$

Similarly,

$$\lim_{\omega \to o} X_m(\omega) = \pi G \delta \left\{ 2z_{N+1}(\sigma_r - \bar{\sigma}) + \delta(\sigma_r - \sigma_o) - \lim_{\omega \to o} \frac{2\delta(N+1)(\sigma_r - \sigma_o)}{\omega} \right\}$$

$$= -\infty \quad \ldots\ldots \quad (25f)$$

Limiting values of $R_1(\omega)$ and $X_1(\omega)$ as $\omega \longrightarrow 0$

From equations (16a) and (15), p.111-2 the Fourier transforms $R_1(\omega)$ and $X_1(\omega)$ of the first derivative of the gravity anomaly, g_s, are given by

$$X_{1S}(\omega) = \frac{c(e^{-\omega z_2}\sinh_2 - e^{-\omega z_1}\sinh_1)}{\omega}$$

$$R_{1S}(\omega) = \frac{-c(e^{-\omega z_2}\cosh_2 - e^{-\omega z_1}\sinh_1)}{\omega}$$

To find the limiting value of $R_{1S}(\omega)$ as $\omega \longrightarrow 0$ we expand the terms within brackets in powers of ω and neglect terms containing powers of ω greater than the first. Taking a typical term, therefore, we have

$$\frac{c}{\omega} e^{-\omega z}\cos(\omega z\tan\beta + \beta)$$

$$\doteq \frac{c}{\omega}(1 - \omega z)\{ \cos\beta - \sin(\omega z\tan\beta)\sin\beta \}$$

$$\doteq \frac{c\cos\beta}{\omega}(1 - \omega z)(1 - \omega z\tan^2\beta)$$

$$\doteq \frac{c\cos\beta}{\omega}(1 - \omega z\sec^2\beta).$$

Combining the effects of the two interfaces at z_1 and z_2, we have

$$\lim_{\omega \longrightarrow 0} R_{1S}(\omega) \doteq \frac{c\cos\beta}{\omega}(z_2 - z_1)\,\omega\sec^2\beta$$

$$\doteq cT\sec\beta$$

$$\doteq 2\pi G\rho T$$

A similar analysis for the imaginary part gives

$$\frac{c}{\omega} e^{-\omega z} \sin(\omega z \tan\beta + \beta) \doteq \frac{c}{\omega} \sin\beta$$

Therefore,

$$\lim_{\omega \longrightarrow o} X_{1S}(\omega) = 0$$

The limiting values of the transform of the first derivative of g_f can be obtained by adding to the results for a block the effect of the two interfaces at z_3 and z_4. It is evident that both $R_{1f}(\omega)$ and $X_{1f}(\omega)$ tend to zero as ω tends to zero.

Limiting value of $\mathbf{F}\left\{g_L - f(x)\right\}$ as $\omega \longrightarrow 0$

If $g_{+\infty}$ and $g_{-\infty}$ are the limiting values of f(x) as x approaches $+\infty$ and $-\infty$ respectively, the corresponding limiting values of the function $g_L - f(x)$ are $(g_L - g_{+\infty})$ and $(g_L + g_{-\infty})$ respectively. It has been shown in Chapter IV that the Fourier transform of the function f(x) may be written in terms of the transforms of the functions $g_L - f(x)$ and g_L. Thus,

$$F\left\{ g_L - f(x)\right\} = F\left\{ g_L\right\} - F\left\{ f(x)\right\}$$

The limiting values of the left-hand side of the above equation can be obtained by finding the limiting values of the two transforms on the R.H.S. of the equation.

It has been shown in Chapter IV that

$$F\left\{g_L\right\} = \frac{g_{+\infty} + g_{-\infty}}{j\omega} + \pi(g_{+\infty} - g_{-\infty})\,\delta(\omega)$$

$$= \frac{2\pi G\rho T}{j\omega} + \pi(g_{+\infty} - g_{-\infty})\,\delta(\omega)$$

since $g_{+\infty} + g_{-\infty}$ = total change in gravity due to the block. Then from the above equations plus equations (25a) and (25b), page 228

$$\lim_{\omega \to 0} F\left\{g_L - g_s(x)\right\} = \left[\lim_{\omega \to 0} \frac{2\pi G\rho T}{j\omega} + \pi(g_{+\infty} - g_{-\infty})\,\delta(\omega)\right]$$

$$- \left[\pi G\rho T \tan\beta(z_1 + z_2) + j\left\{\pi G\rho T(z_1 + z_2)\right.\right.$$

$$\left.\left. - 2\pi G\rho T \lim_{\omega \to 0} \left(\frac{1}{\omega}\right)\right\}\right]$$

$$\doteq \pi(g_{+\infty} - g_{-\infty})\,\delta(\omega) - \pi G\rho T \tan\beta(z_1 + z_2)$$

$$- j\pi G\rho T(z_1 + z_2).$$

If R_S' and X_S' are the real and the imaginary parts of the limiting values of $F\left\{g_L - f(x)\right\}$, we then have

$$R_S' \doteq \pi(g_{+\infty} - g_{-\infty})\,\delta(\omega) - \pi G\rho T \tan\beta(z_1 + z_2) \quad \ldots\ (38a)$$

and

$$X_S' \doteq -\pi G\rho T(z_1 + z_2) \quad \ldots\ (38b)$$

since $\delta(\omega) = 0$ when $\omega \neq 0$, for very small values of ω the limiting value R_S' is approximately given by

$$R_S' \doteq -\pi G\rho T \tan\beta(z_1 + z_2) \quad \ldots\ (38c)$$

For a fault cutting a series of N beds, the corresponding limiting values R_m' and X_m' for very small values of ω are given by

$$R_m' = -\pi G\delta \tan\beta \left[2z_{N+1}(\sigma_r - \bar{\sigma}) + \delta(\sigma_r - \sigma_o)\right] \quad \ldots . \quad (39a)$$

$$X_m' = -\pi G\delta \left[2z_{N+1}(\sigma_r - \bar{\sigma}) + \delta(\sigma_r - \sigma_o)\right] \quad \ldots . \quad (39b)$$

where $$\bar{\sigma} = \frac{\sigma_o z_1 + \sigma_1 t_1 + \ldots . \sigma_N t_N}{z_{N+1}}$$

BIBLIOGRAPHY

Bancroft, A.M. (1960): Gravity anomalies over a buried step: contrib. from Dom Obs. Ottawa, 3, n. 27, reprinted from J. Geoph. Res. 65.

Baranov, V. (1953): Calcul du gradient vertical du champ de gravité ou du champ magnétique measuré à la surface du sol: Geophysical prospecting vol. 1, pp. 172-191.

Barton, D.C. (1938): Gravitational methods of prospecting in The Science of Petroleum ed. by A.E. Dunstan et al., v. 1, p. 364-381: London, Oxford Univ. Press.

Belyea, Helen R. (1952): Deep wells and subsurface stratigraphy of part of the St. Lawrence Lowlands, Quebec. Geol. Sur. Canada, Bull. 22.

Bhattacharya, B.K. (1965): Two-dimensional harmonic analysis as a tool for magnetic interpretation: Geophysics, vol. 30, pp. 829-857.

Billings, M.P. (1942): Structural geology: Prentice-Hall, New York.

Bott, M.H.P. (1962): A simple criterion for interpreting negative gravity anomalies: Geophysics, vol. 27, pp. 376-381.

Bracewell, R. (1965): The Fourier transforms and its application: New York, McGraw-Hill Book Co. Inc.

Clark, T.H. (1934): Structure and stratigraphy of S. Quebec: Bull. Geol. Soc. Am. 45, n. 1, pp. 1-20.

Clark, T.H. (1952): Montreal area - Laval and Lachine: Que. Dept. of Mines, Geol. Rept. 46.

Clark, T.H. (1955): St. Jean-Beloeil area: Que. Dept. of Mines, Geol. Rept. 66.

Dean, W.G. (1958): Frequency analysis for gravity and magnetic interpretation: Geophysics, vol. 23, pp. 97-127.

Dobrin, M.B. (1960): Introduction to geophysical prospecting: McGraw-Hill, New York.

Elkins, T.A. and Hammer, S. (1938): The resolution of combined effects with applications to gravitational and magnetic data: Geophysics, Vol. 3, pp. 315-331.

Elkins, T.A. (1951): The second derivative methods of gravity interpretation: Geophysics, vol. 16, pp. 29-50.

Evjen, H.M. (1936): The place of the vertical gradient in gravitational interpretations: Geophysics, vol. 1, pp. 127-136.

Geldart, L.P., Gill, D.E. and Sharma, B. (1966): Gravity anomalies of two-dimensional faults: Geophysics, vol. 31, pp. 372-397.

Grant, F.S. and West, G.F. (1965): Interpretation theory in applied geophysics: McGraw-Hill, New York.

Griffin, W.R. (1949): Residual gravity in theory and practice: Geophysics, vol. 14, pp. 39-56.

Guillemin, E.A. (1950): The mathematics of circuit analysis: John Wiley and Sons, New York.

Hammer, S. (1950): Density determinations by underground gravity measurements: Geophysics, vol. 15, pp. 637-652.

Hammer, S. (1963): Rock densities and vertical gradient of gravity in the earth's crust: Jour. of Geoph. Res., vol. 69, pp. 603-604.

Hedstrom, H. (1938): A new gravimeter for ore prospecting: Am. Inst. Min. Met. Eng., Tech. pub. 953, pp. 1-23.

Heiland, C. A. (1946): Geophysical exploration: New York, Prentice-Hall, Inc.

Heiskanen, W.A. and Vening Meinesez, F.A. (1958): The earth and its gravity field: McGraw-Hill, New York.

Henderson, R.G. and Zietz, I. (1949): Second vertical derivatives of geomagnetic fields: Geophysics, vol. 14, pp. 508-516.

Hosain, I. (1965): Gravity survey in the St. Lawrence Lowlands, M.S. thesis, Department of Mining and Applied Geophysics, McGill University, Montreal, Que., Canada.

Hubbert, M.K. (1948a): Gravitational terrain effects of two-dimensional topographic features: Geophysics, vol. 13, pp. 226-254.

Hubbert, M.K. (1948b): A line integral method of computing the gravimetric effects of two-dimensional masses, ibid., pp. 215-225.

Innes, M.J.S. and Thomson, L.G.D. (1953): The establishment of primary gravimeter bases in Canada: Pub. Dom. Obs. Ottawa, 16, n. 8.

Jakosky, J.J. (1950): Exploration Geophysics, Second Edition: Trija Publishing Co., Los Angeles.

Kantas, K. (1959): The gravitational potential and its vertical derivatives: Geofisica pure e applicata, vol. 1, pp. 20-24.

Kellog, O.D. (1953): Foundations of potential theory: Dover, New York.

Kumarapelli, P.S. and Saull, V.A. (1966): The St. Lawrence Valley system: A North American equivalent of the East African Rift Valley system: Publ. in Canadian Journal of Earth Sciences, pp. 639-658.

Logan, Sir W.E. (1863): Report on the Geology of Canada: Geol. Survey of Canada, Rept. of prog. to 1863.

McDonald, D.G. (1965): Gravity field studies in the St. Lawrence Lowlands: M.S. thesis, Department of Mining and Applied Geophysics, McGill University, Montreal, Que., Canada.

Nettleton, L.L. (1940): Geophysical prospecting for oil: McGraw-Hill, New York.

Nettleton, L.L. (1954): Regionals residuals and structures: Geophysics, vol. 19, pp. 1-22.

Odegard, M.E. and Berg, J.W. (1965): Gravity interpretation using the Fourier Integral: Geophysics, vol. 30, pp. 424-438.

Papoulis, Athanasios (1962); The Fourier Integral and its applications: McGraw-Hill, New York.

Parasnis, D.S. (1962): Principles of applied geophysics: Methuen, London.

Phillpotts, A.R. (1961): Preliminary report on part of Grenville Township: Quebec Department of Natural Resources, P.R. No. 467.

Ramsey, A.S. (1940): An introduction to the theory of Newtonian Potential: Cambridge Univ. Press, London.

Robertson, L.P. (1960): Precise and secondary levelling in Quebec, South of the St. Lawrence River: Geodetic Sur. Canada, Pub. 16 (revised 1960).

Romberg, F.E. (1958): Key variables in gravity: Geophysics, vol. 23, pp. 684-700.

Rosenbach, O. (1954): Quantitative studies concerning the vertical derivative methods of gravity interpretation: Geophysical Prospecting, vol. 2, pp. 128-138.

Rosenbach, O. (1954): A comparison of second derivative method of gravity interpretation with reflection seismics and geological findings in the Offenburg area: Geophysical Prospecting, vol. 2, pp. 1-123.

Saxov, S. (1956): A gravity survey in the vicinity of Ottawa: Pub. Dom. Obs. Ottawa, 18, n. 11.

Shaw, H. (1932): Interpretation of gravitational anomalies: Geophysical Prospecting, AIMM transactions, pp. 271-335.

Sharma, B. (1964): The vertical gradient of gravity in gravitational interpretation: M.S. thesis, Department of Geology and Geophysics, University of Minnesota, Minneapolis.

Sharma, B. and Geldart, L.P. (1967): Interpretation of gravity anomalies of two-dimensional faults by Fourier transforms (to be published).

Skeels, D.C. (1947): Ambiguity in gravity interpretation: Geophysics, vol. 12, pp. 43-56.

Thomson, L.G.D. and Garland, G.D. (1957): Gravity measurements in Quebec (South of Latitude 52°N): Pub. Dom. Obs. Ottawa, 19, n. 4.

Thyssen-Bornemisze, S. (1963): The vertical gradient in bore-hole exploration: Geophysics, vol. 28, pp. 1072-1073.

Vacquier, V. (1951): Interpretation of aeromagnetic maps: Geol. Soc. of Am. Mem. 47.

am